Stimuli-Responsive and Self-Healing Nanocomposite Hydrogels Based on Reversible and Dynamic Crosslinks

by

Meng Wu

A thesis submitted in partial fulfillment of the requirements for the degree of

Doctor of Philosophy

in

Materials Engineering

Department of Chemical and Materials Engineering
University of Alberta

Abstract

Hydrogels, due to their soft and water abundant natures, highly resemble human skins and tissues and thereby have attracted extensive attention in recent years. Functional hydrogels showing responsiveness to various stimuli such as pH, temperature, strain and pressure are promising for a wide range of biomedical and electrical applications. However, traditional hydrogels crosslinked via permanent covalent bonds are generally weak, brittle and lack of functionalities. Incorporation of reversible and dynamic crosslinks into hydrogel networks can effectively improve their mechanical performances, introduce multiple responsiveness, and endow the hydrogels with self-healing capability. On the other hand, introduction of stiff nanomaterials into hydrogel matrix is an effective approach towards strong and functional gel materials. The combination of the nanofillers and appropriate interfacial reversible and dynamic interactions provides a promising method for the fabrication of high-performance multifunctional hydrogels to meet the increasing needs of modern materials. In this thesis, a review on hydrogels based on reversible and dynamic crosslinks, stimuli-responsive and self-healing functions, and nanocomposite hydrogels was presented first followed by three original research projects on developing nanocomposite hydrogels with stimuli sensitivity and self-healing property based on reversible interactions for biomedical and electrical applications.

Injectable, self-healing and pH-responsive hydrogels are great intelligent drug delivery vehicles for controlled and localized therapeutic release. Hydrogels that show pH-sensitive behaviors in mildly acidic range are ideal to be used for the treatment of regions showing local acidosis like tumors, wounds and infections. In the first project, we

present a facile preparation of an injectable, self-healing and super-sensitive pH-responsive nanocomposite hydrogel based on Schiff base reactions between aldehyde-functionalized polymers and amine-modified silica nanoparticles. The hydrogel shows fast gelation, injectability and rapid self-healing capability. Moreover, the hydrogel demonstrates excellent stability under neutral physiological conditions while a sharp gel-sol transition induced by faintly acidic environment. The pH-responsiveness of the hydrogel is ultra-sensitive, where the mechanical properties, hydrolytic degradation and drug release behaviors can alter significantly when subjected to a slight pH change of 0.2. The novel injectable, self-healing and sensitive pH-responsive hydrogel serves as a promising candidate as localized drug carriers with controlled delivery capability triggered by acidosis, holding great promise for cancer therapy, wound healing and infection treatment.

Conductive hydrogels are of great significance for soft electronic devices. In the second project, we have developed a novel hydrogel ionic conductor by integrating nanofiller reinforcement with micelle cross-linking. The hydrogel was facilely prepared via one-pot polymerization of acrylamide and an amino-functionalized monomer in the presence of carbon nanotubes, aldehyde-modified F127 and LiCl. The dynamic chemical and physical interactions of the cross-linked network offers the hydrogel with a wide spectrum of properties, including excellent stretchability, toughness, exceptional elasticity, resistance to damage by sharp materials, self-healing property and high conductivity. In addition, the hydrogel demonstrated cooling-induced whitening optical behavior. When exploited as a strain and pressure sensor to monitor diverse human motions, the prepared hydrogel sensor showed excellent sensitivity and reliability. The hydrogel was further integrated with an eye mask to monitor human sleep and showed

high reliability for the detection of rapid eye movement (REM) sleep. This work provides new insights into the fabrication of multifunctional, smart and conductive materials, holding great promise for a broad range of applications like wearable sensors, artificial skins, and soft robotics.

In the third project, we have developed an ionic conductive nanocomposite hydrogel with ultra-stretchability and intelligent sensing functions. By leveraging the dynamic feature of multiple intermolecular interactions, polymer/carbon nanotube networks with excellent mechanical performances (i.e., tensile strength, stretchability and toughness up to 1.09 MPa, 4075% and 12.8 MJ/m^3, respectively) were achieved. Additionally, the hydrogel is soft, elastic, transparent and self-healing. The rational combination of the mechanical and electrical properties renders the as-prepared hydrogel with excellent sensing performances and cycling stability, and therefore enables it to perform as a sensory unit of a complete platform for the recognition of some complicated human behaviors. Specifically, with the integration of machine learning module, the hydrogel-based platform exhibits great recognition accuracies to human handwriting motions from single letters to words and phrases after proper training. The combination of superior mechanical performances and intelligent sensing functions within this hydrogel-based ionic skin unlocks its potential as the intelligent human-device interface, which promotes the application of artificial intelligence in customized electronic devices.

Preface

This thesis is an original work conducted by Meng Wu under the supervision from Dr. Hongbo Zeng, containing published contents from the peer-reviewed journals as described below.

Part of Chapter 1 of this thesis has been published as Wu, M.; Peng, Q.; Han, L.; Zeng, H. Self-Healing Hydrogels and Underlying Reversible Intermolecular Interactions. *Chin. J. Polym. Sci.* **2021**, 39, 1246-1261. I was responsible for the manuscript composition. Dr. Qiongyao Peng and Dr. Lingbo Han contributed to the manuscript revision. Dr. Hongbo Zeng was the corresponding author.

Chapter 2 of this thesis has been published as Wu, M.; Chen, J.; Huang, W.; Yan, B.; Peng, Q.; Liu, J.; Chen, L.; Zeng, H. Injectable and Self-Healing Nanocomposite Hydrogels with Ultrasensitive Ph-Responsiveness and Tunable Mechanical Properties: Implications for Controlled Drug Delivery. *Biomacromolecules* **2020**, 21, 2409-2420. I was responsible for materials synthesis, data collection and analysis, as well as the manuscript composition. Dr. Jingsi Chen, Dr. Qiongyao Peng and Dr. Jifang Liu contributed to the manuscript revision. Dr. Bin Yan instructed the polymer synthesis. Dr. Weijuan Huang and Dr. Lingyun Chen helped to conduct the cytocompatibility tests. Dr. Hongbo Zeng was the corresponding author and was involved in the experimental design and manuscript composition.

Chapter 3 of this thesis has been published as Wu, M.; Chen, J.; Ma, Y.; Yan, B.; Pan, M.; Peng, Q.; Wang, W.; Han, L.; Liu, J.; Zeng, H. Ultra Elastic, Stretchable, Self-Healing Conductive Hydrogels with Tunable Optical Properties for Highly Sensitive Soft

Electronic Sensors. *J. Mater. Chem. A* **2020**, 8, 24718-24733. I was responsible for materials synthesis, data collection and analysis, as well as the manuscript composition. Dr. Jingsi Chen, Dr. Wenda Wang, Dr. Lingbo Han and Dr. Jifang Liu contributed to the manuscript revision. Dr. Yuhao Ma contributed to the experimental design of the sleep monitoring experiment. Dr. Bin Yan synthesized the monomer. Mingfei Pan conducted the AFM imaging experiments. Dr. Hongbo Zeng was the corresponding author and was involved inthe experimental design and manuscript composition.

Chapter 4 of this thesis has been submitted to *Chemical Engineering Journal* as Wu, M.; Pan, M.; Qiao, C.; Ma, Y.; Yan, B.; Yang. W.; Peng, Q.; Zeng, H. Ultra stretchable, tough, elastic and transparent hydrogel skins integrated with self-evolving sensing functions enabled by machine learning algorithms. I was responsible for materials synthesis, data collection and analysis, as well as the manuscript composition. Mingfei Pan conducted the AMF force measurements. Chenyu Qiao wrote the software for writing recognition tests. Dr. Bin Yan instructed the monomer synthesis process. Dr. Yuhao Ma contributed to the monomer synthesis. Wenshuai Yang conducted the SEM characterizations. Dr. Qiongyao Peng contributed to the manuscript revision. Dr. Hongbo Zeng was the corresponding author and was involved in the experimental design and manuscript composition.

Dedicated to

My parents, my husband Yuhao, and my son Xianshuo

Acknowledgements

First and foremost, I would like to express my deep gratitude to my supervisor, Dr. Hongbo Zeng, for giving me the great opportunity to study and do research in the University of Alberta and providing invaluable guidance throughout my PhD study. I am extremely grateful for his immerse knowledge on materials science, enthusiasm towards scientific research, patience and kindness to everyone and his encouragement to me for pursuing academic research and career.

Sincere thanks to all my group members, both past and present, for the warm help and friendship. My deep thanks go to Dr. Bin Yan for the help on monomer and polymer synthesis and Dr. Jingsi Chen for the research advices and help on manuscript revision.

Besides, I am appreciated to Alberta Innovates for the financial supports.

Finally, I would like to thank my family members. Thanks to my parents for their love, caring, support and sacrifices for educating me and preparing me for my future. I am very grateful to my husband, Yuhao, for the support, encouragement, company and insightful ideas. I would also thank my son, Xianshuo, for bringing me a lot of happiness.

Table of Contents

Abstract ..... *ii*

Preface ..... *v*

Acknowledgements ..... *viii*

Table of Contents ..... *ix*

List of Tables ..... *xiii*

List of Figures ..... *xiv*

Abbreviations and Symbols ..... *xxiv*

CHAPTER 1 Introduction *1*

1.1 Hydrogels Through Dynamic and Reversible Crosslinks **1**

1.1.1 Physical Interactions in Hydrogel Networks **2**

1.1.2 Dynamic Chemical Bonding in Hydrogel Networks **7**

1.2 Stimuli-Responsive and Self-healing Functions **10**

1.2.1 Stimuli-Responsiveness **10**

1.2.2 Self-Healing Property **13**

1.3 Nanocomposite Hydrogels **16**

1.3.1 Nanofillers **17**

1.3.2 Nanocomposites toward Tough Hydrogels **20**

1.4 Objectives and Outline of this Thesis **22**

CHAPTER 2 Injectable and Self-healing Nanocomposite Hydrogels with Ultra-sensitive pH-Responsiveness and Tunable Mechanical Properties: Implications for Controlled Drug Delivery *25*

2.1 Introduction **25**

2.2 Experimental Methods **30**

2.2.1 Materials **30**

2.2.2 FBEMA Synthesis 31

2.2.3 P(MPC-co-FBEMA) Synthesis 31

2.2.4 Characterization of ASNP 32

2.2.5 Preparation of Hydrogels 32

2.2.6 SEM Characterization 33

2.2.7 Rheological Tests 33

2.2.8 The pH-Regulated Hydrogel Degradation and *In Vitro* Drug Release 35

2.2.9 Cytotoxicity 36

2.3 Experimental Methods 37

2.3.1 Aldehyde-Functionalized Monomer Synthesis and Hydrogel Fabrication 37

2.3.2 Injectability and Self-Healing Property 41

2.3.3 Effect of Composition on the Mechanical Performance of Hydrogels 44

2.3.4 pH-Dependence of the Rheological and Degradation Properties 45

2.3.5 *In Vitro* Release 49

2.3.6 Cytotoxicity 51

2.4 Conclusions 52

CHAPTER 3 Ultra Elastic, Stretchable, Self-Healing Conductive Hydrogels with Tunable Optical properties for Highly Sensitive Soft Electronic Sensors 54

3.1 Introduction 54

3.2 Experimental Methods 58

3.2.1 Materials 58

3.2.2 Synthesis of F127-CHO 58

3.2.3 Synthesis of Amine-Functionalized Monomer 59

3.2.4 Preparation of Hydrogels 60

3.2.5 Mechanical Properties of the Hydrogels 60

3.2.6 Self-Healing Property of the Hydrogels 61

3.2.7 Temperature-Responsive Properties of the Hydrogels 62

3.2.8 Electrical and Sensing Performances of Hydrogels 63

3.3 Results and Discussion 64

3.3.1 Design and Synthesis of PAAFC-L Hybrid Hydrogel 64

3.3.2 Mechanical Properties 66

3.3.3 Self-Healing Properties 71

3.3.4 Thermo-Responsive Optical Properties 74

3.3.5 Electrical Properties 77

3.3.6 Sensing Performances 79

3.4 Conclusions 86

CHAPTER 4 Ultra Stretchable, Tough, Elastic and Transparent Hydrogel Skins Integrated with Self-Evolving Sensing Functions Enabled by Machine Learning Algorithms 88

4.1 Introduction 88

4.2 Experimental Methods 91

4.2.1 Materials 91

4.2.2 Synthesis of Amine-Modified Monomer (AEAM) 91

4.2.3 Preparation of Hydrogels 92

4.2.4 Transparency and Micromorphology of Hydrogels 92

4.2.5 Mechanical Properties of hydrogels 93

4.2.6 AFM Characterization 93

4.2.7 Self-Healing Performances of Hydrogels 95

4.2.8 Electrical and Sensing Performances 95

4.2.9 Handwriting Recognition 96

4.3 Results and Discussion **97**

4.3.1 Fabrication of Nanocomposite Hydrogels **97**

4.3.2 Mechanical Performances of Hydrogels **98**

4.3.3 AFM Force Measurements **103**

4.3.4 Self-Healing Properties **106**

4.3.5 Electrical and Sensing Performances **107**

4.3.6 Writing Recognition **111**

4.4 Conclusions **115**

CHAPTER 5 Conclusions and Prospects ***116***

5.1 Conclusions and contributions **116**

5.2 Prospects **118**

Bibliography ***120***

Appendices ***151***

Appendix A Supporting Information for Chapter 2 ..... **151**

Appendix B Supporting Information for Chapter 3 ..... **156**

Appendix C Supporting Information for Chapter 4 ..... **168**

List of Tables

Table 2.1. Characteristics of synthesized P(MPC-co-FBEMA) random copolymers determined by ^{1}H NMR and GPC. 38

Table S3.1. Water contents of hydrogels with different compositions. 157

Table S3.2. Comparison of reported elastic hydrogels with this work 166

Table S4.1. Water contents of hydrogels with different compositions. 169

Table S4.2. Comparison of reported tough hydrogels and ionic skins or e-skins with this work 175

List of Figures

Figure 1.1. Dynamic and reversible interactions involved in the construction of hydrogel networks. (a−e) reversible physical interactions and (f−i) dynamic covalent bonds..... 2

Figure 1.2. Schematic demonstration of the self-healing process of hydrogels. 14

Figure 1.3. Schematic representation of the network of nanocomposite hydrogels. 16

Figure 2.1. Synthesis routes of (a) 4-formylbenzoate ethyl methacrylate (FBEMA) and (b) P(MPC-co-FBEMA). 38

Figure 2.2. (a) Schematic of PMF-S hydrogel formed through Schiff base linkage between ASNP and P(MPC-co-FBEMA). (b) Oscillatory time sweep with PMF10-S 10-13 hydrogel formed in situ on the rheometer stage at 37 °C. (c, d) SEM images of the cross-section of the cryo-dried hydrogel..... 41

Figure 2.3. (a) PMF10-S 10-13 hydrogel injected from a 23-gauge needle. (b) Rheological steady flow sweep at 37 °C showing the relationship between viscosity and shear rate. (c-e) Photographs illustrating the self-healing property of PMF10-S 10-13 hydrogel, (c) two separate hydrogel pieces, (d) two pieces adhering to each other instantly when brought into contact, (e) the healed gel supporting its own weight. (f) Oscillatory strain sweep of PMF10-S 10-13 hydrogel followed by an oscillatory time sweep at a strain of 1% and 37 °C. (g) Strain-step test with strain altering between 1% and 200% for four cycles at 37 °C..... 43

Figure 2.4. Oscillatory rheological properties of hydrogels prepared from (a) 10 wt% PMF with different MPC:FBEMA molar ratio and 13 wt% ASNP, (b) different loadings of PMF10 and 13 wt% ASNP, and (c) 10 wt% PMF10 and different loadings of ASNP..... 45

Figure 2.5. (a) Rheological time sweeps (strain 1%, angular frequency 10 rad/s) showing

reversible gel−sol−gel transition of PMF10-S 10-13 hydrogel by changing pH, and (b) pictures showing the reversible gel−sol−gel transitions for two cycles. (c, d) Rheological characterization of the pH-dependent behavior of PMF10-S 10-13 hydrogel at 37 °C and strain of 1% by (c) oscillatory frequency sweeps, and (d) G' and G'' versus pH at 10 rad/s. (e) Zeta potentials of ASNP at pH varying from 4 to 8.5. (f) Swelling and hydrolytic degradation of PMF10-S 10-13 hydrogel in 10 mM PBS of various pH at 37 °C. Inserted picture was taken after 96 h of degradation. 48

Figure 2.6. (a) Cumulative release of model drug (i.e., congo red) from PMF10-S 10-13 hydrogel immersed in 10 mM PBS of various pH at 37 °C, and (b) Korsmeyer-Peppas fitting of the congo red release data. (c) Cumulative release of BSA-FITC from the hydrogel in 10 mM PBS of various pH at 37 °C. (d) Photographs showing the release of the two model molecules at the beginning and at the end (120 h) of the experiments. 51

Figure 2.7. Cell viability of HDFa cells after 24 h incubation with (a) various concentrations of mixtures of PMF10-S 10-13 hydrogel components, and (b) different dilution percentages of the 100% hydrogel extracts. 52

Figure 3.1. Synthesis routes of (a) aldehyde-modified F127 (F127-CHO) and (b) 2-aminoethyl acrylamide hydrochloride (AEAM). (c) Schematic illustration of the synthetic process, hierarchical network and dynamic interactions involved in the network construction of the hybrid PAAFC-L hydrogel. 66

Figure 3.2. Mechanical properties of the PAAFC-L hydrogel. (a) Stress-strain curves of hydrogels with different compositions. (b) Photographs showing a PAAFC-L hydrogel knot being stretched 10 times its original length. (c) Tensile loading/unloading cycles with various maximum strains for the composite hydrogel. (d) Compression-relaxation

cycles with maximum strain of 90%. (e) Images demonstrating a PAAFC-L bulk hydrogel withstood cutting and recovered instantly after release with no visible scar left. (f) Schematic of the proposed mechanism for the tensile and compressive elasticity of the PAAFC-L hydrogel. 70

Figure 3.3. Self-healing properties of the PAAFC-L hydrogel. (a) Rheological oscillatory strain sweep of the hybrid hydrogel (left) followed by oscillatory time sweep at a strain of 1% (right). (b) G′ and G″ of cyclic steps with shear strain shifting between 1% and 200%. (c) Optical demonstration of a healed hydrogel withstanding its own weight, bending and stretching. Scale bar: 1 cm. (d) Tensile stress-strain curves of hydrogel samples healing for different time. (e) Illuminance variation of an LED bulb during the hydrogel cut/healing process. The red rectangle indicates the healing zone of the hydrogel, and the scale bar is applied to all three images. (f) Time-dependent current change with the cutting and healing of PAAFC-L hydrogel for several cycles. 73

Figure 3.4. (a) Photographs showing the thermo-responsive optical property of PAAFC-L hydrogel. (b) Optical spectra in visible light range of the hydrogel at 10, 20 and 37 °C. (c) Transmittance change at 550 nm for PAAFC-L hydrogel with the increasing of temperature. (d) Images demonstrating the repeatability of the temperature-tunable transparency variation of PAAFC-L hydrogel shaped as “UA”. (e) DLS size characterizations of F127-CHO micelles at various temperatures ranging from 10 to 60 °C. AFM topography images of F127-CHO micelles prepared at (f) 20 °C and (g) 60 °C... 76

Figure 3.5. (a) Conductivities of hydrogels with different compositions. (b) Relative electric resistance change as a function of tensile strain for the PAAFC-L hydrogel. (c) Relative resistance response under repeated loading-unloading processes with maximum

strain of 100% for 100 cycles. (d) Cyclic relative resistance variations with maximum strain of 100, 200 and 500%. (e) Relative resistance changes as a function of pressure for the hydrogel. Insert figure showing the pressure sensitivity (S) of the hydrogel at different pressure ranges. 79

Figure 3.6. Real-time monitoring of human motions by the PAAFC-L hydrogel electronic sensor. (a) Schematic showing the sensing locations. Signals of relative electric resistance during (b) finger bending, (c) wrist bending, (d) handwriting, (e) elbow bending, (f) knee bending, (g) walking and running, (h) squatting, and (i) sitting..... 81

Figure 3.7. Real-time tracking of human subtle physiological signals by the PAAFC-L hydrogel electronic sensor. Time-dependent relative resistance variations during (a) swallowing, (b) speaking different phrases, (c) making expressions of frowning and astonishing, (d) smile and laugh, (e) breathing with the hydrogel sensor attached on the tummy, and (f) wrist pulse before and after exercise. Variations of wrist pulse patterns: (g) “moderate” pulse with unnoticeable tidal wave before exercise and (h) “taut” pulse with a high tidal peak after exercise. 83

Figure 3.8. (a) Scheme showing the experimental setup of the sleep monitoring experiment. (b) One-night relative resistance changes with time during sleeping. Left insert figure indicating the slow rolling or pendular eye movements during deep sleep. Middle insert figure showing the rapid and jerky eye movements during REM sleep. Right insert figure demonstrating head movement signals during light sleep. (c) Sleep record obtained from the mobile app “Sleep monitor”. 85

Figure 4.1. (a) Scheme showing the synthesis process of nanocomposite PAMAC-L hydrogels. (b) Schematic illustration of the binary ionic interactions in the hydrogel

network. (c) UV-Vis spectrum of the hydrogel in visible light range and an image showing the high transparency..... 98

Figure 4.2. Mechanical properties of the hydrogels. (a) Tensile stress-strain curves of PAM and PAMAC composite hydrogels with various ratios of MTAC to AEAM (MT:AE). (b) Average strength and toughness of PAM and PAMAC composite hydrogels with different cationic monomer ratios calculated from three stress-strain curves. (c) Tensile stress-strain curves of the nanocomposite hydrogel with LiCl concentrations ranging from 0 to 1000 mM. (d) Average strength and toughness of the hydrogels with different LiCl concentrations. (e) Images showing the PAMAC-L hydrogel before and during stretching. (f) Tensile stress-strain curves of the PAMAC-L gel subjected to successive loading/unloading cycles with maximum strain setting from 100−1500%. Tensile stress-strain curves for loading/unloading cycles with maximum strain of (g) 100% and (h) 1000%. (i) Images demonstrating the hydrogel withstanding damage by sharp materials like a blade and recover to its original shape. Compressing stress-strain curves for loading/unloading cycles with maximum strain of (j) 50% and (k) 90%. 102

Figure 4.3. Force measurements of the dual electrostatic interactions. (a) Schematic illustration of a typical AFM force measurement experiment. Topographic AFM images of (b) PAM-MT coating (RMS roughness ~ 0.874 nm) and (c) PAM-AE coating (RMS roughness ~ 0.583 nm) on mica surfaces. Interaction force profiles of a COOH-coated AFM tip and a PAM-MT-coated surface in PB solution (pH 7.4, 5 mM) containing (d) 0, (e) 50, and (f) 1000 mM LiCl, and (g) average adhesion forces for PAM-MT. Interaction force profiles of the COOH-coated AFM tip and a PAM-AE coating in PB solution

containing (h) 0, (i) 50, and (j) 1000 mM LiCl, and (k) the average adhesions calculated from force curves for PAM-AE. 105

Figure 4.4. Self-healing properties of the PAMAC-L hydrogel. (a) Images demonstrating a self-healed gel to withstand lifting, bending and stretching. Scale bar in all images is 1 cm. (b) Rheological oscillatory strain sweep followed by time sweep of the hydrogel. (c) Cyclic oscillatory time sweep with the shear strain shifting between 1% and 1000% for three cycles. (d) Photographs showing the illuminance variation of an LED bulb during the hydrogel's cutting-healing process. (e) Real-time current changes with the cutting and healing of the gel. 107

Figure 4.5. Electrical properties of the hydrogels. (a) Conductivities of different hydrogels. Relative resistance changes vs (b) tensile strain and (c) pressure for the PAMAC-L hydrogel. (d) Cyclic relative resistance responses under repeated tensile loading/unloading processes with maximum strain of 100, 200 and 500%. (e) Relative resistance variation with maximum strain of 100% for 100 cycles. (f) Relative resistance changes under cyclic pressure loading of 2.5, 5 and 12 kPa. (g) Relative resistance response under cyclic pressure of 5 kPa for 200 loading/unloading cycles. 109

Figure 4.6. Sensing performances of PAMAC-L hydrogel. Real-time monitoring (a) finger bending and (b) human wrist pulse before and after exercise using a hydrogel strain sensor. Real-time detection of (c) touch and pressing, and (d) water dropping by a hydrogel pressure sensor. 111

Figure 4.7. Writing recognition by PAMAC-L hydrogel. (a) Scheme showing the handwriting recognition procedure. Recognition results from the software for handwriting of the word (b) "letter" and (c) "hydrogel" on paper. (d) Word recognition accuracies for

these two words calculated from 10 writings of each word. Recognition results for writing of (e) “letter”, (f) “hydrogel”, (g) “ionic skin”, and (h) “how are you” by the tester’s forefinger in the air. (i)Average recognition accuracies for handwriting in air. For the recognition results shown below processed signals, the letters out of the parentheses are the input ones and in the parentheses are the output letters. Blue indicating right recognition and red indicating wrong recognition. 114

Figure S2.1. ^{1}H NMR spectra of (a) FBEMA, (b) PMF10 with CD_3OD as solvent and (b′) PMF10 with D_2O as solvent. 151

Figure S2.2. (a) DLS and (b) XPS results of ASNP. 152

Figure S2.3. Rheological frequency sweeps (1% strain and 37 °C) of (a) PMF10 (20 wt%) and ASNP (26 wt%) solutions, and (b) mixtures of pure polymer of 2-methacryloyloxyethyl phosphorylcholine (PMPC) and different concentrations of amine-modified silica nanoparticle (ASNP). The mixtures were denoted as PMPC-S x-y, where S represents ASNP, x and y are the weight percent of polymer and nanoparticles in the mixture, respectively. It is noted that the fluctuation of some of the data points in Figure S3 was due to the very low viscosities of the related samples and the measured torques were close to the detection limits (in the cone-plate geometry) of the instrument. 153

Figure S2.4. Injected bulk hydrogels of (a) PMF10-S 10-13, and (b) PMF5-S 10-13 through 23-gauge needles. 154

Figure S2.5. Rheological characterization of the pH dependent behavior of PMF5-S 10-13 hydrogel at 37 °C and strain of 1%. (a) Oscillatory frequency sweeps, and (b) G′ and G″ versus pH at 10 rad/s. 154

Figure S2.6. Fitting of BSA-FITC release data of first 24 hours according to Korsmeyer-

Peppas equation. Inset table shows the fitting parameters. 155

Figure S3.1. (a) ^{1}H NMR and (b) FTIR spectra of F127-CHO. 156

Figure S3.2. ^{1}H NMR spectrum of 2-aminoethyl acrylamide hydrochloride (AEAM). 157

Figure S3.3. Weight change of PAAFC hydrogel with LiCl, NaCl and without addition of ions under ambient condition (70−80 RH%, 20 °C). 158

Figure S3.4. (a) Toughness and (b) true stress of hydrogels with different compositions. 158

Figure S3.5. SEM images of the cross-sections of freeze-dried (a) PAM hydrogel, (b) PAAFC hydrogel, (c) and (d) PAAFC at higher magnifications. Red arrows indicating the MWCNTs. 159

Figure S3.6. Stress-strain curves of (a) PAAFC-L, PAM/MWCNT and P(AM-co-AEMA)/MWCNT hydrogels, (b) hydrogels with different concentrations of LiCl, (c) PAAFC-L hydrogels prepared at different pH, and (d) PAAFC-L hydrogels with various MWCNT concentrations. 160

Figure S3.7. Photographs showing the PAAFC-L hydrogel self-healing for 24 h (a) before and (b) during stretching. 161

Figure S3.8. DLS size characterization results of unmodified F127 micelles at various temperatures ranging from 10 to 60 °C. 161

Figure S3.9. (a) Rheological oscillatory temperature sweeps of PAAFC-L hydrogel at an angular frequency of 10 rad/s and a strain of 1%. (b) Stress-strains curves of PAAFC-L hydrogels healed at different temperatures. 162

Figure S3.10. Electrochemical impedance spectra of hydrogels of various compositions. 163

Figure S3.11. (a) Plot of gauge factor versus strain for PAAFC-L hydrogel calculated from the differentiation of the fitting curve of relative resistance change versus strain

experimental data. (b) Relative resistance change-tensile strain loading-unloading curves of PAAFC-L hydrogel. Dash line indicating the recovery process. 163

Figure S3.12. (a) Relative resistance variation as a function of compression strain for PAAFC-L hydrogel. (b) Relative resistance response of the PAAFC-L hydrogel under cyclic pressure loading of 3 kPa (compression strain of 10%) for 100 cycles. (c) Magnified signal during 80-90 cycles..... 164

Figure S3.13. Relative resistance changes of (a) slow and large eye movements, (b) rapid and small eye movements, and (c) head movements measured under awake state. (d) Relative resistance change curve showing the transition from deep to REM sleep. 165

Figure S4.1. (a) Synthetic route and (b) ^{1}H NMR spectrum of 2-aminoethyl acrylamide hydrochloride (AEAM)..... 168

Figure S4.2. SEM images of the cross-sections of freeze-dried PAMAC-L hydrogel at (a) lower magnification and (b) higher magnification. Red arrows indicating the MWCNTs. 168

Figure S4.3. (a) Tensile stress−strain curves and (b) Average strength and toughness of PAM, PAM-MT, PAM-AE hydrogels with or without MWCNTs. 169

Figure S4.4. (a) Tensile stress−strain curves and (b) Average strength and toughness of PAMAC hydrogels with various concentrations of MWCNTs. 170

Figure S4.5. (a) Zeta potentials of COOH-MWCNT, PAM-MT and PAM-AE. (b) Average zeta potentials calculated from three runs. 170

Figure S4.6. Topographic AFM images of bare mica..... 171

Figure S4.7. Electrochemical impedance spectra of hydrogels of different compositions. 171

Figure S4.8. Relative resistance changes for PAMAC-L hydrogel during a loading-unloading cycle for (a) 200% tensile strain and (b) 5 kPa pressure, and subjected to (c)

100 loading/unloading tensile cycles of 100% maximum strain, and (d) 200 loading/unloading compressing cycles of 5 kPa maximum pressure. 172

Figure S4.9. Waveform of a single wrist pulse before exercise. 172

Figure S4.10. (a) Representative current signals for writing English letters from “a” to “z” on paper. (b) Confusion matrix that validates the classifier performance of the trained model. Typical current−time curves of writing words (c) “letter” and (d) “hydrogel”. 173

Figure S4.11. (a) Representative current signals for writing English letters from “a” to “z” in air. (b) Confusion matrix that validates the classifier performance of the trained model. Typical current−time curves of writing words (c) “letter”, (d) “hydrogel”, (e) “ionic skin” and (f) “how are you”. 174

Abbreviations and Symbols

0D	zero-dimensional
1D	one-dimensional
2D	two- dimensional
3D	three-dimensional
PAM	polyacrylamide
PAA	polyacrylic acid
UPy	2-ureido-4[1H]-pyrimidinone
DDAA	donor-donor-acceptor-acceptor
PIC	polyion complexes
NaAMPS	2-acrylamido-2-methylpropanesulfonate
MPTC	3-(methacryloylamino) propyl-trimethylammonium chloride
NaSS	sodium p-styrenesulfonate
DMAEA-Q	acryloyloxethyltrimethylammonium chloride
PAH	poly(allylamine hydrochloride)
C18	stearyl methacrylate
SDS	sodium dodecyl sulfate
CTAB	cetyltrimethylammonium bromide
PEO-PPO-PEO	poly (ethylene oxide)-b-poly(propylene oxide)-b-poly(ethylene oxide)
PNIPAM	poly(N-isopropylacrylamide)
DMAA	N,N-dimethylacrylamide
MAA	methacrylic acid
PEG	poly(ethylene glycol)
CD	cyclodextrin

CB[n]	cucurbit[n]uril
PVA	poly(vinyl alcohol)
PBA	phenylboronic acid
NaCl	sodium chloride
LiCl	lithium chloride
DMF	N,N-dimethylformamide
$CaCO_3$	calcium carbonate
PEI	polyethyleneimine
$HAuCl_4$	chloroauric acid
$AgNO_3$	silver nitrate
Fe_3O_4	iron(II) iron(III) oxide
CNT	carbon nanotube
CNC	cellulose nanocrystal
GO	graphene oxide
PDA	polydopamine
PBS	phosphate-buffered saline
MWCNT	multiwalled carbon nanotube
F127	Pluronic® F127
MPC	2-methacryloyloxyethyl phosphorylcholine
FBEMA	4-formylbenzoate ethyl methacrylate
APTES	3-aminopropyl triethoxysilane
ASNP	APTES-modified silica nanoparticles (ASNP)
HDFa	human dermal fibroblast cell
HEMA	2-hydroxyethyl methacrylate

AIBN	2,2’-azobis (2-methylpropionitrile)
DCC	N,N’-dicyclohexylcarbodiimide
BSA-FITC	bovine serum albumin-fluorescein isothiocyanate conjugate
FB	4-Formylbenzoic acid
DMAP	4-dimethylaminopyridine
AEAM	2-aminoethyl acrylamide hydrochloride
F127-CHO	aldehyde-terminated PEO-PPO-PEO
AIBA	2,2'-azobis(isobutyramidine hydrochloride)
MTAC	2-methacryloyloxy ethyl trimethylammonium chloride
PMF	P(MPC-co-FBEMA)
HCl	hydrochloric acid
THF	tetrahydrofuran
$CHCl_3$	chloroform
CD_3OD	deuterated methanol
DMSO-d6	dimethyl sulfoxide-d6
D_2O	deuterium oxide
GPC	gel permeation chromatography
XPS	X-ray photoelectron spectrometer
DLS	dynamic light scattering
SEM	scanning electron microscope
UV-Vis	ultraviolet-visible
AFM	atomic force microscope
ECM	extracellular matrices
RES	reticuloendothelial system

DN	double-network
NC	nanocomposite
e-skin	electronic skin
LED	light-emitting diode
PSG	polysomnography
HWR	handwriting recognition
pKa	negative decadic logarithm of the acid dissociation constant
LCST	lower critical transition temperature
G'	storage modulus
G''	loss modulus
γ	oscillatory strain
ω	angular frequency
$OD_{570\ nm}$	optical density at 570 nm
M_t/M_∞	cumulative release fraction
PDI	polydispersity index
σ	conductivity
GF	gauge factor
Z	impedance
$\Delta R/R_0$	relative resistance change

CHAPTER 1 Introduction

1.1 Hydrogels Through Dynamic and Reversible Crosslinks

Hydrogels are water-swollen polymeric materials that maintain a distinct three-dimensional (3D) structure.[1-3] They have been widely used in biomedical applications including drug delivery, tissue engineering and wound healing owing to their high resemblance with biological tissues and extracellular matrices (ECM) by sharing common natures of water-abundant, soft and highly porous structures.[3-16] Also, hydrogels with some advanced features like conductivity and stretchability can serve as ideal candidates for soft electronics such as implantable bioelectronics, wearable sensory devices, artificial electronic skins, flexible touch panels, actuators and triboelectric generators.[17-26] In addition, the 3D network, porous structure and high water retention of hydrogels make them promising in environmental applications like wastewater treatment.[27-31]

Traditional hydrogels are crosslinked through permanent covalent bonds and are generally weak and brittle. Therefore, various dynamic and reversible interactions that can effectively dissipate energy upon force loading were introduced as crosslinks including reversible physical bonds (e.g., hydrogen bonding, electrostatic forces, hydrophobic interactions, metal-ligand coordination and host-guest interactions) and dynamic covalent chemistries (e.g., Schiff base or imines, boronate complexations, hydrazones, disulfide bonds), as shown in Figure 1.[32-37] Besides the mechanical performances, these interactions render the corresponding hydrogels with diverse functionalities such as stimuli responsiveness, self-healing capability and injectability,

which makes them to better fulfill the increasing demands of advanced and multifunctional modern materials.

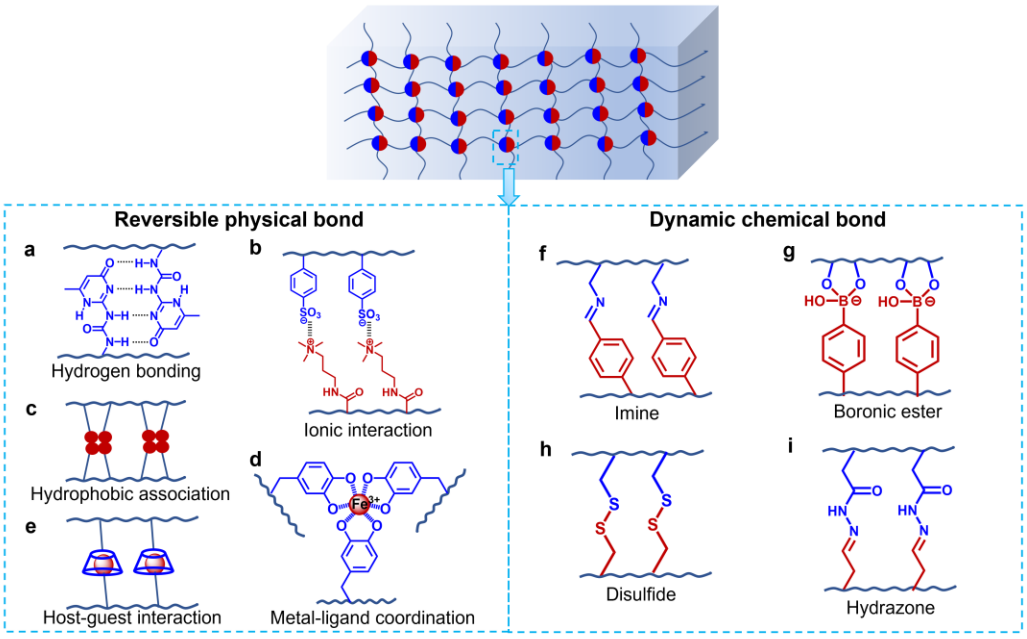

Figure 1.1. Dynamic and reversible interactions involved in the construction of hydrogel networks. (a−e) reversible physical interactions and (f−i) dynamic covalent bonds.

1.1.1 Physical Interactions in Hydrogel Networks

1.1.1.1 Hydrogen Bonding

Hydrogen bonding is a weak and reversible physical interaction that ubiquitously exist in biological systems. It has been widely adopted for the preparation of hydrogels. Some polymers like polyacrylamide (PAM) and polyacrylic acid (PAA) alone can generate hydrogels without the addition of crosslinkers through their multiple intermolecular hydrogen bonding. However, these gels undergo swelling and dissolution when immersed in water due to hydrogen bonds competitively formed with water

molecules. Inspired by the assembly behaviors of biological molecules (e.g., double-helical DNA and protein β-sheets), complementary multiple hydrogen bonds have been increasingly used in the self-assembly of supramolecular structures and materials.[38-40] Considering the insufficient stability of many multiple hydrogen bonds, Meijer and co-workers found that 2-ureido-4[1H]-pyrimidinone (UPy) could dimerize strongly (dimerization constant $K_{dim} > 10^6$ M^{-1} in $CHCl_3$) in a self-complementary DDAA (donor-donor-acceptor-acceptor) array of four cooperative hydrogen bonds (Figure 1a).[41] Prompted by this finding, they further use units of UPy as the associating end group in reversible self-assembling polymers.[42] The quadruple hydrogen bonding formed by UPy is reversible, strong, directional and thermo-responsive, which makes it widely used for the fabrication of hydrogels in recent years.[43-46]

1.1.1.2 Ionic Interactions

Ionic bonding refers to reversible electrostatic interactions between oppositely charged ions. Hydrogels via ionic crosslinks between certain combinations of polyelectrolytes and/or counter ions have been successfully prepared. A typical hydrogel category via ionic crosslinks is that formed between oppositely charged polyelectrolytes. Especially, benefiting from the various strength and lifetime of the ionic bonds formed by different pairs of polyelectrolytes, the mechanical properties of the resultant hydrogels can be tuned in a wide range. For example, Gong and co-workers[47] reported a class of polyion complexes (PIC) hydrogels, where two-step polymerization and water dialysis were involved for preparation. They found the PIC formed by anionic sodium 2-acrylamido-2-methylpropanesulfonate (NaAMPS) and cationic 3-(methacryloylamino) propyl-trimethylammonium chloride (MPTC) is soft and stretchable with a fracture stress

of 0.02 MPa and a breaking strain of 3500%, whereas another pair of polyions, i.e., sodium p-styrenesulfonate (NaSS) and acryloyloxethyltrimethylammonium chloride (DMAEA-Q), resulted in a strong and stiff gel with fracture stress to be 5.1 MPa and stretchability of 1180%. On the other hand, polyampholytes from one-step polymerization can also generate tough and strong hydrogels,[48] but with some drawbacks like random and uncontrollable charge sequence and globule conformation due to intrachain ionic bonds. Another type of hydrogels via ionic crosslinks is those constructed between polyelectrolyte and multivalent ions, such as poly(allylamine hydrochloride) (PAH) and phosphate or citrate.[49]

1.1.1.3 Hydrophobic Associations

Hydrophobic associations are easily formed from the aggregation of hydrophobic moieties or hydrophobes in aqueous media and can quickly reform when disturbed.[50] Micelle crosslinking is a common strategy to incorporate hydrophobic structures into hydrogel networks. Large hydrophobes like stearyl methacrylate (C18) can be solubilized into surfactant micelles such as sodium dodecyl sulfate (SDS) and cetyltrimethylammonium bromide (CTAB) by the addition of salt. Subsequent micelle copolymerization with hydrophilic monomers like AM and AA led to hydrogels with good mechanical performances.[51, 52] Copolymers that can intrinsically form micellar structures have also been incorporated in the hydrogel networks to prepare functional materials. For example, poly (ethylene oxide)-b-poly(propylene oxide)-b-poly(ethylene oxide) (PEO-PPO-PEO) triblock copolymers have been incorporated to fabricate thermo-responsive and elastic hydrogels for biomedical applications.[53, 54] Besides acting as reversible and strong crosslinks, hydrophobic associations provide essential protection to

other crosslinking mechanisms especially hydrogen bonding that is susceptible to water, giving rise to high-performing hydrogels. For example, Zeng and coworkers reported a hydrogel with excellent self-healing capability by entrapping catechol binary hydrogen bonding in the hydrophobic poly(N-isopropylacrylamide) (PNIPAM) microdomains to protect it from environmental oxidation.[55] In another research, an extremely stretchable and fast self-healing hydrogel was prepared by embedding UPy motifs in the SDS micelle.[56] Also, tough and strong hydrogels were generated through weak hydrogen bonding between N,N-dimethylacrylamide (DMAA) and methacrylic acid (MAA) due to polymer-rich aggregates stabilized by hydrophobic interactions among α-methyl groups of PMAA.[57]

1.1.1.4 Metal-Ligand Coordination

Metal-ligand coordination is a dynamic and reversible interaction between a metal ion and a ligand (electron doner), resulting in the formation of complexes of a preferred coordination geometry.[50] By incorporating different metal ions and ligands, hydrogels with various mechanical properties and functionalities have been prepared. For instance, Messersmith and coworkers developed a self-healing hydrogel based on catechol-Fe^{3+} interpolymer cross-linking between catechol-terminated 4-arm poly(ethylene glycol) (PEG) and ferric ions in $FeCl_3$ solution.[58] The hydrogel demonstrated pH-mediated gelation behavior, i.e., being a fluid at acidic condition (pH ~5), forming a sticky gel at pH~8 and turning into an elastomeric gel at basic pH of 12, which was attributed to the stoichiometric transitions of the catechol-Fe^{3+} complexes at different pH (monospecies at pH < 5.6, bis- at 5.6 <pH < 9.1, and tris- at pH > 9.1). Hydrogels based on dynamic Ca^{2+}-bisphosphonate coordination have been reported to form under physiologic neutral conditions and used in tissue engineering.[59] Tough hydrogels have also been fabricated

by incorporating metal-ligand complexation between Ca^{2+} and carboxyl groups on alginate chain as reversible sacrificial bond to dissipate energy.[60]

1.1.1.5 Host-Guest Interactions

Host-guest interaction is a commonly exploited physical interaction in supramolecular chemistry, where a unique complementary inclusion structure is formed via the insertion of one chemical entity (the "guest") into another chemical entity (the "host").[50, 61] The inclusion process is spontaneous and driven by forces like geometric compatibility, hydrogen bonding, hydrophobic, electrostatic and van der Waals interactions.[61] Due to their unique cavity structure, macrocycles especially cavitands (including cyclodextrins (CDs), calixarenes and cucurbit[n]urils (CB[n]s)) are frequently used "host" in aqueous solutions, and also in hydrogel preparations. Among the CDs, α-, β-, and γ-CD with increased cavity have been extensively studied. α-CD is able to form inclusion complexes with PEG and thus has been widely reported for the construction of hydrogels with PEG or copolymers containing PEG segments.[62-64] The gels formed are usually thixotropic and reversible. β-CD with larger cavity has been widely reported to form hydrogel with a variety of guest moieties including adamantane,[65] azobenzene,[66] ferrocene,[67] and cholesterol[68]. CB[n]s, which exhibit higher binding strength and large cavity compared to CDs,[69, 70] have also been exploited in hydrogel network construction. For example, Scherman and coworkers developed a hydrogel based on CB[8] host–guest complexes with two 1-benzyl-3-vinylimidazolium guest groups inserting into one CB[8] molecular.[71] Owing to the reversible dissociation/reformation of the host-guest interaction, the gel demonstrated excellent elasticity (complete recovery from 800% tensile strain in 2 min).

1.1.2 Dynamic Chemical Bonding in Hydrogel Networks

1.1.2.1 Schiff base

Imine bond (−N═CH−) is a dynamic chemical bond formed from the condensation reaction between aldehydes and primary amines. The imine formation reaction was discovered by Schiff[72] in 1864, and thereby imines are also referred to as Schiff bases. Hydrolysis of the Schiff base will take place under acidic conditions.[73-75] The bond is reversible and dynamic under mildly acidic to slightly basic conditions due to the imine hydrolysis/reformation reaction reaching a dynamic equilibrium and the rapid imine exchange reaction occurred under such conditions.[36, 74, 76] Owing to their ready formation and dynamic nature under neutral conditions, and stimuli-responsive properties, Schiff base bonds have been extensively adopted in the fabrication of functional self-healing hydrogels. Hydrogels based on natural macromolecules bearing primary amino groups like chitosan[53, 77-81] and gelation[82, 83] crosslinked by aldehydes like oxidized polysaccharide[80, 82] and synthetic benzaldehyde-modified difunctional PEG[77-79] have been widely reported, and applied in various biomedical applications like wound healing,[53, 81] drug or cell delivery,[79, 83] and central nervous regeneration[78].

1.1.2.2 Boronic ester

Boronic ester bond is another dynamic covalent bond that has been widely used in the preparation of hydrogels. Boronate esters are generated by the condensation of boronic acid compounds and 1,2-/1,3-diols. The hydrogel networks formed by this type of bonds are considered to be transient due to the reversible hydrolysis and reformation of the boronic acid–diol complexes under certain conditions.[84] The gelation of boronic ester-based hydrogels are closely related to the pH of the system, i.e., the boronic ester

formation is favored at the pH near or higher than the pKa of boronic acids.[85-88] Deuel et al. reported the first borate-diol crosslinked hydrogel upon mixing borax and poly(vinyl alcohol) (PVA) around seven decades ago.[89] Until now, numerous boronic ester-based hydrogels have been developed through the reactions between borax[90-92] or phenylboronic acids (PBAs)-functionalized polymers[88, 93-95] and different diols (e.g., PVA,[91, 96] sugar moieties-modified polymers or glycopolymers,[97, 98] catechol-containing polymers[87, 88, 99]). One challenge for the fabrication of hydrogels via boronic acid–diol complexation is the gelation normally occurred under alkaline conditions, which may impede their further use in biomedical applications. Tremendous efforts have been dedicated to address this issue with several strategies developed: using diols with high affinity for boronic acid at lower pH like salicylhydroxamic acid moiety;[93] making use of PBAs with intramolecular coordination to stabilize the boronate ester formation such as 2-acrylamidophenylboronic acid;[87] using PBA derivatives with lower pKa like benzoxaborole with pKa value ~7.2;[88] increasing the pH of the microenvironment around the boronic acid by copolymerizing PBA-modified monomers with N,N-dimethylaminopropyl acrylamide[100].

1.1.2.3 Disulfide

Disulfide bond is a biologically relevant bond involved in multiple biological processes such as the folding of proteins and maintenance of intracellular redox potential. The bond is reversible and dynamic because of the rapid disulfide exchange reaction. The disulfide exchange occurs either through nucleophilic displacement of a thiolate anion from the disulfide by another thiolate anion, or displacement of a thiyl radical from the disulfide by another thiyl radical. This reaction is highly pH dependent, lowering pH to acidic values giving rise to kinetically locked S-S bonds due to the protonation of

thiolates. The disulfide bond is cleavable under reductive conditions and can be reformed on oxidation. Light stimulus can also lead to the cleavage of the S-S bond by creating sulfur radicals that can exchange and recombine. The dynamic and multi-stimuli sensitive nature make the disulfide bond well suited for preparation of dynamic hydrogels with self-healing and stimuli-responsive properties. Small molecular crosslinkers containing disulfide bond have been widely used for the preparation of dynamic disulfide exchange-based hydrogels.[101-103] Cyclic disulfides, which have higher reactivity compared to linear disulfides due to the ring tension, have been utilized to prepare disulfide exchange-based hydrogels with structurally dynamic networks and self-healing properties under neutral conditions.[104-106] By introducing gold(I) ions to form gold(I)−thiolate (Au−S) species, disulfide-based hydrogels that show dynamic networks under neutral conditions have also been developed.[107-109]

1.1.2.4 Hydrazone

Hydrazone bond is formed from the condensation reaction between an aldehyde or a ketone and a hydrazide (R-$NHNH_2$). It forms very slowly under neutral conditions without catalyst, while its formation can be greatly accelerated under mildly acidic conditions or by nucleophilic catalyst such as aniline.[102] Harsh acidic conditions can cause the decomposition of this bond. Hydrazone hydrolysis and exchange occur rapidly at acidic pH values, at high temperatures, or under catalyzation, which renders the bond with reversibility and dynamic nature under these conditions, whereas it tends to be kinetically inert under neutral conditions. Hydrazones have been widely used as dynamic crosslinks in hydrogels, where, in most cases, acryhydrazone crosslinks are adopted. This is because the electron-withdrawing acryl group increases the electrophilicity of the acryhydrazone and therefore accelerates the hydrolysis and exchange reactions and

makes the bond more dynamic. Natural polysaccharides like hyaluronic acid,[110-112] carboxyethyl cellulose,[113] and alginate,[80, 114, 115] and synthetic polymers including PEG[116-118] and PNIPAM[119, 120] have been involved for the preparation of hydrazone-crosslinked hydrogels.

1.2 Stimuli-Responsive and Self-healing Functions

1.2.1 Stimuli-Responsiveness

1.2.1.1 Thermo Responsiveness

Thermo-responsive hydrogels are the hydrogels that undergo property changes including sol-gel transition, appearance change, mechanical property alternation and/or volume variation under thermo stimulus. Thermo-triggered sol-gel transition is an appealing feature for hydrogels in various applications, which renders the gels with injectability and shape remoldability. For example, hydrogels that were solution at low temperatures whereas turned into freestanding gels at body temperature have been developed based on the temperature-sensitive hydrophobic association of polymers with lower critical transition temperature (LCST) like PNIPAM or PEG copolymers as crosslinkers.[55, 121] These hydrogels are promising injectable carriers of bioactive molecules like drugs, proteins and DNAs that allow non-invasive administration for controlled drug delivery. Besides hydrophobic interaction, hydrogen bonding is known to be temperature-responsive, raising temperature would result in its dissociation. By employing UPy as the major crosslinking strategy, Chen et al. have prepared a hydrogel that was an elastic gel at room temperature but transformed into a viscous liquid over 45 °C, which made it to be injectable and remoldable at elevated temperatures.[46]

For some hydrogels that involve multiple crosslinking mechanisms, if the major

crosslinking force is not thermo-responsive, the corresponding hydrogels would undergo physical appearance, mechanical and/or volume changes instead of sol-gel transition. PNIPAM-containing hydrogels can be transparent at room temperature while turn into turbid at temperature higher than LCST.[122, 123] Hydrogels with fast and reversible whiteness changes are promising for thermo-responsive color displays, smart windows, and optical switches. Mechanical modulus variations of hydrogels triggered by temperature changes have also been widely reported. For instance, a micelle crosslinking hydrogel (C18/SDS) experienced a reversible 20-fold decrease in the elastic modulus with the temperature rising from 5 to 80 °C as a result of the increased solubility of hydrophobic moieties at high temperatures, which was demonstrated for shape memory applications.[51] Hydrogels showing thermo stimuli-triggered volume change especially asymmetric swelling have been reported to act as actuators using in micromanipulators, sensors and optical devices.[124]

1.2.1.2 pH responsiveness

pH is a common stimulus in nature. Especially, the pH varies in different parts or tissues in human body, which makes it possible to serve as an internal stimulus to trigger the release of drugs and thus the pH-responsive materials have been extensively reported in biomedical applications. One category of pH-sensitive hydrogels is that based on pH-sensitive polymers including acidic polymers (e.g., poly(carboxylic acid)s, poly(phosphoric acid)s and poly(boronic acid)s) and basic polymers (e.g., the polymers containing amine, tertiary amine, pyrrolidine, morpholino, imidazole, piperazine, and pyridine groups).[125] The pH transition of the gels derived from pH-sensitive polymers depends on the pKa of the corresponding polymers that determines their ionization/deionization behaviors. Among them, poly(carboxylic acid)s with pKa ~4−5 are widely used for pH-responsive hydrogel preparations due to their potential

applications in gastric environment. For example, a pH-responsive injectable hydrogel that can form a gel under pH 3 but decomposed at neutral pH has been developed by introducing a carboxyl-containing monomer, acryloyl-6-aminocaproic acid, into block copolymer chains.[126] By injection of the hydrogel to the gastric perforation site of a rat, local gelation was observed and the perforation healing process was enhanced.

Another kind of pH-sensitive hydrogels is that relies on the association/dissociation of crosslinking bonds. Hydrogels based on dynamic covalent bonds open up new opportunities for pH-responsive hydrogels. Almost all commonly exploited dynamic covalent bonds in hydrogels are sensitive to pH stimulus with the pH-responsive range highly depending on the reaction species. Schiff base-crosslinked hydrogels decompose in mildly acidic conditions and demonstrate reversible sol-gel transition triggered by pH stimulus.[54, 77] Hydrazone debonding occurs in a more acidic environment.[113] Boronic esters are unstable under acidic to slightly basic pHs based on the reacting boronic acid and diol species.[98] These interactions that demonstrate mildly acidic pH-responsive behaviors are attractive for the fabrication of hydrogels in biomedical applications for the treatment of regions showing local acidosis like tumors, wounds and infections.

1.2.1.3 Strain and Pressure Responsiveness

Due to the water abundant nature, many hydrogels are intrinsically conductive, which enables them to sense strain and pressure changes in electrical circuit. Soft hydrogel strain/pressure sensors hold great potential in various applications such as wearable devices, sport monitoring, health diagnosis, and soft robotics. Normally, the conductivity of hydrogels should be enhanced to fulfill the needs of practical sensory applications. There are two strategies that have been adopted for the enhancement of

hydrogels' conductivity and strain/pressure sensitivity. One is the incorporation of conductive fillers[127-129] (e.g., carbon nanotubes, graphene, MXene and silver nanowires), or intrinsic conductive polymers[46, 130] (e.g., polythiophene and polyaniline) to establish electronic conductive gels whose conductivity and strain/pressure sensitivity originate from moving electrons via tunneling effect and contact effect. Another is to introduce ions[21, 131] (e.g., NaCl and LiCl) into hydrogel matrixes or utilizing polyelectrolytes[132], which generates ionic conductive hydrogels. Their conductivity depends on the movement of ions in free water. The sensitivity to strains and pressures is ascribed to geometrical changes. Both strategies have their advantages and disadvantages. Electron-conductive hydrogels are generally in dark color while many ion-conductive gels are transparent. Losing water would lead to the increase of the conductivity of the former but decreased conductivity for the latter due to their different conducting mechanisms.[23] The electronic conductive gels commonly possess higher tensile strain sensitivity (gauge factor (GF) ~ 3−100) than that for ionic conductive hydrogels (GF ~ 1−3).[23] Since many conductive fillers are hydrophobic, relatively complicated chemical modification is needed to incorporate these materials into hydrogel networks whereas introduction of salt ions is a facile method to improve hydrogels' conductivity.

1.2.2 Self-Healing Property

Self-healing generally refers to a material's capability to spontaneously heal or mend fractures and defects, restoring their structures and functionalities after inflicted damage.[33, 34, 133] Self-healing is a common phenomenon in nature, such as bone fracture healing and blood vessel coalesce,[134] but rarely seen in traditional artificial materials because, in most cases, the building blocks of the materials are organized into rigid architectures which lack the ability to migrate across fractures longer than molecular

scale.[135] However, it is possible for macromolecular components in hydrogels based on reversible physical or dynamic chemical bonds to move across defects, reform bonds and repair fractures. Self-healing hydrogels have attracted considerable attention over the past decade. With self-healing ability, the lifetime of hydrogels can be greatly extended, and their reliability, durability and safety can be enhanced. Macroscopically, a hydrogel self-healed from cutting should be able to bond back to withstand its own weight, shaking, bending and/or stretching. Rheological test is another commonly employed method to characterize the self-recovery ability of hydrogel networks, in which the recovery of the internal damage caused by rheological deformation was reflected by a material's viscoelastic properties.

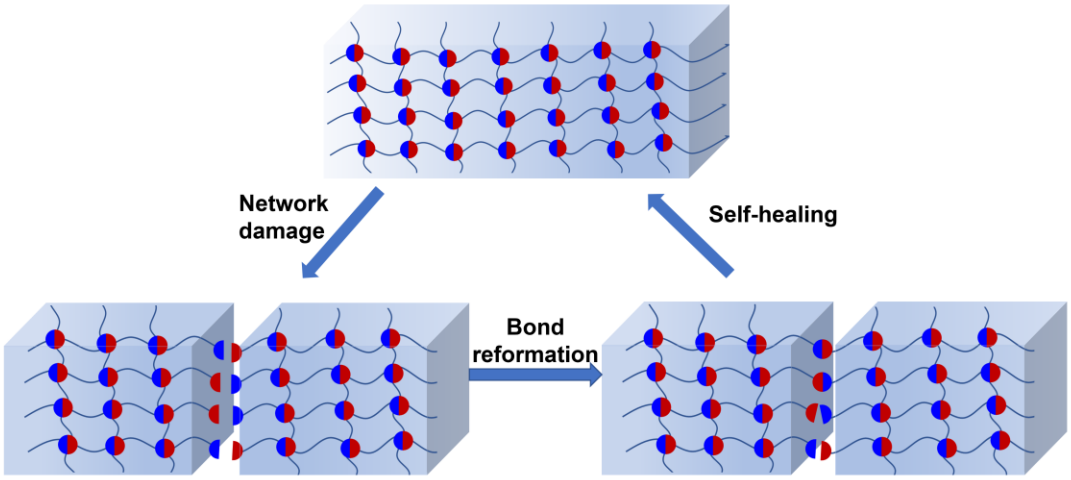

Figure 1.2. Schematic demonstration of the self-healing process of hydrogels.

Two factors play critical roles in determination of a hydrogel's self-healing capability, i.e., the reversibility of crosslinking bonds and the molecular chain mobility. Dynamic hydrogels crosslinked via transient linkages generally demonstrated complete self-healing ability with two gel halves merging into one piece after healing or a punched

hole disappearing.[77, 87, 108] Dynamic covalent interactions are common transient linkages, reversible formation/exchange reactions giving rise to the self-healing of corresponding hydrogels. However, the dynamic nature of the dynamic covalent linkages was only observed under certain conditions. Schiff base bond is reversible under mildly acidic to neutral pH but becomes permanent under basic conditions. Hydrogels based on boronate complexations demonstrated best self-healing ability at the pH near the boronic acid pKa under which the exchange between the boronic esters and the starting components is most effective.[85] Hydrazone and disulfide exchange reactions occur under acidic and basic conditions, respectively, both bonds tending to be kinetically locked under neutral conditions.[102] Physical interactions are generally considered to be reversible while the self-healing of the hydrogels based on these forces are also shown with limitations. For example, hydrogen bonding is generally reversible and dynamic, however, solvation of the bonds hindering the self-healing of relevant hydrogels. Protecting the hydrogen bonding with hydrophobic associations is an effective way to endow the corresponding hydrogel with good self-healing property.[56] For tough hydrogels in which the molecular chains are well-connected into 3D networks and thus have limited mobility, complete self-healing is relatively hard to achieve. Different approaches that can soften the hydrogels and enhance the chain movements across interfaces have been applied. For example, saline solution (3 M NaCl) was used to treat the cut surface of the hydrogel composed of oppositely charged polyelectrolytes, resulting in the self-healed hydrogel with ~2 MPa breaking stress and ~600% fracture strain.[47] For hydrogels involving hydrophobic associations, organic solvents like N,N-dimethylformamide (DMF) that can dissolve hydrophobic domains have been used to facilitate the self-repairing process.[136] In addition, treating the cut surface with surfactant is an effective way to enhance the healing efficiency of micelle crosslinking hydrogels.[51] Raising temperature is a common

strategy for the enhancement of the self-healing efficiency.

1.3 Nanocomposite Hydrogels

Nanocomposite (NC) hydrogels are hydrogels that incorporate nanomaterials into polymer/water matrixes, forming complex nanometer-scale structures.[137] The performances of the composite hydrogels are related to both the polymer matrix and the nanofillers. Taking advantage of the mechanical stiffness, various functionalities and large surface areas of nanomaterials, NC gels possess enhanced mechanical performances and functionalities, which makes them attractive for a wide range of applications. Depending on the miscibility of polymers/water and nanomaterials, different approaches have been adopted to fabricate NC gels such as direct mixing, *in situ* polymerization and *in situ* nanofiller formation.

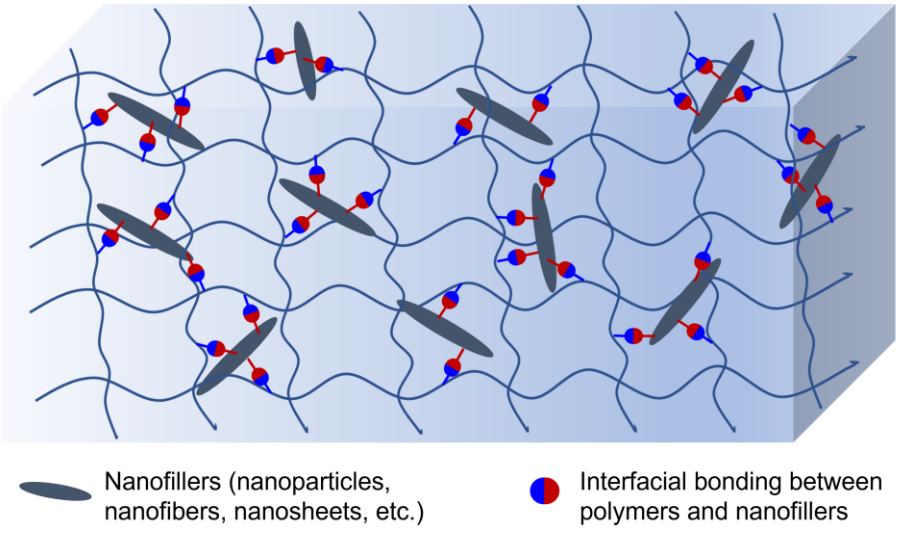

Figure 1.3. Schematic representation of the network of nanocomposite hydrogels.

1.3.1 Nanofillers

Nanomaterials are those of which at least one dimension is confined to nanoscale (<100 nm). They can be categorized into three main types based on their dimensions: zero-dimensional (0D) nanoparticles, one-dimensional (1D) nanofibers and two-dimensional (2D) nanosheets.[138]

1.3.1.1 Nanoparticles

The incorporation of nanoparticles can improve the mechanical performances of hydrogels. For instance, silica nanoparticle-crosslinked hydrogels have been developed with good stretchability and toughness by *in situ* copolymerizing vinyl-functionalized silica nanoparticles with hydrophilic monomers like AM and AA.[139-141] Quantum dots like carbon dots have been introduced into PAM gel networks through *in situ* polymerization, resulting in highly stretchable and elastic hybrid hydrogels.[142] The addition of high content of amorphous $CaCO_3$ nanoparticles into PAA/alginate hydrogels endowed the gels with robust yet compliable mechanical properties, which made them promising for the application as artificial ionic skins.[143] Besides, by introducing functional nanoparticles, hydrogels with various functionalities have been developed. For example, aldehyde-modified carbon dots have been prepared from different aldehyde precursors and mixed with branched polyethylenimine (PEI), producing imine-crosslinked self-healing hydrogels demonstrating fluorescence emissions of different colors.[144] Gold nanoparticles that can act as light absorbers for photothermal therapy have been incorporated into hydrogel networks by in-situ formation from chloroauric acid ($HAuCl_4$) and the resultant hydrogels were utilized for tumor treatment.[145] Similarly, silver nanoparticles were usually introduced into the gel networks via in-situ formation from precursor solutions like $AgNO_3$, to render the hydrogel with antibacterial property and/or conductivity.[146, 147] Magnetic hydrogels have been fabricated by incorporating

Fe_3O_4 nanoparticles, which can be used for tumor treatment though the heating effect induced by alternating current magnetic field.[148, 149]

1.3.1.2 Nanofibers

Nanofibers including nanowires, nanotubes and nanorods have been widely incorporated for the reinforcement of hydrogel networks or providing functionalities. Carbon nanotubes (CNTs), which consist of sp^2-connected carbon atoms and possess high aspect ratio (>1000), exceptional electrical (10^9 A cm^{-2}) and mechanical properties (tensile strength ~ 11–63 GPa, Young's modulus ~ 1–1.8 TPa),[150] have been widely utilized as nanofillers in nanocomposite hydrogels for bioengineering[151-154] and electrical[155, 156] applications. Since CNTs are hydrophobic, surface modification like oxidation to produce carboxy-bearing CNTs are commonly adopted strategy to enable their dispersion in water.[157] In order to avoid agglomeration of oxidized CNTs of high loadings, molecules like gelatin that can form interactions with the surface functional groups have been introduced.[156] Virgin CNTs can also be dispersed into hydrogels through involving hydrophobic associations such as adding surfactant[155] or π–π interactions like decorating with β-CD[158]. Silver nanowires are also commonly used nanofibrous fillers in hydrogels due to their excellent conductivity and bioactivity. They can be incorporated either through in-situ formation from $AgNO_3$[159] or post-treatment like dipping Ag nanowire solutions onto hydrogel surfaces followed by annealing[160]. Gold nanowires, with good conductivity, have also been utilized as conductive agent in composite hydrogel. For example, PAM hydrogels have been integrated with Au nanowires through in-situ polymerization and micropattern technology for wearable pressure sensors.[161] Cellulose nanocrystals (CNCs), strong and stiff rodlike nanomaterials extracted from natural cellulose resources, is a promising reinforcement agent for

hydrogels. They have been used for the reinforcement of hydrophilic polymers like PAA and PVA due to their good compatibility with these polymers.[162, 163] Owing to their excellent biocompatibility, they have also been incorporated with natural polymers for biomedical applications. For instance, by mixing aldehyde-functionalized CNCs with carboxymethyl chitosan, an injectable and self-healing hydrogel have been prepared for deep burn wound healing.[164] Additionally, the CNCs can also be employed as medium for the deposition of metal nanoparticles to facilitate their dispersion in the hydrogel matrix for electrical applications.[146]

1.3.1.3 Nanosheets

Clay nanosheets is a commonly utilized reinforcement agent in hydrogel systems. Haraguchi and coworkers reported the first clay-crosslinked tough hydrogel by *in situ* polymerization of NIPAM in exfoliated clay solutions. Compared to chemically crosslinked gel, the extensibility of the hydrogel dramatically increased from 10−30% to over 1000%.[165] In another example, Wang et al. reported a facile way of preparing clay-reinforced hydrogel with the storage modulus as high as ~400 kPa by directing mixing a positively charged dendrimer with anionic polyacrylate-exfoliated clay nanosheets.[166] Graphene oxide (GO) and reduced GO (rGO) nanosheets, 2D carbon nanomaterials with good water dispersion, high mechanical strength, conductivity (for rGO) and thermal conductivity, have been extensively used for the preparation of tough hydrogels[167, 168] and conductive hydrogels[169-171]. Mxene nanosheets, made of the carbides and nitrides of transition metals, are newly emerging 2D materials with excellent conductivity and water dispersion and thus have been utilized for the preparation of high-performance conductive hydrogels.[172-174]

1.3.2 Nanocomposites toward Tough Hydrogels

Traditional hydrogels crosslinked via permanent covalent bonds are brittle and weak mainly due to two reasons. First, conventional hydrogels, prepared by free radical polymerization of hydrophilic monomers and crosslinkers, generally have highly random or heterogeneous networks, which will cause stress localization upon loading and thereby easily fracture of the material.[175] Second, traditional hydrogels generally lack effective energy dissipation mechanisms when experiencing force loadings. Various strategies have been developed for the preparation of tough hydrogels (tensile strength > 0.1 MPa and fracture energy > 100 J/m^2) by improving network homogeneity like preparation of tetra-PEG hydrogels[176] and using γ-radiation for initiation,[177] or introducing energy dissipation mechanisms such as integration of reversible crosslinks,[47, 51, 178, 179] and by construction of double-networks (DN),[60, 136, 180] introduction of nanofillers,[165, 168, 181] and assembly of anisotropic structures[182-184]. Among these approaches toward tough hydrogels, the introduction of nanomaterials into hydrogel matrix can simultaneously lead to even distribution of stress by homogeneously dispersed nanofillers and introduce interfacial bonding to dissipate energy.

The mechanical robustness of NC hydrogels relies on the well dispersion of nanomaterials in hydrogel matrix and robust interfacial interactions between polymers and nanofillers. The dispersion of nanomaterials is related to various factors like their hydrophilicity, concentration, and the interaction with polymers. The interfacial bonding is of critical importance to the corresponding hydrogel's mechanical performance by providing effective energy dissipation, enabling forces transfer between soft polymers and stiff fillers, and avoiding the slide of nanomaterials within the matrix when subjected to external forces. Permanent chemical bonds as interfacial interactions between silica

nanoparticle surfaces and hydrophilic polymers (PAA and PAM) led to stretchable hydrogels with medium tensile strength ~100−300 kPa and stretchability ~1000−4000%, however, similar to covalently crosslinked hydrogels, elevating nanofiller content resulting in significantly impaired mechanical performance. Hydrogen bonding have also been introduced at the interfaces of polymers and nanomaterials. Due to the ubiquitously presented polar groups on nanomaterials with good water dispersion and hydrophilic polymers used for hydrogel preparation, hydrogen bonding widely exist at polymer/nanofiller interfaces. However, in many cases, it is not strong enough to generate tough hydrogels. Other interactions[156, 168] or special hydrogen bonding[169, 185] should be integrated. Polydopamine (PDA) surface coating is a facile strategy to introduce functional catechol groups on nanofiller surfaces that enable the hydrogen bonding with polymer matrixes as well as endow the material with self-healing and adhesive properties. For example, PDA-modified GO and clay have been incorporated with PAM to produce ultra-stretchable hydrogels (strain at break > 4000%, tensile strength ~50−200 kPa).[169, 185] Ionic interaction is a commonly utilized strong physical interaction between nanofillers and polymers. The brilliant mechanical property of the first tough NC gel, clay/PNIPAM, was attributed to the strong ionic interaction between clay nanosheets and the persulfate initiator.[186] In another example, the introduction of ionic forces and hydrogen bonding into interfaces between CNTs and polymers enabled well dispersion of high concentrations of the nanomaterials, and led to a tough hydrogel with high tensile strength of ~0.7 MPa.[156]

1.4 Objectives and Outline of this Thesis

Owing to the unique water abundant and biomimetic nature, hydrogel materials hold great promise to fulfill the diverse needs of modern biomedical and electrical engineering applications. Despite the great progress made in developing multifunctional hydrogels that are mechanically strong, stimuli-responsive and/or self-healing, challenges still exist to achieve highly performing hydrogels that mingle multiple functionalities to meet specific applications. The combination of reversible physical and chemical interactions with nanomaterial fillers opens up new opportunity for the development of multifunctional and tough hydrogels. The overall objective of this thesis is to develop novel NC hydrogels incorporated with reversible interfacial bonding, and use them in specific bioengineering and electrical applications like controlled drug delivery vehicles and flexible sensors. The research work in this thesis contains three parts. The first part (Chapter 2) is the development of ultra pH-sensitive hydrogels and the implication for controlled drug delivery. The second (Chapter 3) and third (Chapter 4) parts are the fabrications of hydrogel materials that combine mechanical, conductive, stimuli-responsive and self-healing properties for wearable sensory applications.

With the development of modern drug delivery systems, hydrogels that can be injected to the local site, self-heal to an integrated piece and release drugs on demand have attracted widespread attention in biomedical community. Hydrogels via dynamic covalent crosslinks like imines make it possible for local mildly acidic pH to trigger the release of carried drugs for the treatment of body regions showing acidosis like tumors, wounds and infections. Nevertheless, the fabrication of hydrogels with slightly acidic pH

responsiveness and narrow and adjustable pH-sensitive ranges still remains a challenge. In chapter 2, we presented a facile preparation of an injectable, self-healing and ultra pH-sensitive hydrogel by direct mixing an aldehyde-functionalized zwitterionic polymer and amine-modified silica nanoparticles. The gelation occurred rapidly in 10 s owning to the fast Schiff base formation between the components. The gel was not only injectable and self-healing, but also demonstrated sharp gel-sol transition located in the faintly acid environment (6.4−7.0) whilst kept stable in neutral PBS buffer. Moreover, a slight pH change of 0.2 in the responsive range led to significant variations of the hydrogel's rheological, dissolution and drug release behaviors.

Hydrogels, with soft, stretchable and conductive features, highly resemble the human skin, and thus are ideal for skin-like flexible sensors to provide comfort human-machine interaction experiences and avoid mechanical mismatch with tissues. Mechanical robustness, fatigue resistance and good conductivity are prerequisite for such applications. Other desirable properties are the self-healing capability, stimuli-responsiveness and transparency. In chapter 3, we report an ultra-elastic, tough, self-healing and ionic conductive hydrogel by simple one-pot polymerization of AM and an amine-bearing monomer in the presence of carboxyl-modified multiwalled carbon nanotubes (MWCNTs), aldehyde-modified F127 micelles and LiCl. In this composite, both the ionic interactions generated between the nanofillers and polymers and the imine bonds between micelles and polymers contribute to the mechanical performances and self-healing of the hydrogel. The elastic nature, recovery from ultra-high tensile and compressive strains, ensures the excellent fatigue resistance of the gel to fulfill the reliability and durability requirement of sensory applications. The gel is thermo-responsive, being turbid at room temperature while turning into transparent at body

temperature. The resultant hydrogel was used for the detection of large human motions, subtle physiological signals like wrist pulse and the monitoring of the human sleeping process with high sensitivity and stability.

In chapter 4, we designed a stretchable, tough, self-healing, transparent and ionic conductive hydrogel based on the dual ionic interactions between the carboxy-modified MWCNTs and functional cations of PAM copolymers. The strong and weak interfacial ionic interactions served as the long lifespan bond for crosslinking of the molecular chains and the sacrificial bond for energy dissipation upon force loading, respectively, which resulted in extremely stretchable (up to ~4000%), strong (up to ~1 MPa) and elastic hydrogels (recovery from 1000% tensile strain). Due to the low MWCNTs concentration, the hydrogel is transparent. It was used as a skin-like strain/pressure sensor for the detection of human motions and wrist pulse signals, as well as touching, pressing and water dropping. The high sensing performance of the gel for fine motions enabled it to be further used for the writing recognition process, with brilliant recognition rate from single letters to more complicated words and sentences.

Finally, in chapter 5, we outlined the conclusions and contributions of this work, and proposed some future research prospects.

CHAPTER 2 Injectable and Self-healing Nanocomposite Hydrogels with Ultra-sensitive pH-Responsiveness and Tunable Mechanical Properties: Implications for Controlled Drug Delivery

2.1 Introduction

In recent years, there has been growing research interest in the development of "smart" or stimuli-responsive drug delivery systems to meet complicated requirements in biomedical applications.[7, 187-191] Smart delivery vehicles are crucial for transporting therapeutic agents as they can help to achieve controlled release of the carried cargos, avoiding side effects of traditional pharmacotherapy techniques.[188, 192] _ENREF_6 Hydrogels, especially stimuli-responsive hydrogels, play an irreplaceable role in drug delivery technologies owing to their unique characteristics like water abundance, soft, high porosity, biocompatibility and high resemblance to ECM.[7-9, 189, 190, 193-196] They can retain the nature of the entrapped therapeutic factors like drugs, proteins, DNA and cells by providing biomimetic wet circumstances and protect these delicate bioactive molecules from undesirable enzymatic or hydrolytic degradation.[197, 198] In addition, compared to nano drug carriers like liposomes, nanoparticles and micelles that suffer from low delivery efficiencies because of quick clearance by human's renal and reticuloendothelial systems (RES), hydrogels can be directly located at the desired sites and realize localized, sustained and on-demand release of the therapeutics.[199-201] Up to now, enormous progress has been made in the development of controlled drug delivery systems based on smart hydrogels that are responsive to specific environmental changes (temperature, pH, magnetic field, electric field, etc.).[187, 190-192, 202-204] Among all the stimuli, since pH value varies in different parts or tissues in human body, it can serve as

an internal stimulus and has been widely exploited to trigger the release of drugs.[7, 205, 206] Traditional pH-responsive hydrogels composed of covalently crosslinked ionic polymers are well developed as drug delivery systems.[7, 205] However, they generally lack injectable and self-healing properties, which makes them face problems like invasive surgical implantation, improper adaption to the defect site, loss of structural integrity and functionality during frequent stress in human body, and increased risk of infections.[50, 123, 207] Another limitation of conventional pH-responsive hydrogels is that they are not suitable for the treatment of regions showing local acidosis such as sites of tumor, wound, infection and ischemia, where pH-sensitive behavior in mildly acidic range is required.[205]

To address these issues and meet the rapidly growing requirements of well-performed and multifunctional biomaterials, hydrogels crosslinked via dynamic covalent bonds,[36, 208] such as imines,[77, 78, 209-211] phenylboronate complexations,[97, 98] hydrazones[118, 212, 213] and disulfide bonds,[102, 104] have attracted widespread attention in biomedical community. Taking advantage of the dynamic, reversible and responsive to external stimuli natures of the dynamic covalent bonds, these hydrogels possess distinct features like self-healing capability, stimuli-responsiveness, shear-thinning property and injectability. They provide an approach to reliable and durable intelligent drug carriers with minimally invasive administration and improved tissue adaptability for localized therapeutic delivery. Among all the dynamic covalent linkages, imines, also known as Schiff bases, which are formed from the condensation reactions between aldehydes and primary amines, have become one of the most commonly used strategy for the fabrication of injectable and self-healing smart hydrogels owing to their readily formation under neutral conditions, outstanding neutral reversibility and pH-dependent stability.[77] Moreover, as imine structures generally decompose in mildly acidic environment,[75] they are attractive candidates for the construction of smart therapeutic delivery platforms to

treat areas of local acidosis. Although some Schiff base-crosslinked hydrogels have been developed as drug carriers for cancer therapy,[54, 214-220] wound healing[53, 219] and local infection treatment,[221] _ENREF_51 they are not able to satisfy the practical needs of the complicated biomedical processes. For example, it is known that the extracellular pH of tumors is mildly acidic due to exuberant production of lactic acid.[222, 223] For cancer therapy through localized drug delivery, the delivery system is required to show a sharp gel-sol transition under faintly acidic physiological conditions (pH 6.0-7.4) to release drugs in tumor microenvironment while maintain gel stability under normal physiological conditions to minimize drug release to surrounding normal tissues.[217, 218, 224] Besides, the degree of tumor acidity increases with the increase of tumor size and growth rate and has considerable variation within different regions of the same tumor.[222] To maximize the therapeutic efficiency, it is highly desired to develop a delivery system with drug release profile precisely regulated by a slight alteration of the local pH. However, the hydrogels reported previously, which are mostly composed of natural polymers (e.g., chitosan or its derivatives, oxidized polysaccharides) or aldehyde-modified PEG, are difficult to be precisely modified and thereafter lack of fine-tuned functionalities such as ultra-sensitive pH-responsiveness and gel stability under neutral physiological conditions. It is still a challenge for the design of synthetic polymeric hydrogels with good neutral stability, tunable and sensitive pH-responsive behaviors as well as injectable and self-healing properties for controlled drug release.

Herein, we report a novel injectable, self-healing and super-sensitive pH-responsive hydrogel based on Schiff base reaction between aldehyde-containing copolymers and amine-modified silica nanoparticles. The copolymer was synthesized through simple free radical polymerization of 2-methacryloyloxyethyl phosphorylcholine (MPC) and an aromatic aldehyde-functionalized monomer, 4-formylbenzoate ethyl

methacrylate (FBEMA). We chose MPC as one of the primary components of the hydrogel because of its cell membrane-mimic molecular structure, super hydrophilicity and excellent biocompatibility.[88, 97, 225, 226] 3-Aminopropyl triethoxysilane (APTES)-modified silica nanoparticles (ASNP) were utilized as another gelator since silica nanoparticles have been extensively investigated as drug delivery platforms and the involvement of nanoparticles in hydrogels has been reported as a facile approach to improve mechanical performances of hydrogels as well as to introduce multiple functionalities.[227-231] It is known that the pH range of Schiff base formation is closely related to the pKa of amines, since protonated amino groups ($-NH_3^+$) lack nucleophilicity to form imines with aldehydes.[73, 74] Amines with low pKa values like chitosan (pKa 6.2-7.0) could lead to corresponding hydrogels to be too stable under local acidosis conditions, i.e., pH-induced hydrogel degradation were only triggered at relatively strong acidic environment (pH<6)[204, 217]. On the other hand, imine-based hydrogels containing synthetic polyamines with high pKa values (pKa >9) like polyethyleneimine (PEI)[123], polylysines[216, 232] and hyperbranched poly(amido amine)[233] face problems like instability under neutral pH, slow or only gel formation under alkaline conditions (pH 8-8.5). Therefore, ASNP with moderate pKa around 7.6[234] is promising for the fabrication of hydrogels with pH responsiveness under mildly acidic conditions and maintenance of gel stability at neutral pH. The hybrid hydrogel was formed after a simple mixing process of the copolymer and nanoparticle solutions. It not only shows fast gelation process (<10 s), injectability, rapid self-healing capability, sharp gel-sol transition located in the faintly acid environment, but also exhibits excellent neutral stability and ultra-sensitive pH-responsive behavior. A slight pH change of 0.2 can cause significant shifts of the hydrogel's rheological, dissolution and drug release behaviors. By varying the composition of the hydrogel, its mechanical and pH-sensitive behaviors can also be

manipulated. In addition, the as-prepared hydrogel shows low cytotoxicity to human dermal fibroblast cells (HDFa). All these features suggest that the hydrogel has great potential in bioengineering applications such as therapeutic delivery vehicle for the treatment of local acidosis (e.g., tumors, wounds and infections).

2.2 Experimental Methods

2.2.1 Materials

2-Methacryloyloxyethyl phosphorylcholine (MPC, 97%), 2-hydroxyethyl methacrylate (HEMA, 97%), 2,2'-azobis (2-methylpropionitrile) (AIBN, 98%), APTES-functionalized silica nanoparticle dispersion in water (ASNP, <30 nm), N,N'-dicyclohexylcarbodiimide (DCC, 99%), congo red and bovine serum albumin-fluorescein isothiocyanate conjugate (BSA-FITC) were purchased from Sigma-Aldrich and used as received. 4-Formylbenzoic acid (FB, 98%), 4-dimethylaminopyridine (DMAP, 99%) and all solvents were purchased from Fisher Scientific.

2.2.2 FBEMA Synthesis

4-Formylbenzoic acid (FB, 2.25g, 0.015 mol), HEMA(1.95g, 0.015 mol) and DMAP (0.25g) were dissolved in 50 ml of dry tetrahydrofuran (THF), followed by the addition of DCC (4.0g, 0.019 mol) under a nitrogen atmosphere. The reaction system was stirred at room temperature for 48 h. The resulting mixture was first filtered to eliminate the white solid (dicyclohexylurea, DCU), and then precipitated in ethyl ether and filtered to remove other dissolved DCU. The obtained solution was concentrated under vacuum and passed through a silica gel column with hexane: ethyl ether 1: 1 as eluent to separate FBEMA from reactants and by-products. After dried in vacuum oven overnight, the product appeared to be a light-yellow liquid with a yield of 43%. Chemical structure of the monomer was confirmed by an Agilent 400-MR DD2 NMR spectrometer. ^{1}H NMR (DMSO-d6, 400 MHz): δ_H (ppm) = 10.08 (s, 1H, C<u>H</u>O), 8.11 (m, 2H, C<u>H</u>CHCCHO), 8.01 (m, 2H, C<u>H</u>CCHO), 6.00 (dq, 1H, C<u>H$_2$</u>C(CH$_3$)COO), 5.65 (p, 1H, C<u>H$_2$</u>C(CH$_3$)COO), 4.55 (m, 2H, C(CH$_3$)COOCH$_2$C<u>H$_2$</u>), 4.44 (m, 2H, C(CH$_3$)COOC<u>H$_2$</u>), 1.83(dd, 3H, CH$_2$C(C<u>H$_3$</u>)COO).

2.2.3 P(MPC-co-FBEMA) Synthesis

The random copolymers of MPC and FBEMA with various contents of FBEMA ranging from 0 to 20 wt% were synthesized through free radical polymerization using AIBN as an initiator. A typical process to synthesis copolymers with FBEMA feeding fraction of 10 mol% is as follows. MPC (1.0 g, 3.4 mmol), FBEMA (0.099 g, 0.38 mmol) and AIBN (0.0062 g, 0.038 mmol, 1 mol% relative to monomers) were dissolved in 10 ml of ethanol. After purged with nitrogen for 20 min, the mixture was allowed to stir at 60 ºC for 24 h. The P(MPC-co-FBEMA) copolymer (denoted as PMF) was precipitated

out by adding the resulting solution dropwise in THF (200 ml), collected by filtration, redissolved in ethanol (10 ml) and precipitated from THF again. The recovered product was then dried under vacuum overnight to yield a white polymer powder. ^{1}H NMR spectra of the copolymers were collected with CD_3OD as the solvent. The molecular weights and polydispersity indexes (PDIs) of copolymers were measured by gel permeation chromatography (GPC) on an Agilent Technologies 1200 series system in water.

2.2.4 Characterization of ASNP

The solid content of ASNP aqueous dispersion was measured by evaporating the dispersion in an oven at 60 ºC overnight and comparing the weights before and after the evaporation. Surface element analysis was done on a Kratos AXIS 165 X-ray photoelectron spectrometer (XPS). The size and PDI of ASNP were characterized by dynamic light scattering (DLS) with a Malvern Zetasizer Nano ZSP. The zeta potentials of ASNP at various pH were also measured on a Malvern Zetasizer with samples prepared by first dissolving 40 μl of ASNP dispersion in 4 ml deionized water followed by adjusting pH using 2 M tris buffer. The amino group content in the ASNP solution was detected through ninhydrin reaction.[235]

2.2.5 Preparation of Hydrogels

The P(MPC-co-FBEMA)-ASNP hydrogels with different compositions were prepared. The hydrogel samples were denoted as PMFx-S y-z, where PMF means the copolymer, S represents the amine-modified silica nanoparticle, x, y and z are the mole fraction of FBEMA in the copolymer, weight percent of copolymer in the hydrogel and weight percent of nanoparticles in the hydrogel, respectively. For a typical fabrication

procedure of PMF10-S 10-13 hydrogel, P(MPC-co-FBEMA) with 10 mol% of FBEMA was first dissolved in deionized water (20 wt%) under a short time of sonication. The pH of the ASNP dispersion (26 wt%) was adjusted to 7.4 using 2 M tris buffer. The polymer solution (100 μl) and nanoparticle dispersion (100 μl) were then mixed well by vortex to give the hydrogel final concentrations of polymer and nanoparticles to be 10 wt% and 13 wt%, respectively.

2.2.6 SEM Characterization

The porous morphology of the hydrogel was characterized using a Zeiss Sigma field emission scanning electron microscope (SEM) at an acceleration voltage of 5 kV. To prepare samples for imaging, 500 μl of hydrogel was cryo-dried and transferred into a liquid nitrogen bath. After 2 h, the frozen sample was taken out and fractured using a sharp blade. A thin layer of gold metal was sputter-coated on the freshly cut surface prior to imaging.

2.2.7 Rheological Tests

The hydrogel's gelation, mechanical, shear-thinning, self-healing and pH-responsive performances were studied through rheological tests on a TA Instruments AR-G2 stress-controlled rheometer. The measurements were conducted using a 20 mm (diameter) 2º cone geometry with a gap of 53 μm and analyzed using TA Instruments TRIOS software. The rheological behaviors of PMF10 copolymer solution (20 wt%), ASNP dispersion (26 wt%, pH 7.4), and mixtures of pure polymer of MPC and ASNP with different concentrations of the nanoparticles were investigated by oscillatory frequency sweeps from 0.1 to 100 rad/s with a constant strain of 1%. For all rheological measurements of hydrogels, the hydrogels were formed *in situ* on the rheometer stage by

adding 50 µl of ASNP dispersions and 50 µl of PMF polymer solutions to the center of the stage. Silicone oil was dropped outside of the hydrogel layer to protect it from possible moisture loss. Dynamic oscillatory time sweeps were performed at a constant angular frequency (ω) of 10 rad/s and a 1% strain amplitude (γ) to measure the gelation process. The hydrogel's shear-thinning property was evaluated by a steady flow sweep with shear rate varying from 1 to 100 1/s. The self-healing property of PMF10-S 10-13 hydrogel was quantitatively studied by an oscillatory strain amplitude sweep (γ from 1% to 200%) with fixed frequency (ω = 10 rad/s) followed by a dynamic time sweep with constant frequency and strain (ω = 10 rad/s, γ = 1%). Cyclic strain experiment was also conducted to examine the repeatability of the self-healing behavior. In the test, the strain was shifted between 1% and 200% for four cycles at a fixed frequency (ω = 10 rad/s).

To measure the pH responsiveness of PMF-S hydrogel, concentrated HCl solution (5 µL, 5 M) was first added to the hydrogel (100 µL) on the stage of the rheometer, after mixing by pre-shearing for around 20 s, rheological behavior of the mixture was recorded by oscillatory time sweep (ω 10 rad/s, γ 1%). After the measurement, concentrated tris solution (10 µL, 5 M) was added to the mixture to increase the pH and regenerate the hydrogel of which the rheological property was immediately recorded by oscillatory time sweep (ω 10 rad/s, γ 1%). The pH of the system was measured before each rheological test step. The reversible sol-gel transitions were also optically demonstrated in a vial by alternatively adding concentrated HCl (10 µL, 5 M) and tris solution (20 µL, 5 M) to a pre-formed hydrogel (200 µL) for two cycles. The rheological properties of hydrogels at different pH values were characterized by oscillatory frequency sweeps from 0.1 to 100 rad/s with constant strain of 1%, where hydrogel samples were formed by mixing ASNP solutions of pH values varying from 4 to 8.5 with copolymer solutions. All rheological

tests were conducted at 37 ºC.

2.2.8 The pH-Regulated Hydrogel Degradation and *In Vitro* Drug Release

For the pH-dependent hydrolytic degradation tests, PMF10-S 10-13 hydrogels were prepared at the bottom of 2 ml glass vials of which the weights (W_v) were recorded before experiments. Then the weights of hydrogel together with glass vial were measured and recorded as W_0. Afterwards, 10 mM PBS buffers (1.5 ml) with pH varying from 6.4 to 7.4 were added on top of the hydrogels and the set-ups were placed into a 37 ºC water bath. At predetermined time intervals, the buffers were carefully pipetted out, the remained hydrogels together with vials were weighed (W_t) and the buffers were put back into the vials again. The weight remaining ratio of hydrogels was thus calculated by the following equation:

$$Weight\ remaining\ ratio\ \% = \frac{W_t - W_v}{W_0 - W_v} \times 100\% \qquad (2.1)$$

In the *in vitro* drug release experiments, congo red and BSA-FITC were used as two model drugs. First, PMF10 copolymers were dissolved in the solutions of congo red (0.4 mg/ml) or BSA-FITC (4 mg/ml). Then the copolymers solutions (100 µl) with model drugs were mixed with equal volumes of ASNP dispersions to form drug-loaded PMF10-S 10-13 hydrogels. Similar to the degradation experiments, the hydrogels were immersed in PBS buffers (1.5 ml) with various pH values. After incubated in 37 ºC water bath for predetermined periods, 1 ml of the aqueous supernatant solutions were taken out for ultraviolet-visible (UV-Vis) analyses on a Thermo Evolution 300 UV-Vis spectroscopy and then put back into the vials after measurements. The absorbances at 510 nm and 495 nm were recorded for congo red and BSA-FITC samples, respectively. Samples of which the absorbances were defined as 100% were prepared by mixing 100 µl of copolymer solutions containing the dye or protein with 1.5 ml deionized water first and then adding

100 µl of ASNP dispersions to the mixtures. All experiments on pH-sensitive degradation and *in vitro* drug release were carried out in triplicate. The release data were fitted using the Korsmeyer-Peppas equation,

$$\frac{M_t}{M_\infty} = kt^n \qquad (2.2)$$

where M_t/M_∞ is the cumulative release fraction, k is a constant incorporating characteristics of the delivery system and the drug, and n indicates the transport mechanism.[236-238]

2.2.9 Cytotoxicity

The cytocompatibility of PMF10-S 10-13 hydrogel toward human primary dermal fibroblast cells (HDFa, ATCC® PCS-201-012™) was assessed by MTT assay. Both mixtures of gel components which were composed of PMF copolymer and ASNP solutions and PMF-S gel extracts were used for the tests. The mixtures of gel components were prepared by diluting a 30 mg/ml polymer/nanoparticle mixture solution (13 mg/ml copolymer, 17 mg/ml nanoparticle) to 2, 1, 0.5, 0.25 mg/mL using complete growth media composed of fibroblast basal media (ATCC® PCS-201-030™) and fibroblast growth kit-low serum (ATCC® PCS-201-041™). Hydrogel extract (100%) was obtained by adding 2 mL of complete growth media to 200 µL hydrogel and incubating in an incubator (37 °C, 5% CO_2) for 24 h, which was further diluted to 50%, 25% and 12.5% gel extracts. Fibroblast cells (100 µL cell suspension) were seeded into a 96-well plate at a density of 7800 cells/well. After incubated in the incubator (37 °C, 5% CO_2) for 24 h, the spent media were discarded and 100 µL of sample solution or control were added. The cells were then allowed to incubate for another 24 h. After that, the sample solutions were removed, and each well was washed with 100 µL Dulbecco's phosphate-buffered saline (DPBS) to remove residual samples before the addition of MTT solution (0.5

mg/mL in DPBS). After incubation of the plate at 37 °C for 4 h, MTT solutions were discarded and 100 μL of dimethyl sulfoxide was added to dissolve the MTT formazan. The optical density at 570 nm ($OD_{570\ nm}$) was measured using a microplate reader, and the cell viability was then calculated by comparing $OD_{570\ nm}$ of cells treated with/without mixtures of gel components or gel extracts.

2.3 Experimental Methods

2.3.1 Aldehyde-Functionalized Monomer Synthesis and Hydrogel Fabrication

An aromatic aldehyde-functionalized monomer FBEMA was synthesized through carbodiimide-catalyzed esterification of HEMA and 4-formylbenzoic acid as shown in **Figure 2.1a**. Its molecular structure was confirmed by ^{1}H NMR spectrum (**Figure S2.1a** in **Appendix A**). In the spectrum, the benzaldehyde functional group gave signals at 10.08 (h), 8.11 (f) and 8.01(g) ppm, and the peaks of carbon-carbon double bond appeared at 6.00 (b) and 5.65 (a) ppm. The integration ratios of all the characteristic peaks showed good consistency with the theoretical values, indicating the successful synthesis of the FBEMA monomer. Then, a series of random copolymers consisting of MPC and FBEMA with the feed fraction of the latter monomer ranging from 0 to 20 mol% were synthesized through facile and efficient free radical polymerization. (**Figure 2.1b**) NMR and GPC were employed to investigate the structures of the corresponding P(MPC-co-FBEMA) statistical copolymers (denoted as PMF), and their characteristics were summarized in **Table 2.1**. ^{1}H NMR spectrum reveals the coexistence of the two monomers (**Figure S2.1b** and **b′** in **Appendix A**), where the actual FBEMA molar contents in the products were determined from the integral values of the characteristic signals. The desired copolymer compositions were easily obtained as suggested by the close feed and actual molar ratios of the aldehyde moiety.

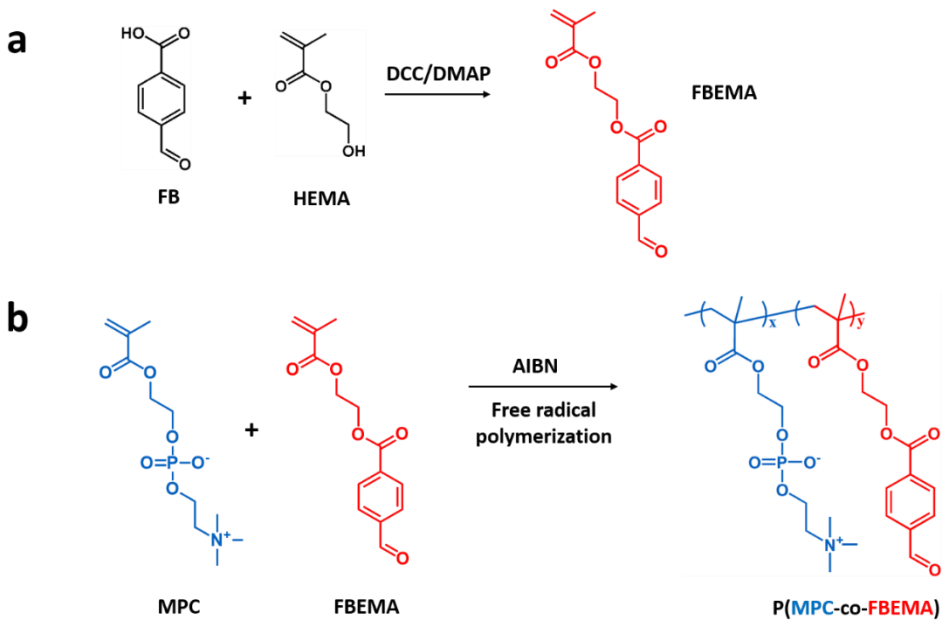

Figure 2.1. Synthesis routes of (a) 4-formylbenzoate ethyl methacrylate (FBEMA) and (b) P(MPC-co-FBEMA).

Table 2.1. Characteristics of synthesized P(MPC-co-FBEMA) random copolymers determined by ^{1}H NMR and GPC.

Polymer[a]	FBMA content (mol%)		Mn (g/mol)	PDI
	Feed	Product		Mw/Mn
PMF 2	2	1.7	1.404×10^{5}	1.695
PMF 5	5	3.9	1.611×10^{5}	1.916
PMF 10	10	9.2	1.310×10^{5}	1.663
PMF 20	20	18.6	2.567×10^{5}	1.373

[a] For polymer PMF x, PMF represents the P(MPC-co-FBMA) copolymer and x is the feed molar fraction of FBEMA.

Nanoparticles were exploited to act as crosslinkers in the hybrid hydrogels. Since their size would exert profound influence on the hydrogel formation, where very big particles tend to result in the failure of polymer bridging of multiple nanoparticles,[227] the ASNP used was relatively small with a z-average diameter around 22 nm and a PDI of 0.18, as indicated by DLS results (**Figure S2.2a**). XPS was utilized to verify the existence of amino groups on the surface of silica nanoparticles, and as shown in **Figure S2.2b** in **Appendix A**, the characteristic signal of N 1s can be clearly distinguished at 399.6 eV. The $–NH_2$ concentration in the ASNP solution (26 wt%) was quantitatively determined to be 0.17 M by ninhydrin reaction.

Hydrogels were generated through a simple mixing process of PMF solutions and ASNP aqueous dispersions. In this work, gel PMF10-S 10-13 (10 mol% of FBEMA in copolymer, 10 wt% of PMF and 13 wt% of ASNP) with the molar ratio of the amino group to the aldehyde group in the final nanocomposite hydrogel of 2:1 was used for all characterizations unless otherwise noted. As illustrated by pictures in **Figure 2.2a** and rheological results in **Figure S2.3a** in **Appendix A**, each solution of PMF or ASNP before mixing appeared to be a low-viscous liquid. The low viscosity of ASNP dispersion of high solid content is attributed to the electrostatic repulsion of the abundant protonated amino groups on the surface of the silica, which avoids their coalescence and further gelation. However, upon blending and agitation of these two components, the mixture lost its mobility and became a freestanding hydrogel within 10 s (from vial inversion test) under neutral pH at room temperature (**Figure 2.2a**). The gelation process was further monitored by rheological oscillatory time sweep (**Figure 2.2b**). With two precursor solutions successively mounted on the rheometer stage, a hydrogel formed *in situ* immediately, where the shear storage modulus (G') surpassed the loss modulus (G'') at

the beginning of the test, signifying a gel-like behavior, and then slowly grew from 1440 to 1568 Pa in 300 s. In contrast, the mixtures of pure polymer of MPC and ASNP appeared to be low-viscous liquids as indicated by the rheological results in **Figure S2.3b** in **Appendix A**. Therefore, the rapid hydrogel formation of PMF-S is induced by the fast Schiff base reaction between aromatic aldehyde groups on copolymers and multiple easy-accessible amino groups on the surface of ASNPs, enabling instant and efficient bridging of nanoparticles by polymer chains to construct the hydrogel network. SEM images in **Figure 2.2c** and **2.2d** display the morphology of the cross-section of the cryo-dried hydrogel sample. The hybrid hydrogel exhibits a uniformly porous structure, and closely packed nanoparticles can be clearly observed at high magnification showing diameters around tens of nanometers.

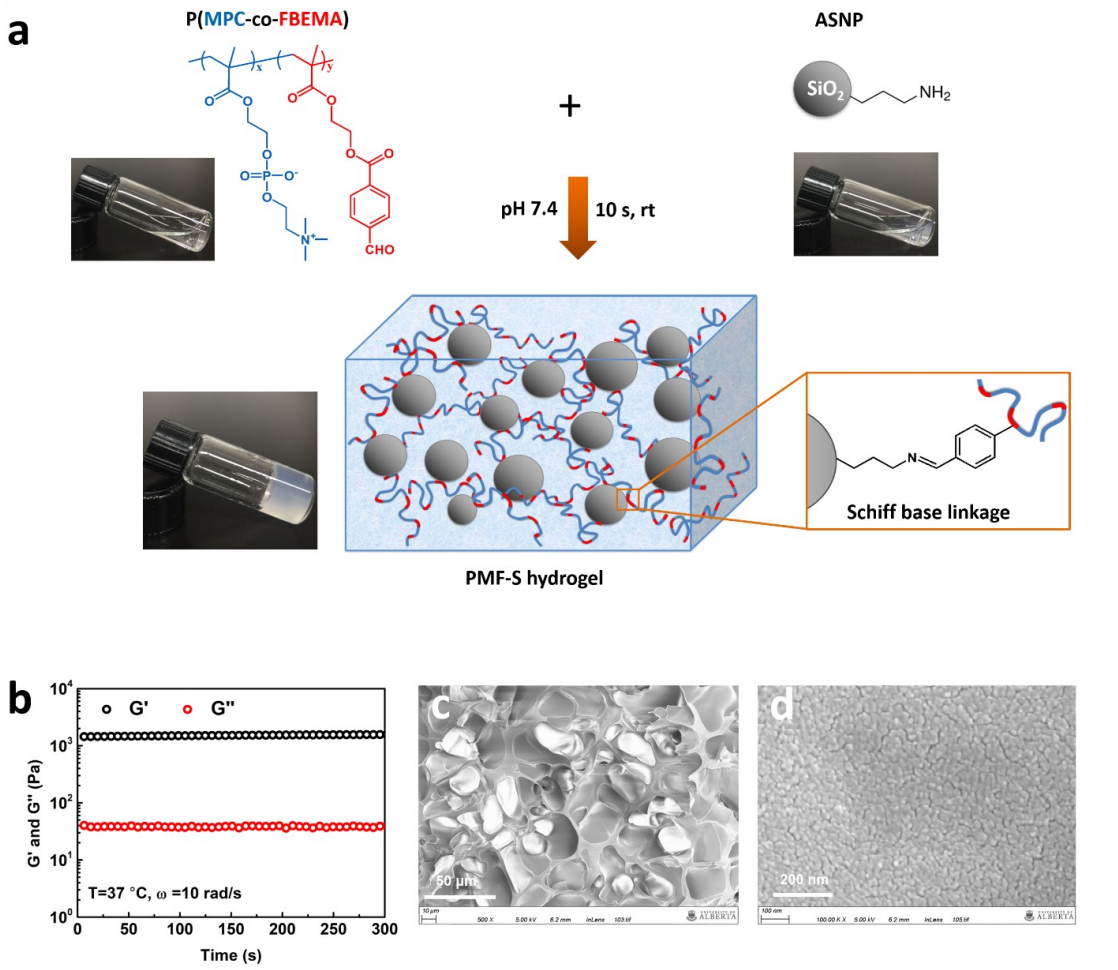

Figure 2.2. (a) Schematic of PMF-S hydrogel formed through Schiff base linkage between ASNP and P(MPC-co-FBEMA). (b) Oscillatory time sweep with PMF10-S 10-13 hydrogel formed in situ on the rheometer stage at 37 °C. (c, d) SEM images of the cross-section of the cryo-dried hydrogel.

2.3.2 Injectability and Self-Healing Property

Injectability is essential in biomedical applications for minimally invasive and localized administration of therapeutic hydrogels. It requires the hydrogel to show viscous flow under shear stress and a rapid recovery when the stress is relaxed.[239] Generally, the viscosity (η) under high shear rate (~100 1/s) should not be higher than 1

Pa·s for convenient injection of the hydrogel through high gauge needles.[227] In our experiments, the PMF-S hydrogel generated upon mixing the polymer and nanoparticle solutions in the syringe could be freely extruded to write letters such as "UA" (**Figure 2.3a**) or to form a bulk gel (**Figure S2.4a** in **Appendix A**) through 23-gauge needles without clogging. This good injectability is attributed to the shear-thinning property of the dynamic imine-crosslinked hydrogel. As demonstrated by the rheological steady flow sweep in **Figure 2.3b**, the hydrogel's viscosity dropped below 1 Pa·s as soon as the shear rate reached 50 1/s and it ended up with 0.6 Pa·s at 100 1/s.

Self-healing property is not only a prerequisite for the recovery of a hydrogel after injection, but also beneficial to a drug-loaded hydrogel to autonomously heal fractures and avoid any possible leakage of loading cargo after inflicted damage in the body.[240] The self-healing process of PMF-S hydrogel is exhibited in **Figure 2.3c, 2.3d** and **2.3e**. When two pieces of a cracked hydrogel were brought into contact, dynamic Schiff base interaction was instantly generated at the contact area, and the adhesion between the two fragments was strong enough to integrate the pieces into a free-standing hydrogel. Oscillatory strain sweep was conducted to further reveal the hydrogel's strain-dependent rheological property and its self-healing ability. In **Figure 2.3f**, G' remained greater than G'' in a broad strain region from 1% to 117%, indicating the PMF-S hydrogel could withstand relatively large deformation. After the strain reached the crossover of G' and G'' (117%), severe dislocation between molecular chains and ASNP occurred and the hydrogel network started to rupture, leading to a quasi-liquid state of the material. Once the stress was relaxed and the strain amplitude reverted to 1%, the material's mechanical property recovered immediately with G' and G'' returning to their original states, manifesting the fast and complete self-healing process of the PMF-S hydrogel. Moreover, the healing process is repeatable, as presented by the step-strain measurement in **Figure**

2.3g, in which the hydrogel was first destroyed at a high magnitude strain of 200%, followed by the reformation at a low magnitude strain of 1%. Both G' and G'' were able to recover their initial values even after several cycles of network breakage and reconstruction, suggesting the reversible and robust nature of the applied Schiff base linkages in PMF-S hydrogel.

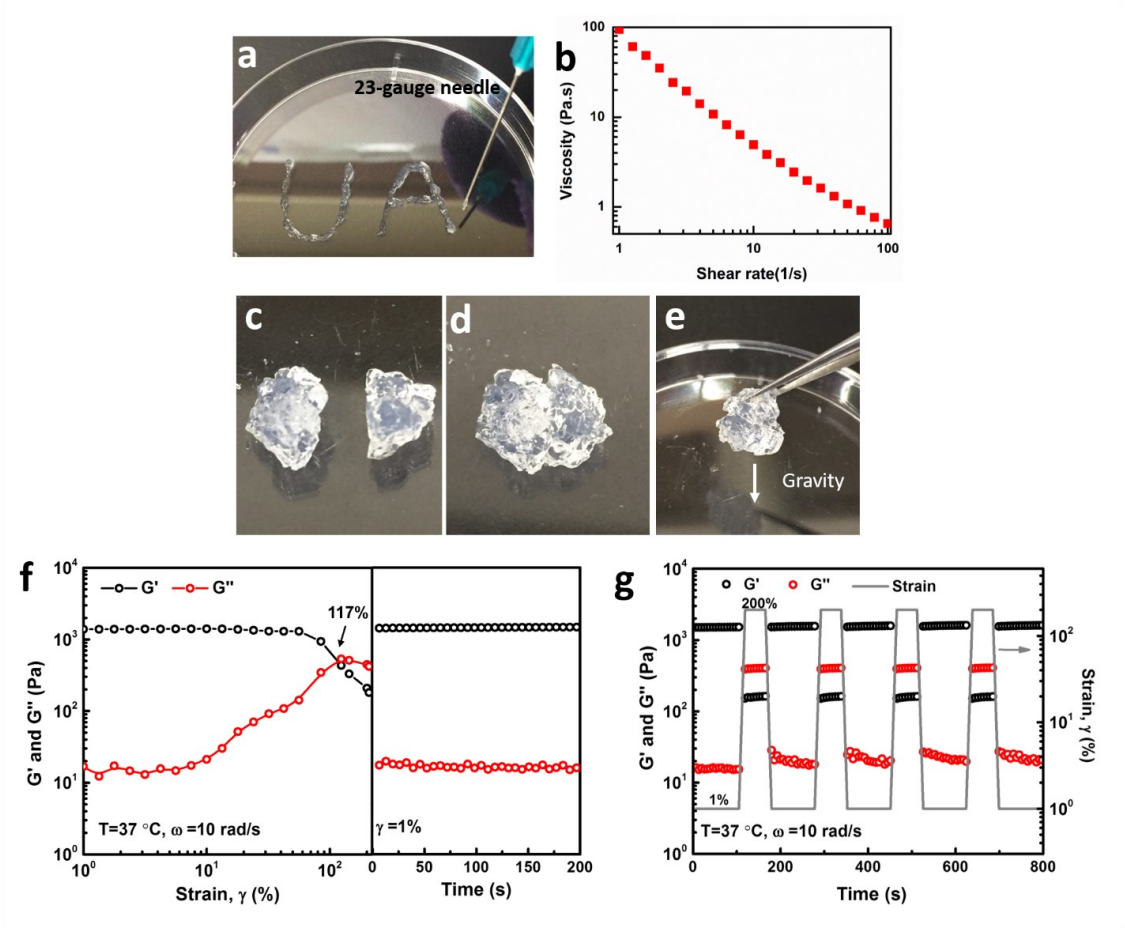

Figure 2.3. (a) PMF10-S 10-13 hydrogel injected from a 23-gauge needle. (b) Rheological steady flow sweep at 37 °C showing the relationship between viscosity and shear rate. (c-e) Photographs illustrating the self-healing property of PMF10-S 10-13 hydrogel, (c) two separate hydrogel pieces, (d) two pieces adhering to each other instantly when brought into contact, (e) the healed gel supporting its own weight. (f) Oscillatory strain sweep of PMF10-S 10-13 hydrogel followed by an oscillatory time sweep at a

strain of 1% and 37 °C. (g) Strain-step test with strain altering between 1% and 200% for four cycles at 37 °C.

2.3.3 Effect of Composition on the Mechanical Performance of Hydrogels

The mechanical performance of the hybrid hydrogel was highly dependent on its composition. As shown in Figure 4, by altering the ratio of two monomers, copolymer or nanoparticle contents, the G' (T=37 °C, ω=10 rad/s, γ=1%) of the prepared PMF-S hydrogels can be finely modulated from several to over 2000 Pa, which enables the hydrogels to serve diverse biomedical applications. To be specific, with FBEMA molar percentage ranging from 2% to 20%, all the resultant copolymers were able to form hydrogels with ASNP (**Figure 2.4a**). The higher the aldehyde-functionalized monomer ratio was, the more Schiff base interactions per unit volume possessed, resulting in significant improvement of storage modulus from 82 to 2211 Pa. The increase of crosslinking degree also induced higher opacity of the hydrogel (**Figure S2.4** in **Appendix A**). Similarly, increasing the loading of PMF copolymers or ASNP would directly enhance the density of Schiff base linkages, consequently improving the hydrogels' modulus. As displayed in Figure 4b, it should be noted that, with only 2% of PMF, a hydrogel with G' around 200 Pa was constructed, and the value jumped to near 1000 Pa when the polymer content increased to 5% (**Figure 2.4b**). The relatively high modulus at low PMF concentration was ascribed to the incorporation of nanoparticles that could not only contribute to the crosslinking degree but also hinder the sliding of polymer molecular chains when the material was under stress. In good agreement, **Figure 2.4c** further demonstrates that a mild increase of the nanoparticle fraction would cause a considerable scale-up of G', and specifically, the G' almost doubled with a slight increase of ASNP content from 10% to 13%. Generally, the tan delta (equal to G''/G') of the as-

formed PMF-S gels located at very low values (< 0.04) except those weak gels with *G′* lower than 100 Pa, indicating high elasticity of the nanocomposite hydrogels.

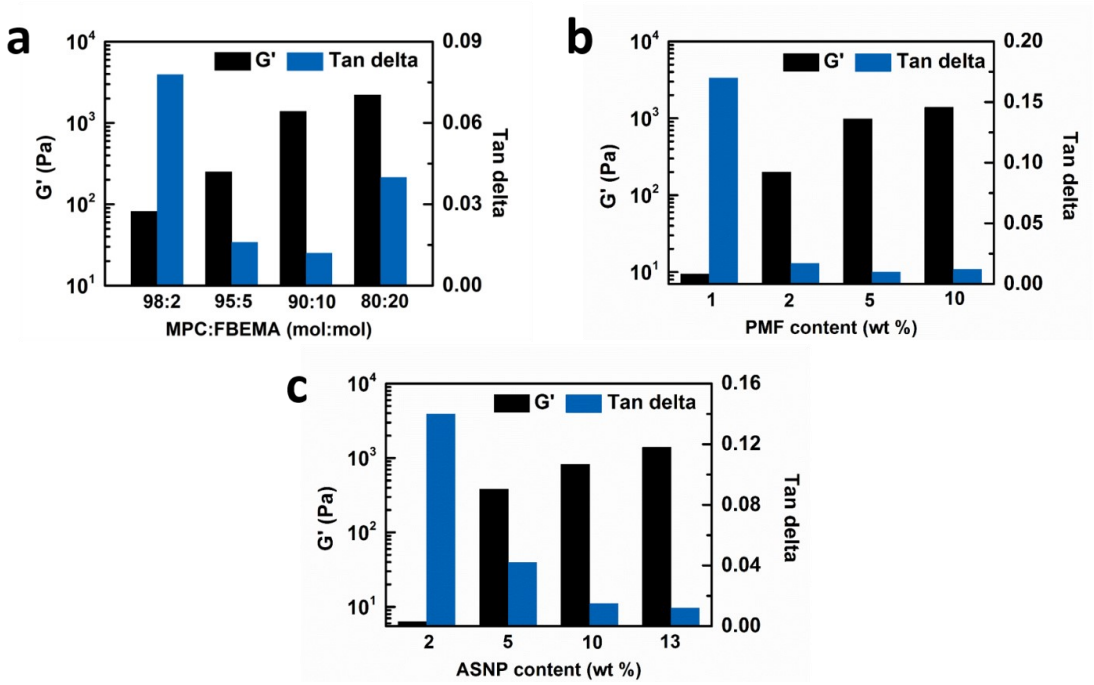

Figure 2.4. Oscillatory rheological properties of hydrogels prepared from (a) 10 wt% PMF with different MPC:FBEMA molar ratio and 13 wt% ASNP, (b) different loadings of PMF10 and 13 wt% ASNP, and (c) 10 wt% PMF10 and different loadings of ASNP.

2.3.4 pH-Dependence of the Rheological and Degradation Properties

It is well known that imine structures would undergo hydrolysis in an acid-sensitive manner, resulting in pH-responsive behaviors of the corresponding hydrogels. The change of hydrogel behaviors when varying the pH of the gels was measured in situ by the rheometer. As shown in **Figure 2.5a**, upon the addition of concentrated HCl solution (5 μL, 5 M), the PMF10-S 10-13 hydrogel was rapidly liquified (pH measured to be ~2) with a sharp drop of G″ to very low values (0.3~0.4 Pa). This result is due to the complete hydrolysis of the dynamic Schiff base bonds between PMF copolymer and ASNP. However, after the acid was neutralized (pH measured to be ~7) by the addition of

tris solution (10 μL, 5 M), gelation occurred immediately with G′ (~1300 Pa) and G″ (~ 20 Pa) recovered close to their original values at the beginning of the rheological sweep, indicating rapid and reversible pH-responsiveness of the PMF-S hydrogel. It should be noted that the slight deterioration of the mechanical performance of the hydrogel was attributed to the slight dilution of the gelators after the addition of acid or base solutions. The reversibility of the pH-sensitive gel-sol-gel transition of the hydrogel was also demonstrated by cyclic tests in **Figure 2.5b**.

The pH-regulated sol-gel transition of the PMF-S hydrogel was also quantitatively investigated by rheological tests with pH ranging from 4 to 8.5. In **Figure 2.5c**, at high pH values (6.8, 7.4, 8.0 and 8.5), the system shows gel-like behaviors with *G′* dominant across the whole range of the applied angular frequencies. However, the hydrogel lost over half of its strength (*G′*) when the pH condition changed from neutral to mildly acidic of 6.8. A further decrease of pH to 6.4 induced a significant drop of *G′* to values comparable to that of *G″*, suggesting a viscous liquid-like behavior at the static state ($\omega <$ 4 rad/s). Rapid decreases of *G′* and *G″* were observed for samples at pH 6, which indicated the mixture completely turned into a liquid with low viscosity. **Figure 2.5d** displays the variations of *G′* and *G″* as a function of pH. A sharp sol-gel transition could be clearly observed in the faintly acidic pH range of 6.0-7.4. In addition, the pH-responsive behaviors of the PMF-S hydrogel could be readily adjusted by varying hydrogel compositions. For example, decreasing the ratio of FBEMA monomer in the copolymer to 5 mol% resulted in a shift of the sol-gel transition to pH range of 6.4-7.4 (**Figure S2.5** in **Appendix A**).

It is known that the protonation state of amino group exerts a profound influence on it reactivity for Schiff base formation, i.e., protonated amino groups ($-NH_3^+$) lack nucleophilicity to react with aldehyde groups for the formation of hydrogels.[73] To better

clarify the pH-responsive gelation behavior of PMF-S hydrogel, the protonation degree of amino groups on ASNP at various pH ranging from 4-8.5 was evaluated by zeta potential measurements. As demonstrated in **Figure 2.5e**, ASNPs were almost fully protonated when pH was lower than 6, pulling the equilibrium of Schiff base reaction toward hydrolysis,[36] and thereby no gelation occurred at such conditions. At higher pH values, the protonation degree of amino groups rapidly decreased with $pK_{1/2}$ (the pH at which half of the surface amino groups are ionized and also denoted as pKa) measured to be 7.6 which is consistent with the value reported in previous studies[234]. Therefore, the Schiff base formation and gelation are greatly accelerated under neutral conditions. The zeta potential results are in good agreement with the pH-dependent rheological performance of PMF-S hydrogel, indicating the critical role ASNP played in determining the pH-responsive behavior of the hydrogel.

The swelling and hydrolytic degradation behaviors of PMF-S hydrogels in PBS buffers with pH ranging from 6.4 to 7.4 were demonstrated in **Figure 2.5f**. All the samples started to swell when they were immersed in PBS solutions, and the swelling ratio was higher with a lower pH value within the first 6 h. This result was because, in a more acidic environment, the larger number of the protonated amino groups tended to lower the crosslinking degrees as well as drive more counter ions migrating into the hydrogel, leading to a higher osmotic pressure. With incubation time increasing, hydrogels in mildly acidic media (6.4, 6.6 and 6.8) exhibited degradation behaviors. Moreover, the degradation rate depended on the acidity of the buffers in an ultra-sensitive manner. The hydrogel completely dissolved in the pH 6.4 PBS medium within 4 days and partially degraded at pH 6.6 in 5 days, while, at pH 6.8, the hydrogel kept most of its integrity within the experimental period. This sensitive pH-controlled hydrolytic degradation profile is attributed to the increased hydrolysis rate of Schiff base under more

acidic conditions and the high hydrophilicity of the as-synthesized PMF copolymer. In contrast, in neutral pH buffer, no hydrogel dissolution was observed, suggesting the excellent gel stability under physiological condition, which is highly desirable in controlled drug release to avoid side effects to normal tissues.

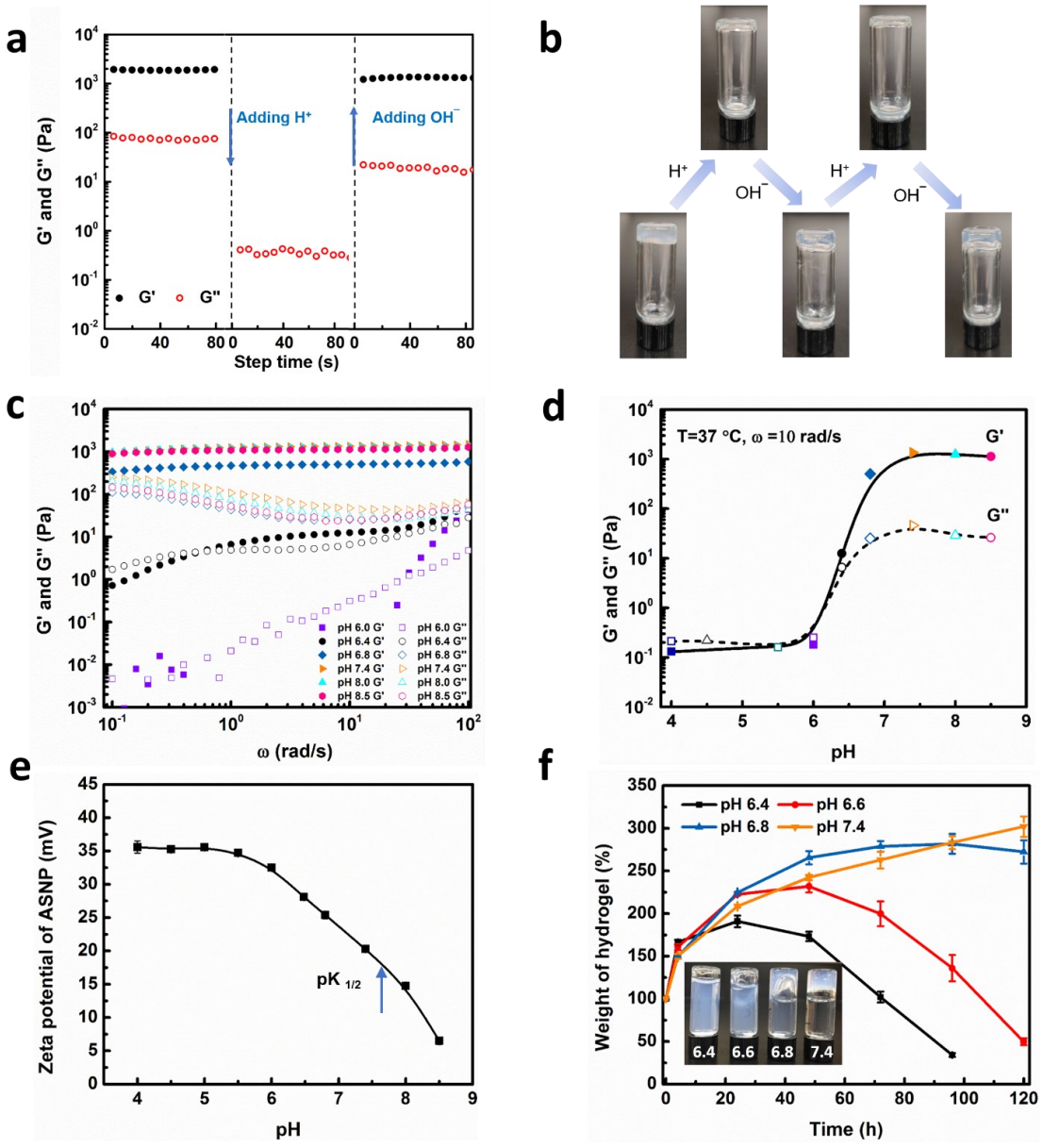

Figure 2.5. (a) Rheological time sweeps (strain 1%, angular frequency 10 rad/s) showing reversible gel−sol−gel transition of PMF10-S 10-13 hydrogel by changing pH, and (b) pictures showing the reversible gel−sol−gel transitions for two cycles. (c, d) Rheological characterization of the pH-dependent behavior of PMF10-S 10-13 hydrogel at 37 °C and

strain of 1% by (c) oscillatory frequency sweeps, and (d) G' and G'' versus pH at 10 rad/s. (e) Zeta potentials of ASNP at pH varying from 4 to 8.5. (f) Swelling and hydrolytic degradation of PMF10-S 10-13 hydrogel in 10 mM PBS of various pH at 37 °C. Inserted picture was taken after 96 h of degradation.

2.3.5 *In Vitro* Release

The pH-responsive *in vitro* release profiles of PMF-S hydrogels were investigated upon soaking the cargo-loaded hydrogels in PBS of pH 6.4, 6.6, 6.8 and 7.4 (**Figure 2.6**). To demonstrate the potential application of the PMF-S hydrogel as a pH-responsive delivery depot for localized release of both small water-soluble molecules and protein drugs, two molecules, congo red and BSA-FITC were selected as model "drugs". Congo red is a low-cost small molecular dye that has been used as a model drug in previous studies[241, 242]. More importantly, it bears an amino group that can react with the aldehyde group in the PMF hydrogel, which makes it of high resemblance to the widely used amine-containing drugs in cancer therapy and wound healing like the anti-tumor drug Dox and anti-bacterial drug amoxicillin. Its release patterns were demonstrated in **Figure 2.6a** and graphically shown in **Figure 2.6d**. In order to better understand the release mechanism, the data were fitted using the well-known Korsmeyer-Peppas equation, $M_t/M_\infty = kt^n$, with high correlations ($r^2 \geq 0.989$) (**Figure 2.6b**). In the equation, the diffusional exponent n is an indication of the mechanism of drug release, i.e., $n \leq 0.5$ characterizing Fickian diffusion controlled rate release, $0.5 < n < 1$ indicating anomalous (non-Fickian) transport of cargos and $n = 1$ reflecting zero-order or case-II relaxational release of drugs which is ascribed to the erosion and/or swelling of hydrogel matrix.[236, 237, 243] As shown in Figure 6a, the PMF-S hydrogel displayed an ultraslow congo red release under neutral physiological pH (7.4) with only 12% of the molecule released after

5 days of incubation, which was ascribed to the imine formation between the amino groups in the dye and the aldehyde moieties in copolymers as well as the outstanding gel stability at neutral pH. According to the Korsmeyer-Peppas fitting curve (n = 0.47), a small portion of dye molecules unbound to the hydrogel network was released from the hydrogel in a Fickian diffusion-controlled profile. The release rate gradually enhanced with the increase of medium acidity, reaching 23% of release after 5 days for the hydrogel at pH 6.8. The exponent n increased to 0.71, indicating the hydrogel dissolution and swelling together with diffusion played roles in the controlled release process.[243, 244] _ENREF_67 It is noted that further mild decreases of pH to 6.6 and 6.4 led to a significant acceleration of the process, with 56% and 93% of drug released at the end of the experiment, respectively. Moreover, zero-order release (n ≈ 1), a highly desirable feature for controlled drug delivery, was realized under these two conditions, owing to the hydrogel erosion-dominated release of the drug.

BSA-FITC, which has been commonly used as a protein model drug[203, 227], was chosen as another model therapeutic. As shown in **Figure 2.6c**, the PMF-S hydrogel exhibited a faster release of BSA within the first 24 h compared to that of congo red due to the weaker drug-hydrogel interaction. Korsmeyer-Peppas fitting of the first-24 h release data gave the exponent n of 0.86~0.89 (**Figure S2.6** in **Appendix A**), which was indicative of the anomalous (non-Fickian) transport mechanism, suggesting the diffusion process of trapped molecules was controlled by the swelling and/or dissolution of hydrogels. After 24 h, similar sensitive pH-regulated release manners were obtained, where high levels of BSA release of ~90% were attained in mildly acid environment (pH 6.4 and 6.6), while only 58% of the proteins were released at neutral pH after 5 days (Figure 6c, 6d). The ultra-sensitive pH-induced release of both agents suggests the PMF-S hydrogel can serve as a promising candidate to fulfill the practical needs in controlled

drug delivery for cancer therapy, wound healing and so forth.

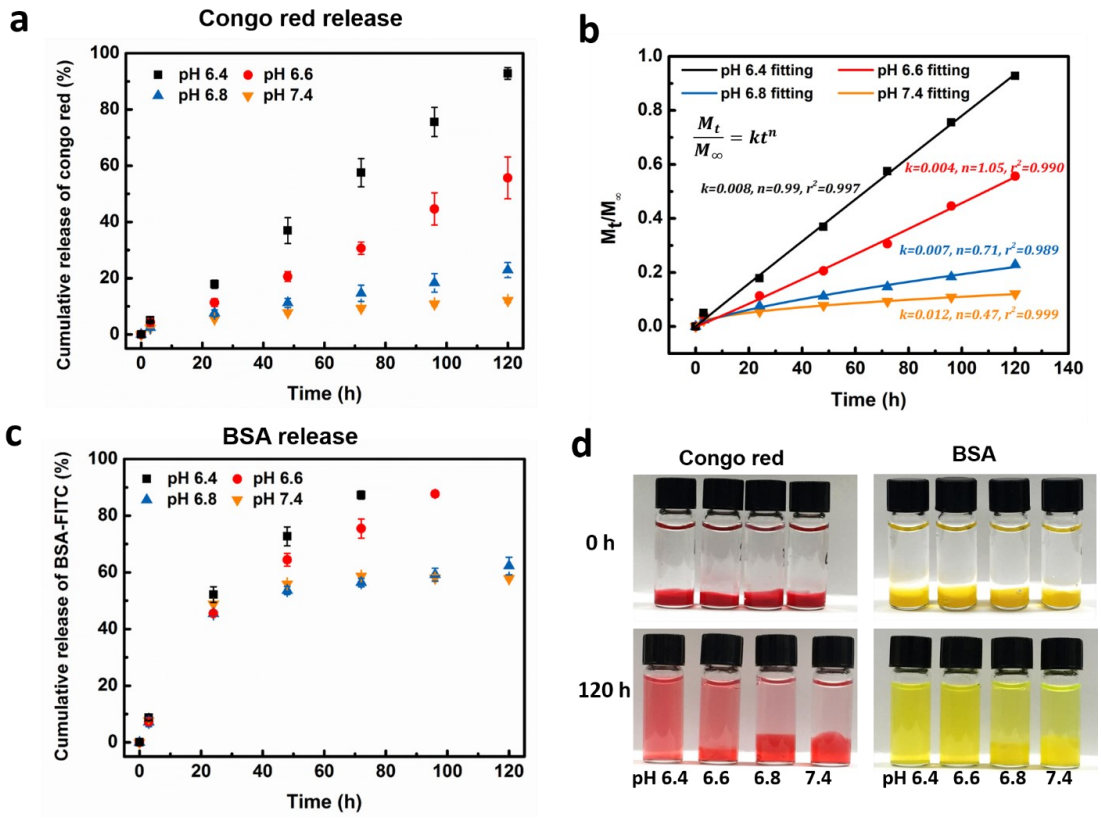

Figure 2.6. (a) Cumulative release of model drug (i.e., congo red) from PMF10-S 10-13 hydrogel immersed in 10 mM PBS of various pH at 37 °C, and (b) Korsmeyer-Peppas fitting of the congo red release data. (c) Cumulative release of BSA-FITC from the hydrogel in 10 mM PBS of various pH at 37 °C. (d) Photographs showing the release of the two model molecules at the beginning and at the end (120 h) of the experiments.

2.3.6 Cytotoxicity

The biocompatibility of the PMF-S hydrogel was examined by MTT assay using human fibroblast cells HDFa and the results are shown in Figure 7. Due to the decomposition of the Schiff base, the potential toxicity of the hydrolysis products of the hydrogel, i.e., PMF copolymer and ASNP, was evaluated by examining the cytotoxicity of the mixtures of these two components. As shown in Figure 7a, after incubation with

the mixtures of hydrogel components for 24 h, the cell viability remained to be more than 88% for samples at all concentrations and even reached 103% for the mixture solution of a concentration as high as 2 mg/ml (**Figure 2.7a**), indicating the potential toxicity of the hydrolysis products of the PMF-S hydrogel is low. The cytotoxicity of hydrogel extracts was also assessed and over 80% of the cell retained viable with highly concentrated 100% gel extract (**Figure 2.7b**). Therefore, the PMF-S hydrogel possessing good cytocompatibility has great potential for biomedical applications.

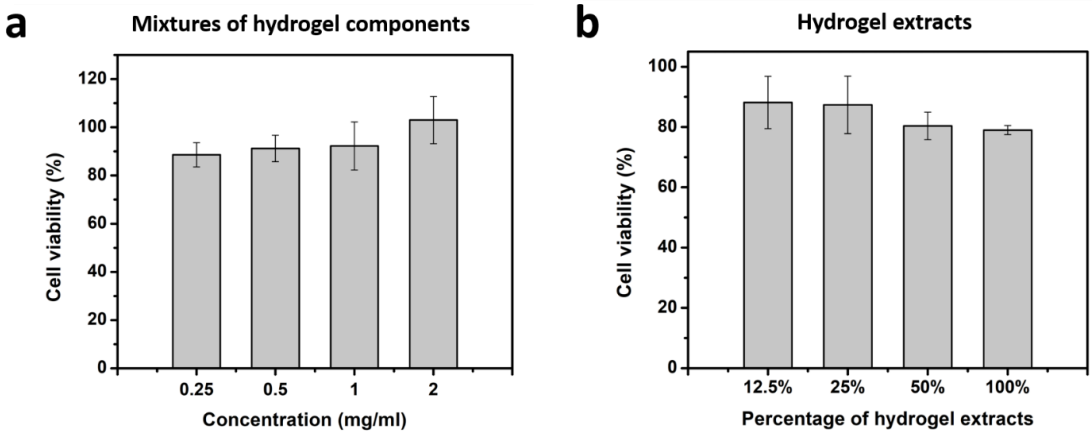

Figure 2.7. Cell viability of HDFa cells after 24 h incubation with (a) various concentrations of mixtures of PMF10-S 10-13 hydrogel components, and (b) different dilution percentages of the 100% hydrogel extracts.

2.4 Conclusions

In this work, we have prepared an injectable, self-healing and ultra-sensitive pH-responsive hydrogel PMF-S through dynamic Schiff base linkages between aldehyde-functionalized zwitterionic polymers and amine-modified silica nanoparticles. The hydrogel shows rapid gelation, shearing-thinning induced injectability, as well as fast and

repeatable self-healing ability. Notably, it decomposes rapidly under mildly acid environment while displays excellent gel stability under neutral physiological pH condition. Very interestingly, the hydrogel's mechanical, hydrolytic degradation and drug release behaviors can be manipulated by varying pH in an ultra-sensitive manner in the faintly acidic range, that is, a slight pH change of 0.2 can induce significant variation of the corresponding properties. Additionally, the hydrogel's mechanical and pH-responsive properties can be readily tuned by its composition. Cytotoxicity tests demonstrate good biocompatibility of the hydrogel. Therefore, our results provide a facile approach for the fabrication of novel drug delivery systems particularly triggered by local acidosis, and the ultra-sensitive pH-responsiveness of the developed hydrogel can be employed for applications demanding a precise control of pH-induced release.

CHAPTER 3 Ultra Elastic, Stretchable, Self-Healing Conductive Hydrogels with Tunable Optical properties for Highly Sensitive Soft Electronic Sensors

3.1 Introduction

Soft electronics have received growing attention in recent years due to their unique advantages such as flexibility, stretchability and human-friendly nature, enabling a broad range of applications including wearable sensory devices, implantable bioelectronics, artificial electronic skins (e-skins), flexible touch panels, actuators and triboelectric generators.[19, 91, 245, 246] Up to now, enormous progress has been made in the development of soft electronic devices using a variety of materials like carbon- or metal-based thin films,[247, 248] conductive hydrogels[21, 249, 250] and elastomers[251, 252]. Among them, hydrogels, which are water-swollen polymeric materials that maintain a distinct 3D structure, have emerged as promising candidates for flexible electronics owing to their soft, water-rich, conformable and biocompatible characteristics.[17, 19, 23, 249, 253-255] Closely resembling human skin, hydrogels are particularly appealing for the fabrication of wearable and biomedical electronics to avoid mechanical mismatch with tissues and provide comfortable human-machine interaction experiences.[18, 91] In order to efficiently transmit electrical signals, hydrogel electronics are required to possess good conductive performance. Several strategies have been adopted to improve the conductivity of hydrogels, including the incorporation of conductive nanofillers[127-129] (e.g., carbon nanotubes, graphene and silver nanowires), intrinsic conductive polymers[46, 130] (e.g., polythiophene and polyaniline) or ions[21, 131] (e.g., NaCl and LiCl) into hydrogel matrixes. While the former two strategies suffer from filler agglomeration, complicated synthetic

processes, high cost and dark color, the introduction of ions appears to be a facile, economical and bio-inspired approach to prepare conductive hydrogels with high transparency and water retention capability.[256]

In practical applications, since soft electronics usually undergo frequent stress caused by stretching, bending, tapping or pressure during usage, it is highly desirable for the conductive hydrogels to have decent mechanical properties such as stretchability, toughness and fatigue resistance. Traditional chemically cross-linked hydrogels are generally weak and brittle due to the lack of energy dissipation mechanisms and network homogeneity.[33, 257, 258] Therefore, dynamic physical bonds like hydrogen bonds, hydrophobic interactions and ionic interactions instead of permanent chemical bonds are generally introduced to allow effective mechanical energy dissipation through hydrogels, and thereby to provide the hydrogels with suitable toughness.[57, 60, 259] More interestingly, the incorporation of dynamic bonds endows hydrogels with self-healing capability, that is, the ability to autonomously heal fractures and restore functionality after damage, which could significantly prolong hydrogels' life spans and enhance their reliability.[34, 260-262] In recent years, dynamic chemical bonds[36, 263] (e.g., imines,[77, 209, 264] phenylboronate complexations,[95, 98] hydrazones[111, 265] and disulfide bonds[105, 266]), which combine the merits of both dynamic physical interactions and traditional covalent bonds, have drawn widespread attention due to their strong, robust yet reversible natures. Among dynamic covalent bonds, imines or Schiff bases, which are formed from the condensation reactions between aldehydes and primary amines, have been extensively employed in the fabrication of hydrogels for various biomedical applications, owing to their dynamic nature, ready formation under neutral conditions, and stimuli-responsive property.[77, 264] However, these interactions have seldom been expanded to the preparation of tough conductive devices to provide these fascinating features.

For the fabrication of tough hydrogels, besides involving dynamic bonds, creating special structures within the hydrogel matrixes is also extensively employed.[33] Up to now, a variety of hydrogels showing good mechanical performances have been developed based on elegant structure design, such as DN hydrogels,[60, 180, 267] NC hydrogels,[23, 165, 268] tetra-arm PEG hydrogels,[176] micelle cross-linked hydrogels[51, 178, 269] and so forth. Among them, the construction of NC hydrogels, which could simultaneously introduce effective energy dissipation mechanisms and increase homogeneity of cross-linked networks,[258, 270] is an effective yet facile approach to reinforce hydrogels and thus is promising for the fabrication of soft electronics. Fatigue resistance or elasticity is another essential feature towards more reliable and durable flexible devices, particularly for applications subjected to constant large deformations like wearable sensory gadgets. Despite a great number of tough conductive hydrogels developed, most of them lack satisfactory elasticity to fulfill practical needs. Micelle cross-linking is an appealing method that could endow corresponding hydrogels with good elasticity owing to the quick reassembly of micelle structures after deformation.[56, 155, 269] However, its adoption in conductive hydrogels has rarely been reported. In recent studies, there has been growing interest in integrating two or more cross-linking mechanisms into one hydrogel to achieve improved mechanical performance as well as multiple functionalities.[53, 116] Therefore, incorporating nanofillers, micelle cross-linking and Schiff base interaction into one platform holds great promise for elastic, tough and self-healing hydrogel conductors. On the other hand, to meet the increasingly complex and multifunctional requirements for modern electronics, it is desired to prepare conductive “smart” hydrogels that can respond to environmental stimuli such as temperature, pH and magnetic field.[204, 271] Although a variety of conductive hydrogels have been developed, they struggle to meet all these performance demands including good conductivity, stretchability, elasticity, self-healing property and

stimuli-responsiveness. It is still a challenge to fabricate such conductive hydrogel that possesses multiple desirable attributes.

Herein, we have developed a novel tough conductive hydrogel showing outstanding elasticity, stretchability, self-healing and stimuli-responsive properties, and high conductivity. The hydrogel was generated from a facile one-pot free radical polymerization process of acrylamide (AM), and 2-aminoethyl acrylamide hydrochloride (AEAM), with the presence of carboxy-modified multiwall carbon nanotubes (MWCNT) and aldehyde-terminated poly(ethylene oxide)-b-poly(propylene oxide)-b-poly(ethylene oxide) (F127-CHO) under neutral condition. Among these components, AM plays a major role in the formation of polymer network through its multiple intermolecular hydrogen bonding.[272, 273] MWCNT was selected to construct a nanocomposite network due to its large aspect ratio and the remarkable reinforcement effect on composite materials.[155, 156, 274] In addition, carboxyl-functionalized MWCNT shows better water dispersity and biocompatibility compared to unmodified CNT,[275] and thus was chosen for the hydrogel preparation. F127, which can self-assemble to micelles in a thermo-sensitive manner,[276] offers hydrophobic associations to the hydrogel as well as endows it with stimuli-responsiveness. Most importantly, the amine-containing monomer AEAM, which can generate ionic interaction and Schiff base bond with MWCNT and F127-CHO, respectively, was introduced to enable strong and dynamic interfacial bonding between gelators. In addition, LiCl was incorporated to improve the ionic conductivity of the hydrogel, and it is chosen over other salts because of the better water retention ability and hygroscopicity.[256] The integration of dynamic Schiff base bonds with nanofiller reinforcement and micelle cross-linking endows the hydrogel with an unique combination of properties, i.e., combining exceptional elasticity with outstanding self-healing performances. The hydrogel reached 97% recovery from 1000% tensile strain and 100%

recovery from 90% compression strain within 1 min, while achieving high stretchability of 635% after self-healing. The well cross-linked network also offers the hydrogel with excellent damage resistance to sharp materials. Meanwhile, the hydrogel possesses sensitive thermo-responsive property, i.e., its optical appearance could be readily tuned from transparent to opaque through altering temperature from high to low. The hydrogel was successfully employed as a strain/pressure sensor to detect human motions including both large movements and tiny physiological activities with extremely sensitive and repeatable responses. Compared to previously reported hydrogel sensors, the as-prepared hybrid hydrogel achieved more favorable multifunctionalities for high-performance sensory devices, which makes it hold great potential in soft intelligent sensors and e-skins.

3.2 Experimental Methods

3.2.1 Materials

Acrylamide (AM, 99%), Pluronic® F127 (F127, 99.99%), N,N'-dicyclohexylcarbodiimide (DCC, 99%), ethylenediamine (99%), ethylenediamine dihydrochloride (98%), hydrochloric acid (HCl, 37%), acryloyl chloride (97%) and 2,2'-azobis(isobutyramidine hydrochloride) (AIBA, 97%), MWCNT (> 8% carboxylic acid functionalized, average diameter × length: 9.5 nm × 1.5 μm) were purchased from Sigma-Aldrich and used as received. 4-Formylbenzoic acid (98%), 4-dimethylaminopyridine (DMAP, 99%), lithium chloride (LiCl, 98.5%) and all solvents were purchased from Fisher Scientific and used as received.

3.2.2 Synthesis of F127-CHO

F127-CHO was synthesized by DCC/DMAP catalyzed esterification reaction between Pluronic® F127 and 4-formylbenzoic acid. First, Pluronic® F127 (10 g, 0.8

mmol), 4-formylbenzoic acid (0.9 g, 6 mmol) and DMAP (0.05 g, 0.4 mmol) were dissolved in 60 mL of tetrahydrofuran (THF) under sonication, followed by the addition of 20 mL THF with DCC (1.6 g, 7.8 mmol) dissolved in. After stirred at room temperature for 40 h, the mixture was concentrated under vacuum and precipitated from ethyl ether twice. The resultant white solid was dried and then dissolved in Milli-Q water. After centrifugation, the supernatant was collected and lyophilized to obtain the white powder product with a yield of 96.1%. Its chemical structure was confirmed by ^{1}H NMR spectrum on an Agilent 400-MR DD2 NMR spectrometer with DMSO-d6 as the solvent and by Fourier transform infrared (FTIR) spectrum on a Nicolet iS50 FTIR spectrometer (Thermo Scientific, USA).

3.2.3 Synthesis of Amine-Functionalized Monomer

For the synthesis of amine-functionalized monomer (AEAM), first, ethylenediamine dihydrochloride (30 g, 0.226 mol), Milli-Q water (120 mL) and ethylenediamine (31.9 g, 0.532 mol) were mixed and stirred at room temperature for 1 h. After the addition of 160 mL methanol, the mixture was allowed to react for another 1 h, followed by cooling down to –30 °C. Acryloyl chloride (48.1 g, 0.532 mol) was then slowly added to the system. After the complete addition of acryloyl chloride, the solution was kept below –20 °C for 1 h before the addition of HCl (37 %) to adjust the pH to 1−2. After the temperature of the system rose to room temperature naturally, solvents were removed under vacuum and lyophilization. The resultant white powder was then dissolved in isopropanol, filtrated and crystallized at –20 °C from the filtrate to obtain the crude product. Finally, the raw product was recrystallized from isopropanol and precipitated from THF to obtain a white powder product with a yield of 25.1%. The chemical structure of the monomer was confirmed by ^{1}H NMR spectrum with D_2O as the

solvent.

3.2.4 Preparation of Hydrogels

For a typical synthesis process of 1.8 mL hydrogel, AM (0.36 g), F127-CHO (0.1 g), AEAM (0.08 g) were first dissolved in 0.9 mL LiCl aqueous solution (2 M), and then mixed with 0.9 mL MWCNT aqueous dispersion (2 mg/L), followed by adjusting pH of the system to 7.4 using NaOH solution. After purged with nitrogen for 20 min and the addition of initiator AIBA (6 mg), the mixture was allowed to polymerize overnight at 30 °C to obtain the final hydrogel in which the concentrations of polymers, MWCNT and LiCl were 300 mg/mL, 1 mg/L and 1 M, respectively. This composite hydrogel was denoted as PAAFC-L, where PAA, F, C and L represent the copolymer of AM and AEAM, F127-CHO, MWCNT and LiCl, respectively. To study the effects of functional gelators on the mechanical performance of the hydrogel, a series of control hydrogels with the same total polymer content were also synthesized following the above procedure. These control hydrogels include pure PAM hydrogel only composed of AM, PAMF hydrogel consisting of AM and unmodified F127, PAAF hydrogel composed of AM, AEAM and F127-CHO, PAM/MWCNT hydrogel, P(AM-co-AEAM)/MWCNT hydrogel, PAAFC hydrogel without the addition of LiCl, PAAFC-L hydrogels with various contents of MWCNT, and PAAFC-L hydrogel prepared under mild acidic pH of 6, respectively. The morphologies of freeze-dried hydrogels and dispersity of MWCNTs in the hydrogel were characterized using a Zeiss Sigma field emission scanning electron microscope (SEM) at an acceleration voltage of 10 kV.

3.2.5 Mechanical Properties of the Hydrogels

Mechanical properties of the hydrogels were characterized on an AGS-X universal tensile testing machine (Shimadzu, Japan) at room temperature. Tensile tests

were performed with a 50 N load cell and rectangular specimens of 20 mm (length) × 5 mm (width) × 1.5 mm (thickness). The stretchability of hydrogels was measured at a constant crosshead speed of 10 mm/min. The true tensile stress of samples was determined by multiplying the tested nominal tensile stress with the tensile strain, and the toughness of hydrogels was calculated from the area below nominal stress-strain curves.[277]

For the measurements of elasticity, cyclic tensile tests were conducted at a constant stretching rate of 20 mm/min and various predetermined maximum strains of 100, 200, 500 and 1000% under ambient condition (room temperature 20°C, 60% humidity). The wait time between cycles was set to be 20 s for 100 and 200% stains, and 60 s for 500 and 1000% stains. Cyclic compression experiments were performed at a constant compressing rate of 5 mm/min and wait time between cycles of 60 s with a 5000 N load cell. In compression tests, cylindrical hydrogel specimens were prepared with a diameter of 17 mm and a height of 8 mm.

3.2.6 Self-Healing Property of the Hydrogels

The self-healing capability of the hydrogels was first studied through rheological tests on a TA Instruments AR-G2 stress-controlled rheometer using a 20 mm (diameter) 2º cone geometry with a gap of 53 μm. Oscillatory strain (γ) amplitude sweep at fixed angular frequency (ω) of 10 rad/s was carried out with γ ranging from 1 to 20000%, followed by a dynamic time sweep at constant frequency of 10 rad/s and strain of 1%. Afterward, the repeatability of the self-healing behavior was examined by cyclic strain experiment with γ shifting between 1% and 2000% for three cycles at a fixed frequency of 10 rad/s. The self-healing property was also macroscopically observed by bringing two pieces of hydrogels into contact. One of the hydrogel pieces was prepared with a trace

amount of Rhodamine B to give a color difference. The stretchability of hydrogels after healing for 2, 24 or 48 h was detected on the AGS-X universal tensile testing machine. Besides, the electrical properties of the hydrogel before and after self-repairing were evaluated by both the light-emitting diode (LED) illumination and the current change during several cutting-healing cycles on an electrochemical workstation (CHI920, CH Instruments, USA). All the autonomous healing experiments were conducted at room temperature.

3.2.7 Temperature-Responsive Properties of the Hydrogels

The thermo-responsive optical property of the hydrogels was captured by images at temperatures of 10, 20, 37 °C. The hydrogels at 10 and 37 °C were obtained by treating the samples in fridge and a water bath at 37 °C, respectively, and the surface temperatures were measured by an infrared thermometer. Additionally, the change of transparency was quantitatively recorded by a microplate reader (Cytation 5, Biotek, USA) at different temperatures in visible light range (400−800 nm), with samples of 6.5 mm diameter and 1.5 mm thickness. The repeatability of the hydrogel's temperature-tuned optical property was evaluated by alternatively float the hydrogel on a 37 °C water bath and an ice-water bath and for several cycles. To reveal the mechanism of the transparency change, the sizes of the unmodified F127 and F127-CHO micelles at various temperatures ranging from 10 to 60 °C were characterized by dynamic light scattering (DLS) with a Malvern Zetasizer Nano ZSP. The topography images of F127-CHO micelles at different temperatures were acquired using a Dimension Icon atomic force microscope (AFM) system (Bruker, Santa Barbara, CA, USA) operated in air in the tapping mode. The samples for AFM imaging were prepared by depositing two drops of micelle aqueous solution (10 mg/mL) onto a cleaned silica substrate. The surfaces were then dried in air at

20 or 60 °C followed by rinsing with Milli-Q water of corresponding temperatures and dried by nitrogen flow.

3.2.8 Electrical and Sensing Performances of Hydrogels

The electrical conductivities (σ) of hydrogels were measured by the electrochemical workstation (CHI920, CH Instruments, USA). Electrochemical impedance spectroscopy was conducted in the frequency range of 10^{-1}–10^{6} Hz with an amplitude of 5 mV at open circuit voltage. The σ values were calculated by the following equation

$$\sigma = \frac{L}{R_b S} \qquad (3.1)$$

where L is the gauge length, S refers to the cross-section area of the hydrogel sample and R_b is the bulk resistance (intercept at Z′ axis). The strain and pressure sensing properties of the PAAFC-L hydrogel upon stretching and compression were evaluated by mounting the samples on an in-house prepared stretching stage and the AGS-X universal tensile testing machine, respectively. In these tests, the real-time I–t (current vs time) curves were recorded and the ratio of resistance change (ΔR) to resistance at t = 0 (R_0) was calculated according to the following equation

$$\frac{\Delta R}{R_0} = \frac{I_0}{I} - 1 \qquad (3.2)$$

where I_0 represents the current at t = 0. Afterwards, the sensing performances of the hydrogel for diverse human activities like finger, wrist, elbow and knee movements were characterized by mounting hydrogels on corresponding positions. The hydrogel sensor was also mounted on face, throat, tummy and radial artery and a sleeping eye mask to detect subtle human motions such as facial expressions, speaking, breathing, wrist pulse and sleeping. The dimensions of the hydrogel sensors for all sensing characterizations

were around 20 mm (length) × 5 mm (width) × 1.5 mm (thickness), except for the wrist pulse tracking where a thinner (thickness ~ 0.7 mm) hydrogel sensor was used to achieve higher sensitivity. A thin layer of Vaseline was applied on the surface of the hydrogel sensors after the fixing of copper foils and conductive wires to the hydrogel to avoid moisture loss.

3.3 Results and Discussion

3.3.1 Design and Synthesis of PAAFC-L Hybrid Hydrogel

In order to introduce dynamic Schiff base interactions into the hybrid hydrogel, first, the triblock copolymer of poly(ethylene oxide)-b-poly(propylene oxide)-b-poly(ethylene oxide), (PEO_{100}-PPO_{65}-PEO_{100}, F127), was functionalized to bear terminal benzaldehyde groups through carbodiimide-catalyzed esterification with 4-formylbenzoic acid (**Figure 3.1a**). The molecular structure of F127-CHO was confirmed by ^{1}H NMR spectrum (**Figure S3.1a** in **Appendix B**), in which the benzaldehyde functional group gave signals at 10.07, 8.12, and 8.02 ppm. The degree of aldehyde modification was 86.6% as calculated from the characteristic peak of the aldehyde group and $-CH_3$ of PPO. The successful aldehyde-modification of F127 was also confirmed by FTIR spectrum. As demonstrated in **Figure S3.1b** in **Appendix B**, compared to unmodified triblock copolymer, extra adsorption peaks of F127-CHO appeared at 1723, 1706 and 761 cm^{-1}, which were assigned to the stretching vibration of C═O bond of ester group, C═O stretching of aldehyde group and out-of-plane C–H bending of aromatic ring, respectively. Next, the amine-containing monomer, AEAM, was synthesized via a two-step reaction as shown in **Figure 3.1b**. Its molecular structure was characterized by ^{1}H NMR, which is shown in **Figure S3.2** in **Appendix B**. According to the spectrum, the

molecule gave characteristic signals of C═C at 6. 13−6.26 and 5.75 ppm, and $-CH_2CH_2-$ at 3.12 and 3.53 ppm. All integrals showed good consistency with the theoretical values, suggesting the successful synthesis of the monomer.

The composite PAAFC-L hydrogel was then fabricated via a facile one-pot polymerization of AM and AEAM with the existence of F127-CHO, carboxy-functionalized MWCNT and LiCl under a mild condition of neutral pH (7.4) and temperature of 30 °C. The synthetic process and hierarchical 3D network of the hydrogel are schematically displayed in **Figure 3.1c**. In the hydrogel, the intermolecular hydrogen bonding among AM contributes to the construction of the primary polymer network. Through copolymerization with AEAM, the P(AM-co-AEAM) random copolymer forms dynamic imine linkages with the aldehyde groups on the surface of F127 micelles. Meanwhile, electrostatic interactions are generated between the copolymer and MWCNT because of the partially protonated amino groups in AEAM (pKa ~ 8.8)[278, 279] and the completely ionized carboxyl groups on MWCNT (pKa ~ 4)[280] under neutral conditions. LiCl was incorporated to enhance the conductivity of the hydrogel as well as improve its water retention capability. Compared to PAAFC hydrogels using NaCl as conducting ions or without the addition of salts, the PAAFC-L hydrogel shows the slowest water loss rate and the best water retention ability in 30 days under ambient condition, as shown in **Figure S3.3**. The water content of prepared hydrogels was around 74%. (**Table S3.1** in **Appendix B**)

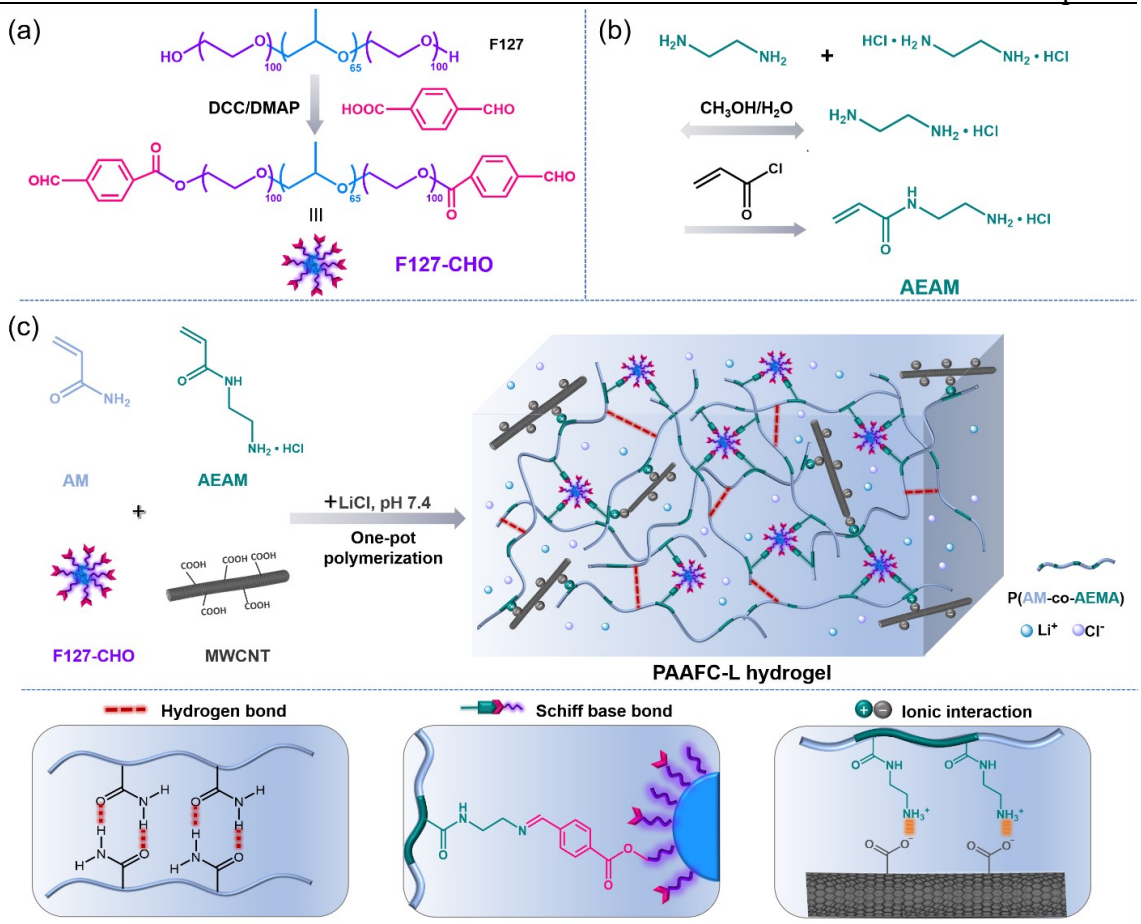

Figure 3.1. Synthesis routes of (a) aldehyde-modified F127 (F127-CHO) and (b) 2-aminoethyl acrylamide hydrochloride (AEAM). (c) Schematic illustration of the synthetic process, hierarchical network and dynamic interactions involved in the network construction of the hybrid PAAFC-L hydrogel.

3.3.2 Mechanical Properties

The mechanical strengths and stretchabilities of the hydrogels were characterized by uniaxial tensile tests, and their nominal stress-strain curves are presented in **Figure 3.2a**. For pure PAM hydrogel, the tensile strength was relatively low and yielding occurred during stretching followed by plastic flow, suggesting the poor elasticity of the PAM hydrogel. The PAMF hydrogel, which was only composed of AM and unmodified

F127, showed improved stretchability but impaired strength due to the weak interfacial interaction between these two components. When AEAM was introduced to the system (denoted as PAAF), the interfacial bonding was greatly enhanced by the formation of Schiff base linkages, and thereby the hydrogel was effectively reinforced with an almost tripled breaking strength of 0.076 MPa. Further incorporation of a tiny amount of MWCNT (1 mg/L) remarkably increased the strength to 0.147 MPa. The strain upon failure and toughness (**Figure S3.4a** in **Appendix B**) of the composite hydrogel reached high values of 1205% and 0.98 MJ/m^3, respectively. Additionally, no typical yielding and well-defined plastic flow region were observed, indicating an elastomer-like tensile behavior of the PAAFC-L hydrogel. Since the cross-section area of samples would gradually decrease during stretching, the true stress that can better reflect a material's tensile performance was also calculated as shown in **Figure S3.4b** in **Appendix B**. The true breaking stress of PAAFC-L hydrogel ended up being 1.77 MPa which was seven times that of pure PAM hydrogel.

The microscopic morphology of hydrogels, which has an important influence on their mechanical performances, was characterized by SEM and are showed in Figure S5. According to **Figure S3.5a** in **Appendix B**, pure PAM hydrogels demonstrated ununiform porous structure, with pore size differing greatly in different regions. After the incorporation of MWCNTs, micelles and dynamic interfacial bonds, the structure homogeneity is remarkably enhanced, as reflected by the uniform porous morphology of PAAFC hydrogel in **Figure S3.5b** in **Appendix B**. Moreover, the pore size of the composite hydrogel is much smaller than that of PAM, which may be attributed to the multiple cross-linking strategies involved in the hydrogel construction and thereby denser hydrogel networks. Also, MWCNTs can be clearly seen from images at higher magnifications (**Figure S3.5c and S3.5d** in **Appendix B**), where no aggregations of the

nanofillers were observed. The good dispersion of the MWCNTs in the hydrogel matrix makes for its significant reinforcement of the composite hydrogel.

It is worth noting that the interfacial ionic interaction between MWCNT and AEAM plays a critical role in the considerable reinforcement effect of MWCNT. This effect was evidenced by the inferior stretching performance of PAM/MWCNT hydrogel in the absence of AEAM and greatly improved mechanical property of P(AM-co-AEMA)/MWCNT hydrogel (**Figure S3.6a** in **Appendix B**). The effect of other factors like LiCl, pH and nanofiller content on the tensile properties were also investigated. As presented in Figure S6b, the stress-strain curves of hydrogels with 1 M or without LiCl almost overlapped, suggesting an ignorant effect of LiCl at such concentration on the hydrogel's mechanical performance. However, with further increasing LiCl concentration from 1M to 3, 5 and 7 M, both the mechanical strength and stretchability of the PAAFC hydrogels gradually decreased, which can be attributed to the suppression of the electrostatic interactions between MWCNTs and P(AM-co-AEAM) at a higher ionic strength.[281] Therefore, PAAFC-L hydrogel with 1 M LiCl was chosen for electrical and sensing experiments. pH also poses great influence (**Figure S3.6c** in **Appendix B**) on the tensile properties of the hydrogel. The hydrogel prepared at pH 6, under which condition the Schiff base tended to be fully hydrolyzed, showed considerably impaired strength and stretchability, also indicating the essential role the imine bond played in the effective mechanical strengthening of the hydrogel. On the other hand, increasing MWCNT content could improve the hydrogel's tensile strength whereas sacrifice its strain at break and transparency (**Figure S3.6d** in **Appendix B**). Therefore, 1 mg/L was chosen as the MWCNT concentration in the composite hydrogel. The outstanding stretchability and flexibility of the PAAFC-L were also demonstrated by images in **Figure 3.2b**, where a hydrogel knot was manually stretched to 10 times its original length without fracture. In

addition, the shape of the hydrogel quickly recovered after stretching, reflecting its good elasticity.

The elasticity and fatigue resistance of the PAAFC-L hybrid hydrogel were quantitatively characterized by cyclic tensile tests with a range of maximum loading strains. As shown in **Figure 3.2c**, the hydrogel was capable to completely recover both its shape and strength after applying a maximum loading strain of 100% for 100 tensile cycles. Similar excellent recovery behaviors were also observed at 200% and 500% strains. Moreover, when an extremely high strain of 1000% was applied, although a slight decrease of energy dissipation (18 %) was observed for the second cycle, good superposition of the following successive cycles was achieved. The PAAFC-L hydrogel restored 94.2 % of its original shape ((1000%-residue strain)/1000%) and 97% of its primary strength at the 20th cycle, which is comparable to the most elastic hydrogel reported to date.[282] The outstanding elasticity was also revealed by compression experiments. As demonstrated in **Figure 3.2d**, upon compression to a high strain of 90% for 10 cycles, the loading/unloading curves of the hydrogel for all cycles overlapped, indicating 100% recovery of the hydrogel network. The compressive modulus was calculated from the first 5% strain of the compression curve, which gave a value of 18.6 kPa, similar to natural skin. In addition to elastically retrieve from tensile or compressive deformation, the hydrogel could bear the damage from sharp materials. For example, the hydrogel recovered its initial state after cut by a sharp steel blade from top to bottom, with no visible scar left once the blade was removed (**Figure 3.2e**). This excellent cut-resistance signifies the well-crosslinked 3D network of the PAAFC-L hydrogel and its effective energy dissipation upon cutting.[283] The brilliant elasticity of the hydrogel is attributed to the reversible deformation and rapid reassembly of micelles, as well as the dynamic breakage and reconfiguration of the Schiff bases and ionic interactions during

tensile or compressive loading/unloading processes (**Figure 3.2f**).

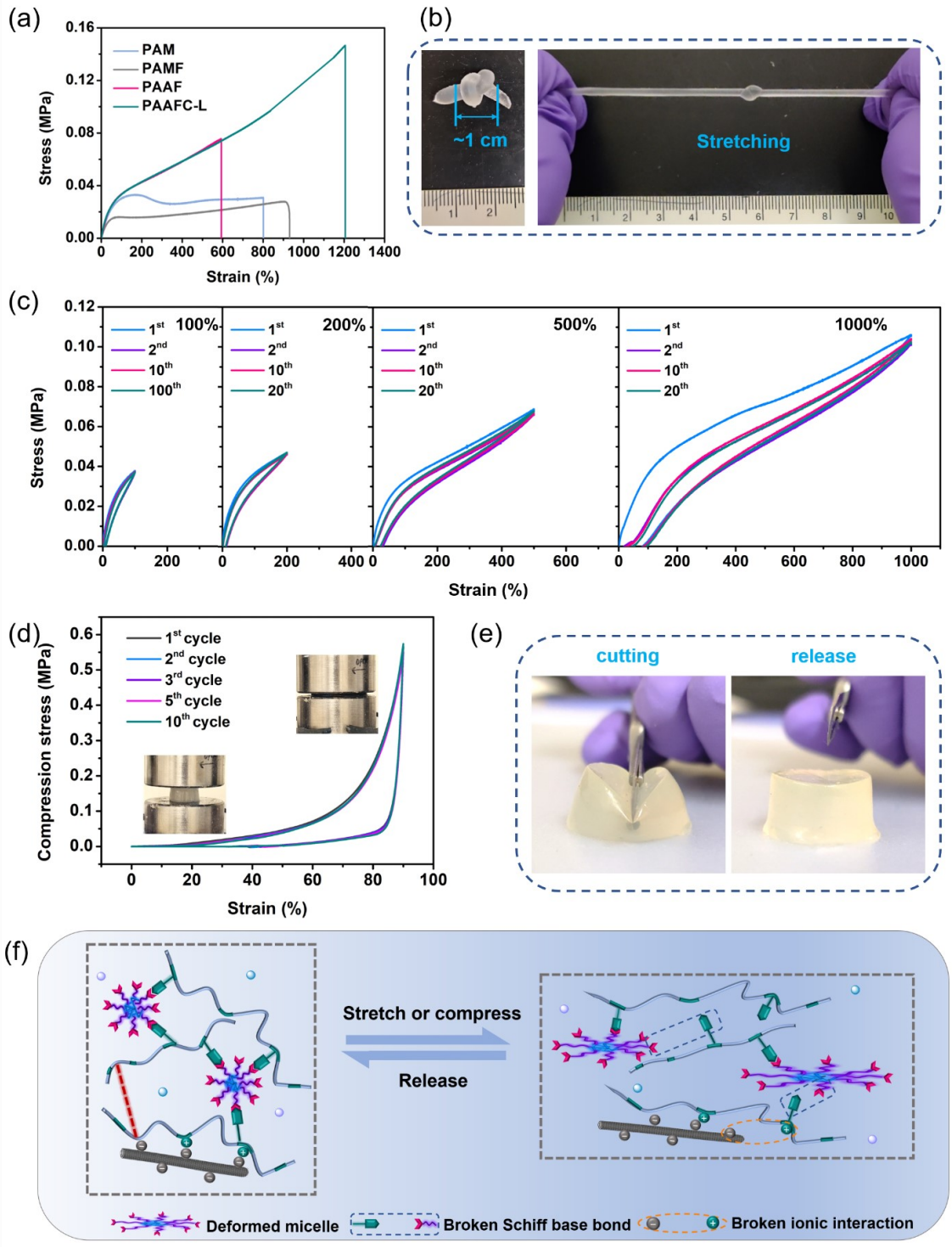

Figure 3.2. Mechanical properties of the PAAFC-L hydrogel. (a) Stress-strain curves of hydrogels with different compositions. (b) Photographs showing a PAAFC-L hydrogel knot being stretched 10 times its original length. (c) Tensile loading/unloading cycles

with various maximum strains for the composite hydrogel. (d) Compression-relaxation cycles with maximum strain of 90%. (e) Images demonstrating a PAAFC-L bulk hydrogel withstood cutting and recovered instantly after release with no visible scar left. (f) Schematic of the proposed mechanism for the tensile and compressive elasticity of the PAAFC-L hydrogel.

3.3.3 Self-Healing Properties

The reversible disengagements of the associations in the hydrogel also endow it with self-healing properties. **Figure 3.3a** and **3.3b** show the rheological characterizations of the self-repairable performance of the hydrogel. In Figure 3a, when oscillatory strain sweep was conducted, the storage modulus (G′) surpassed the loss modulus (G″) in a broad strain range until a high shear strain of 1172% applied, where the crossover of G′ and G″ manifested the rupture of the hydrogel network. This result suggested the capability of the hydrogel to endure large shear deformations. Once the strain reverted to 1%, the network immediately self-healed as indicated by the instant and complete recovery of G′ and G″, indicating fast regeneration of the dynamic interactions in the hybrid hydrogel. The cyclic experiment with shear strain shifted between 1% and 2000% shows the excellent repeatability of the self-healing performance (**Figure 3.3b**).

The hydrogel's self-mending property was also displayed macroscopically by images in **Figure 3.3c**. When the hydrogel specimens (one of them stained to give a color difference) were cut into halves and then brought into contact at room temperature, the adhesion force generated from the dynamic bonds on the interface was strong enough to integrate the fragments into a free-standing gel. The healed hydrogel can instantly support its own weight and bear bending. After healing for 1 h, the gel was able to withstand

stretching of ~200% strain. To quantify the self-healing efficiency, tensile tests were performed on cut and healed hydrogels from one original samples with a healing time of 2, 24 and 48 h, respectively (**Figure 3.3d** and **Figure S3.7** in **Appendix B**). The elongations at break were 291% and 523% for the sample after 2 h and 24 h healing, respectively. The hydrogel allowed to self-repair for 48 h could be stretched over 7 times its initial length and achieved a healing efficiency of 53% (the ratio of breaking strain of the healed specimen to that of the original hydrogel). Although the hydrogel did not reach 100% self-healing, which was limited by the diffusion ability of hydrophobic species across ruptured interfaces,[180] its self-healing efficiency and stretchability after healing outperform most of the elastic hydrogels reported (**Table S3.2** in **Appendix B**).

The self-healing ability was further demonstrated in electrical circuits. In **Figure 3.3e**, a LED bulb was illuminated with a piece of hydrogel as part of the circuit, manifesting the conductive nature of the hydrogel. The light went out once the hydrogel in the closed loop was cut into two halves and appeared again after the two gel pieces brought into contact. Real-time current measurement confirmed the good self-repairing electrical property. As shown in **Figure 3.3f**, the current disappeared when the hydrogel was cut into two fragments, however retrieved the original value after an increase caused by gentle pressure during healing, suggesting the rapid and complete reconstruction of the conductive paths. Moreover, after several cutting-healing cycles, the current could be fully restored, indicating good repeatability of this self-repairable electrical property.

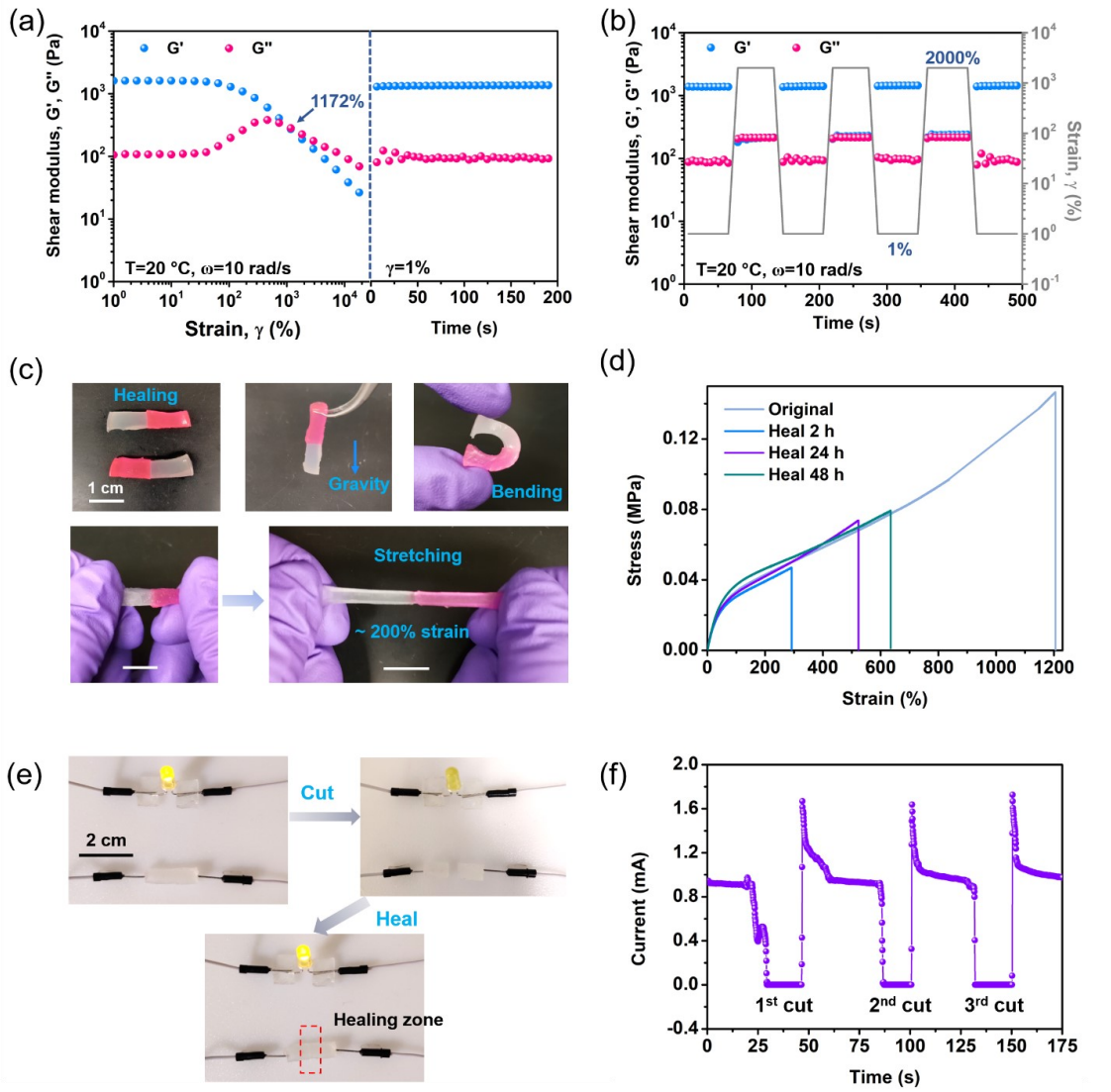

Figure 3.3. Self-healing properties of the PAAFC-L hydrogel. (a) Rheological oscillatory strain sweep of the hybrid hydrogel (left) followed by oscillatory time sweep at a strain of 1% (right). (b) G′ and G″ of cyclic steps with shear strain shifting between 1% and 200%. (c) Optical demonstration of a healed hydrogel withstanding its own weight, bending and stretching. Scale bar: 1 cm. (d) Tensile stress-strain curves of hydrogel samples healing for different time. (e) Illuminance variation of an LED bulb during the hydrogel cut/healing process. The red rectangle indicates the healing zone of the hydrogel, and the scale bar is applied to all three images. (f) Time-dependent current change with the cutting and healing of PAAFC-L hydrogel for several cycles.

3.3.4 Thermo-Responsive Optical Properties

The optical property of the PAAFC-L hydrogel can be readily tuned by temperature. The hydrogel was opaque at 10 °C, became translucent at 20 °C and turned to entirely transparent when heated to body temperature of 37 °C (**Figure 3.4a**). This transparency change was quantitatively characterized by optical spectroscopy in visible light range of 400−800 nm. As demonstrated in **Figure 3.4b** and **3.4c**, the transmittance of the hydrogel remarkably increased with the increasing of temperature, reaching around 90% at 37 °C and then leveling off when further raising the temperature. Moreover, such optical transition process occurred rapidly in air and was highly repeatable, as displayed in **Figure 3.4d**, where a hydrogel sample shaped as capital letters of "UA" was successively float on a 37 °C water bath and an ice-water bath for several cycles. The optical property shift of the hydrogel was most likely attributed to the size change of F127 micelles with temperature, where the sizes of unmodified F127 and F127-CHO at various temperatures were detected by DLS and the results are shown in **Figure S3.8** in **Appendix B** and **Figure 3.4e**, respectively. Both the micelles displayed thermo-sensitive size distribution, however, in different manners. The unfunctionalized F127 micelle was small at low temperatures (< 25 °C), while exhibited growth as the temperature further rose. This result is due to the dehydration of PEO heads of F127 at elevated temperatures, thus reducing steric repulsions between the heads and allowing more molecules to associate in a micelle.[276, 284] In contrast, for aldehyde terminated F127 (F127-CHO), below the critical temperature of 25 °C, the size greatly increased as compared to that of F127, which may be attributed to the increased hydrophobicity of the PEG head due to the existence of benzaldehyde groups and thereby led to the formation of micelle clusters. The generation of aggregates at relatively low temperatures was evident in AFM topography images of F127-CHO prepared at 20 °C (**Figure 3.4f**), while homogeneous

dispersed small micelles of F127-CHO were observed at 60 °C (**Figure 3.4g**). Therefore, the thermo-tunable optical property of the hydrogel can be interpreted in terms of the local hydrophobic domains formed through the thermo-induced phase transition of the F127-CHO micelles, which also led to slight increase of G′ of the hydrogel during cooling from 60 to 10°C, as displayed by rheological temperature sweeps in **Figure S9a** in **Appendix B**. Temperature also poses a significant influence on the self-healing behavior of the hydrogel. As shown in **Figure S9b** in **Appendix B**, the hydrogel showed the highest self-healing efficiency at room temperature, both lowering and raising temperature would impair the stretchability of self-healed PAAFC-L hydrogel. The demonstrated tunable whiteness of the hydrogel broadens its applications such as in the field of switchable color display.[122]

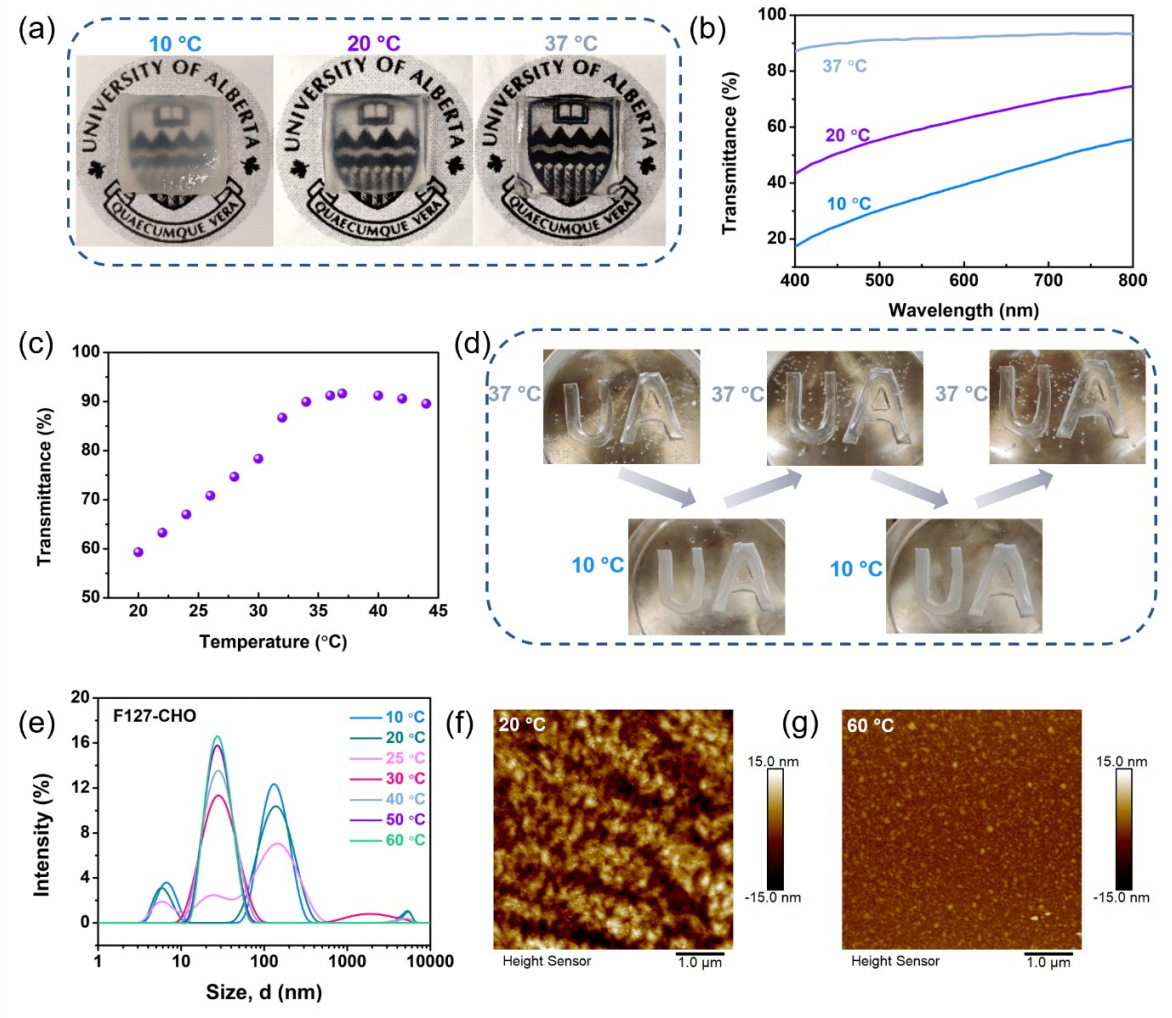

Figure 3.4. (a) Photographs showing the thermo-responsive optical property of PAAFC-L hydrogel. (b) Optical spectra in visible light range of the hydrogel at 10, 20 and 37 °C. (c) Transmittance change at 550 nm for PAAFC-L hydrogel with the increasing of temperature. (d) Images demonstrating the repeatability of the temperature-tunable transparency variation of PAAFC-L hydrogel shaped as "UA". (e) DLS size characterizations of F127-CHO micelles at various temperatures ranging from 10 to 60 °C. AFM topography images of F127-CHO micelles prepared at (f) 20 °C and (g) 60 °C.

3.3.5 Electrical Properties

The conductivities of the hydrogels were calculated from the electrochemical impedance spectra (**Figure S3.10** in **Appendix B**) measured by an electrochemical workstation. As shown in **Figure 3.5a**, the conductivities of pure PAM and PAMF hydrogel were relatively low (~0.08 S/m) due to the absence of ions. When AEAM was introduced to the hydrogel, the values were greatly enhanced to 0.66 S/m because of the existence of counterions to protonated amino groups. Further incorporation of MWCNT, however, did not further enhance the conductivity, suggesting no electric conductive paths formed by MWCNT due to its low content. After 1 M LiCl was incorporated, the electrical conductivity was dramatically improved to 3.96 S/m, which is higher than that of many reported gel ionic conductors.[283] **Figure 3.5b** shows the relative resistance change $\Delta R/R_0$ (equals to $(R-R_0)/R_0$) of the PAAFC-L hydrogel to the applied tensile strain. Following previous studies,[250, 285] the experimental data were fitted into a parabolic equation $y = A\varepsilon^2 + B\varepsilon$ with high correlation (r^2=0.9999), where y represents the relative resistance change and ε is the tensile strain. The gauge factor, which reflects the sensitivity of the resistance change with strain, was thus calculated from the differentiation of the fitting curve (**Figure S3.11a** in **Appendix B**). The value increased with the stretching of the hydrogel, being 1.07 at 100% strain and reaching 2.32 at 900% strain. The moderate gauge factor values ensured good sensitivity of the hydrogel, and meanwhile retained its conductive nature upon applying extremely high strains, enabling a wide workable strain range (0−930%) of the conductor.

The repeatability of the strain-sensitive electrical performance was then evaluated by cyclic tests. As demonstrated in **Figure 3.5c**, the hydrogel shows stable and

reproducible response signals after 100 successive cycles of 100% strain as indicated by the well-preserved amplitude. Benefiting from the elastic nature of the PAAFC-L hydrogel, no obvious hysteresis was observed during tensile loading/unloading processes (**Figure S3.11b** in **Appendix B**). Furthermore, identical waveforms in each cycle were also obtained when larger strains of 200% and 500% were applied for 20 cycles (**Figure 3.5d**). Besides responding to tensile strains, the hydrogel displays high sensitivity to pressures or compressive strains, where $\Delta R/R_0$ value decreased with the compression of the sample, as demonstrated in **Figure 3.5e** and **Figure S3.12a** in **Appendix B**. The pressure sensitivity of the hydrogel is 0.25 kPa^{-1} at low pressures (< 2 kPa) and remains to be 0.053 kPa^{-1} at higher pressures (~ 5 kPa), indicating its wide workable pressure range. Similarly, stable and repeatable pressure response signals were obtained when cyclic pressure loading of 3 kPa (compression strain of 10%) was applied to the hydrogel for 100 successive cycles (**Figure S3.12b** and **S3.12c** in **Appendix B**). Combining the excellent stretchability, skin-mimetic modulus, brilliant fatigue resistance and good electrical performances, the hydrogel is therefore promising to act as soft electronic devices, especially for applications that experience constant large deformations like wearable sensors. Moreover, together with its self-healing and thermo-responsive properties, the PAAFC-L hydrogel that processes multiple desirable features stands out of the reported elastic hydrogels (**Table S3.2** in **Appendix B**), which enables it to serve as a great candidate for more durable and reliable smart electronics.

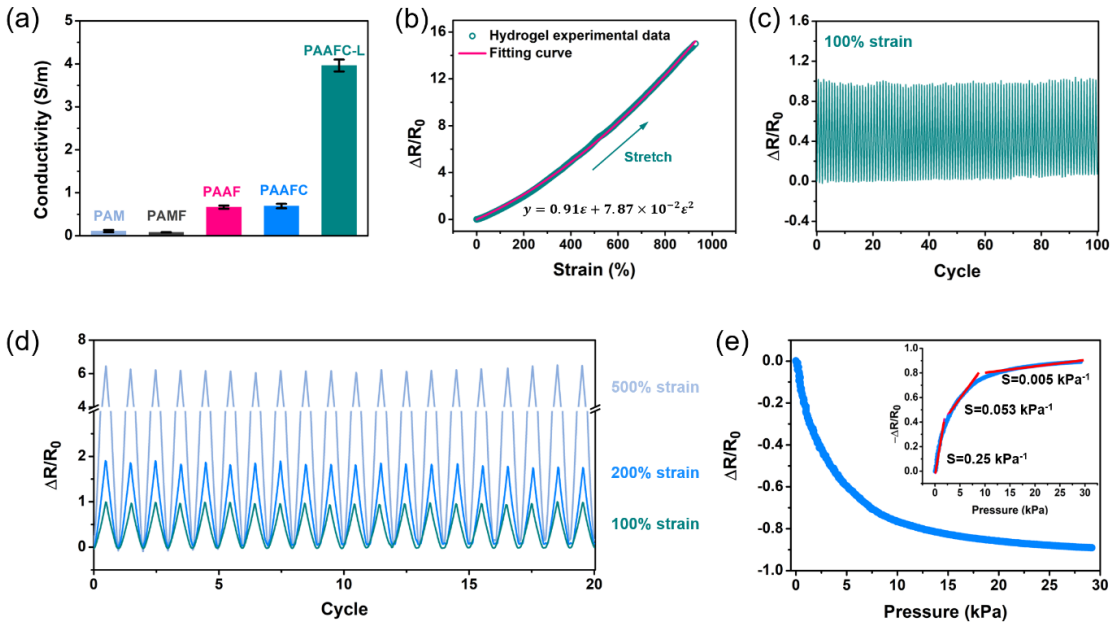

Figure 3.5. (a) Conductivities of hydrogels with different compositions. (b) Relative electric resistance change as a function of tensile strain for the PAAFC-L hydrogel. (c) Relative resistance response under repeated loading-unloading processes with maximum strain of 100% for 100 cycles. (d) Cyclic relative resistance variations with maximum strain of 100, 200 and 500%. (e) Relative resistance changes as a function of pressure for the hydrogel. Insert figure showing the pressure sensitivity (S) of the hydrogel at different pressure ranges.

3.3.6 Sensing Performances

To demonstrate the hydrogel's practical application as a wearable strain/pressure sensor, it was directly mounted on diverse parts of the human body (**Figure 3.6a**) to monitor a wide range of human activities in real time. **Figure 3.6b** shows the relative resistance change of the hydrogel with the bending of the forefinger. Apparent relative resistance variations were observed when the bending angle was sequentially set as 15°,

30°, 60° and 90°. Also, at each specific angle, the electrical signals were highly repeatable and stable. Similarly, when the hydrogel sensor was attached to other joints like wrist, elbow and knee, the bending of the joints can be detected sensitively and repeatedly, as shown in **Figure 3.6c, 3.6e** and **3.6f**, respectively. This desired strain-dependent sensing property allowed the hydrogel to recognize fine human activities such as handwriting. As displayed in Figure 6d, when a tester wrote capital letters of "A", "B" and "C" with the hydrogel sensor mounted on the wrist, the corresponding electrical patterns of each letter were highly reproducible and could be clearly distinguished from the others. In addition, precise recognition of human walking and running was achieved by the differentiated frequencies of the resistance change and waveforms of the signals (**Figure 3.6g**). Large human motions like squat and sitting can also be readily detected as displayed in Figure 6h and 6i, respectively.

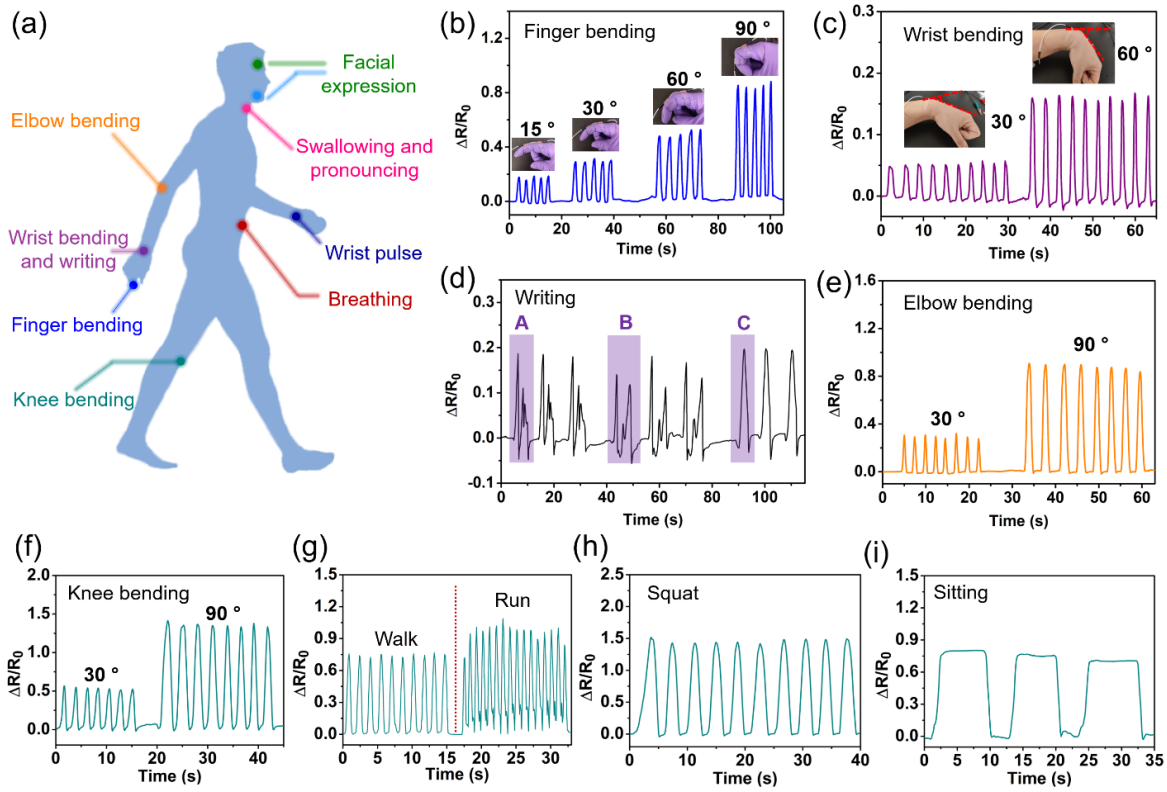

Figure 3.6. Real-time monitoring of human motions by the PAAFC-L hydrogel electronic sensor. (a) Schematic showing the sensing locations. Signals of relative electric resistance during (b) finger bending, (c) wrist bending, (d) handwriting, (e) elbow bending, (f) knee bending, (g) walking and running, (h) squatting, and (i) sitting.

Taking advantage of the excellent sensitivity of both tensile strain and pressure, where easily distinguishable positive and negative $\Delta R/R_0$ values were shown, respectively, the hydrogel sensor was then exploited to discern subtle human motions. As shown in **Figure 3.7a**, when a piece of hydrogel was attached to the volunteer's throat, the pressure caused by swallowing generated corresponding electric variations that could be clearly distinguished, which gave incredibly detailed information of the throat movement. In addition, tiny yet complicated muscle movements involved in speaking can also be recorded accordingly. **Figure 3.7b** shows the time-dependent relative resistance

change curves with the tester pronouncing different phrases of “hello”, “how are you”, “hydrogel” and “sensor”, where distinct and repeatable characteristic signal was obtained for each phrase. Besides, facial expressions recognition has been readily realized as shown in **Figure 3.7c** and **3.7d**. In **Figure 3.7c**, when the tester made expressions like frowning and astonishing, the corresponding relative resistance variations exhibited opposite valleys and peaks as a result of the compression and stretching of the hydrogel sensor, respectively, indicating the high sensitivity of the hydrogel device. Similarly, expressions of smiling and laughing can be recognized by the disparate intensity of the $\Delta R/R_0$ value (**Figure 3.7d**). Furthermore, the hydrogel sensor was used for real-time tracking of human physiological signals like breathing and radial artery pulse by assembling it on the tester’s tummy and over wrist radial artery, respectively (**Figure 3.7e** and **3.7f**). Notably, as shown in **Figure 3.7f**, the wrist pulses that reflect the complicated blood flow and heartbeat information were detected with excellent sensitivity and accuracy. In relaxation, the pulse gave electrical signals of well-defined percussion peak, dicrotic notch associated with the close action of the valve in heart, and dicrotic peak in each beat (**Figure 3.7g**), which were typically obtained from healthy people.[286] After exercise, not only the pulse rate increased from 73 beats/min to107 beats/min. Also, the pulse pattern change was acquired from “moderate” to “taut” with an elevated tidal peak shown up (**Figure 3.7h**), according to classification in traditional Chinese pulse diagnosis (TCPD).[287] This waveform alternation is due to the straining of subject’s muscle that led to increased systolic pressure.[288] Such high sensitivity for pulse waveform detection has seldom been reported in simple hydrogel systems.

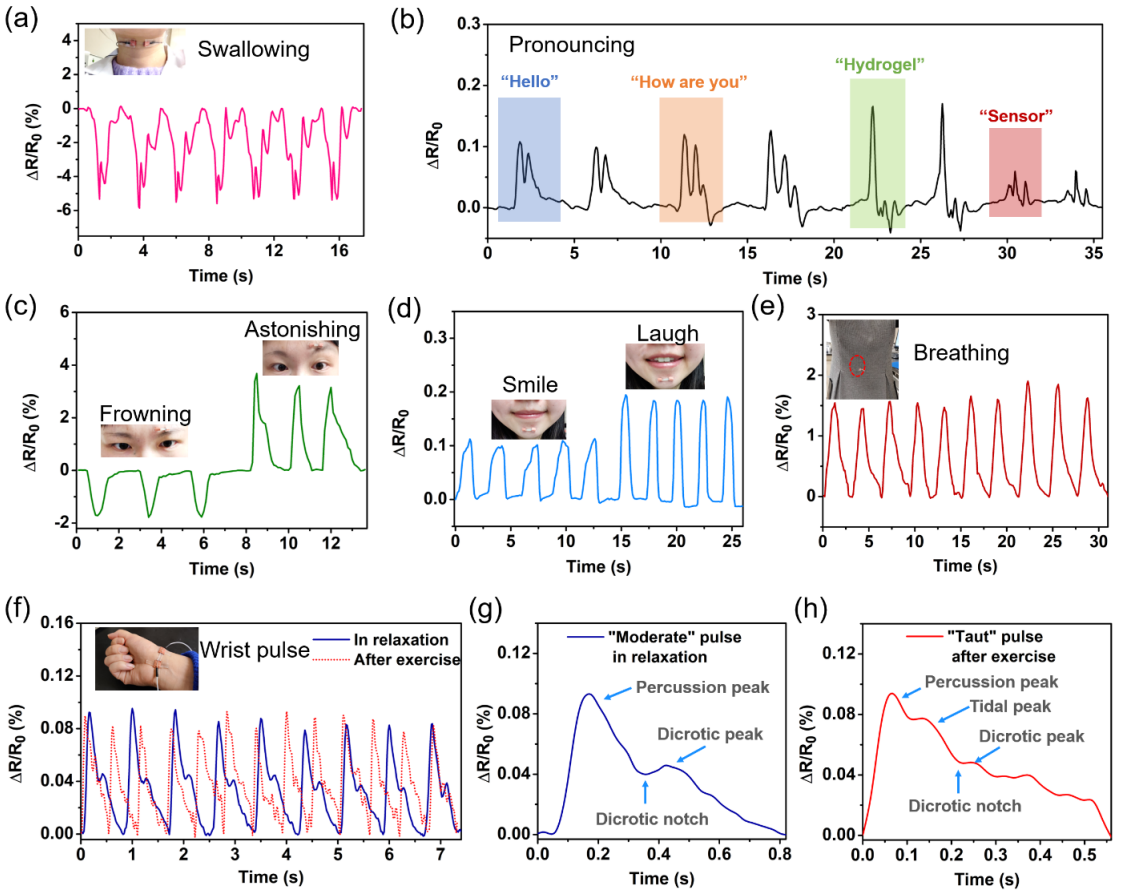

Figure 3.7. Real-time tracking of human subtle physiological signals by the PAAFC-L hydrogel electronic sensor. Time-dependent relative resistance variations during (a) swallowing, (b) speaking different phrases, (c) making expressions of frowning and astonishing, (d) smile and laugh, (e) breathing with the hydrogel sensor attached on the tummy, and (f) wrist pulse before and after exercise. Variations of wrist pulse patterns: (g) "moderate" pulse with unnoticeable tidal wave before exercise and (h) "taut" pulse with a high tidal peak after exercise.

Next, to further demonstrate the hydrogel's potential application in real life, the PAAFC-L hydrogel sensor was integrated with a sleep mask to make a "smart" eye mask for real-time monitoring of human sleep. The experimental setup is shown in **Figure 3.8a**. The hydrogel sensor surface was covered by a thin layer of polyethylene film to

segregate it from the eyelid, which could avoid possible irritation to the skin as well as minimize water loss from the hydrogel. Eye and head activities that might occur during sleep were first detected during awake state of a healthy subject. There are mainly two types of eye movement involved in sleeping process. One is slow, rolling or pendular eye movements and the other is rapid and jerky ocular movements with the latter occurring during Rapid Eye Movement (REM) sleep.[289] These two kinds of eye movement can be clearly distinguished by the different relative resistance variation signals caused by pressure change, as shown in **Figure S3.13a** and **S3.13b** in **Appendix B**. Since light sleep stage generally features head and body movements,[290] the electrical signals of head movements were also recorded and displayed much larger amplitude of $\Delta R/R_0$ than that of eye movements (**Figure S3.13c** in **Appendix B**). The one-night sleep of the subject was then recorded as shown in **Figure 3.8b**. The sleep process was divided into three stages: deep, light and REM sleep as marked in different colors in **Figure 3.8b**. Light sleep was differentiated from a deeper stage of sleep according to its relatively frequent head movement signals. Particularly, the smart sleep mask shows excellent sensitivity for the detection of rapid eye movement (REM) sleep that is associated with intense neuronal activity and dreaming and thereby of high research and public interest, giving signals with obviously recognizable boundary between REM and deep sleep (**Figure S3.13d** in **Appendix B**). Compared to the sleep recorded by a popular sleep monitoring mobile app "Sleep Monitor" (**Figure 3.8c**) that measures sleep only based on the body movements and voices, the sleeping process measured by the smart sleep mask shows much higher reliability for the recognition of REM sleep. Total REM time was calculated to be 1 h 55 min (28% of total sleep time), in good accordance with the previously reported average REM sleep time (~25% of total time asleep) for healthy people between 25 to 50 years old.[291] In addition, compared to Polysomnography (PSG) that has been usually used to

monitor sleep in hospital,[290] the sleep mask is much less costly, easier to apply and non-intrusive to sleep itself, thus being more applicable to the general public. Owing to the outstanding sensing performances, the PAAFC-L hydrogel sensor is promising for a broad range of applications ranging from wearable sensors for health care, sports and disease diagnosis to artificial electronic skins.

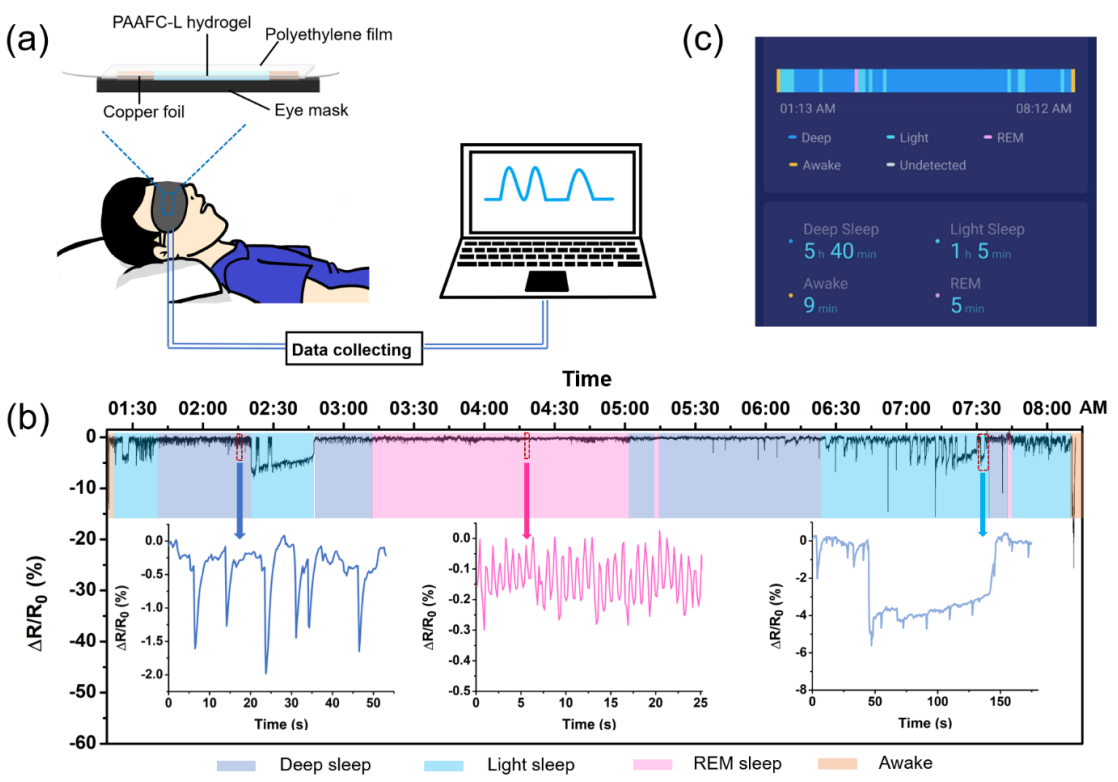

Figure 3.8. (a) Scheme showing the experimental setup of the sleep monitoring experiment. (b) One-night relative resistance changes with time during sleeping. Left insert figure indicating the slow rolling or pendular eye movements during deep sleep. Middle insert figure showing the rapid and jerky eye movements during REM sleep. Right insert figure demonstrating head movement signals during light sleep. (c) Sleep record obtained from the mobile app "Sleep monitor".

3.4 Conclusions

In this work, we have prepared an ultra elastic, stretchable, self-healing and stimuli-responsive ionic conductive hydrogel PAAFC-L. The hydrogel was fabricated via facile one-pot free radical polymerization of AM and amine-containing monomer AEAM, with the presence of aldehyde-functionalized F127 micelles, MWCNT and LiCl. Through the Schiff base bonds between AEAM and F127-CHO as well as the ionic interactions between AEAM and MWCNT, the hydrogel possesses robust and dynamic interfacial bonding which results in outstanding mechanical properties and self-healing capability. The as-prepared hydrogel PAAFC-L can be stretched over 13 times its original length and almost fully recover from an extremely high strain of 1000% with in 1min. Additionally, the PAAFC-L hydrogel completely restores its shape and strength after compression to 90% strain and shows superior damage resistance to sharp materials. Moreover, the autonomously self-healed PAAFC-L hydrogel samples can withstand stretching over 7 times its original length. Very interestingly, the PAAFC-L hydrogel's optical properties can be readily tuned by thermal stimuli, that is, being translucent at room temperature while turning into entirely transparent at body temperature of 37 °C. Electrical characterization evidenced the high sensitivity of the hydrogel in broad strain and pressure windows. This multifunctional PAAFC-L hydrogel was successfully applied as a flexible sensor to monitor a variety of human activities including large motions and tiny physiological signals. Notably, when employed for the acquisition of wrist radial artery pulses, the hydrogel sensory device detected about not only the frequency of the beats but also ultra-detailed pattern of each pulse, which has seldom been reported in previous hydrogel sensory systems. The hydrogel was also integrated with a sleep mask to monitor human sleep and showed excellent reliability for the detection of REM sleep.

Therefore, the ultrasensitive smart hydrogel sensor is promising for a variety of applications including health and sports monitoring, disease diagnosis, remote control through vocal or facial recognition, artificial muscles and skins, soft robotics, etc. The developed strategy of combining dynamic covalent chemistry with nanofiller reinforcement and micelle crosslinking opens up new prospects for designing highly sensitive soft electronic sensors.

CHAPTER 4 Ultra Stretchable, Tough, Elastic and Transparent Hydrogel Skins Integrated with Self-Evolving Sensing Functions Enabled by Machine Learning Algorithms

4.1 Introduction

Human skin is soft, mechanically tough, stretchable, elastic, capable to feel a variety of environmental changes such as pressure, strain, temperature, etc. To develop artificial skin-like materials that imitate the properties and functions of our skin is of great significance, and has attracted growing attentions.[292-294] Among the various mimics of different sophistication, "ionic skins", which are ionic conductive skin-mimetic materials, emphasize the flexible and sensory properties of the skins, and thereby find a broad range of applications in the fields of wearable sensors, soft robotics and machines, personal health monitoring and diagnosis, triboelectric nanogenerators, etc.[131, 295-298] Especially, ionic conductive hydrogels, simulating the natural skins in various aspects like water abundance, stretchability, softness and biocompatibility, are ideal ionic skins.[246, 299]

Skins are tough and elastic while traditional hydrogels are generally fragile and/or undergo plastic deformation upon large strains. Despite great efforts dedicate into ionic skins with a range of systems developed including polyacrylamide/NaCl hydrogel[295], polyacrylic acid/alginate/amorphous $CaCO_3$ hydrogel[131] and so forth, to develop hydrogel ionic conductors that combine the decent mechanical performances and sensitive feeling abilities of skins is still a great challenge. Tough hydrogels, through their elegant network design, can achieve high strength and toughness, and thus are promising for ionic skins. Multiple strategies such as construction of double-networks (DN),[60, 136, 180] introduction

of nanofillers,[165, 168, 181] assembly of anisotropic structures,[182-184] using oppositely charged polyelectrolytes[47] and integration of micelle cross-linking[51, 178, 179] have been adopted for the fabrication of tough hydrogels. Among these approaches, introducing nanofillers to construct nanocomposite (NC) hydrogels, which can simultaneously provide effective energy dissipation and increase homogeneity of the gel networks, is an effective yet facile way to enhance the hydrogels' mechanical performances.[33, 300]

Besides the strong, elastic and tough features, it is highly desirable to design tough hydrogels with skin-like low elastic moduli and high stretchability to achieve good sensory capabilities comparable to human skin, to ensure conformable contact with curved surfaces and to avoid mechanical mismatch with tissues.[18, 131, 301, 302] However, many existing tough hydrogels with good strength are too stiff for applications as skin-like sensors. On the other hand, our skin can autonomously heal from wound. It is of great interest for a skin-mimetic material of high sophistication to be self-healing, which can significantly prolong its lifespan and enhance its reliability.[34, 303, 304] Another desirable feature for ionic skins is the transparency, which renders the materials with the ability to transmit optical signals and therefore considerably broadens their applications.[305] Regrettably, a majority of the current high-performing tough hydrogels are not or only partially transparent due to the existence of associated micro domains, high loadings of nanofillers or anisotropic structures.

Here, we have developed a new class of ionic skins based on tough NC hydrogels that demonstrated a wide range of attractive features including ultra stretchability, high toughness, skin-mimetic moduli, elasticity, self-healing property, transparency, fatigue resistance and great sensing performances. The materials were fabricated by a simple one-step free radical polymerization of acrylamide (AM), an amino-functionalized monomer and a quaternary ammonium-bearing monomer in the presence of small

amounts of carboxyl-modified multiwalled carbon nanotubes (MWCNTs) and LiCl. In the hydrogel, hydrogen bonding between acrylamide comprises the primary network. MWCNT was selected as a reinforcement agent for our NC hydrogel due to its large aspect ratio and ultra-high mechanical strength. However, high loadings of the MWCNTs will inevitably darken the material. It is a challenge for MWCNTs of a low concentration to effectively reinforce the material and lead to a transparent hydrogel, which might be achieved by the introduction of strong and dynamic interfacial interactions. In this work, the interfacial connection between the polymer and the reinforcement agent, the MWCNTs, was built by introducing dual electrostatic interactions between carboxyl groups on MWCNTs and the two cationic comonomers. Benefiting from the efficient force transduction within the gel network, a trace amount of MWCNTs could remarkably improve the resultant NC gel's mechanical performances with toughness reaching up to 46.9 times that of PAM hydrogel and stretchability up to 4075%. The two ionic interactions play different roles in the hydrogel network. The strong amine-carboxylate interaction acts as relatively permanent crosslinkers while the weak quaternary ammonium-carboxylate crosslinkings break/reform reversibly to dissipate energy upon deformation, as confirmed by atomic force microscopy (AFM) force measurements. Meanwhile, considering that high salts loadings in ionic skins might impair the materials' biocompatibility or cause skin irritation,[306] LiCl of a low concentration was added into the system, which not only ensures the excellent sensory capabilities but also demonstrates positive effect on the gel's toughness. The desired combination of mechanical and electrical properties enables the skin-like hydrogel sensor with brilliant sensibility and cycling stability. Strains during human motions and subtle wrist pulsing were accurately detected. Small pressures originated from water droplets falling were also sensitively discerned. Moreover, a complete platform to recognize handwriting in

two manners (writing on paper and in air) was developed for the first time, which shows high recognition accuracies from writing single letters to more complicated words, phrases and short sentences. Taking advantages of the facile one-step synthesis, tough yet soft nature, decent sensory performances, and integration of the favorable self-healing and transparent properties, the developed skin-like hydrogels hold great potential for various applications including intelligent and wearable sensors, health diagnosis and soft robotics.

4.2 Experimental Methods

4.2.1 Materials

Acrylamide (AM, 99%), 2-methacryloyloxy ethyl trimethylammonium chloride (MTAC, 80 wt% in water solution), acryloyl chloride (97%), ethylenediamine (99%), ethylenediamine dihydrochloride (98%), hydrochloric acid (HCl, 37%), MWCNT (> 8% carboxylic acid functionalized, average diameter × length: 9.5 nm × 1.5 μm) and 2,2'-azobis(isobutyramidine hydrochloride) (AIBA, 97%) were purchased from Sigma-Aldrich and used as received. Lithium chloride (LiCl, 98.5%) and all solvents were purchased from Fisher Scientific and used as received.

4.2.2 Synthesis of Amine-Modified Monomer (AEAM)

The amine-functionalized monomer, 2-aminoethyl acrylamide hydrochloride (AEAM), was synthesized following the method reported in our previous research. Briefly, ethylenediamine dihydrochloride (30 g, 0.226 mol), Milli-Q water (120 ml) and ethylenediamine (31.9 g, 0.532 mol) were mixed and allowed to react for 1 h at room temperature under stirring, followed by the addition of methanol (160 ml) and reaction for another 1 h. After cooling the system to -20 °C, acryloyl chloride (48.1 g, 0.532 mol)

was slowly added to the mixture within 2 h, followed by stirring for another 1 h. HCl (37 %) was then added to adjust the pH of the system to 1−2. After removal of the solvents under vacuum and lyophilization, the resultant solid was dissolved in isopropanol and filtrated. The filtrate was crystallized at –20 °C and recrystallized twice. Finally, the raw product was precipitated from THF to obtain a white powder. The chemical structure of the monomer was confirmed by ^{1}H NMR spectrum on an Agilent 400-MR DD2 NMR spectrometer with D_2O as the solvent.

4.2.3 Preparation of Hydrogels

The hydrogels were prepared through one-pot polymerizations. To achieve the optimal mechanical and electrical performances, a series of hydrogels with various ratios of MTAC to AEAM (MT:AE), LiCl concentrations and carboxyl-functionalized MWCNT contents were synthesized and characterized. For a typical synthetic process of 1.8 ml composite hydrogel with MT:AE of 7:3, 50 mM LiCl and 2 mg/L MWCNT, acrylamide (0.6 g), MTAC (0.07 g) and AEAM (0.03 g) were mixed in 1.6 ml of MWCNT dispersion (2 mg/L) with 50 mM LiCl dissolved in, followed by the addition of ~ 10 μL 1 M NaOH solution to adjust the pH to ~7.4. After purging with nitrogen for 20 min and the addition of the initiator, AIBA (8 mg dissolved in 0.2 ml MWCNT dispersion), the mixture was allowed to react overnight at 30 °C. The resultant hydrogel was denoted as PAMAC-L, where PAMA is the copolymer of AM, MTAC and AEAM, C represents the MWCNT, and L refers to LiCl.

4.2.4 Transparency and Micromorphology of Hydrogels

The transparency of the composite hydrogel was measured using ultraviolet-visible (UV-Vis) spectroscopy (Thermo Evolution 300 UV-Vis) with a hydrogel sample thickness of 3 mm. The micromorphology of the hydrogel cross-section was

characterized using a Zeiss Sigma field emission scanning electron microscope (SEM) at an acceleration voltage of 10 kV. For the preparation of SEM samples, hydrogel strips were first quenched in a liquid nitrogen bath, cut into two pieces and cryo-dried, followed by the sputtering of gold prior to imaging.

4.2.5 Mechanical Properties of hydrogels

The mechanical performances of the hydrogels were characterized on an AGS-X universal tensile testing machine (Shimadzu, Japan) equipped with either a 50 N load cell for tensile tests or a 5000 N load cell for compression characterizations. For tensile tests, rectangular hydrogel specimens with dimensions around 20 mm (length) × 4 mm (width) × 0.8 mm (thickness) were used, and a constant crosshead speed of 50 mm/min was applied. Cyclic tensile measurements were performed at various predetermined maximum strains. The wait time between cycles was set to be 20 s for 100% and 60s for other strains, respectively. All the tensile tests were conducted at room temperature (20 °C) and humidity around 60%. A thin layer of Vaseline was applied on the surfaces of the hydrogels to avoid moisture loss. The cyclic compression performances of hydrogels were characterized with cylindrical specimens (diameter of 17 mm and height of 10 mm) at a constant compressing rate of 5 mm/min and room temperature. The interval between cycles was set to be 60 s.

4.2.6 AFM Characterization

To better understand the intermolecular interactions involved in the construction of the hydrogel networks, a nanomechanical tool, AFM, was employed to quantitatively characterize the intermolecular forces. Other than the hydrogen bonding between AM, the ionic interactions between the carboxyl groups on MWCNT and two cationic moieties

(amino groups of AEAM and trimethylammonium groups of MTAC) on the copolymers were proposed to play critical roles in the formation and reinforcement of the hydrogel. Therefore, to measure these two ionic interactions, first, two copolymers, i.e., the copolymer of AM and MTAC (PAM-MT) and the copolymer of AM and AEAM (PAM-AE) were synthesized following the same procedure that of the hydrogel synthesis and the same acrylamide to functional monomers weight ratio (6:1). Next, freshly cleaved mica sheets were immersed in the copolymer solutions (0.1 wt% polymer dissolved in 100 mM NaCl solution) for 24 h to obtain PAM-MT- or PAM-AE-coated surfaces. The surfaces were washed with DI water for 3 times to remove free polymer chains and dried with nitrogen blow. The surface morphologies were confirmed by AFM imaging.

The interaction forces were then measured between the polymer-coated mica surfaces and carboxyl-functionalized AFM tips in Phosphate Buffer solution (PB, 5 mM that is similar to the salinity in PAMAC hydrogel) at a neutral pH of 7.4 with different LiCl salinity, using an MPF-3D AFM (Asylum Research, Santa Barbara, CA, USA). The COOH-coated AFM tips were prepared by immersing the AFM tip (NPV-10, Bruker, Santa Barbara, CA) in 6-mercaptohexanoic acid solution (10 mM, in anhydrous ethanol) for 2 h followed by water/ethanol wash to remove the loosely bonded residues.[307, 308] After positioning the COOH-coated AFM tip over the polymer-coated mica surfaces, in a typical force measurement experiment, the AFM cantilever was first driven to approach the mica surface at a fixed velocity of 2 μm/s until a pre-set force load of 5 nN was reached, and then retracted from the substrate to obtain a force-distance curve. In the experiment, the force was calculated from the deflection and spring constant of the AFM cantilever via the Hooke's law, with the deflection detected through a laser beam reflected onto a 4-quadrant photodiode detector. Force mapping was conducted on a 20 μm x 20 μm surface to obtain more than 50 force curves for the calculation of the average

adhesion forces between the cationic copolymers and the carboxyl groups.

4.2.7 Self-Healing Performances of Hydrogels

The self-healing capability of the PAMAC-L hydrogel was investigated by bringing two hydrogel pieces into contact with one of them stained by methyl orange to give a color difference. Rheological experiments were also carried out to quantitatively evaluate the self-repairing behavior of the hydrogel on a stress-controlled rheometer (TA Instruments, AR-G2) using a plate-plate geometry (20 mm diameter) at a gap of 200 μm. First, oscillatory strain (γ) sweep was performed with γ ranging from 1 to 3000% to rupture the hydrogel network at a constant angular frequency (ω = 10 rad/s), followed by an oscillation time sweep at a small strain (1%) to allow the recovery of the network. The repeatability of the self-healing process was assessed by cyclic strain experiment with the strain shifted between 1% and 1000% for three cycles. In addition, the electrical self-healing performances of the hydrogel were investigated by monitoring the cutting-healing processes using either the light-emitting diode (LED) illumination with a hydrogel strip as part of an electrical circuit or the current change measured by an electrochemical workstation (CHI920, CH Instruments, USA). All self-healing experiments were conducted at room temperature.

4.2.8 Electrical and Sensing Performances

The electrical conductivity (σ) values of the hydrogels were calculated by electrochemical impedance spectroscopy measured on the electrochemical workstation in a frequency range of 10^{-1}–10^{6} Hz with an amplitude of 5 mV at open circuit voltage, following the equation 3.1 in chapter 3. The tensile strain and pressure sensitivities of the PAAFC-L hydrogel were determined by the real-time current vs time (I–t) curves recorded during the stretching or compression process at constant speeds same with those

for mechanical tests. Cyclic tensile and compressing experiments were also carried out to evaluate the electrical signal repeatability of the hydrogel, where the testing speed was set to be 150 and 20 mm/min for tensile and compressing cycles, respectively. The relative resistance changes were calculated from the I−t curves according to the following equation 3.2 in chapter 3. Next, the PAMAC-L hydrogel integrated with copper foils and conductive wires were used for the sensing of human activities like finger bending and physiological signals such as wrist pulses, and for the detection of finger pressing and water dropping.

4.2.9 Handwriting Recognition

To further explore the practical application of the PAMAC-L hydrogel, the hydrogel sensing system was used for the monitoring of human writing processes and the recognition of handwriting. By mounting the hydrogel device on the forefinger of the tester, the finger motions reflecting the writing activity were recorded through real-time I−t curves. Two manners of writing, i.e., handwriting on paper and writing using the forefinger in air, were monitored. The collected current signals were then processed in a self-developed software which was written in Matlab R2021b. For the recognition of writing signals, first, multiple current signals for each of the 26 letters from a to z were collected and used for the training of models through the Machine Learning toolbox of Matlab. For the model training, the peak features of each letter were extracted first, trained in the Machine Learning toolbox using all available algorithms and the model showing the best predicted accuracy (Ensemble Classifier: Bagged Trees) was selected. Afterwards, the current curves of the written words and short sentences were processed with the trained models to give final recognition results.

4.3 Results and Discussion

4.3.1 Fabrication of Nanocomposite Hydrogels

The amino-functionalized monomer, AEAM, was first synthesized via a two-step reaction and characterized by ^{1}H NMR (**Figure S4.1** in **Appendix C**). From the NMR spectrum, the characteristic peaks of C═C can be observed at 6.20−6.32 and 5.78−5.82 ppm, and −CH_2CH_2− can be found at 3.19 and 3.59 ppm, which confirmed the successful synthesis of the monomer. The nanocomposite hydrogel was fabricated via a facile one-pot free radical polymerization of AM, MTAC and AEAM in the presence of carboxyl-modified MWCNTs and LiCl under mild conditions of 30 °C and physiological neutral pH, as illustrated in **Figure 4.1a**. In this hydrogel (denoted as PAMAC-L), AM comprises the main network via their intermolecular hydrogen bonding. Since good interfacial interactions between matrix and nanofillers are critical for the mechanical robustness of nanocomposite materials, strong/reversible ionic interactions were introduced to the polymer-MWCNT interfaces by introducing functional cationic and anionic moieties. Specifically, dual electrostatic interactions were generated under the experimental pH conditions, i.e., the interactions between ionized carboxyl groups (pKa ~ 4)[280] on MWCNT and the two cations including quaternary ammonium cations in MTAC (pKa ~ 9.4)[309] and protonated amino groups of AEAM (pKa ~ 8.8)[278, 279] (**Figure 4.1b**). As shown in **Figure 4.1c**, the yielded hybrid hydrogel is homogeneous and transparent, demonstrating high transmittances over 90% within the visible light range of 410-700 nm, which is attributed to the excellent dispersion and low concentration of the nanotubes. Microscopically, a uniform interconnected porous morphology was observed from SEM images of the freeze-dried hydrogel cross-section (**Figure S4.2a** in **Appendix C**). MWCNTs can be clearly seen in higher magnification of the SEM image (**Figure**

S4.2b in **Appendix C**), whilst no apparent aggregations of the nanofillers were found, also indicating their good dispersion.

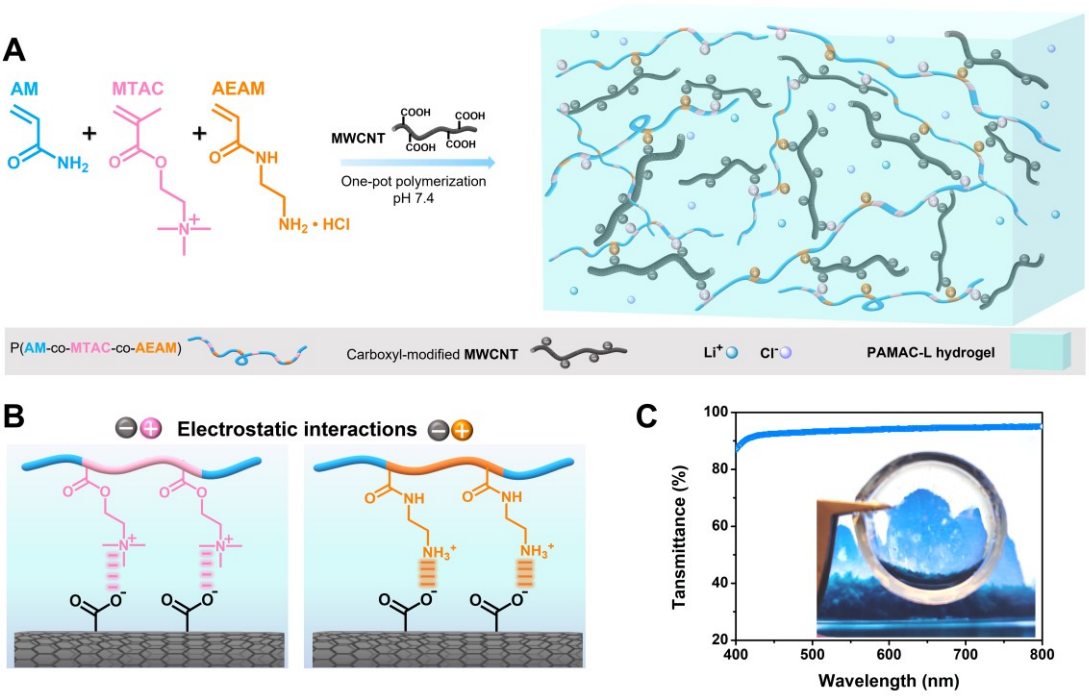

Figure 4.1. (a) Scheme showing the synthesis process of nanocomposite PAMAC-L hydrogels. (b) Schematic illustration of the binary ionic interactions in the hydrogel network. (c) UV-Vis spectrum of the hydrogel in visible light range and an image showing the high transparency.

4.3.2 Mechanical Performances of Hydrogels

The mechanical properties of the resultant hydrogels are presented in Figure 2. The water content of all hydrogels was fixed at 70% (**Table S4.1** in **Appendix C**). According to the nominal tensile stress-strain curves in **Figure 4.2a**, original PAM gel is weak and relatively brittle. Yielding followed by plastic flow were clearly observed,

giving a final fracture strength and strain of 0.05 MPa and 555%, respectively. In contrast, the breaking strain of the hydrogel composed of AM, MTAC and a tiny amount of MWCNTs (PAM-MT-C, MT:AE=1:0) was drastically increased to 3818%. Meanwhile, by introducing AEAM and MWCNT to the PAM gel (PAM-AE-C, MT:AE=0:1), a high fracture strength of 0.39 MPa was reached. The improvements of the mechanical performances were attributed to the electrostatic forces generated between $-N(CH_3)_3^+$ or $-NH_3^+$ on copolymers and $-COO^-$ on the nanotubes that provides effective ways for force transduction and energy dissipation. The role of ionic interactions was evidenced by the poor tensile performances of the hydrogels composed of only AM and the nanotubes (PAM-C), PAM-MT and PAM-AE without the additions of MWCNTs (**Figure S4.3** in **Appendix C**). The nanocomposite solely involving one of the cationic monomers, however, suffers from either poor strength (in the case of MTAC) or limited stretchability (in the case of AEAM), which restricts their further applications. Surprisingly, incorporation of dual cations into the composite resulted in strong and highly stretchable hydrogels (PAMAC) that combines the merits of both functional moieties, suggesting the synergetic effect of these two interactions. As demonstrated in **Figure 4.2a** and **4.2b**, by adjusting the weight ratio of MTAC to AEAM to 7:3, optimized tensile properties were achieved, i.e., the fracture stress reached up to 0.67 MPa and the toughness was attained up to 6.92 MJ/m^3 that was 22.6 times that of PAM hydrogel. The concentration of MWCNTs also poses effects on the mechanical properties of the composite gels. Raising MWCNTs' content led to enhanced strength and fracture elongation while too high concentrations resulted in macroscopic aggregations of the nanofillers and thus inferior performances, giving an optimizing MWCNTs concentration of 2 mg/L (**Figure S4.4** in **Appendix C**).

On the other hand, introducing salt ions is a facile, economical and bio-inspired

strategy for the enhancement of a hydrogel's conductivity as well as favoring the water retention capability of a gel, and thus has been widely adopted in hydrogel conductors. Considering the suppressing effect of the ions on the electrostatic interactions,[281] the tensile properties of the nanocomposite PAMAC-L hydrogels containing various LiCl concentrations were investigated, as shown in **Figure 4.2c** and **4.2d**. It is interesting that, with the addition of a small amount of LiCl (50 mM), the stretchability of the hybrid hydrogel was increased up to a remarkably high value of 4075%, which resulted in a fracture strength as high as 1.09 MPa (average breaking strength of 0.68 MPa) and an impressing toughness of 12.8 MJ/m^3 (average toughness of 9.11 MJ/m^3). The excellent stretchability of the PAMAC-L hydrogel was also demonstrated by the image in **Figure 4.2e**. Further increasing the LiCl concentration caused the dropping of both the strength and stretchability of the hydrogel as a result of the shielded ionic interactions, confirming the key role of the binary interfacial electrostatic interactions to the nanocomposites' strength and toughness. Therefore, PAMAC-L with 50 mM LiCl was used in all other characterizations unless otherwise noticed. Also, under such concentration, the salt was considered to be safe to human cells.[310]

The elasticity or fatigue resistance of the hybrid PAMAC-L hydrogel was characterized by cyclic elongation and compression tests. The hydrogel was first allowed to be cyclically stretched to a series of predetermined maximum strains ranging from 100% to 1500%. As shown in **Figure 4.2f**, the gel was capable to completely recover both its shape and strength before the strain of 500%. After that, small residue deformations were observed while full recovery of the strength was achieved until a high strain of 1000%. It should be noted that the material was still able to recover 92% of the deformation ((maximum strain-residue strain)/maximum strain) even when an ultra-high strain of 1500% was applied. The excellent elasticity was also confirmed by the good

superposition of the loading/unloading curves for 100 successive cycles of 100% strain (**Figure 4.2g**). When the hydrogel was subjected to 20 cycles of 1000% maximum strain (**Figure 4.2h**), although an energy dissipation decrease of 28% was observed from the 2nd cycle, the stress-strain curves for the 2^{nd} to 20^{th} cycles overlapped, indicating a stabilized network after the first cycle. Besides, the PAMAC-L hydrogel restored 92% of its primary strength and recovered 90% of the maximum strain even after 20 cycles of the large tensile deformation. The well-connected 3D network and the efficient energy dissipation of the involved interactions also endows the hydrogel with the capability to resist damage by sharp materials, which highly resembles the human skin's protection function. As demonstrated in **Figure 4.2i**, when a cylindrical gel was cut by a sharp steel blade from top to bottom, the hydrogel was not damaged but elastically retrieved to its original shape with no visible scar left once the blade was removed. Also, the hydrogel is robust to bear compression strain with a compressive modulus of 96.0 kPa (calculated from the first 5% of the compression curve of 50% strain), similar to the modulus of human skins[311]. Moreover, it could completely recover from 10 consecutive compression cycles of 50% maximum strain as reflected by the overlapped loading/unloading curves of different cycles (**Figure 4.2j**). When a large strain of 90% was applied, the compressive stress reached as high as 2.52 MPa. The composite hydrogel retained the strength of 2.09 MPa after 10 rounds of loading and unloading processes (**Figure 4.2k**). Compared to previously reported tough hydrogels as summarized in **Table S4.2** in **Appendix C**, the prepared PAMAC-L hydrogel outstands in aspects of ultra extensibility, skin-mimetic modulus, repeatable recovery from large strains and high transparency, which made it extremely suitable for ionic skins. Also, the NC gel outperforms the previous ionic skins and e-skins (**Table S4.2** in **Appendix C**) owing to its mechanically stretchable, tough and strong nature.

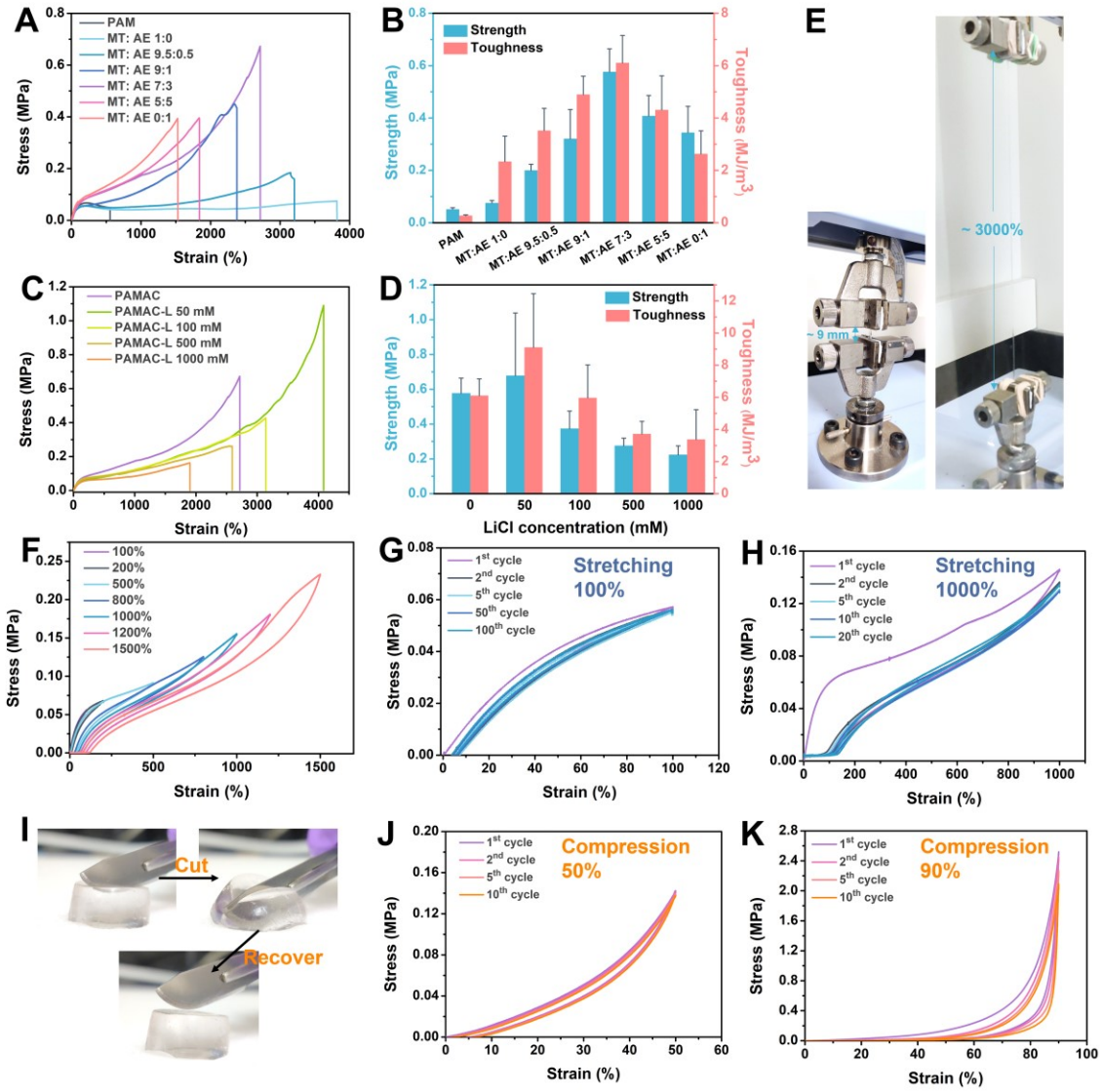

Figure 4.2. Mechanical properties of the hydrogels. (a) Tensile stress-strain curves of PAM and PAMAC composite hydrogels with various ratios of MTAC to AEAM (MT:AE). (b) Average strength and toughness of PAM and PAMAC composite hydrogels with different cationic monomer ratios calculated from three stress-strain curves. (c) Tensile stress-strain curves of the nanocomposite hydrogel with LiCl concentrations ranging from 0 to 1000 mM. (d) Average strength and toughness of the hydrogels with different LiCl concentrations. (e) Images showing the PAMAC-L

hydrogel before and during stretching. (f) Tensile stress-strain curves of the PAMAC-L gel subjected to successive loading/unloading cycles with maximum strain setting from 100−1500%. Tensile stress-strain curves for loading/unloading cycles with maximum strain of (g) 100% and (h) 1000%. (i) Images demonstrating the hydrogel withstanding damage by sharp materials like a blade and recover to its original shape. Compressing stress-strain curves for loading/unloading cycles with maximum strain of (j) 50% and (k) 90%.

4.3.3 AFM Force Measurements

To better understand the role of the dual electrostatic interactions in the hydrogel's network and elucidate the reinforcement mechanism, AFM was employed to directly measure forces between carboxyl groups and the two functional cations. The AFM experimental setup is schematically depicted in **Figure 4.3a**.[312] Cationic-functionalized copolymers PAM-MT and PAM-AE were synthesized and coated on mica surfaces. Carboxyl groups were dressed on AFM tips. The COOH-coated AFM tip was brought into contact with the polymer coatings and then retracted from the substrate surfaces to obtain force–distance curves. To mimic circumstances in the hydrogels, force measurements were conducted under a neutral pH of 7.4 with different LiCl salinity, under which carboxyl groups were negatively charged and the amino or quaternary ammonium groups carried positive charges as confirmed by zeta potential tests (**Figure S4.5** in **Appendix C**). The morphologies of the PAM-MT- and PAM-AE-coated surfaces were first characterized by topographic AFM imaging as shown in **Figure 4.3b** and **4.3c** using bare mica as the reference (**Figure S4.6** in **Appendix C**), suggesting the high coverage and low roughness of the surfaces.

Force mapping was then conducted on a 20 μm x 20 μm area to obtain more than

50 force curves and average adhesion between AFM tips and the surfaces was calculated. Representative force–distance curves of $-COO^-$ interacting with PAM-MT and PAM-AE without LiCl are presented in **Figure 4.3d** and **4.3h**, respectively. In both cases, an apparent attractive force was measured during the approaching process, featuring electrostatic interactions between the oppositely charged moieties. Upon separation, significant adhesions were measured between the carboxylate and both cations with the adhesion energy (Force/Radius, F/R) value for PAM-MT (17.0 ± 3.6 mM/m) much lower than that for PAM-AE (115.3 ± 27.4 mM/m). This coincides with the tensile result that the PAM-AE-C hydrogel was much stronger than PAM-MT-C, whilst weaker yet possibly more dynamic carboxylate-quaternary ammonium interaction gave rise to hydrogels with better stretchability. After the additions of 50 mM LiCl, both interactions were suppressed with the F/R values to be 6.0 ± 1.6 and 72.7 ± 22.1 mM/m for PAM-MT and PAM-AE, respectively, as demonstrated by force–distance curves in **Figure 4.3e and 4.3i**, along with summaries of the F/R averages in **Figure 4.3h** and **4.3k**. Partially shielded ionic interaction at a low LiCl concentration surprisingly led to enhanced stretchability (from 2531 ± 256% for PAMAC to 3652 ± 619% for PAMAC-L) and toughness of the hydrogels, which might be ascribed to the lowered interaction energies facilitating the dynamic dissociation/reassociation of reversible electrostatic bindings during stretching processes. Further increasing the ionic strength to 1000 mM severely suppressed the ionic forces (**Figure 4.3f** and **4.3j**), which is consistent with the mechanical results. According to the force measurement results, it is clear that there exists two types of ionic interactions that contribute to the assembly of the gel networks. The strong and stretchable nature of the composite hydrogel originates from the synergetic effect of both forces, i.e., carboxylate-protonated amino complexes provide robust backbone to the network while carboxylate-quaternary ammonium interactions

offer effective energy dissipation to the hydrogel upon deformation.

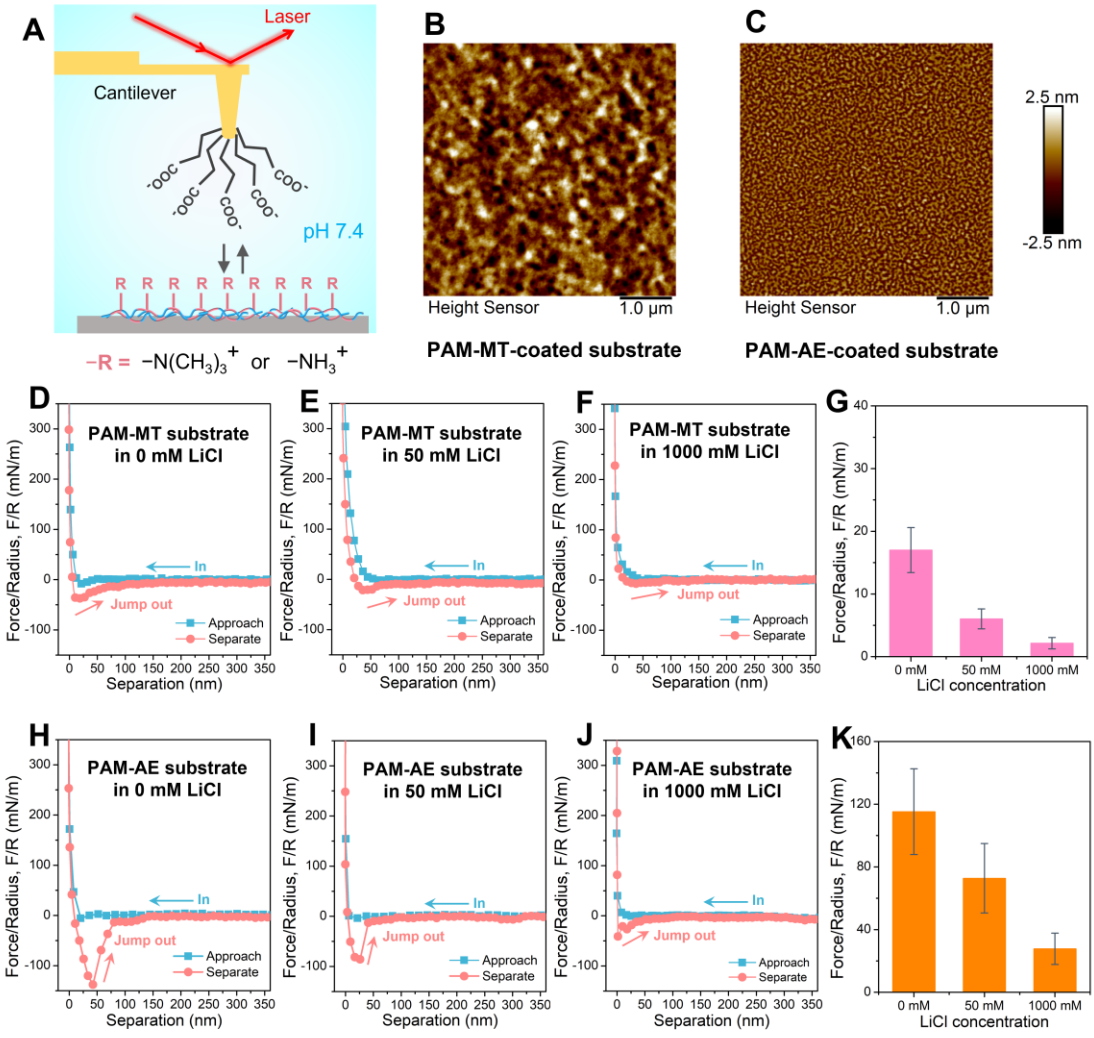

Figure 4.3. Force measurements of the dual electrostatic interactions. (a) Schematic illustration of a typical AFM force measurement experiment. Topographic AFM images of (b) PAM-MT coating (RMS roughness ~ 0.874 nm) and (c) PAM-AE coating (RMS roughness ~ 0.583 nm) on mica surfaces. Interaction force profiles of a COOH-coated AFM tip and a PAM-MT-coated surface in PB solution (pH 7.4, 5 mM) containing (d) 0, (e) 50, and (f) 1000 mM LiCl, and (g) average adhesion forces for PAM-MT. Interaction force profiles of the COOH-coated AFM tip and a PAM-AE coating in PB solution

containing (h) 0, (i) 50, and (j) 1000 mM LiCl, and (k) the average adhesions calculated from force curves for PAM-AE.

4.3.4 Self-Healing Properties

The reversible physical crosslinks including ionic interactions and hydrogen bonding endows the PAMAC-L hydrogel with autonomous self-healing capability as shown in Figure 4, which is highly favorable for prolonging the lifespan and enhancing the durability of the material. **Figure 4.4a** demonstrates that a self-repaired hydrogel can bear lifting, vigorous shaking and bending after healing for 2 h, as well as being stretched around 100% of its original length with 24 h self-healing. The viscoelastic behaviors as characterized by rheological tests in **Figure 4.4b** and **4.4c** also confirmed the self-recovery of the nanocomposite's network under oscillation shear stress. In Figure 4B, the storage modulus (G′) of the PAMAC-L showed high values of ~8500 Pa and surpassed the loss modulus (G″) until a large shear strain of 364.2% was reached, after which the network ruptured. Recovery of the network was observed once the stress was released with strain reset to 1%, as indicated by the completely restored G′ and G″. Cyclic rheological result in Figure 4C suggests the repeatability of the self-healing processes, where fully recovered shear moduli were obtained with the hydrogel cyclically subjected to a large deformation of 1000%. Electrically, a hydrogel strip was connected into a circuit to form a closed loop, with either an LED bulb (**Figure 4.4d**) or real-time current measurement (**Figure 4.4e**) to monitor its cutting-healing processes. In both cases, the LED light or the current can immediately retrieve their initial states after self-repairing of the composite, manifesting the fast reconstruction of the conductive paths in the hydrogel. In addition, the repeatability of this self-recoverable electrical property was evidenced by the complete restoration of the current after cycles of the cutting-healing process.

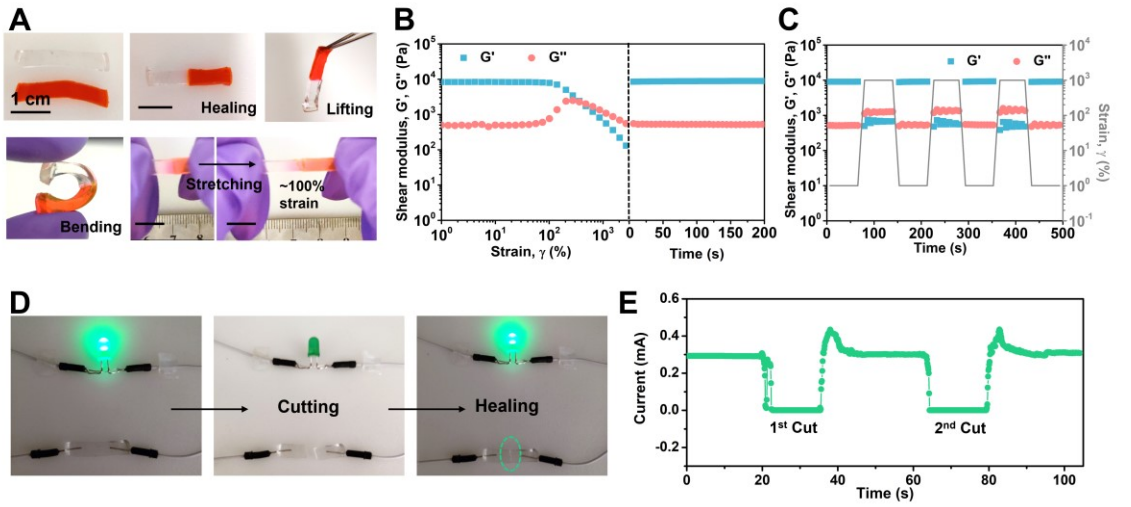

Figure 4.4. Self-healing properties of the PAMAC-L hydrogel. (a) Images demonstrating a self-healed gel to withstand lifting, bending and stretching. Scale bar in all images is 1 cm. (b) Rheological oscillatory strain sweep followed by time sweep of the hydrogel. (c) Cyclic oscillatory time sweep with the shear strain shifting between 1% and 1000% for three cycles. (d) Photographs showing the illuminance variation of an LED bulb during the hydrogel's cutting-healing process. (e) Real-time current changes with the cutting and healing of the gel.

4.3.5 Electrical and Sensing Performances

Conductivity is an essential requirement for ionic skins. The conductivities (σ) of the prepared gels were measured via electrochemical impedance spectroscopy as demonstrated in **Figure 4.5a** and **Figure S4.7** in **Appendix C**. PAM hydrogel is less conductive with σ around 0.1 S/m, while introducing cationic functional monomers and MWCNTs sextupled the value. The similar conductivities of PAMA without MWCNTs and PAMAC hydrogel evidenced that the MWCNTs did not form conductive paths due to their low concentration. Further incorporation with LiCl raised the average σ value to

0.85 S/m. Sensitivities of the PAMAC-L to tensile strains and pressures were characterized and showed in **Figure 4.5b** and **4.5c**, respectively. According to **Figure 4.5b**, the gel ionic conductor is workable over an extremely wide strain range (0-1800%) superior to most of the previously reported hydrogel sensors or ionic skins. The relative resistance changes ($\Delta R/R_0$) increased sensitively with tensile deformations, giving gauge factors (GF) to be 0.98, 2.19 and 3.35 over strain ranges of 0−300%, 300−800% and 800−1800%, respectively. Compared with previously reported ionic conductive hydrogels of high ion loadings (**Table S4.2**), the PAMAC-L possesses comparable or even higher GFs but much lower risk of skin irritation and biotoxicity caused by high concentrations of salts. Also, the moderate GF values enable the material to keep conductive at strains as high as 1800% as well as ensure stable and sensitive current responses during deformation. Pressures also trigger sensitive changes of the resistances over a large range of 0−15 kPa but led to negative $\Delta R/R_0$ values. The pressure sensitivity (S) was 0.062 within pressure range of 0−5 kPa, remaining values of 0.022 and 0.008 when reaching high pressures of 5−9 kPa and 9−15 kPa, respectively. Taking advantages of the elastic recovery under tensile/compressive strains, the skin-like PAMAC-L sensor demonstrated repeatable and stable strain/pressure response signals within wide ranges. As illustrated in **Figure 4.5d** and **4.5f**, identical waveforms were obtained when the hydrogel was subjected to stretching or compressing for 20 cycles with maximum strains to be 100, 200 and 500% or pressures of 2.5, 5 and 12 kPa. Also, there is no cyclic loading-unloading hysteresis was detected for 200% stretching process as shown in **Figure S4.8A**. Slight hysteresis was observed for 5 kPa compression loading-unloading cycle (**Figure S4.8B**). Besides, well-preserved $\Delta R/R_0$ amplitudes were observed for 100 consecutive cycles of 100% tensile strain and 200 successive cycles under 5 kPa pressure as shown in **Figure 4.5e and 4.5g**, respectively, and in **Figure S4.8C** and **S4.8D** in

Appendix C, validating the long-term durability of the ionic composite skins for electrical sensory applications.

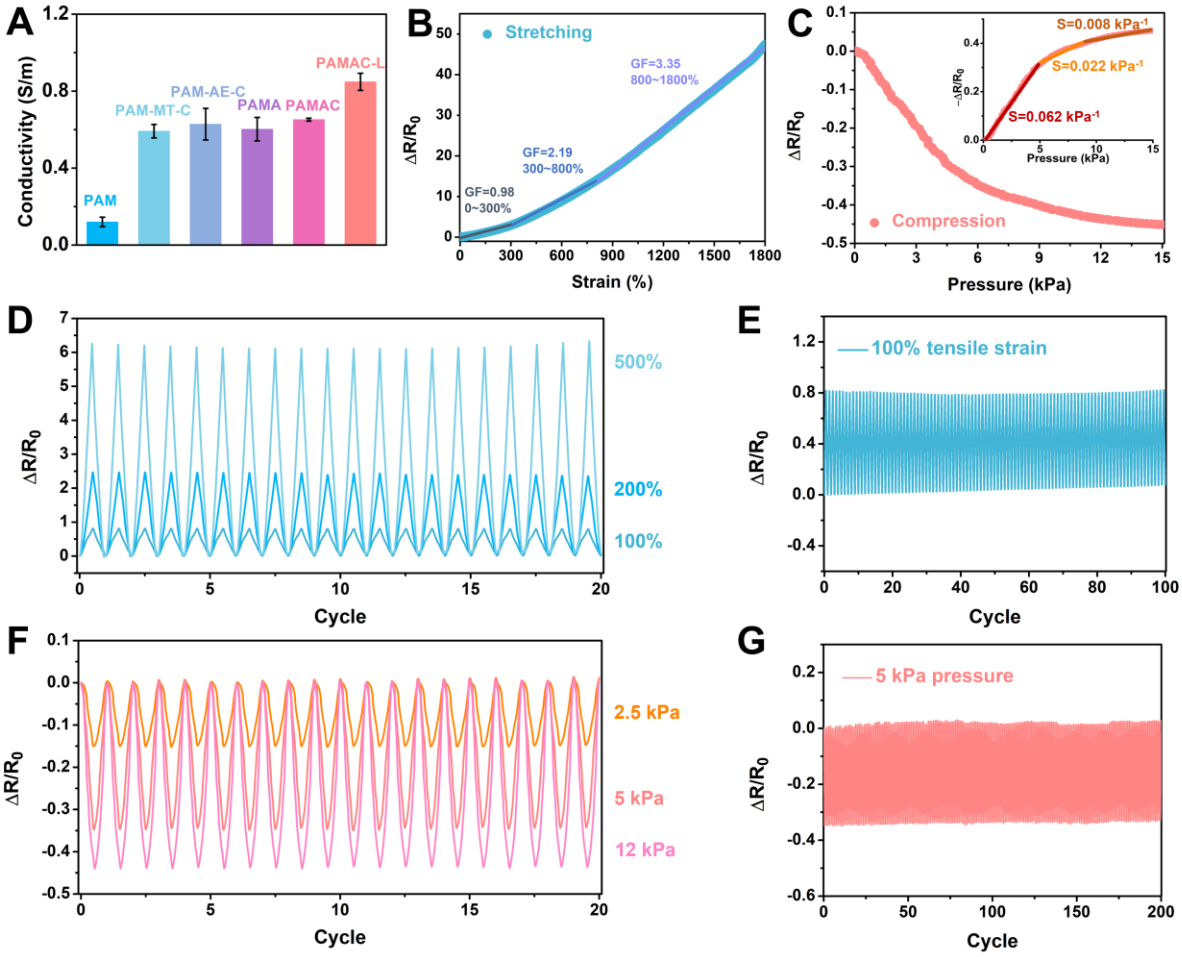

Figure 4.5. Electrical properties of the hydrogels. (a) Conductivities of different hydrogels. Relative resistance changes vs (b) tensile strain and (c) pressure for the PAMAC-L hydrogel. (d) Cyclic relative resistance responses under repeated tensile loading/unloading processes with maximum strain of 100, 200 and 500%. (e) Relative resistance variation with maximum strain of 100% for 100 cycles. (f) Relative resistance changes under cyclic pressure loading of 2.5, 5 and 12 kPa. (g) Relative resistance response under cyclic pressure of 5 kPa for 200 loading/unloading cycles.

The desirable strain-responsive electrical properties enable the hydrogel to detect human activities and subtle motions with high sensitivity and accuracy. For example, when a hydrogel sensor was mounted on the tester's finger, stable and reproducible relative resistance changes were measured when the finger sequentially bended to angles of 15°, 30°, 45° and 90° (**Figure 4.6a**). Subtle human physiological signals like wrist pulse can also be discerned with a thin hydrogel sensor fixed over the wrist radial artery of the tester (**Figure 4.6b**). Particularly, the soft sensor precisely detected both the systolic and diastolic processes of the pulses, giving clearly distinguishable percussion peak (systolic peak), dicrotic notch and dicrotic peak (diastolic peak) in each beat (**Figure S4.9** in **Appendix C**) and a heartbeat rate of 84.5/min. After exercise (20 squats), both the changes of the heartbeat rate and the pulse's waveform were readily acquired. An increase in heartbeat rate to 140.4/min was detected. In addition, the pulse signals featured weakened dicrotic peaks, reflecting the deficient cardiovascular compensation of the subject after exercise[288]. The recovery of the dicrotic wave and pulse rate could be clearly observed 90 s after the exercise. These results suggest the superb sensitivity and stability of the ionic hydrogel strain sensor, and its great potential in health diagnostic applications. On the other hand, when a gel layer was integrated to be a pressure sensor as shown in **Figure 4.6c**, both slight touch and pressing were detected in good sensitivity. Notably, the hydrogel pressure sensor is able to discern very subtle pressure changes like water dropping. As displayed in **Figure 4.6d**, when a small water droplet was allowed to fall from a constant height (15 cm) and gently removed, a sharp negative $\Delta R/R_0$ signal indicating the moment of the water droplet hitting the surface (in ~0.18 s) was first sensitively detected as shown in the insert image of **Figure 4.6d**, followed by slowly recovery of the $\Delta R/R_0$ to 0 reflecting the water removal. The signal for falling water droplets is also highly reproducible.

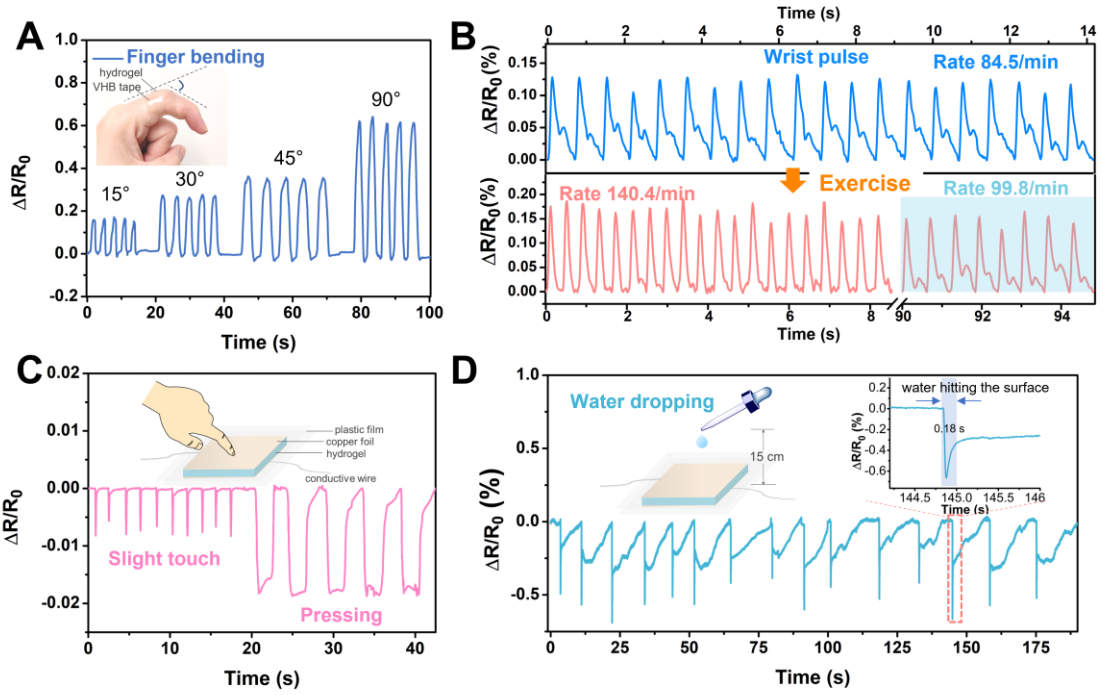

Figure 4.6. Sensing performances of PAMAC-L hydrogel. Real-time monitoring (a) finger bending and (b) human wrist pulse before and after exercise using a hydrogel strain sensor. Real-time detection of (c) touch and pressing, and (d) water dropping by a hydrogel pressure sensor.

4.3.6 Writing Recognition

Writing is a common activity in our daily life and a keyway for recording and communication. Despite the growing utilization of typing by keyboards, handwriting still comprises a critical part of many people's writing activities. Therefore, handwriting recognition (HWR), which aims to translate handwritten input from papers, touch-screens and other devices into a digital format that the computer understands,[313] have attracted much attention. Different from tradition HWR based on the artificial graphical marks on a surface, hydrogel sensors detect writing processes by monitoring the relevant joint

movements, however, previous sensors[146, 179, 314, 315] halted at the motion recording step due to limited mechanical performance, sensitivity, signal stability and/or lack of appropriate platform. Benefiting from the great sensitivities of the PAMAC-L ionic skin to fine motions, it holds great potential in writing sensation. Here, we developed a complete English writing recognition platform including signal collection, processing and output by monitoring forefinger joint motions of the tester using the PAMAC-L gel and processing the collected signals using a self-developed software. As shown in **Figure 4.7a** (upper left), first, traditional handwriting on paper using a pen was investigated. By writing 26 English letters in lower case from "a" to "z" in the size of daily handwriting, the slight movements of the finger were sensitively detected, and a series of current signals was gathered where each letter demonstrated clearly distinguishable and highly repeatable waveform (**Figure S4.10a** in **Appendix C**). These signals were then used for the training of a model in the Matlab machine learning toolbox. The trained model originated from nearly a thousand current signals gave a good letter prediction accuracy of 70% (**Figure S4.10b** in **Appendix C**). Afterward, English words like "letter" (**Figure 4.7b** and **Figure S4.10c** in **Appendix C**) and "hydrogel" (**Figure 4.7c** and **Figure S4.10d** in **Appendix C**) were written, and the obtained electrical signals were processed in the software using the pre-trained model. The average recognition rates calculated from 10 writings of each word reached 87% and 68% for these two words, respectively (**Figure 4.7d**).

On the other hand, in modern life, there have been growing interests in more portable, comfortable, intelligent and wearable devices to accomplish daily writing. Thus, another handwriting manner, i.e., writing in the air using the forefinger as schematically shown in **Figure 4.7a** (lower left), was monitored and recognized, by which the writing

activity can be readily translate into digital text even without using of a keyboard or a touch panel. Similarly, letter current signals were first collected to train a model with ultra high accuracy of 92% (**Figure S4.11a** and **S4.11b** in **Appendix C**). Next, words writing was recorded by current changes and recognized in the software. Writing English words "letter" (**Figure 4.7e** and **Figure S4.11c** in **Appendix C**) and "hydrogel" (**Figure 4.7f** and **Figure S4.11d** in **Appendix C**) gave excellent recognition rates of 97% and 91%, respectively (**Figure 4.7i**). According to **Figure 4.7i**, even for more complicated phrases and short sentences, good recognitions can be acquired with the average success rates of 82% for "ionic skin" (**Figure 4.7g** and **Figure S4.11e** in **Appendix C**) and 86% for "how are you" (**Figure 4.7h** and **Figure S4.11f** in **Appendix C**). From these results, the skin-like PAMAC-L gel-based platform shows great feasibility for the monitoring of human writing process and is promising towards more intelligent and wearable writing electronic devices. Since the writing habits of different person may vary a lot, the integration of flexible sensor with machine learning module can provide a promising approach towards customized and evolvable iontronics.

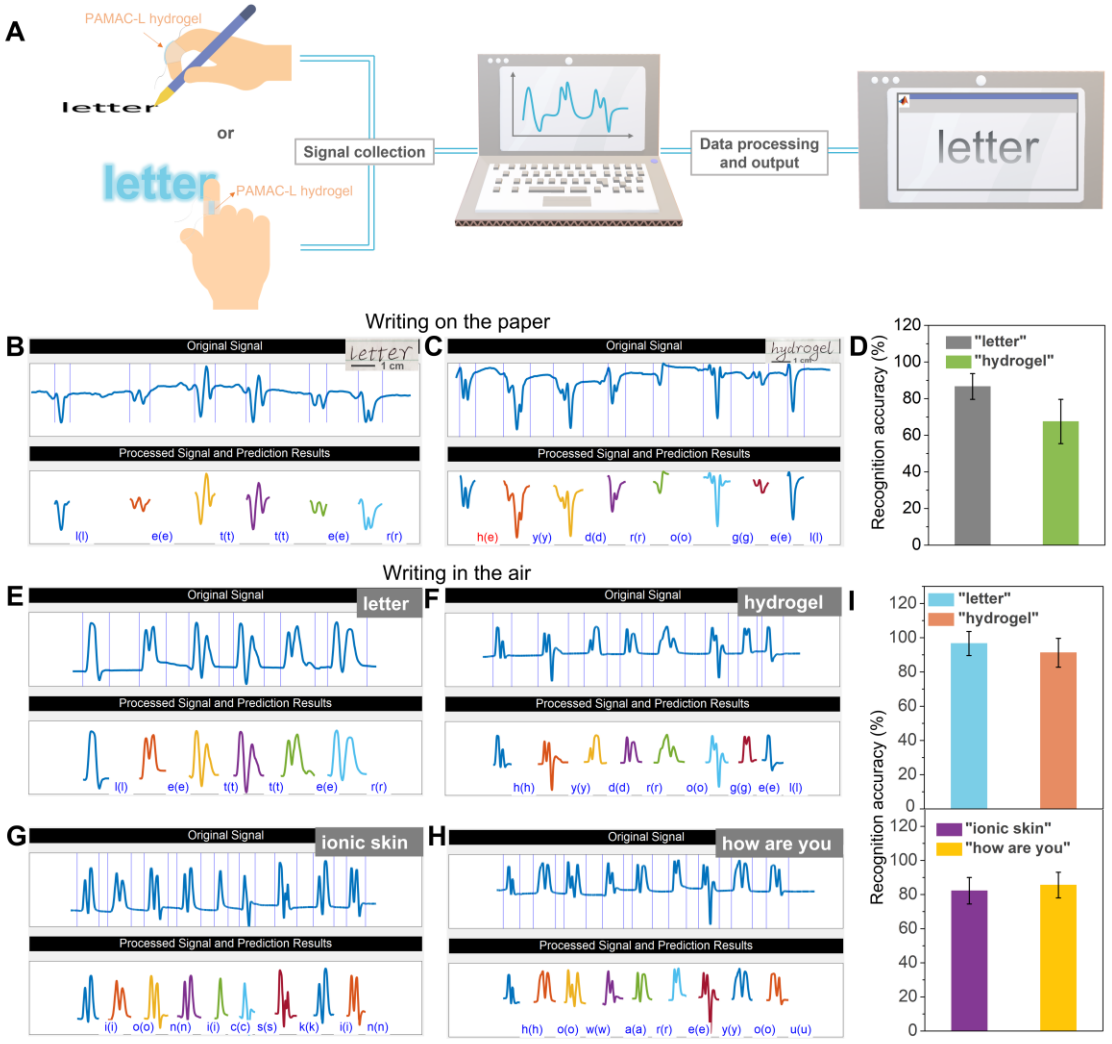

Figure 4.7. Writing recognition by PAMAC-L hydrogel. (a) Scheme showing the handwriting recognition procedure. Recognition results from the software for handwriting of the word (b) “letter” and (c) “hydrogel” on paper. (d) Word recognition accuracies for these two words calculated from 10 writings of each word. Recognition results for writing of (e) “letter”, (f) “hydrogel”, (g) “ionic skin”, and (h) “how are you” by the tester’s forefinger in the air. (i)Average recognition accuracies for handwriting in air. For the recognition results shown below processed signals, the letters out of the parentheses are the input ones and in the parentheses are the output letters. Blue indicating right recognition and red indicating wrong recognition.

4.4 Conclusions

In this work, we have fabricated a novel type of ionic conductive hydrogel via simple one-pot polymerization of AM and two cationic functional monomers in the presence of MWCNTs and LiCl. Owing to the binary strong/dynamic interfacial electrostatic interactions, the resultant skin-like material possesses a wide spectrum of desirable properties including outstanding stretchability, strength, toughness, elasticity, transparency, self-healing ability and stable electrical cycling performance. The hydrogel ionic skin was used as a strain and pressure sensor to monitor the human motion, wrist pulse, touching, pressing and water dropping with excellent sensitivity and signal repeatability. More importantly, with the integration of machine learning module, the hydrogel ionic skin demonstrated its great potential in recognition of complicated human behavior (i.e., handwriting in air and on paper) by detecting finger movements during writing and translating the analog current signal into digital text with high accuracies. Therefore, the skin-like hydrogel sensor is promising in various applications including wearable devices, health monitoring and diagnosis, soft robotics, etc. The developed strategy also provides new insights into the development of multifunctional tough hydrogels and opens up new prospects for the application of artificial intelligence in next generation ionic skins with customized requirements.

CHAPTER 5 Conclusions and Prospects

5.1 Conclusions and contributions

In this thesis work, by incorporating nanomaterials and reversible crosslinking strategies, we have developed three novel NC hydrogels demonstrating responsiveness to various stimuli including pH, temperature, strain and pressure, and self-healing capability. These multifunctional materials have been applied in different biomedical and electrical applications. In the first project, a hydrogel that demonstrates sensitive pH responsiveness at mildly acidic range and excellent stability under neutral conditions superior to previous studies has been prepared, which made it a promising candidate as a drug carrier for cancer therapy and wound healing that require accurate drug delivery triggered by local acidosis but avoid harm to surrounding normal tissues. In the second project, by combining dynamic chemical and physical crosslinking mechanisms, ultra-elasticity and excellent self-healing property were achieved in one single hydrogel, which provides new insights towards the fabrication of tough self-healing hydrogels. In the third project, a transparent and ultra-stretchable tough hydrogel that stands out of the previous opaque tough hydrogels has been prepared through a simple one-step method. By the integration of machine learning module, the hydrogel sensor was endowed with intelligent sensing functions that has not been reported in previous studies.

To be specific, the major conclusions and original contributions are as follows.

(1) An ultra pH-responsive hydrogel with sharp and faintly acidic responsive range has been fabricated based on imine bonds formation by facilely mixing aldehyde-functionalized polymer and amine-modified silica nanoparticle. The gel is injectable and

can autonomously heal from fractures. Moreover, it was stable in neutral aqueous media, whereas decomposed under mildly acidic conditions right located at the local acidosis range, which made it promising to be used as vehicles for the controlled delivery of bioactive molecules to regions like tumors, wounds and infections. This ultrasensitive pH-responsive behavior was attributed to the utilization of the ASNPs with medium pKa (7.6) to enable the mildly acidic decomposition of imine bonds in the gel while ensure the neutral stability. We further demonstrated the feasibility of this hydrogel to be used as a drug delivery vehicle by *in vitro* experiments, where a slight drop of pH (0.2) in the region of 6.4−7.0 can trigger significant release of the loading model drugs.

(2) An elastic, stretchable, self-healing and ionic conductive hydrogel that integrate nanomaterials with micelle crosslinking in one system has been prepared through simple one-pot polymerization. Especially, the gel can recover from extremely large tensile strain of 1000%. The self-healed hydrogel can be stretched up to 7 times its original length. The combination of the excellent mechanical and self-healing properties is ascribed to the reversibly crosslinked 3D networks generated from the ionic interactions between MWCNTs and protonated amine-bearing PAM copolymers, and the imine bonds between aldehyde groups on micelles and the amino moiety of the copolymer. In addition, the thermo-responsive behavior of the aldehyde-modified F127 micelles endows the corresponding hydrogel with sensitive temperature-dependent optical properties. This hydrogel was successfully used as a strain and pressure sensor for the detection of diverse human activities. Particularly, it can be used to distinguish the subtle wrist pulse changes before and after exercise, and the slight eye movement variations during human sleep.

(3) A tough, ultra-stretchable, self-healing and transparent hydrogel has been

prepared via synergetic ionic interactions between MWCNTs and PAM copolymers containing two types of cationic moieties. The gel can be stretched up to 40 times its original length, and reach high average strength of 0.7 MPa, whilst keep elastic in large strains (< 1000%). The two interfacial ionic interactions, stronger one between protonated amine of copolymers and carboxyl groups on MWCNTs and weaker one between quaternary ammonium on polymers and the carboxylate, endow the hydrogel with strong and reversible crosslinks to effectively transfer forces between polymers and nanomaterials and dissipate energy upon force loading. The resultant hydrogel was utilized as a strain and pressure sensor for the detection of human motions and subtle signals. To further demonstrate its practical application, we developed a platform combining the electrical signal collection, processing and output for the recognition of human activities with high success rate.

5.2 Prospects

In this study, we have explored the possibility of using functional nanomaterials and introducing reversible interfacial interactions to render the hydrogels with specific responsiveness and improve their mechanical and self-healing performances, together with investigating their applications in biomedical and electrical areas. For the future studies, *in vivo* and animal tests can be conducted to further evaluate their practical biomedical applications. Since dynamic covalent interactions like imines possessing some inviting features like the pH sensitivity and dynamicity, different modification strategies and synthesis routes can be developed to enable them to be used in a broader range of hydrogel systems. For example, water soluble aldehyde-containing monomer can be synthesized and utilized in relevant Schiff base-crosslinked materials. On the other hand, the fabrication of tough self-healing hydrogels, despite the huge efforts

devoted, remains a great challenge. A possible solution is to introduce interactions with good dynamicity like dynamic covalent interactions to tough hydrogel systems, to allow multiple crosslinking mechanisms. In addition, as introducing nanomaterials is a promising approach for enhanced mechanical performances, optimizing interfacial interactions and generating anisotropic structures are possible strategies to further develop NC hydrogels with superior mechanical properties. Finally, for the applications as flexible sensors, intelligent and wireless devices can be developed to fulfill the practical needs of modern electronics. For example, the intelligent writing recognition functions of our third system can be further enhanced by utilizing the finger movement signals of multiple fingers and involving writing manners of different person into the model training process.

Bibliography

(1) Ahmed, E. M. Hydrogel: Preparation, Characterization, and Applications: A Review. *J. Adv. Res.* **2015**, 6, 105-121

(2) Ganji, F.; Vasheghani, F. S.; VASHEGHANI, F. E. Theoretical Description of Hydrogel Swelling: A Review. *IRAN. POLYM. J.* **2010**, 19, 375-398

(3) Kopeček, J. Hydrogel Biomaterials: A Smart Future? *Biomaterials* **2007**, 28, 5185-5192

(4) Billiet, T.; Vandenhaute, M.; Schelfhout, J.; Van Vlierberghe, S.; Dubruel, P. A Review of Trends and Limitations in Hydrogel-Rapid Prototyping for Tissue Engineering. *Biomaterials* **2012**, 33, 6020-6041

(5) Vashist, A.; Vashist, A.; Gupta, Y.; Ahmad, S. Recent Advances in Hydrogel Based Drug Delivery Systems for the Human Body. *J. Mater. Chem. B* **2014**, 2, 147-166

(6) Kamoun, E. A.; Kenawy, E.-R. S.; Chen, X. A Review on Polymeric Hydrogel Membranes for Wound Dressing Applications: Pva-Based Hydrogel Dressings. *J. Adv. Res.* **2017**, 8, 217-233

(7) Gupta, P.; Vermani, K.; Garg, S. Hydrogels: From Controlled Release to Ph-Responsive Drug Delivery. *Drug Discov. Today* **2002**, 7, 569-579

(8) Peppas, N. A.; Hilt, J. Z.; Khademhosseini, A.; Langer, R. Hydrogels in Biology and Medicine: From Molecular Principles to Bionanotechnology. *Adv. Mater.* **2006**, 18, 1345-1360

(9) Hoffman, A. S. Hydrogels for Biomedical Applications. *Adv. Drug Deliv. Rev.* **2012**, 64, 18-23

(10) Van Vlierberghe, S.; Dubruel, P.; Schacht, E. Biopolymer-Based Hydrogels as Scaffolds for Tissue Engineering Applications: A Review. *Biomacromolecules* **2011**, 12, 1387-1408

(11) Zhu, J.; Marchant, R. E. Design Properties of Hydrogel Tissue-Engineering Scaffolds. *Expert Rev. Med. Devices* **2011**, 8, 607-626

(12) Dhivya, S.; Padma, V. V.; Santhini, E. Wound Dressings - a Review. *BioMedicine* **2015**, 5, 22-22

(13) Sirousazar, M.; Yari, M. Dehydration Kinetics of Polyvinyl Alcohol Hydrogel Wound Dressings During Wound Healing Process. *Chin. J. Polym. Sci.* **2010**, 28, 573-580

(14) Yang, X.; Li, P.; Tang, W.; Du, S.; Yu, M.; Lu, H.; Tan, H.; Xing, X. A Facile Injectable Carbon Dot/Oxidative Polysaccharide Hydrogel with Potent Self-Healing and High Antibacterial Activity. *Carbohydr. Polym.* **2021**, 251, 117040

(15) Chen, L.; Li, X.-q.; Cao, L.-p.; Li, X.-l.; Meng, J.-r.; Dong, J.; Yu, L.; Ding, J.-d. An Injectable Hydrogel with or without Drugs for Prevention of Epidural Scar Adhesion after Laminectomy in Rats. *Chin. J. Polym. Sci.* **2016**, 34, 147-163

(16) Zhu, F.-b.; Yu, H.-c.; Lei, W.-x.; Ren, K.-f.; Qian, J.; Wu, Z.-l.; Zheng, Q. Tough Polyion Complex Hydrogel Films of Natural Polysaccharides. *Chin. J. Polym. Sci.* **2017**, 35, 1276-1285

(17) Yuk, H.; Lu, B.; Zhao, X. Hydrogel Bioelectronics. *Chem. Soc. Rev.* **2019**, 48, 1642-1667

(18) Liu, Y.; Liu, J.; Chen, S.; Lei, T.; Kim, Y.; Niu, S.; Wang, H.; Wang, X.; Foudeh, A. M.; Tok, J. B.-H. Soft and Elastic Hydrogel-Based Microelectronics for Localized Low-Voltage Neuromodulation. *Nat. Biomed. Eng.* **2019**, 3, 58-68

(19) Wang, C.; Wang, C.; Huang, Z.; Xu, S. Materials and Structures toward Soft Electronics. *Adv. Mater.* **2018**, 30, 1801368

(20) Lai, Y.-C.; Wu, H.-M.; Lin, H.-C.; Chang, C.-L.; Chou, H.-H.; Hsiao, Y.-C.; Wu, Y.-C. Entirely, Intrinsically, and Autonomously Self-Healable, Highly Transparent, and Superstretchable Triboelectric Nanogenerator for Personal Power Sources and Self-Powered Electronic Skins. *Adv. Funct. Mater.* **2019**, 29, 1904626

(21) Kim, C.-C.; Lee, H.-H.; Oh, K. H.; Sun, J.-Y. Highly Stretchable, Transparent Ionic Touch Panel. *Science* **2016**, 353, 682-687

(22) Peng, Q.; Chen, J.; Wang, T.; Peng, X.; Liu, J.; Wang, X.; Wang, J.; Zeng, H. Recent Advances in Designing Conductive Hydrogels for Flexible Electronics. *InfoMat* **2020**, 2, 843-865

(23) Sun, X.; Yao, F.; Li, J. Nanocomposite Hydrogel-Based Strain and Pressure Sensors: A Review. *J. Mater. Chem. A* **2020**, 8, 18605-18623

(24) Wang, Z.; Cong, Y.; Fu, J. Stretchable and Tough Conductive Hydrogels for Flexible Pressure and Strain Sensors. *J. Mater. Chem. B* **2020**, 8, 3437-3459

(25) Ionov, L. Hydrogel-Based Actuators: Possibilities and Limitations. *Mater. Today* **2014**, 17, 494-503

(26) Wang, J.-J.; Zhang, Q.; Ji, X.-X.; Liu, L.-B. Highly Stretchable, Compressible, Adhesive, Conductive Self-Healing Composite Hydrogels with Sensor Capacity. *Chin. J. Polym. Sci.* **2020**, 38, 1221-1229

(27) Van Tran, V.; Park, D.; Lee, Y.-C. Hydrogel Applications for Adsorption of Contaminants in Water and Wastewater Treatment. *Environ. Sci. Pollut. Res.* **2018**, 25, 24569-24599

(28) Guo, H.; Jiao, T.; Zhang, Q.; Guo, W.; Peng, Q.; Yan, X. Preparation of Graphene Oxide-Based Hydrogels as Efficient Dye Adsorbents for Wastewater Treatment. *Nanoscale Res. Lett.* **2015**, 10, 1-10

(29) Pakdel, P. M.; Peighambardoust, S. J. Review on Recent Progress in Chitosan-Based Hydrogels for Wastewater Treatment Application. *Carbohydr. Polym.* **2018**, 201, 264-279

(30) Pakdel, P. M.; Peighambardoust, S. J. A Review on Acrylic Based Hydrogels and Their Applications in Wastewater Treatment. *J. Environ. Manage.* **2018**, 217, 123-143

(31) Zhang, P.-B.; Tang, A.-Q.; Wang, Z.-H.; Lu, J.-Y.; Zhu, B.-K.; Zhu, L.-P. Tough Poly(L-Dopa)-Containing Double Network Hydrogel Beads with High Capacity of Dye Adsorption. *Chin. J. Polym. Sci.* **2018**, 36, 1251-1261

(32) Wang, W.; Narain, R.; Zeng, H. Chapter 10 - Hydrogels. In: Narain R, ed. *Polymer Science and Nanotechnology*. Elsevier; 2020:203-244.

(33) Wang, W.; Narain, R.; Zeng, H. Rational Design of Self-Healing Tough Hydrogels: A Mini Review. *Front. Chem.* **2018**, 6, 497

(34) Taylor, D. L.; in het Panhuis, M. Self‐Healing Hydrogels. *Adv. Mater.* **2016**, 28, 9060-9093

(35) Kilic, R.; Sanyal, A. Self-Healing Hydrogels Based on Reversible Covalent Linkages: A Survey of Dynamic Chemical Bonds in Network Formation. In: Creton C, Okay O, eds. *Self-Healing and Self-Recovering Hydrogels*. Cham: Springer International Publishing; 2020:243-294.

(36) Corbett, P. T.; Leclaire, J.; Vial, L.; West, K. R.; Wietor, J.-L.; Sanders, J. K.; Otto, S. Dynamic Combinatorial Chemistry. *Chem. Rev.* **2006**, 106, 3652-3711

(37) Wang, P.; Huang, C.; Xing, Y.; Fang, W.; Ren, J.; Yu, H.; Wang, G. Nir-Light- and Ph-Responsive Graphene Oxide Hybrid Cyclodextrin-Based Supramolecular Hydrogels. *Langmuir* **2019**, 35, 1021-1031

(38) Sherrington, D. C.; Taskinen, K. A. Self-Assembly in Synthetic Macromolecular Systems Multiple Hydrogen Bonding Interactions. *Chem. Soc. Rev.* **2001**, 30, 83-93

(39) Chen, J.; Yan, B.; Wang, X.; Huang, Q.; Thundat, T.; Zeng, H. Core Cross-Linked Double Hydrophilic Block Copolymer Micelles Based on Multiple Hydrogen-Bonding Interactions. *Polym. Chem.* **2017**, 8, 3066-3073

(40) Brunsveld, L.; Folmer, B. J. B.; Meijer, E. W.; Sijbesma, R. P. Supramolecular Polymers. *Chem. Rev.* **2001**, 101, 4071-4098

(41) Beijer, F. H.; Sijbesma, R. P.; Kooijman, H.; Spek, A. L.; Meijer, E. Strong Dimerization of Ureidopyrimidones Via Quadruple Hydrogen Bonding. *J. Am. Chem. Soc.* **1998**, 120, 6761-6769

(42) Sijbesma, R. P.; Beijer, F. H.; Brunsveld, L.; Folmer, B. J.; Hirschberg, J. K.; Lange, R. F.; Lowe, J. K.; Meijer, E. Reversible Polymers Formed from Self-Complementary Monomers Using Quadruple Hydrogen Bonding. *Science* **1997**, 278, 1601-1604

(43) Cui, J.; del Campo, A. Multivalent H-Bonds for Self-Healing Hydrogels. *Chem. Commun.* **2012**, 48, 9302-9304

(44) Hou, S.; Wang, X.; Park, S.; Jin, X.; Ma, P. X. Rapid Self‐Integrating, Injectable Hydrogel for Tissue Complex Regeneration. *Adv. Healthc. Mater.* **2015**, 4, 1491-1495

(45) Jeon, I.; Cui, J.; Illeperuma, W. R.; Aizenberg, J.; Vlassak, J. J. Extremely Stretchable and Fast Self‐Healing Hydrogels. *Adv. Mater.* **2016**, 28, 4678-4683

(46) Chen, J.; Peng, Q.; Thundat, T.; Zeng, H. Stretchable, Injectable, and Self-Healing Conductive Hydrogel Enabled by Multiple Hydrogen Bonding toward Wearable Electronics. *Chem. Mater.* **2019**, 31, 4553-4563

(47) Luo, F.; Sun, T. L.; Nakajima, T.; Kurokawa, T.; Zhao, Y.; Sato, K.; Ihsan, A. B.; Li, X.; Guo, H.; Gong, J. P. Oppositely Charged Polyelectrolytes Form Tough, Self-Healing, and Rebuildable Hydrogels. *Adv. Mater.* **2015**, 27, 2722-2727

(48) Sun, T. L.; Kurokawa, T.; Kuroda, S.; Ihsan, A. B.; Akasaki, T.; Sato, K.; Haque, M. A.; Nakajima, T.; Gong, J. P. Physical Hydrogels Composed of Polyampholytes Demonstrate High Toughness and Viscoelasticity. *Nat. Mater.* **2013**, 12, 932-937

(49) Huang, Y.; Lawrence, P. G.; Lapitsky, Y. Self-Assembly of Stiff, Adhesive and Self-Healing Gels from Common Polyelectrolytes. *Langmuir* **2014**, 30, 7771-7777

(50) Taylor, D. L.; in het Panhuis, M. Self-Healing Hydrogels. *Adv. Mater.* **2016**, 28, 9060-9093

(51) Gulyuz, U.; Okay, O. Self-Healing Poly (Acrylic Acid) Hydrogels with Shape Memory Behavior of High Mechanical Strength. *Macromolecules* **2014**, 47, 6889-6899

(52) Tuncaboylu, D. C.; Sari, M.; Oppermann, W.; Okay, O. Tough and Self-Healing Hydrogels Formed Via Hydrophobic Interactions. *Macromolecules* **2011**, 44, 4997-5005

(53) Qu, J.; Zhao, X.; Liang, Y.; Zhang, T.; Ma, P. X.; Guo, B. Antibacterial Adhesive Injectable Hydrogels with Rapid Self-Healing, Extensibility and Compressibility as Wound Dressing for Joints Skin Wound Healing. *Biomaterials* **2018**, 183, 185-199

(54) Ding, C.; Zhao, L.; Liu, F.; Cheng, J.; Gu, J.; Dan, S.-.; Liu, C.; Qu, X.; Yang, Z. Dually Responsive Injectable Hydrogel Prepared by in Situ Cross-Linking of Glycol Chitosan and Benzaldehyde-Capped Peo-Ppo-Peo. *Biomacromolecules* **2010**, 11, 1043-1051

(55) Li, L.; Yan, B.; Yang, J.; Chen, L.; Zeng, H. Novel Mussel-Inspired Injectable Self-Healing Hydrogel with Anti-Biofouling Property. *Adv. Mater.* **2015**, 27, 1294-1299

(56) Jeon, I.; Cui, J.; Illeperuma, W. R. K.; Aizenberg, J.; Vlassak, J. J. Extremely Stretchable and Fast Self-Healing Hydrogels. *Adv. Mater.* **2016**, 28, 4678-4683

(57) Hu, X.; Vatankhah‐Varnoosfaderani, M.; Zhou, J.; Li, Q.; Sheiko, S. S. Weak Hydrogen Bonding Enables Hard, Strong, Tough, and Elastic Hydrogels. *Adv. Mater.* **2015**, 27, 6899-6905

(58) Holten-Andersen, N.; Harrington, M. J.; Birkedal, H.; Lee, B. P.; Messersmith, P. B.; Lee, K. Y. C.; Waite, J. H. Ph-Induced Metal-Ligand Cross-Links Inspired by Mussel Yield Self-Healing Polymer Networks with near-Covalent Elastic Moduli. *PNAS* **2011**, 108, 2651-2655

(59) Shi, L.; Wang, F.; Zhu, W.; Xu, Z.; Fuchs, S.; Hilborn, J.; Zhu, L.; Ma, Q.; Wang, Y.; Weng, X.; Ossipov, D. A. Self-Healing Silk Fibroin-Based Hydrogel for Bone Regeneration: Dynamic Metal-Ligand Self-Assembly Approach. *Adv. Funct. Mater.* **2017**, 27, 1700591

(60) Sun, J.-Y.; Zhao, X.; Illeperuma, W. R.; Chaudhuri, O.; Oh, K. H.; Mooney, D. J.; Vlassak, J. J.; Suo, Z. Highly Stretchable and Tough Hydrogels. *Nature* **2012**, 489, 133

(61) Liu, G.; Yuan, Q.; Hollett, G.; Zhao, W.; Kang, Y.; Wu, J. Cyclodextrin-Based Host–Guest Supramolecular Hydrogel and Its Application in Biomedical Fields. *Polym. Chem.* **2018**, 9, 3436-3449

(62) Li, J.; Harada, A.; Kamachi, M. Sol–Gel Transition During Inclusion Complex Formation between A-Cyclodextrin and High Molecular Weight Poly(Ethylene Glycol)S in Aqueous Solution. *Polym. J.* **1994**, 26, 1019-1026

(63) Simões, S. M. N.; Veiga, F.; Torres-Labandeira, J. J.; Ribeiro, A. C. F.; Sandez-Macho, M. I.; Concheiro, A.; Alvarez-Lorenzo, C. Syringeable Pluronic–A-Cyclodextrin Supramolecular Gels for Sustained Delivery of Vancomycin. *European Journal of Pharmaceutics and Biopharmaceutics* **2012**, 80, 103-112

(64) Huh, K. M.; Ooya, T.; Lee, W. K.; Sasaki, S.; Kwon, I. C.; Jeong, S. Y.; Yui, N. Supramolecular-Structured Hydrogels Showing a Reversible Phase Transition by Inclusion Complexation between Poly(Ethylene Glycol) Grafted Dextran and A-Cyclodextrin. *Macromolecules* **2001**, 34, 8657-8662

(65) Sheng, J.; Wang, Y.; Xiong, L.; Luo, Q.; Li, X.; Shen, Z.; Zhu, W. Injectable Doxorubicin-Loaded Hydrogels Based on Dendron-Like B-Cyclodextrin–Poly(Ethylene Glycol) Conjugates. *Polym. Chem.* **2017**, 8, 1680-1688

(66) Rosales, A. M.; Rodell, C. B.; Chen, M. H.; Morrow, M. G.; Anseth, K. S.; Burdick, J. A. Reversible Control of Network Properties in Azobenzene-Containing Hyaluronic Acid-Based Hydrogels. *Bioconjugate Chem.* **2018**, 29, 905-913

(67) Tomatsu, I.; Hashidzume, A.; Harada, A. Redox-Responsive Hydrogel System Using the Molecular Recognition of B-Cyclodextrin. *Macromol. Rapid Commun.* **2006**, 27, 238-241

(68) van de Manakker, F.; van der Pot, M.; Vermonden, T.; van Nostrum, C. F.; Hennink, W. E. Self-Assembling Hydrogels Based on B-Cyclodextrin/Cholesterol Inclusion Complexes. *Macromolecules* **2008**, 41, 1766-1773

(69) Liu, S.; Ruspic, C.; Mukhopadhyay, P.; Chakrabarti, S.; Zavalij, P. Y.; Isaacs, L. The Cucurbit[N]Uril Family: Prime Components for Self-Sorting Systems. *J. Am. Chem. Soc.* **2005**, 127, 15959-15967

(70) Kim, J.; Jung, I.-S.; Kim, S.-Y.; Lee, E.; Kang, J.-K.; Sakamoto, S.; Yamaguchi, K.; Kim, K. New Cucurbituril Homologues: Syntheses, Isolation, Characterization, and X-Ray Crystal Structures of Cucurbit[N]Uril (N = 5, 7, and 8). *J. Am. Chem. Soc.* **2000**, 122, 540-541

(71) Liu, J.; Tan, C. S. Y.; Yu, Z.; Lan, Y.; Abell, C.; Scherman, O. A. Biomimetic Supramolecular Polymer Networks Exhibiting Both Toughness and Self‐Recovery. *Adv. Mater.* **2017**, 29, 1604951

(72) Schiff, H. Mittheilungen Aus Dem Universitätslaboratorium in Pisa: Eine Neue Reihe Organischer Basen. *Justus Liebigs Annalen der Chemie* **1864**, 131, 118-119

(73) Wang, T.; Turhan, M.; Gunasekaran, S. Selected Properties of Ph‐Sensitive, Biodegradable Chitosan–Poly (Vinyl Alcohol) Hydrogel. *Polym. Int.* **2004**, 53, 911-918

(74) Godoy‐Alcántar, C.; Yatsimirsky, A. K.; Lehn, J. M. Structure‐Stability Correlations for Imine Formation in Aqueous Solution. *J. Phys. Org. Chem.* **2005**, 18, 979-985

(75) Xin, Y.; Yuan, J. Schiff's Base as a Stimuli-Responsive Linker in Polymer Chemistry. *Polym. Chem.* **2012**, 3, 3045-3055

(76) Wojtecki, R. J.; Meador, M. A.; Rowan, S. J. Using the Dynamic Bond to Access Macroscopically Responsive Structurally Dynamic Polymers. *Nat. Mater.* **2011**, 10, 14

(77) Zhang, Y.; Tao, L.; Li, S.; Wei, Y. Synthesis of Multiresponsive and Dynamic Chitosan-Based Hydrogels for Controlled Release of Bioactive Molecules. *Biomacromolecules* **2011**, 12, 2894-2901

(78) Tseng, T. C.; Tao, L.; Hsieh, F. Y.; Wei, Y.; Chiu, I. M.; Hsu, S. h. An Injectable, Self‐Healing Hydrogel to Repair the Central Nervous System. *Adv. Mater.* **2015**, 27, 3518-3524

(79) Dong, R.; Zhao, X.; Guo, B.; Ma, P. X. Self-Healing Conductive Injectable Hydrogels with Antibacterial Activity as Cell Delivery Carrier for Cardiac Cell Therapy. *ACS Appl. Mater. Interfaces* **2016**, 8, 17138-17150

(80) Wei, Z.; Yang, J. H.; Liu, Z. Q.; Xu, F.; Zhou, J. X.; Zrinyi, M.; Osada, Y.; Chen, Y. M. Novel Biocompatible Polysaccharide-Based Self-Healing Hydrogel. *Adv. Funct. Mater.* **2015**, 25, 1352-1359

(81) Chen, G.; Yu, Y.; Wu, X.; Wang, G.; Ren, J.; Zhao, Y. Bioinspired Multifunctional Hybrid Hydrogel Promotes Wound Healing. *Adv. Funct. Mater.* **2018**, 28,

(82) Pettignano, A.; Haering, M.; Bernardi, L.; Tanchoux, N.; Quignard, F.; Diaz Diaz, D. Self-Healing Alginate-Gelatin Biohydrogels Based on Dynamic Covalent Chemistry: Elucidation of Key Parameters. *Mater. Chem. Front.* **2017**, 1, 73-79

(83) Vahedi, M.; Barzin, J.; Shokrolahi, F.; Shokrollahi, P. Self-Healing, Injectable Gelatin Hydrogels Cross-Linked by Dynamic Schiff Base Linkages Support Cell Adhesion and Sustained Release of Antibacterial Drugs. *Macromol. Mater. Eng.* **2018**, 303,

(84) Guan, Y.; Zhang, Y. Boronic Acid-Containing Hydrogels: Synthesis and Their Applications. *Chem. Soc. Rev.* **2013**, 42, 8106-8121

(85) Brooks, W. L. A.; Sumerlin, B. S. Synthesis and Applications of Boronic Acid-Containing Polymers: From Materials to Medicine. *Chem. Rev.* **2016**, 116, 1375-1397

(86) Yan, J.; Springsteen, G.; Deeter, S.; Wang, B. The Relationship among Pka, Ph, and Binding Constants in the Interactions between Boronic Acids and Diols—It Is Not as Simple as It Appears. *Tetrahedron* **2004**, 60, 11205-11209

(87) Deng, C. C.; Brooks, W. L. A.; Abboud, K. A.; Sumerlin, B. S. Boronic Acid-Based Hydrogels Undergo Self-Healing at Neutral and Acidic Ph. *ACS Macro Lett.* **2015**, 4, 220-224

(88) Chen, Y.; Diaz-Dussan, D.; Wu, D.; Wang, W.; Peng, Y.-Y.; Asha, A. B.; Hall, D. G.; Ishihara, K.; Narain, R. Bioinspired Self-Healing Hydrogel Based on Benzoxaborole-Catechol Dynamic Covalent Chemistry for 3d Cell Encapsulation. *ACS Macro Lett.* **2018**, 7, 904-908

(89) Deuel, v. H.; Neukom, H. Über Die Reaktion Von Borsäure Und Borax Mit Polysacchariden Und Anderen Hochmolekularen Polyoxy ‐ Verbindungen. *Die Makromolekulare Chemie* **1949**, 3, 13-30

(90) He, L.; Szopinski, D.; Wu, Y.; Luinstra, G. A.; Theato, P. Toward Self-Healing Hydrogels Using One-Pot Thiol-Ene Click and Borax-Diol Chemistry. *ACS Macro Lett.* **2015**, 4, 673-678

(91) Lai, Y. C.; Wu, H. M.; Lin, H. C.; Chang, C. L.; Chou, H. H.; Hsiao, Y. C.; Wu, Y. C. Entirely, Intrinsically, and Autonomously Self ‐ Healable, Highly Transparent, and Superstretchable Triboelectric Nanogenerator for Personal Power Sources and Self ‐ Powered Electronic Skins. *Adv. Funct. Mater.* **2019**, 1904626

(92) Tseng, T.-C.; Hsieh, F.-Y.; Theato, P.; Wei, Y.; Hsu, S.-h. Glucose-Sensitive Self-Healing Hydrogel as Sacrificial Materials to Fabricate Vascularized Constructs. *Biomaterials* **2017**, 133, 20-28

(93) Roberts, M. C.; Hanson, M. C.; Massey, A. P.; Karren, E. A.; Kiser, P. F. Dynamically Restructuring Hydrogel Networks Formed with Reversible Covalent Crosslinks. *Adv. Mater.* **2007**, 19, 2503-2507

(94) Yesilyurt, V.; Ayoob, A. M.; Appel, E. A.; Borenstein, J. T.; Langer, R.; Anderson, D. G. Mixed Reversible Covalent Crosslink Kinetics Enable Precise, Hierarchical Mechanical Tuning of Hydrogel Networks. *Adv. Mater.* **2017**, 29,

(95) Yesilyurt, V.; Webber, M. J.; Appel, E. A.; Godwin, C.; Langer, R.; Anderson, D. G. Injectable Self-Healing Glucose-Responsive Hydrogels with Ph-Regulated Mechanical Properties. *Adv. Mater.* **2016**, 28, 86-+

(96) Amaral, A. J. R.; Emamzadeh, M.; Pasparakis, G. Transiently Malleable Multi-Healable Hydrogel Nanocomposites Based on Responsive Boronic Acid Copolymers. *Polym. Chem.* **2018**, 9, 525-537

(97) Chen, Y.; Wang, W.; Wu, D.; Nagao, M.; Hall, D. G.; Thundat, T.; Narain, R. Injectable Self-Healing Zwitterionic Hydrogels Based on Dynamic Benzoxaborole-Sugar Interactions with Tunable Mechanical Properties. *Biomacromolecules* **2018**, 19, 596-605

(98) Wu, D.; Wang, W. D.; Diaz-Dussan, D.; Peng, Y. Y.; Chen, Y. J.; Narain, R.; Hall, D. G. In Situ Forming, Dual-Crosslink Network, Self-Healing Hydrogel Enabled by a Bioorthogonal Nopoldiol-Benzoxaborolate Click Reaction with a Wide Ph Range. *Chem. Mater.* **2019**, 31, 4092-4102

(99) He, L.; Fullenkamp, D. E.; Rivera, J. G.; Messersmith, P. B. Ph Responsive Self-Healing Hydrogels Formed by Boronate–Catechol Complexation. *Chem. Commun.* **2011**, 47, 7497-7499

(100) Kitano, S.; Hisamitsu, I.; Koyama, Y.; Kataoka, K.; Okano, T.; Sakurai, Y. Effect of the Incorporation of Amino Groups in a Glucose‐Responsive Polymer Complex Having Phenylboronic Acid Moieties. *Polym. Adv. Technol.* **1991**, 2, 261-264

(101) Wu, D.-C.; Loh, X. J.; Wu, Y.-L.; Lay, C. L.; Liu, Y. 'Living' Controlled in Situ Gelling Systems: Thiol−Disulfide Exchange Method toward Tailor-Made Biodegradable Hydrogels. *J. Am. Chem. Soc.* **2010**, 132, 15140-15143

(102) Deng, G.; Li, F.; Yu, H.; Liu, F.; Liu, C.; Sun, W.; Jiang, H.; Chen, Y. Dynamic Hydrogels with an Environmental Adaptive Self-Healing Ability and Dual Responsive Sol-Gel Transitions. *ACS Macro Lett.* **2012**, 1, 275-279

(103) Sun, P.; Ren, S.; Liu, F.; Wu, A.; Sun, N.; Shi, L.; Zheng, L. Smart Low Molecular Weight Hydrogels with Dynamic Covalent Skeletons. *Soft Matter* **2018**, 14, 6678-6683

(104) Barcan, G. A.; Zhang, X.; Waymouth, R. M. Structurally Dynamic Hydrogels Derived from 1,2-Dithiolanes. *J. Am. Chem. Soc.* **2015**, 137, 5650-5653

(105) Zhang, X.; Waymouth, R. M. 1,2-Dithiolane-Derived Dynamic, Covalent Materials: Cooperative Self-Assembly and Reversible Cross-Linking. *J. Am. Chem. Soc.* **2017**, 139, 3822-3833

(106) Yu, H.; Wang, Y.; Yang, H.; Peng, K.; Zhang, X. Injectable Self-Healing Hydrogels Formed Via Thiol/Disulfide Exchange of Thiol Functionalized F127 and Dithiolane Modified Peg. *J. Mater. Chem. B* **2017**, 5, 4121-4127

(107) Casuso, P.; Pérez-San Vicente, A.; Iribar, H.; Gutiérrez-Rivera, A.; Izeta, A.; Loinaz, I.; Cabañero, G.; Grande, H.-J.; Odriozola, I.; Dupin, D. Aurophilically Cross-Linked "Dynamic" Hydrogels Mimicking Healthy Synovial Fluid Properties. *Chem. Commun.* **2014**, 50, 15199-15201

(108) Casuso, P.; Odriozola, I.; Perez-San Vicente, A.; Loinaz, I.; Cabanero, G.; Grande, H.-J.; Dupin, D. Injectable and Self-Healing Dynamic Hydrogels Based on Metal(I)-Thiolate/Disulfide Exchange as Biomaterials with Tunable Mechanical Properties. *Biomacromolecules* **2015**, 16, 3552-3561

(109) Perez-San Vicente, A.; Peroglio, M.; Ernst, M.; Casuso, P.; Loinaz, I.; Grande, H.-J.; Alini, M.; Eglin, D.; Dupin, D. Self-Healing Dynamic Hydrogel as Injectable Shock-Absorbing Artificial Nucleus Pulposus. *Biomacromolecules* **2017**, 18, 2360-2370

(110) Wang, L. L.; Highley, C. B.; Yeh, Y.-C.; Galarraga, J. H.; Uman, S.; Burdick, J. A. Three-Dimensional Extrusion Bioprinting of Single- and Double-Network Hydrogels Containing Dynamic Covalent Crosslinks. *J. Biomed. Mater. Res. A* **2018**, 106, 865-875

(111) Yu, F.; Cao, X.; Du, J.; Wang, G.; Chen, X. Multifunctional Hydrogel with Good Structure Integrity, Self-Healing, and Tissue-Adhesive Property Formed by Combining Die Is Alder Click Reaction and Acylhydrazone Bond. *ACS Appl. Mater. Interfaces* **2015**, 7, 24023-24031

(112) Wang, H.; Zhu, D.; Paul, A.; Cai, L.; Enejder, A.; Yang, F.; Heilshorn, S. C. Covalently Adaptable Elastin-Like Protein-Hyaluronic Acid (Elp-Ha) Hybrid Hydrogels with Secondary Thermoresponsive Crosslinking for Injectable Stem Cell Delivery. *Adv. Funct. Mater.* **2017**, 27,

(113) Yang, X.; Liu, G.; Peng, L.; Guo, J.; Tao, L.; Yuan, J.; Chang, C.; Wei, Y.; Zhang, L. Highly Efficient Self-Healable and Dual Responsive Cellulose-Based Hydrogels for Controlled Release and 3d Cell Culture. *Adv. Funct. Mater.* **2017**, 27,

(114) Wang, L.; Deng, F.; Wang, W.; Li, A.; Lu, C.; Chen, H.; Wu, G.; Nan, K.; Li, L. Construction of Injectable Self-Healing Macroporous Hydrogels Via a Template-Free Method for Tissue Engineering and Drug Delivery. *ACS Appl. Mater. Interfaces* **2018**, 10, 36721-36732

(115) Yan, S.; Wang, W.; Li, X.; Ren, J.; Yun, W.; Zhang, K.; Li, G.; Yin, J. Preparation of Mussel-Inspired Injectable Hydrogels Based on Dual-Functionalized Alginate with Improved Adhesive, Self-Healing, and Mechanical Properties. *J. Mater. Chem. B* **2018**, 6, 6377-6390

(116) Wang, P.; Deng, G.; Zhou, L.; Li, Z.; Chen, Y. Ultrastretchable, Self-Healable Hydrogels Based on Dynamic Covalent Bonding and Triblock Copolymer Micellization. *ACS Macro Lett.* **2017**, 6, 881-886

(117) Sharma, P. K.; Taneja, S.; Singh, Y. Hydrazone-Linkage-Based Self-Healing and Injectable Xanthan-Poly(Ethylene Glycol) Hydrogels for Controlled Drug Release and 3d Cell Culture. *ACS Appl. Mater. Interfaces* **2018**, 10, 30936-30945

(118) Sharma, P. K.; Singh, Y. Glyoxylic Hydrazone Linkage-Based Peg Hydrogels for Covalent Entrapment and Controlled Delivery of Doxorubicin. *Biomacromolecules* **2019**, 20, 2174-2184

(119) Patenaude, M.; Hoare, T. Injectable, Mixed Natural-Synthetic Polymer Hydrogels with Modular Properties. *Biomacromolecules* **2012**, 13, 369-378

(120) Patenaude, M.; Hoare, T. Injectable, Degradable Thermoresponsive Poly (N-Isopropylacrylamide) Hydrogels. *ACS Macro Lett.* **2012**, 1, 409-413

(121) Li, L.; Yan, B.; Yang, J.; Huang, W.; Chen, L.; Zeng, H. Injectable Self-Healing Hydrogel with Antimicrobial and Antifouling Properties. *ACS Appl. Mater. Interfaces* **2017**, 9, 9221-9225

(122) Eklund, A.; Zhang, H.; Zeng, H.; Priimagi, A.; Ikkala, O. Fast Switching of Bright Whiteness in Channeled Hydrogel Networks. *Adv. Funct. Mater.* **2020**, 2000754

(123) Wang, W. D.; Xiang, L.; Gong, L.; Hu, W. H.; Huang, W. J.; Chen, Y. J.; Asha, A. B.; Srinivas, S.; Chen, L. Y.; Narain, R.; Zeng, H. B. Injectable, Self-Healing Hydrogel with Tunable Optical, Mechanical, and Antimicrobial Properties. *Chem. Mater.* **2019**, 31, 2366-2376

(124) Shang, J.; Le, X.; Zhang, J.; Chen, T.; Theato, P. Trends in Polymeric Shape Memory Hydrogels and Hydrogel Actuators. *Polym. Chem.* **2019**, 10, 1036-1055

(125) Kocak, G.; Tuncer, C.; Bütün, V. Ph-Responsive Polymers. *Polym. Chem.* **2017**, 8, 144-176

(126) Wang, W.; Zeng, Z.; Xiang, L.; Liu, C.; Diaz-Dussan, D.; Du, Z.; Asha, A. B.; Yang, W.; Peng, Y.-Y.; Pan, M.; Narain, R.; Liu, J.; Zeng, H. Injectable Self-Healing Hydrogel Via Biological Environment-Adaptive Supramolecular Assembly for Gastric Perforation Healing. *ACS Nano* **2021**, 15, 9913-9923

(127) Ahadian, S.; Ramón-Azcón, J.; Estili, M.; Liang, X.; Ostrovidov, S.; Shiku, H.; Ramalingam, M.; Nakajima, K.; Sakka, Y.; Bae, H. Hybrid Hydrogels Containing Vertically Aligned Carbon Nanotubes with Anisotropic Electrical Conductivity for Muscle Myofiber Fabrication. *Scientific reports* **2014**, 4, 4271

(128) Liu, X.; Miller, A. L.; Park, S.; Waletzki, B. E.; Zhou, Z.; Terzic, A.; Lu, L. Functionalized Carbon Nanotube and Graphene Oxide Embedded Electrically Conductive Hydrogel Synergistically Stimulates Nerve Cell Differentiation. *ACS Appl. Mater. Interfaces* **2017**, 9, 14677-14690

(129) Lim, C.; Shin, Y.; Jung, J.; Kim, J. H.; Lee, S.; Kim, D.-H. Stretchable Conductive Nanocomposite Based on Alginate Hydrogel and Silver Nanowires for Wearable Electronics. *APL Materials* **2019**, 7, 031502

(130) Feig, V. R.; Tran, H.; Lee, M.; Bao, Z. Mechanically Tunable Conductive Interpenetrating Network Hydrogels That Mimic the Elastic Moduli of Biological Tissue. *Nat. Commun.* **2018**, 9, 1-9

(131) Lei, Z.; Wang, Q.; Sun, S.; Zhu, W.; Wu, P. A Bioinspired Mineral Hydrogel as a Self‐Healable, Mechanically Adaptable Ionic Skin for Highly Sensitive Pressure Sensing. *Adv. Mater.* **2017**, 29, 1700321

(132) Wang, L.; Gao, G.; Zhou, Y.; Xu, T.; Chen, J.; Wang, R.; Zhang, R.; Fu, J. Tough, Adhesive, Self-Healable, and Transparent Ionically Conductive Zwitterionic Nanocomposite Hydrogels as Skin Strain Sensors. *ACS Appl. Mater. Interfaces* **2019**, 11, 3506-3515

(133) Hager, M. D. Self‐Healing Materials. *Handbook of Solid State Chemistry* **2017**, 201-225

(134) Hager, M. D.; Greil, P.; Leyens, C.; van der Zwaag, S.; Schubert, U. S. Self‐Healing Materials. *Adv. Mater.* **2010**, 22, 5424-5430

(135) South, A. B.; Lyon, L. A. Autonomic Self‐Healing of Hydrogel Thin Films. *Angew. Chem.* **2010**, 122, 779-783

(136) Zhang, H. J.; Sun, T. L.; Zhang, A. K.; Ikura, Y.; Nakajima, T.; Nonoyama, T.; Kurokawa, T.; Ito, O.; Ishitobi, H.; Gong, J. P. Tough Physical Double-Network Hydrogels Based on Amphiphilic Triblock Copolymers. *Adv. Mater.* **2016**, 28, 4884-4890

(137) Haraguchi, K. Nanocomposite Hydrogels. *Curr. Opin. Solid State Mater. Sci.* **2007**, 11, 47-54

(138) Sabah, A.; Hornyak, G. L. Nanofibers and Nanowires. In: Javad S, Butt A, eds. *Nanobotany*. Cham: Springer International Publishing; 2018:67-82.

(139) Huang, Y.; Zhong, M.; Huang, Y.; Zhu, M.; Pei, Z.; Wang, Z.; Xue, Q.; Xie, X.; Zhi, C. A Self-Healable and Highly Stretchable Supercapacitor Based on a Dual Crosslinked Polyelectrolyte. *Nat. Commun.* **2015**, 6, 10310

(140) Shi, F.-K.; Wang, X.-P.; Guo, R.-H.; Zhong, M.; Xie, X.-M. Highly Stretchable and Super Tough Nanocomposite Physical Hydrogels Facilitated by the Coupling of Intermolecular Hydrogen Bonds and Analogous Chemical Crosslinking of Nanoparticles. *J. Mater. Chem. B* **2015**, 3, 1187-1192

(141) Zhong, M.; Liu, X.-Y.; Shi, F.-K.; Zhang, L.-Q.; Wang, X.-P.; Cheetham, A. G.; Cui, H.; Xie, X.-M. Self-Healable, Tough and Highly Stretchable Ionic Nanocomposite Physical Hydrogels. *Soft Matter* **2015**, 11, 4235-4241

(142) Hu, M.; Gu, X.; Hu, Y.; Wang, T.; Huang, J.; Wang, C. Low Chemically Cross-Linked Pam/C-Dot Hydrogel with Robustness and Superstretchability in Both as-Prepared and Swelling Equilibrium States. *Macromolecules* **2016**, 49, 3174-3183

(143) Lei, Z.; Wang, Q.; Sun, S.; Zhu, W.; Wu, P. A Bioinspired Mineral Hydrogel as a Self-Healable, Mechanically Adaptable Ionic Skin for Highly Sensitive Pressure Sensing. *Adv. Mater.* **2017**, 29, 1700321

(144) Bhattacharya, S.; Phatake, R. S.; Barnea, S. N.; Zerby, N.; Zhu, J. J.; Shikler, R.; Lemcoff, N. G.; Jelinek, R. Fluorescent Self-Healing Carbon Dot/Polymer Gels. *Acs Nano* **2019**, 13, 1433-1442

(145) Xing, R.; Liu, K.; Jiao, T.; Zhang, N.; Ma, K.; Zhang, R.; Zou, Q.; Ma, G.; Yan, X. An Injectable Self-Assembling Collagen–Gold Hybrid Hydrogel for Combinatorial Antitumor Photothermal/Photodynamic Therapy. *Adv. Mater.* **2016**, 28, 3669-3676

(146) Lin, F.; Wang, Z.; Shen, Y.; Tang, L.; Zhang, P.; Wang, Y.; Chen, Y.; Huang, B.; Lu, B. Natural Skin-Inspired Versatile Cellulose Biomimetic Hydrogels. *J. Mater. Chem. A* **2019**, 7, 26442-26455

(147) Murali Mohan, Y.; Lee, K.; Premkumar, T.; Geckeler, K. E. Hydrogel Networks as Nanoreactors: A Novel Approach to Silver Nanoparticles for Antibacterial Applications. *Polymer* **2007**, 48, 158-164

(148) Wu, H.; Liu, L.; Song, L.; Ma, M.; Gu, N.; Zhang, Y. Enhanced Tumor Synergistic Therapy by Injectable Magnetic Hydrogel Mediated Generation of Hyperthermia and Highly Toxic Reactive Oxygen Species. *ACS Nano* **2019**, 13, 14013-14023

(149) Zhang, Y.; Yang, B.; Zhang, X.; Xu, L.; Tao, L.; Li, S.; Wei, Y. A Magnetic Self-Healing Hydrogel. *Chem. Commun.* **2012**, 48, 9305-9307

(150) Mehrali, M.; Thakur, A.; Pennisi, C. P.; Talebian, S.; Arpanaei, A.; Nikkhah, M.; Dolatshahi-Pirouz, A. Nanoreinforced Hydrogels for Tissue Engineering: Biomaterials That Are Compatible with Load-Bearing and Electroactive Tissues. *Adv. Mater.* **2017**, 29, 1603612

(151) Yoon, I.-K.; Hwang, J.-Y.; Seo, J.-w.; Jang, W.-C.; Kim, H.-W.; Shin, U. S. Carbon Nanotube-Gelatin-Hydroxyapatite Nanohybrids with Multilayer Core–Shell Structure for Mimicking Natural Bone. *Carbon* **2014**, 77, 379-389

(152) Chahine, N. O.; Collette, N. M.; Thomas, C. B.; Genetos, D. C.; Loots, G. G. Nanocomposite Scaffold for Chondrocyte Growth and Cartilage Tissue Engineering: Effects of Carbon Nanotube Surface Functionalization. *Tissue Engineering Part A* **2014**, 20, 2305-2315

(153) Ramón-Azcón, J.; Ahadian, S.; Estili, M.; Liang, X.; Ostrovidov, S.; Kaji, H.; Shiku, H.; Ramalingam, M.; Nakajima, K.; Sakka, Y.; Khademhosseini, A.; Matsue, T. Dielectrophoretically Aligned Carbon Nanotubes to Control Electrical and Mechanical Properties of Hydrogels to Fabricate Contractile Muscle Myofibers. *Adv. Mater.* **2013**, 25, 4028-4034

(154) Shin, S. R.; Jung, S. M.; Zalabany, M.; Kim, K.; Zorlutuna, P.; Kim, S. b.; Nikkhah, M.; Khabiry, M.; Azize, M.; Kong, J.; Wan, K.-t.; Palacios, T.; Dokmeci, M. R.; Bae, H.; Tang, X.; Khademhosseini, A. Carbon-Nanotube-Embedded Hydrogel Sheets for Engineering Cardiac Constructs and Bioactuators. *ACS Nano* **2013**, 7, 2369-2380

(155) Qin, Z.; Sun, X.; Yu, Q.; Zhang, H.; Wu, X.; Yao, M.; Liu, W.; Yao, F.; Li, J. Carbon Nanotubes/Hydrophobically Associated Hydrogels as Ultrastretchable, Highly

Sensitive, Stable Strain, and Pressure Sensors. *ACS Appl. Mater. Interfaces* **2020**, 12, 4944-4953

(156) Sun, X.; Qin, Z.; Ye, L.; Zhang, H.; Yu, Q.; Wu, X.; Li, J.; Yao, F. Carbon Nanotubes Reinforced Hydrogel as Flexible Strain Sensor with High Stretchability and Mechanically Toughness. *Chem. Eng. J.* **2020**, 382, 122832

(157) Kovtyukhova, N. I.; Mallouk, T. E.; Pan, L.; Dickey, E. C. Individual Single-Walled Nanotubes and Hydrogels Made by Oxidative Exfoliation of Carbon Nanotube Ropes. *J. Am. Chem. Soc.* **2003**, 125, 9761-9769

(158) Guo, K.; Zhang, D.-L.; Zhang, X.-M.; Zhang, J.; Ding, L.-S.; Li, B.-J.; Zhang, S. Conductive Elastomers with Autonomic Self-Healing Properties. *Angew. Chem. Int. Ed.* **2015**, 54, 12127-12133

(159) Mandal, B.; Rameshbabu, A. P.; Soni, S. R.; Ghosh, A.; Dhara, S.; Pal, S. In Situ Silver Nanowire Deposited Cross-Linked Carboxymethyl Cellulose: A Potential Transdermal Anticancer Drug Carrier. *ACS Appl. Mater. Interfaces* **2017**, 9, 36583-36595

(160) Kumar, K. S.; Zhang, L.; Kalairaj, M. S.; Banerjee, H.; Xiao, X.; Jiayi, C. C.; Huang, H.; Lim, C. M.; Ouyang, J.; Ren, H. Stretchable and Sensitive Silver Nanowire-Hydrogel Strain Sensors for Proprioceptive Actuation. *ACS Appl. Mater. Interfaces* **2021**, 13, 37816-37829

(161) Yin, M.-j.; Zhang, Y.; Yin, Z.; Zheng, Q.; Zhang, A. P. Micropatterned Elastic Gold-Nanowire/Polyacrylamide Composite Hydrogels for Wearable Pressure Sensors. *Advanced Materials Technologies* **2018**, 3, 1800051

(162) Liu, X.; Yang, K.; Chang, M.; Wang, X.; Ren, J. Fabrication of Cellulose Nanocrystal Reinforced Nanocomposite Hydrogel with Self-Healing Properties. *Carbohydr. Polym.* **2020**, 240, 116289

(163) Li, B.; Zhang, Y.; Wu, C.; Guo, B.; Luo, Z. Fabrication of Mechanically Tough and Self-Recoverable Nanocomposite Hydrogels from Polyacrylamide Grafted Cellulose Nanocrystal and Poly(Acrylic Acid). *Carbohydr. Polym.* **2018**, 198, 1-8

(164) Huang, W.; Wang, Y.; Huang, Z.; Wang, X.; Chen, L.; Zhang, Y.; Zhang, L. On-Demand Dissolvable Self-Healing Hydrogel Based on Carboxymethyl Chitosan and Cellulose Nanocrystal for Deep Partial Thickness Burn Wound Healing. *ACS Appl. Mater. Interfaces* **2018**, 10, 41076-41088

(165) Haraguchi, K.; Takehisa, T. Nanocomposite Hydrogels: A Unique Organic–Inorganic Network Structure with Extraordinary Mechanical, Optical, and Swelling/De‐Swelling Properties. *Adv. Mater.* **2002**, 14, 1120-1124

(166) Wang, Q.; Mynar, J. L.; Yoshida, M.; Lee, E.; Lee, M.; Okuro, K.; Kinbara, K.; Aida, T. High-Water-Content Mouldable Hydrogels by Mixing Clay and a Dendritic Molecular Binder. *Nature* **2010**, 463, 339-343

(167) Pan, C.; Liu, L.; Chen, Q.; Zhang, Q.; Guo, G. Tough, Stretchable, Compressive Novel Polymer/Graphene Oxide Nanocomposite Hydrogels with Excellent Self-Healing Performance. *ACS Appl. Mater. Interfaces* **2017**, 9, 38052-38061

(168) Cong, H.-P.; Wang, P.; Yu, S.-H. Highly Elastic and Superstretchable Graphene Oxide/Polyacrylamide Hydrogels. *Small* **2014**, 10, 448-453

(169) Han, L.; Lu, X.; Wang, M.; Gan, D.; Deng, W.; Wang, K.; Fang, L.; Liu, K.; Chan, C. W.; Tang, Y.; Weng, L.-T.; Yuan, H. A Mussel-Inspired Conductive, Self-Adhesive, and Self-Healable Tough Hydrogel as Cell Stimulators and Implantable Bioelectronics. *Small* **2017**, 13, 1601916

(170) Jin, X.; Jiang, H.; Li, G.; Fu, B.; Bao, X.; Wang, Z.; Hu, Q. Stretchable, Conductive Pani-Paam-Gocs Hydrogels with Excellent Mechanical Strength, Strain Sensitivity and Skin Affinity. *Chem. Eng. J.* **2020**, 394, 124901

(171) Jing, X.; Mi, H.-Y.; Peng, X.-F.; Turng, L.-S. Biocompatible, Self-Healing, Highly Stretchable Polyacrylic Acid/Reduced Graphene Oxide Nanocomposite Hydrogel Sensors Via Mussel-Inspired Chemistry. *Carbon* **2018**, 136, 63-72

(172) Zhang, Y.-Z.; Lee, K. H.; Anjum, D. H.; Sougrat, R.; Jiang, Q.; Kim, H.; Alshareef, H. N. Mxenes Stretch Hydrogel Sensor Performance to New Limits. *Science Advances* **2018**, 4, eaat0098

(173) Liao, H.; Guo, X.; Wan, P.; Yu, G. Conductive Mxene Nanocomposite Organohydrogel for Flexible, Healable, Low-Temperature Tolerant Strain Sensors. *Adv. Funct. Mater.* **2019**, 29, 1904507

(174) Zhang, Y.; Chen, K.; Li, Y.; Lan, J.; Yan, B.; Shi, L.; Ran, R. High-Strength, Self-Healable, Temperature-Sensitive, Mxene-Containing Composite Hydrogel as a Smart Compression Sensor. *ACS Appl. Mater. Interfaces* **2019**, 11, 47350-47357

(175) Razal, J. M.; Brown, H. R.; Spinks, G. M.; Whitten, P. G.; Naficy, S. Progress toward Robust Polymer Hydrogels. **2011**,

(176) Sakai, T.; Matsunaga, T.; Yamamoto, Y.; Ito, C.; Yoshida, R.; Suzuki, S.; Sasaki, N.; Shibayama, M.; Chung, U.-i. Design and Fabrication of a High-Strength Hydrogel with Ideally Homogeneous Network Structure from Tetrahedron-Like Macromonomers. *Macromolecules* **2008**, 41, 5379-5384

(177) Wang, X.; Wang, H.; Brown, H. R. Jellyfish Gel and Its Hybrid Hydrogels with High Mechanical Strength. *Soft Matter* **2011**, 7, 211-219

(178) Sun, P.; Zhang, H.; Xu, D.; Wang, Z.; Wang, L.; Gao, G.; Hossain, G.; Wu, J.; Wang, R.; Fu, J. Super Tough Bilayer Actuators Based on Multi-Responsive Hydrogels Crosslinked by Functional Triblock Copolymer Micelle Macro-Crosslinkers. *J. Mater. Chem. B* **2019**, 7, 2619-2625

(179) Wu, M.; Chen, J.; Ma, Y.; Yan, B.; Pan, M.; Peng, Q.; Wang, W.; Han, L.; Liu, J.; Zeng, H. Ultra Elastic, Stretchable, Self-Healing Conductive Hydrogels with Tunable Optical Properties for Highly Sensitive Soft Electronic Sensors. *J. Mater. Chem. A* **2020**, 8, 24718-24733

(180) Chen, Q.; Zhu, L.; Chen, H.; Yan, H.; Huang, L.; Yang, J.; Zheng, J. A Novel Design Strategy for Fully Physically Linked Double Network Hydrogels with Tough, Fatigue Resistant, and Self‐Healing Properties. *Adv. Funct. Mater.* **2015**, 25, 1598-1607

(181) Shao, C.; Wang, M.; Meng, L.; Chang, H.; Wang, B.; Xu, F.; Yang, J.; Wan, P. Mussel-Inspired Cellulose Nanocomposite Tough Hydrogels with Synergistic Self-Healing, Adhesive, and Strain-Sensitive Properties. *Chem. Mater.* **2018**, 30, 3110-3121

(182) Hua, M.; Wu, S.; Ma, Y.; Zhao, Y.; Chen, Z.; Frenkel, I.; Strzalka, J.; Zhou, H.; Zhu, X.; He, X. Strong Tough Hydrogels Via the Synergy of Freeze-Casting and Salting Out. *Nature* **2021**, 590, 594-599

(183) Yan, G.; He, S.; Ma, S.; Zeng, A.; Chen, G.; Tang, X.; Sun, Y.; Xu, F.; Zeng, X.; Lin, L. Catechol-Based All-Wood Hydrogels with Anisotropic, Tough, and Flexible Properties for Highly Sensitive Pressure Sensing. *Chem. Eng. J.* **2022**, 427, 131896

(184) Mredha, M. T. I.; Le, H. H.; Tran, V. T.; Trtik, P.; Cui, J.; Jeon, I. Anisotropic Tough Multilayer Hydrogels with Programmable Orientation. *Materials Horizons* **2019**, 6, 1504-1511

(185) Han, L.; Lu, X.; Liu, K.; Wang, K.; Fang, L.; Weng, L.-T.; Zhang, H.; Tang, Y.; Ren, F.; Zhao, C.; Sun, G.; Liang, R.; Li, Z. Mussel-Inspired Adhesive and Tough Hydrogel Based on Nanoclay Confined Dopamine Polymerization. *ACS Nano* **2017**, 11, 2561-2574

(186) Haraguchi, K.; Li, H.-J.; Matsuda, K.; Takehisa, T.; Elliott, E. Mechanism of Forming Organic/Inorganic Network Structures During in-Situ Free-Radical Polymerization in Pnipa−Clay Nanocomposite Hydrogels. *Macromolecules* **2005**, 38, 3482-3490

(187) Siegel, R. A. Stimuli Sensitive Polymers and Self Regulated Drug Delivery Systems: A Very Partial Review. *J. Controlled Release* **2014**, 190, 337-351

(188) Li, Z.; Song, N.; Yang, Y.-W. Stimuli-Responsive Drug-Delivery Systems Based on Supramolecular Nanovalves. *Matter* **2019**, 1, 345-368

(189) Vashist, A.; Vashist, A.; Gupta, Y. K.; Ahmad, S. Recent Advances in Hydrogel Based Drug Delivery Systems for the Human Body. *J. Mater. Chem. B* **2014**, 2, 147-166

(190) Knipe, J. M.; Peppas, N. A. Multi-Responsive Hydrogels for Drug Delivery and Tissue Engineering Applications. *Regen. Biomater.* **2014**, 1, 57-65

(191) Qiu, Y.; Park, K. Environment-Sensitive Hydrogels for Drug Delivery. *Adv. Drug Deliv. Rev.* **2001**, 53, 321-339

(192) Norouzi, M.; Nazari, B.; Miller, D. W. Injectable Hydrogel-Based Drug Delivery Systems for Local Cancer Therapy. *Drug Discov. Today* **2016**, 21, 1835-1849

(193) Hoare, T. R.; Kohane, D. S. Hydrogels in Drug Delivery: Progress and Challenges. *Polymer* **2008**, 49, 1993-2007

(194) De Laporte, L.; Shea, L. D. Matrices and Scaffolds for DNA Delivery in Tissue Engineering. *Adv. Drug Deliv. Rev.* **2007**, 59, 292-307

(195) Murakami, T.; Brown, H. R.; Hawker, C. J. One‐Pot Fabrication of Robust Interpenetrating Hydrogels Via Orthogonal Click Reactions. *J. Polym. Sci., Part A: Polym. Chem.* **2016**, 54, 1459-1467

(196) Lin, P.; Ma, S.; Wang, X.; Zhou, F. Molecularly Engineered Dual-Crosslinked Hydrogel with Ultrahigh Mechanical Strength, Toughness, and Good Self-Recovery. *Adv. Mater.* **2015**, 27, 2054-2059

(197) Kashyap, N.; Kumar, N.; Kumar, M. N. V. R. Hydrogels for Pharmaceutical and Biomedical Applications. **2005**, 22, 107-150

(198) Li, J.; Mooney, D. J. Designing Hydrogels for Controlled Drug Delivery. *Nat. Rev. Mater.* **2016**, 1, 16071

(199) Shi, J.; Guobao, W.; Chen, H.; Zhong, W.; Qiu, X.; Xing, M. M. Q. Schiff Based Injectable Hydrogel for in Situ Ph-Triggered Delivery of Doxorubicin for Breast Tumor Treatment. *Polym. Chem.* **2014**, 5, 6180-6189

(200) Yoo, J.-W.; Doshi, N.; Mitragotri, S. Adaptive Micro and Nanoparticles: Temporal Control over Carrier Properties to Facilitate Drug Delivery. *Adv. Drug Deliv. Rev.* **2011**, 63, 1247-1256

(201) Tacar, O.; Sriamornsak, P.; Dass, C. R. Doxorubicin: An Update on Anticancer Molecular Action, Toxicity and Novel Drug Delivery Systems. *J. Pharm. Pharmacol.* **2013**, 65, 157-170

(202) Zhang, L.; Wang, L.; Guo, B.; Ma, P. X. Cytocompatible Injectable Carboxymethyl Chitosan/N-Isopropylacrylamide Hydrogels for Localized Drug Delivery. *Carbohydr. Polym.* **2014**, 103, 110-118

(203) Zhao, J.; Zhao, X.; Guo, B.; Ma, P. X. Multifunctional Interpenetrating Polymer Network Hydrogels Based on Methacrylated Alginate for the Delivery of Small Molecule Drugs and Sustained Release of Protein. *Biomacromolecules* **2014**, 15, 3246-3252

(204) Qu, J.; Zhao, X.; Ma, P. X.; Guo, B. Injectable Antibacterial Conductive Hydrogels with Dual Response to an Electric Field and Ph for Localized "Smart" Drug Release. *Acta Biomater.* **2018**, 72, 55-69

(205) Rizwan, M.; Yahya, R.; Hassan, A.; Yar, M.; Azzahari, A. D.; Selvanathan, V.; Sonsudin, F.; Abouloula, C. N. Ph Sensitive Hydrogels in Drug Delivery: Brief History, Properties, Swelling, and Release Mechanism, Material Selection and Applications. *Polymers* **2017**, 9, 137

(206) Wu, J.; Chen, A.; Zhou, Y.; Zheng, S.; Yang, Y.; An, Y.; Xu, K.; He, H.; Kang, J.; Luckanagul, J. A.; Xian, M.; Xiao, J.; Wang, Q. Novel H2s-Releasing Hydrogel for Wound Repair Via in Situ Polarization of M2 Macrophages. *Biomaterials* **2019**, 222, 119398

(207) Yu, L.; Ding, J. Injectable Hydrogels as Unique Biomedical Materials. *Chem. Soc. Rev.* **2008**, 37, 1473-1481

(208) Rowan, S. J.; Cantrill, S. J.; Cousins, G. R.; Sanders, J. K.; Stoddart, J. F. Dynamic Covalent Chemistry. *Angew. Chem. Int. Ed.* **2002**, 41, 898-952

(209) Yan, B.; Huang, J.; Han, L.; Gong, L.; Li, L.; Israelachvili, J. N.; Zeng, H. Duplicating Dynamic Strain-Stiffening Behavior and Nanomechanics of Biological Tissues in a Synthetic Self-Healing Flexible Network Hydrogel. *ACS nano* **2017**, 11, 11074-11081

(210) Xie, W.; Gao, Q.; Guo, Z.; Wang, D.; Gao, F.; Wang, X.; Wei, Y.; Zhao, L. Injectable and Self-Healing Thermosensitive Magnetic Hydrogel for Asynchronous

Control Release of Doxorubicin and Docetaxel to Treat Triple-Negative Breast Cancer. *ACS Appl. Mater. Interfaces* **2017**, 9, 33660-33673

(211) Yang, L.; Li, Y.; Gou, Y.; Wang, X.; Zhao, X.; Tao, L. Improving Tumor Chemotherapy Effect Using an Injectable Self-Healing Hydrogel as Drug Carrier. *Polym. Chem.* **2017**, 8, 3071-3076

(212) Chang, R.; Wang, X.; Li, X.; An, H.; Qin, J. Self-Activated Healable Hydrogels with Reversible Temperature Responsiveness. *ACS Appl. Mater. Interfaces* **2016**, 8, 25544-25551

(213) Yang, X.; Liu, G.; Peng, L.; Guo, J.; Tao, L.; Yuan, J.; Chang, C.; Wei, Y.; Zhang, L. Highly Efficient Self‐Healable and Dual Responsive Cellulose‐Based Hydrogels for Controlled Release and 3d Cell Culture. *Adv. Funct. Mater.* **2017**, 27, 1703174

(214) Shi, J.; Guobao, W.; Chen, H.; Zhong, W.; Qiu, X.; Xing, M. M. Schiff Based Injectable Hydrogel for in Situ Ph-Triggered Delivery of Doxorubicin for Breast Tumor Treatment. *Polym. Chem.* **2014**, 5, 6180-6189

(215) Saito, H.; Hoffman, A. S.; Ogawa, H. I. Delivery of Doxorubicin from Biodegradable Peg Hydrogels Having Schiff Base Linkages. *J. Bioact. Compat. Polym.* **2007**, 22, 589-601

(216) Wu, X.; He, C.; Wu, Y.; Chen, X. Synergistic Therapeutic Effects of Schiff's Base Cross-Linked Injectable Hydrogels for Local Co-Delivery of Metformin and 5-Fluorouracil in a Mouse Colon Carcinoma Model. *Biomaterials* **2016**, 75, 148-162

(217) Qu, J.; Zhao, X.; Ma, P. X.; Guo, B. Ph-Responsive Self-Healing Injectable Hydrogel Based on N-Carboxyethyl Chitosan for Hepatocellular Carcinoma Therapy. *Acta Biomater.* **2017**, 58, 168-180

(218) Qian, C.; Zhang, T.; Gravesande, J.; Baysah, C.; Song, X.; Xing, J. Injectable and Self-Healing Polysaccharide-Based Hydrogel for Ph-Responsive Drug Release. *Int. J. Biol. Macromol.* **2018**, 123, 140-148

(219) Li, Q. W.; Wen, J. R.; Liu, C. L.; Jia, Y. P.; Wu, Y. Z.; Shan, Y.; Qian, Z. Y.; Liao, J. F. Graphene-Nanoparticle-Based Self-Healing Hydrogel in Preventing Postoperative Recurrence of Breast Cancer. *ACS Biomater. Sci. Eng.* **2019**, 5, 768-779

(220) Liang, Y.; Zhao, X.; Ma, P. X.; Guo, B.; Du, Y.; Han, X. Ph-Responsive Injectable Hydrogels with Mucosal Adhesiveness Based on Chitosan-Grafted-Dihydrocaffeic Acid and Oxidized Pullulan for Localized Drug Delivery. *J. Colloid Interface Sci.* **2019**, 536, 224-234

(221) Hu, J.; Zheng, Z.; Liu, C.; Hu, Q.; Cai, X.; Xiao, J.; Cheng, Y. A Ph-Responsive Hydrogel with Potent Antibacterial Activity against Both Aerobic and Anaerobic Pathogens. *Biomater. Sci.* **2019**, 7, 581-584

(222) Wike-Hooley, J.; Haveman, J.; Reinhold, H. The Relevance of Tumour Ph to the Treatment of Malignant Disease. *Radiother. Oncol.* **1984**, 2, 343-366

(223) McCarty, M. F.; Whitaker, J. Manipulating Tumor Acidification as a Cancer Treatment Strategy. *Altern Med Rev* **2010**, 15, 264-272

(224) Popescu, M.-T.; Mourtas, S.; Pampalakis, G.; Antimisiaris, S. G.; Tsitsilianis, C. Ph-Responsive Hydrogel/Liposome Soft Nanocomposites for Tuning Drug Release. *Biomacromolecules* **2011**, 12, 3023-3030

(225) Sinclair, A.; O'Kelly, M. B.; Bai, T.; Hung, H. C.; Jain, P.; Jiang, S. Self‐Healing Zwitterionic Microgels as a Versatile Platform for Malleable Cell Constructs and Injectable Therapies. *Adv. Mater.* **2018**, 30, 1803087

(226) Hayward, J. A.; Chapman, D. Biomembrane Surfaces as Models for Polymer Design: The Potential for Haemocompatibility. *Biomaterials* **1984**, 5, 135-142

(227) Appel, E. A.; Tibbitt, M. W.; Webber, M. J.; Mattix, B. A.; Veiseh, O.; Langer, R. Self-Assembled Hydrogels Utilizing Polymer–Nanoparticle Interactions. *Nat. Commun.* **2015**, 6, 6259

(228) Li, Q.; Barrett, D. G.; Messersmith, P. B.; Holten-Andersen, N. Controlling Hydrogel Mechanics Via Bio-Inspired Polymer–Nanoparticle Bond Dynamics. *ACS nano* **2016**, 10, 1317-1324

(229) Cheang, T.-y.; Tang, B.; Xu, A.-w.; Chang, G.-q.; Hu, Z.-j.; He, W.-l.; Xing, Z.-h.; Xu, J.-b.; Wang, M.; Wang, S.-m. Promising Plasmid DNA Vector Based on Aptes-Modified Silica Nanoparticles. *Int. J. Nanomedicine* **2012**, 7, 1061

(230) He, Q.; Shi, J. Mesoporous Silica Nanoparticle Based Nano Drug Delivery Systems: Synthesis, Controlled Drug Release and Delivery, Pharmacokinetics and Biocompatibility. *J. Mater. Chem.* **2011**, 21, 5845-5855

(231) Maan, O.; Song, P.; Chen, N.; Lu, Q. An in Situ Procedure for the Preparation of Zeolitic Imidazolate Framework‐8 Polyacrylamide Hydrogel for Adsorption of Aqueous Pollutants. *Adv. Mater. Interfaces* **2019**, 6, 1801895

(232) Cheng, C.; Zhang, X.; Meng, Y.; Zhang, Z.; Chen, J.; Zhang, Q. Multiresponsive and Biocompatible Self-Healing Hydrogel: Its Facile Synthesis in Water, Characterization and Properties. *Soft Matter* **2017**, 13, 3003-3012

(233) Yang, W.; Wu, X.; Liu, F.; Dou, Y.; Hu, Z.; Hao, W. A Fluorescent, Self-Healing and Ph Sensitive Hydrogel Rapidly Fabricated from Hpamam and Oxidized Alginate with Injectability. *Rsc Advances* **2016**, 6, 34254-34260

(234) Rajendra, R. B.; Jan, G. Tuning the Number Density of Nanoparticles by Multivariant Tailoring of Attachment Points on Flat Substrates. *Nanotechnology* **2007**, 18, 25301-25301

(235) Sarin, V. K.; Kent, S. B.; Tam, J. P.; Merrifield, R. B. Quantitative Monitoring of Solid-Phase Peptide Synthesis by the Ninhydrin Reaction. *Anal. Biochem.* **1981**, 117, 147-157

(236) Ritger, P. L.; Peppas, N. A. A Simple Equation for Description of Solute Release I. Fickian and Non-Fickian Release from Non-Swellable Devices in the Form of Slabs, Spheres, Cylinders or Discs. *J. Controlled Release* **1987**, 5, 23-36

(237) Ritger, P. L.; Peppas, N. A. A Simple Equation for Description of Solute Release Ii. Fickian and Anomalous Release from Swellable Devices. *J. Controlled Release* **1987**, 5, 37-42

(238) Peppas, N. A.; Sahlin, J. J. A Simple Equation for the Description of Solute Release. Iii. Coupling of Diffusion and Relaxation. *Int. J. Pharm.* **1989**, 57, 169-172

(239) Guvendiren, M.; Lu, H. D.; Burdick, J. A. Shear-Thinning Hydrogels for Biomedical Applications. *Soft matter* **2012**, 8, 260-272

(240) Li, L.; Smitthipong, W.; Zeng, H. Mussel-Inspired Hydrogels for Biomedical and Environmental Applications. *Polym. Chem.* **2015**, 6, 353-358

(241) Wang, J.; Wang, Z.; Gao, J.; Wang, L.; Yang, Z.; Kong, D.; Yang, Z. Incorporation of Supramolecular Hydrogels into Agarose Hydrogels—a Potential Drug Delivery Carrier. *J. Mater. Chem.* **2009**, 19, 7892-7896

(242) Yao, S.; Liu, H.; Yu, S.; Li, Y.; Wang, X.; Wang, L. Drug-Nanoencapsulated Plga Microspheres Prepared by Emulsion Electrospray with Controlled Release Behavior. *Regen. Biomater.* **2016**, 3, 309-317

(243) Singhvi, G.; Singh, M. In-Vitro Drug Release Characterization Models. *Int J Pharm Stud Res* **2011**, 2, 77-84

(244) Kataria, K.; Sharma, A.; Garg, T.; K Goyal, A.; Rath, G. Novel Technology to Improve Drug Loading in Polymeric Nanofibers. *Drug Deliv. Lett.* **2014**, 4, 79-86

(245) Hammock, M. L.; Chortos, A.; Tee, B. C. K.; Tok, J. B. H.; Bao, Z. 25th Anniversary Article: The Evolution of Electronic Skin (E ‐ Skin): A Brief History, Design Considerations, and Recent Progress. *Adv. Mater.* **2013**, 25, 5997-6038

(246) Zhou, Y.; Wan, C.; Yang, Y.; Yang, H.; Wang, S.; Dai, Z.; Ji, K.; Jiang, H.; Chen, X.; Long, Y. Highly Stretchable, Elastic, and Ionic Conductive Hydrogel for Artificial Soft Electronics. *Adv. Funct. Mater.* **2019**, 29, 1806220

(247) De, S.; Higgins, T. M.; Lyons, P. E.; Doherty, E. M.; Nirmalraj, P. N.; Blau, W. J.; Boland, J. J.; Coleman, J. N. Silver Nanowire Networks as Flexible, Transparent, Conducting Films: Extremely High Dc to Optical Conductivity Ratios. *ACS nano* **2009**, 3, 1767-1774

(248) Chae, S. H.; Lee, Y. H. Carbon Nanotubes and Graphene Towards Soft Electronics. *Nano Convergence* **2014**, 1, 15

(249) Peng, Q.; Chen, J.; Wang, T.; Peng, X.; Liu, J.; Wang, X.; Wang, J.; Zeng, H. Recent Advances in Designing Conductive Hydrogels for Flexible Electronics. *InfoMat*,

(250) Cai, G.; Wang, J.; Qian, K.; Chen, J.; Li, S.; Lee, P. S. Extremely Stretchable Strain Sensors Based on Conductive Self ‐ Healing Dynamic Cross ‐ Links Hydrogels for Human ‐ Motion Detection. *Advanced Science* **2017**, 4, 1600190

(251) Chen, J.; Liu, J.; Thundat, T.; Zeng, H. Polypyrrole-Doped Conductive Supramolecular Elastomer with Stretchability, Rapid Self-Healing, and Adhesive Property for Flexible Electronic Sensors. *ACS Appl. Mater. Interfaces* **2019**, 11, 18720-18729

(252) Cao, Y.; Morrissey, T. G.; Acome, E.; Allec, S. I.; Wong, B. M.; Keplinger, C.; Wang, C. A Transparent, Self ‐ Healing, Highly Stretchable Ionic Conductor. *Adv. Mater.* **2017**, 29, 1605099

(253) Chen, J.; Peng, Q.; Peng, X.; Han, L.; Wang, X.; Wang, J.; Zeng, H. Recent Advances in Mechano-Responsive Hydrogels for Biomedical Applications. *ACS Applied Polymer Materials* **2020**, 2, 1092-1107

(254) Reis, L. A.; Chiu, L. L.; Liang, Y.; Hyunh, K.; Momen, A.; Radisic, M. A Peptide-Modified Chitosan–Collagen Hydrogel for Cardiac Cell Culture and Delivery. *Acta Biomater.* **2012**, 8, 1022-1036

(255) Mandal, A.; Clegg, J. R.; Anselmo, A. C.; Mitragotri, S. Hydrogels in the Clinic. *Bioengineering & Translational Medicine* **2020**, 5, e10158

(256) Bai, Y.; Chen, B.; Xiang, F.; Zhou, J.; Wang, H.; Suo, Z. Transparent Hydrogel with Enhanced Water Retention Capacity by Introducing Highly Hydratable Salt. *Appl. Phys. Lett.* **2014**, 105, 151903

(257) Naficy, S.; Brown, H. R.; Razal, J. M.; Spinks, G. M.; Whitten, P. G. Progress toward Robust Polymer Hydrogels. *Aust. J. Chem.* **2011**, 64, 1007-1025

(258) Chung, H. J.; Charaya, H.; Liu, L.; Li, X. Tough Hydrogels: Toughening Mechanisms and Their Utilization in Stretchable Electronics and in Regenerative Medicines. *Hybrid Organic‐Inorganic Interfaces: Towards Advanced Functional Materials* **2018**, 535-580

(259) Liu, Y.; He, W.; Zhang, Z.; Lee, B. P. Recent Developments in Tough Hydrogels for Biomedical Applications. *Gels* **2018**, 4, 46

(260) Li, L.; Yan, B.; Yang, J.; Chen, L.; Zeng, H. Novel Mussel‐Inspired Injectable Self‐Healing Hydrogel with Anti‐Biofouling Property. *Adv. Mater.* **2015**, 27, 1294-1299

(261) Zhang, Q.; Liu, L.; Pan, C.; Li, D. Review of Recent Achievements in Self-Healing Conductive Materials and Their Applications. *Journal of Materials Science* **2018**, 53, 27-46

(262) Zhang, G.; Yang, Y.; Chen, Y.; Huang, J.; Zhang, T.; Zeng, H.; Wang, C.; Liu, G.; Deng, Y. A Quadruple‐Hydrogen‐Bonded Supramolecular Binder for High‐Performance Silicon Anodes in Lithium‐Ion Batteries. *Small* **2018**, 14, 1801189

(263) Kilic, R.; Sanyal, A. Self-Healing Hydrogels Based on Reversible Covalent Linkages: A Survey of Dynamic Chemical Bonds in Network Formation. **2020**,

(264) Wu, M.; Chen, J.; Huang, W.; Yan, B.; Peng, Q.; Liu, J.; Chen, L.; Zeng, H. Injectable and Self-Healing Nanocomposite Hydrogels with Ultrasensitive Ph-Responsiveness and Tunable Mechanical Properties: Implications for Controlled Drug Delivery. *Biomacromolecules* **2020**, 21, 2409-2420

(265) Deng, G.; Tang, C.; Li, F.; Jiang, H.; Chen, Y. Covalent Cross-Linked Polymer Gels with Reversible Sol− Gel Transition and Self-Healing Properties. *Macromolecules* **2010**, 43, 1191-1194

(266) Banerjee, S. L.; Bhattacharya, K.; Samanta, S.; Singha, N. K. Self-Healable Antifouling Zwitterionic Hydrogel Based on Synergistic Phototriggered Dynamic Disulfide Metathesis Reaction and Ionic Interaction. *ACS Appl. Mater. Interfaces* **2018**, 10, 27391-27406

(267) Zhu, P.; Hu, M.; Deng, Y.; Wang, C. One‐Pot Fabrication of a Novel Agar‐Polyacrylamide/Graphene Oxide Nanocomposite Double Network Hydrogel with High Mechanical Properties. *Adv. Eng. Mater.* **2016**, 18, 1799-1807

(268) Zhu, P.; Deng, Y.; Wang, C. Graphene/Cyclodextrin-Based Nanocomposite Hydrogel with Enhanced Strength and Thermo-Responsive Ability. *Carbohydr. Polym.* **2017**, 174, 804-811

(269) Sun, Y.-n.; Gao, G.-r.; Du, G.-l.; Cheng, Y.-j.; Fu, J. Super Tough, Ultrastretchable, and Thermoresponsive Hydrogels with Functionalized Triblock Copolymer Micelles as Macro-Cross-Linkers. *ACS Macro Lett.* **2014**, 3, 496-500

(270) Haraguchi, K. Nanocomposite Hydrogels. *Curr. Opin. Solid State Mater. Sci.* **2007**, 11, 47-54

(271) Shi, Y.; Ma, C.; Peng, L.; Yu, G. Conductive "Smart" Hybrid Hydrogels with Pnipam and Nanostructured Conductive Polymers. *Adv. Funct. Mater.* **2015**, 25, 1219-1225

(272) Tanaka, N.; Ito, K.; Kitano, H. Raman Spectroscopic Study of Hydrogen Bonding of Polyacrylamide in Heavy Water. *Macromolecules* **1994**, 27, 540-544

(273) Ilmain, F.; Tanaka, T.; Kokufuta, E. Volume Transition in a Gel Driven by Hydrogen Bonding. *Nature* **1991**, 349, 400-401

(274) Esawi, A. M.; Farag, M. M. Carbon Nanotube Reinforced Composites: Potential and Current Challenges. *Materials & design* **2007**, 28, 2394-2401

(275) Liu, Z.; Dong, X.; Song, L.; Zhang, H.; Liu, L.; Zhu, D.; Song, C.; Leng, X. Carboxylation of Multiwalled Carbon Nanotube Enhanced Its Biocompatibility with L02 Cells through Decreased Activation of Mitochondrial Apoptotic Pathway. *J. Biomed. Mater. Res. A* **2014**, 102, 665-673

(276) Briganti, G.; Puvvada, S.; Blankschtein, D. Effect of Urea on Micellar Properties of Aqueous Solutions of Nonionic Surfactants. *J. Phys. Chem.* **1991**, 95, 8989-8995

(277) Yi, J.; Nguyen, K.-C. T.; Wang, W.; Yang, W.; Pan, M.; Lou, E.; Major, P. W.; Le, L. H.; Zeng, H. Polyacrylamide/Alginate Double-Network Tough Hydrogels for Intraoral Ultrasound Imaging. *J. Colloid Interface Sci.* **2020**, 578, 598-607

(278) Alidedeoglu, A. H.; York, A. W.; McCormick, C. L.; Morgan, S. E. Aqueous Raft Polymerization of 2 - Aminoethyl Methacrylate to Produce Well - Defined, Primary Amine Functional Homo - and Copolymers. *J. Polym. Sci., Part A: Polym. Chem.* **2009**, 47, 5405-5415

(279) Deng, Z.; Bouchékif, H.; Babooram, K.; Housni, A.; Choytun, N.; Narain, R. Facile Synthesis of Controlled - Structure Primary Amine - Based Methacrylamide Polymers Via the Reversible Addition - Fragmentation Chain Transfer Process. *J. Polym. Sci., Part A: Polym. Chem.* **2008**, 46, 4984-4996

(280) Azehara, H.; Kasanuma, Y.; Ide, K.; Hidaka, K.; Tokumoto, H. Distinct Chemical Contrast in Adhesion Force Images of Hydrophobic–Hydrophilic Patterned Surfaces Using Multiwalled Carbon Nanotube Probe Tips. *Jpn. J. Appl. Phys.* **2008**, 47, 3594

(281) Hu, Y.; Guo, T.; Ye, X.; Li, Q.; Guo, M.; Liu, H.; Wu, Z. Dye Adsorption by Resins: Effect of Ionic Strength on Hydrophobic and Electrostatic Interactions. *Chem. Eng. J.* **2013**, 228, 392-397

(282) Zhang, X.; Sheng, N.; Wang, L.; Tan, Y.; Liu, C.; Xia, Y.; Nie, Z.; Sui, K. Supramolecular Nanofibrillar Hydrogels as Highly Stretchable, Elastic and Sensitive Ionic Sensors. *Materials Horizons* **2019**, 6, 326-333

(283) Liu, Z.; Liang, G.; Zhan, Y.; Li, H.; Wang, Z.; Ma, L.; Wang, Y.; Niu, X.; Zhi, C. A Soft yet Device-Level Dynamically Super-Tough Supercapacitor Enabled by an Energy-Dissipative Dual-Crosslinked Hydrogel Electrolyte. *Nano Energy* **2019**, 58, 732-742

(284) Alexandridis, P.; Athanassiou, V.; Hatton, T. A. Pluronic-P105 Peo-Ppo-Peo Block Copolymer in Aqueous Urea Solutions: Micelle Formation, Structure, and Microenvironment. *Langmuir* **1995**, 11, 2442-2450

(285) Sun, Z.; Wang, L.; Jiang, X.; Bai, L.; Wang, W.; Chen, H.; Yang, L.; Yang, H.; Wei, D. Self-Healing, Sensitive and Antifreezing Biomass Nanocomposite Hydrogels Based on Hydroxypropyl Guar Gum and Application in Flexible Sensors. *Int. J. Biol. Macromol.* **2019**,

(286) Thakker, B.; Vyas, A. L.; Farooq, O.; Mulvaney, D.; Datta, S. Wrist Pulse Signal Classification for Health Diagnosis. *2011 4th International Conference on Biomedical Engineering and Informatics (BMEI)*. 2011;4:1799-1805

(287) Zhang, D.; Zuo, W.; Zhang, D.; Zhang, H.; Li, N. Classification of Pulse Waveforms Using Edit Distance with Real Penalty. *EURASIP Journal on Advances in Signal Processing* **2010**, 2010, 303140

(288) Xu, L.; Wang, K.; Wang, L.; Li, N. Pulse Contour Variability before and after Exercise. *19th IEEE Symposium on Computer-based Medical Systems (CBMS'06)*. 2006:237-240

(289) Aserinsky, E.; Kleitman, N. Regularly Occurring Periods of Eye Motility, and Concomitant Phenomena, During Sleep. *Science* **1953**, 118, 273-274

(290) Mantua, J.; Gravel, N.; Spencer, R. Reliability of Sleep Measures from Four Personal Health Monitoring Devices Compared to Research-Based Actigraphy and Polysomnography. *Sensors* **2016**, 16, 646

(291) Cao, J.; Herman, A. B.; West, G. B.; Poe, G.; Savage, V. M. Unraveling Why We Sleep: Quantitative Analysis Reveals Abrupt Transition from Neural Reorganization to Repair in Early Development. *Science Advances* **2020**, 6, eaba0398

(292) Kim, D.-H.; Lu, N.; Ma, R.; Kim, Y.-S.; Kim, R.-H.; Wang, S.; Wu, J.; Won, S. M.; Tao, H.; Islam, A.; Yu, K. J.; Kim, T.-i.; Chowdhury, R.; Ying, M.; Xu, L.; Li, M.; Chung, H.-J.; Keum, H.; McCormick, M.; Liu, P.; Zhang, Y.-W.; Omenetto, F. G.; Huang, Y.; Coleman, T.; Rogers, J. A. Epidermal Electronics. *Science* **2011**, 333, 838-843

(293) Hammock, M. L.; Chortos, A.; Tee, B. C.-K.; Tok, J. B.-H.; Bao, Z. 25th Anniversary Article: The Evolution of Electronic Skin (E-Skin): A Brief History, Design Considerations, and Recent Progress. *Adv. Mater.* **2013**, 25, 5997-6038

(294) Wang, M.; Luo, Y.; Wang, T.; Wan, C.; Pan, L.; Pan, S.; He, K.; Neo, A.; Chen, X. Artificial Skin Perception. *Adv. Mater.* **2021**, 33, 2003014

(295) Sun, J. Y.; Keplinger, C.; Whitesides, G. M.; Suo, Z. Ionic Skin. *Adv. Mater.* **2014**, 26, 7608-7614

(296) Parida, K.; Kumar, V.; Jiangxin, W.; Bhavanasi, V.; Bendi, R.; Lee, P. S. Highly Transparent, Stretchable, and Self-Healing Ionic-Skin Triboelectric Nanogenerators for Energy Harvesting and Touch Applications. *Adv. Mater.* **2017**, 29, 1702181

(297) Liu, Z.; Wang, Y.; Ren, Y.; Jin, G.; Zhang, C.; Chen, W.; Yan, F. Poly(Ionic Liquid) Hydrogel-Based Anti-Freezing Ionic Skin for a Soft Robotic Gripper. *Materials Horizons* **2020**, 7, 919-927

(298) Lei, Z.; Wu, P. A Supramolecular Biomimetic Skin Combining a Wide Spectrum of Mechanical Properties and Multiple Sensory Capabilities. *Nat. Commun.* **2018**, 9, 1-7

(299) Yang, C.; Suo, Z. Hydrogel Ionotronics. *Nat. Rev. Mater.* **2018**, 3, 125-142

(300) Chung, H.-J.; Charaya, H.; Liu, L.; Li, X. Tough Hydrogels: Toughening Mechanisms and Their Utilization in Stretchable Electronics and in Regenerative Medicines. *Hybrid Organic‐Inorganic Interfaces*. 2018:535-580.

(301) Chortos, A.; Liu, J.; Bao, Z. Pursuing Prosthetic Electronic Skin. *Nat. Mater.* **2016**, 15, 937-950

(302) Lai, Y. C.; Wu, H. M.; Lin, H. C.; Chang, C. L.; Chou, H. H.; Hsiao, Y. C.; Wu, Y. C. Entirely, Intrinsically, and Autonomously Self‐Healable, Highly Transparent, and Superstretchable Triboelectric Nanogenerator for Personal Power Sources and Self‐Powered Electronic Skins. *Adv. Funct. Mater.* **2019**, 29, 1904626

(303) Deng, Z.; Wang, H.; Ma, P. X.; Guo, B. Self-Healing Conductive Hydrogels: Preparation, Properties and Applications. *Nanoscale* **2020**, 12, 1224-1246

(304) Wu, M.; Peng, Q.-Y.; Han, L.-B.; Zeng, H.-B. Self-Healing Hydrogels and Underlying Reversible Intermolecular Interactions. *Chin. J. Polym. Sci.* **2021**, 39, 1246-1261

(305) Zhang, C.; Zhou, Y.; Han, H.; Zheng, H.; Xu, W.; Wang, Z. Dopamine-Triggered Hydrogels with High Transparency, Self-Adhesion, and Thermoresponse as Skinlike Sensors. *ACS Nano* **2021**, 15, 1785-1794

(306) Aral, H.; Vecchio-Sadus, A. Toxicity of Lithium to Humans and the Environment—a Literature Review. *Ecotoxicology and Environmental Safety* **2008**, 70, 349-356

(307) Schuetze, B.; Mayer, C.; Loza, K.; Gocyla, M.; Heggen, M.; Epple, M. Conjugation of Thiol-Terminated Molecules to Ultrasmall 2 Nm-Gold Nanoparticles Leads to Remarkably Complex 1 H-Nmr Spectra. *J. Mater. Chem. B* **2016**, 4, 2179-2189

(308) Ivanov, M. R. Covalently Functionalized Gold Nanoparticles: Synthesis, Characterization, and Integration into Capillary Electrophoresis. **2011**,

(309) Tan, F.; Xu, X.; Deng, T.; Yin, M.; Zhang, X.; Wang, J. Fabrication of Positively Charged Poly (Ethylene Glycol)-Diacrylate Hydrogel as a Bone Tissue Engineering Scaffold. *Biomedical materials* **2012**, 7, 055009

(310) Yuan, J.; Hou, Q.; Chen, D.; Zhong, L.; Dai, X.; Zhu, Z.; Li, M.; Fu, X. Chitosan/Licl Composite Scaffolds Promote Skin Regeneration in Full-Thickness Loss. *Science China Life Sciences* **2020**, 63, 552-562

(311) Kalra, A.; Lowe, A.; Al-Jumaily, A. Mechanical Behaviour of Skin: A Review. *J. Mater. Sci. Eng* **2016**, 5, 1000254

(312) Xie, L.; Liu, F.; Liu, J.; Zeng, H. A Nanomechanical Study on Deciphering the Stickiness of Sars-Cov-2 on Inanimate Surfaces. *ACS applied materials & interfaces* **2020**,

(313) Silfverberg, M. Chapter 1 - Historical Overview of Consumer Text Entry Technologies. In: MacKenzie IS, Tanaka-Ishii K, eds. *Text Entry Systems*. Burlington: Morgan Kaufmann; 2007:3-25.

(314) Peng, W.; Han, L.; Huang, H.; Xuan, X.; Pan, G.; Wan, L.; Lu, T.; Xu, M.; Pan, L. A Direction-Aware and Ultrafast Self-Healing Dual Network Hydrogel for a Flexible Electronic Skin Strain Sensor. *J. Mater. Chem. A* **2020**, 8, 26109-26118

(315) Huang, H.; Han, L.; Fu, X.; Wang, Y.; Yang, Z.; Pan, L.; Xu, M. Multiple Stimuli Responsive and Identifiable Zwitterionic Ionic Conductive Hydrogel for Bionic Electronic Skin. *Advanced Electronic Materials* **2020**, 6, 2000239

(316) Guthrie, J. P. Carbonyl Addition Reactions: Factors Affecting the Hydrate–Hemiacetal and Hemiacetal–Acetal Equilibrium Constants. *Can. J. Chem.* **1975**, 53, 898-906

(317) Clayden, J.; Greeves, N.; Warren, S. Chapter 14 Nucleophilic Substitution at C= O with Loss of Carbonyl Oxygen. *Organic Chemistry, First Edition, Oxford University Press* **2001**, 342-343

(318) Ashley, D. L.; Orti, D. L.; Hill Jr, R. H. Proton Nuclear Magnetic Resonance Evidence for Two Configurations of the Hemiacetals of Aflatoxin B1 and Sterigmatocystin. *J. Agric. Food. Chem.* **1987**, 35, 782-785

(319) Evans, D. A.; Gauchet-Prunet, J. A. Diastereoselective Synthesis of Protected Syn 1, 3-Diols by Base-Catalyzed Intramolecular Conjugate Addition of Hemiacetal-Derived Alkoxide Nucleophiles. *J. Org. Chem.* **1993**, 58, 2446-2453

(320) Zhao, S.; Abu-Omar, M. M. Recyclable and Malleable Epoxy Thermoset Bearing Aromatic Imine Bonds. *Macromolecules* **2018**, 51, 9816-9824

(321) Chao, A.; Negulescu, I.; Zhang, D. Dynamic Covalent Polymer Networks Based on Degenerative Imine Bond Exchange: Tuning the Malleability and Self-Healing Properties by Solvent. *Macromolecules* **2016**, 49, 6277-6284

(322) Matsumoto, M.; Dasari, R. R.; Ji, W.; Feriante, C. H.; Parker, T. C.; Marder, S. R.; Dichtel, W. R. Rapid, Low Temperature Formation of Imine-Linked Covalent Organic Frameworks Catalyzed by Metal Triflates. *J. Am. Chem. Soc.* **2017**, 139, 4999-5002

(323) Annabi, N.; Shin, S. R.; Tamayol, A.; Miscuglio, M.; Bakooshli, M. A.; Assmann, A.; Mostafalu, P.; Sun, J. Y.; Mithieux, S.; Cheung, L. Highly Elastic and Conductive Human‐Based Protein Hybrid Hydrogels. *Adv. Mater.* **2016**, 28, 40-49

(324) Liu, Y.-J.; Cao, W.-T.; Ma, M.-G.; Wan, P. Ultrasensitive Wearable Soft Strain Sensors of Conductive, Self-Healing, and Elastic Hydrogels with Synergistic "Soft and Hard" Hybrid Networks. *ACS Appl. Mater. Interfaces* **2017**, 9, 25559-25570

(325) Odent, J.; Wallin, T. J.; Pan, W.; Kruemplestaedter, K.; Shepherd, R. F.; Giannelis, E. P. Highly Elastic, Transparent, and Conductive 3d‐Printed Ionic Composite Hydrogels. *Adv. Funct. Mater.* **2017**, 27, 1701807

(326) Pei, X.; Zhang, H.; Zhou, Y.; Zhou, L.; Fu, J. Stretchable, Self-Healing and Tissue-Adhesive Zwitterionic Hydrogels as Strain Sensors for Wireless Monitoring of Organ Motions. *Materials Horizons* **2020**,

(327) Lin, P.; Ma, S.; Wang, X.; Zhou, F. Molecularly Engineered Dual‐Crosslinked Hydrogel with Ultrahigh Mechanical Strength, Toughness, and Good Self‐Recovery. *Adv. Mater.* **2015**, 27, 2054-2059

(328) Li, T.; Wang, Y.; Li, S.; Liu, X.; Sun, J. Mechanically Robust, Elastic, and Healable Ionogels for Highly Sensitive Ultra-Durable Ionic Skins. *Adv. Mater.* **2020**, 32, 2002706

(329) Li, S.; Pan, H.; Wang, Y.; Sun, J. Polyelectrolyte Complex-Based Self-Healing, Fatigue-Resistant and Anti-Freezing Hydrogels as Highly Sensitive Ionic Skins. *J. Mater. Chem. A* **2020**, 8, 3667-3675

(330) He, Z.; Yuan, W. Adhesive, Stretchable, and Transparent Organohydrogels for Antifreezing, Antidrying, and Sensitive Ionic Skins. *ACS Appl. Mater. Interfaces* **2021**, 13, 1474-1485

(331) Zhang, Z.; Wang, L.; Yu, H.; Zhang, F.; Tang, L.; Feng, Y.; Feng, W. Highly Transparent, Self-Healable, and Adhesive Organogels for Bio-Inspired Intelligent Ionic Skins. *ACS Appl. Mater. Interfaces* **2020**, 12, 15657-15666

Appendices

Appendix A Supporting Information for Chapter 2

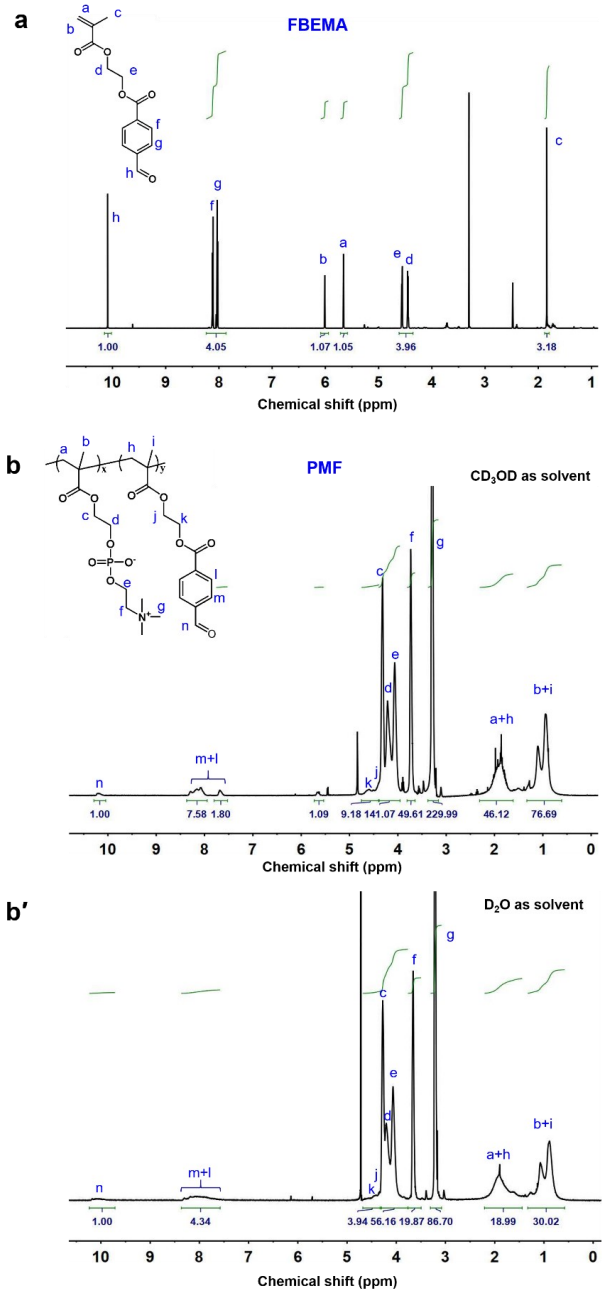

Figure S2.1. ^{1}H NMR spectra of (a) FBEMA, (b) PMF10 with CD_3OD as solvent and (b′) PMF10 with D_2O as solvent.

In Figure S1b, when CD_3OD was used as the NMR solvent for PMF copolymer, the integration ratio of the peak for formyl proton (n) to aromatic ring signals (m+l) is less than the theoretical value, while the ratio shows good consistency with the theoretical value when using D_2O as the solvent as shown in Figure S1b′. This difference is due to the reaction between the PMF copolymer and d-methanol, leading to the formation of hemiacetal, which was evidenced by the broad peak assigned to hemiacetal α-proton at chemical shift of 5.6 ppm in Figure S1b.[316-319] The integration ratio of the sum of formyl proton peak and hemiacetal α-proton peak to aromatic ring signals (m+l) is around 1/4, which is in good agreement with the theoretical value. Since CD_3OD gives sharper NMR peaks and more detailed information of the functional aldehyde group while the peaks are broad with D_2O because of the limited solubility of the benzaldehyde moiety in D_2O, the actual aldehyde contents in the copolymers were calculated from the integral values of the characteristic aromatic ring signals (m+l) of FBEMA and characteristic peaks of MPC (c+d+e). It's worth noting that although hemiacetals between aldehyde groups and the solvent might form when ethanol was used as the solvent for copolymer synthesis, the unstable hemiacetals would decompose to aldehydes when the polymer was purified with the removal of ethanol[2].

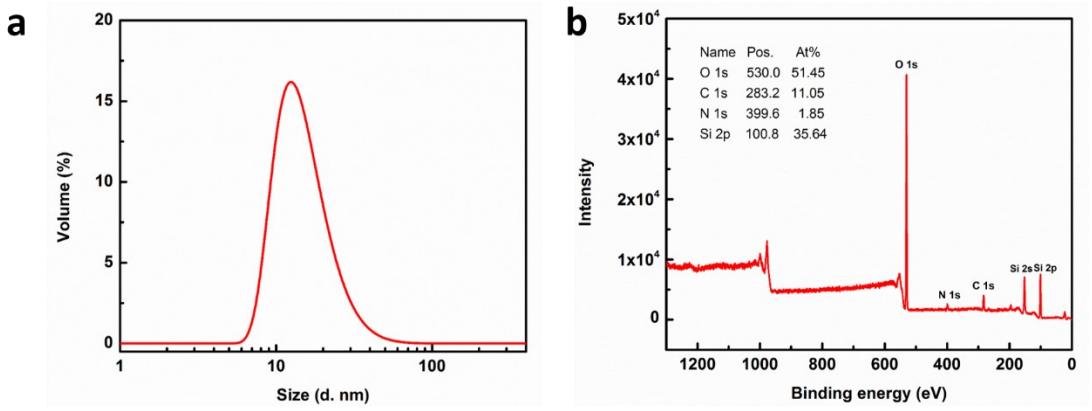

Figure S2.2. (a) DLS and (b) XPS results of ASNP.

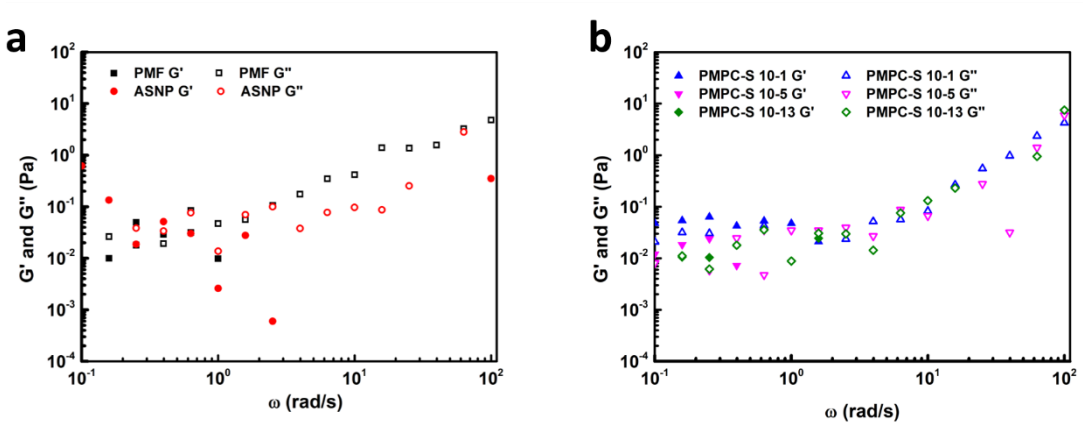

Figure S2.3. Rheological frequency sweeps (1% strain and 37 °C) of (a) PMF10 (20 wt%) and ASNP (26 wt%) solutions, and (b) mixtures of pure polymer of 2-methacryloyloxyethyl phosphorylcholine (PMPC) and different concentrations of amine-modified silica nanoparticle (ASNP). The mixtures were denoted as PMPC-S x-y, where S represents ASNP, x and y are the weight percent of polymer and nanoparticles in the mixture, respectively. It is noted that the fluctuation of some of the data points in Figure S3 was due to the very low viscosities of the related samples and the measured torques were close to the detection limits (in the cone-plate geometry) of the instrument.

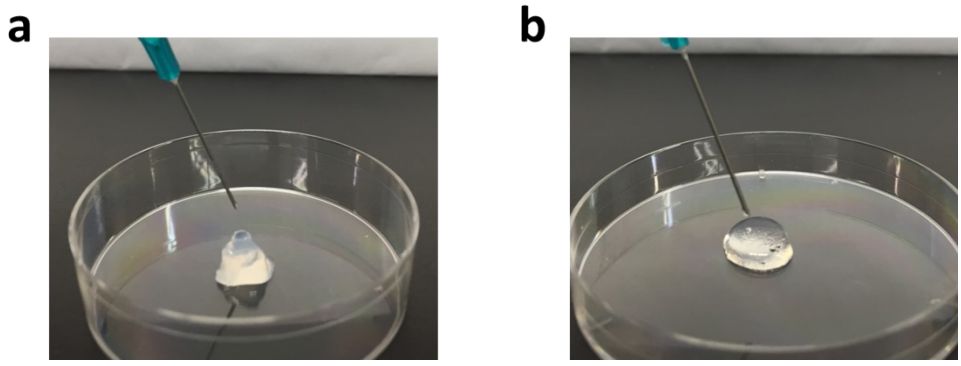

Figure S2.4. Injected bulk hydrogels of (a) PMF10-S 10-13, and (b) PMF5-S 10-13 through 23-gauge needles.

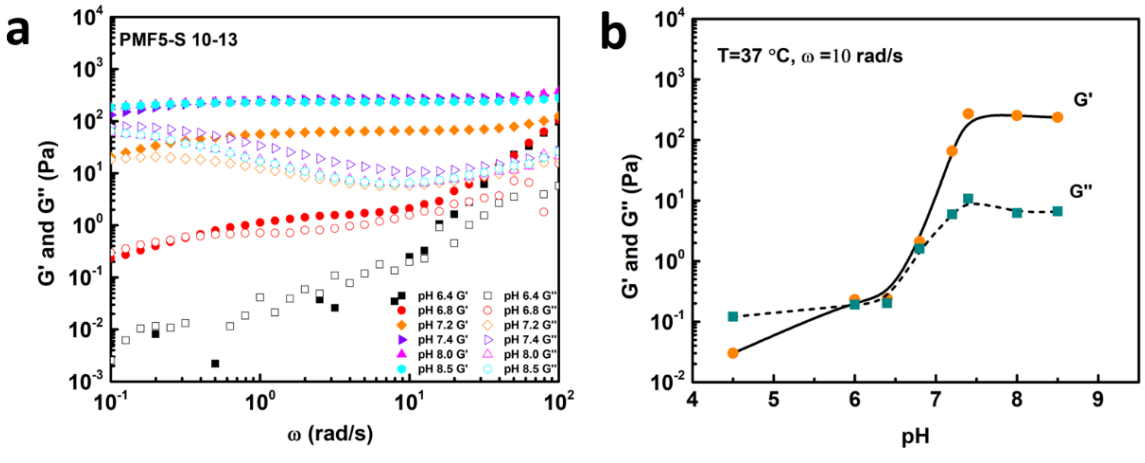

Figure S2.5. Rheological characterization of the pH dependent behavior of PMF5-S 10-13 hydrogel at 37 °C and strain of 1%. (a) Oscillatory frequency sweeps, and (b) G′ and G″ versus pH at 10 rad/s.

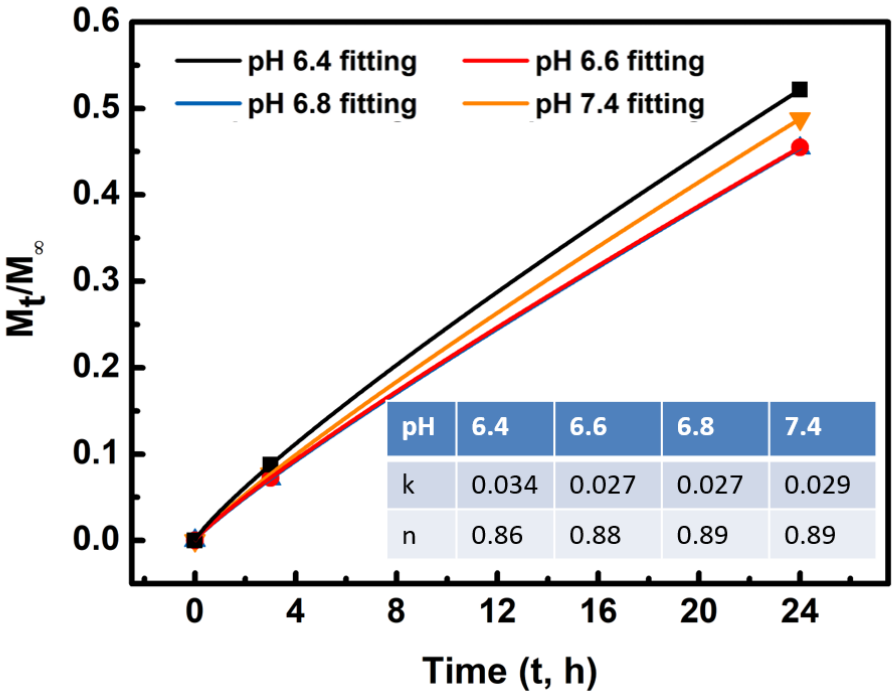

Figure S2.6. Fitting of BSA-FITC release data of first 24 hours according to Korsmeyer-Peppas equation. Inset table shows the fitting parameters.

Appendix B Supporting Information for Chapter 3

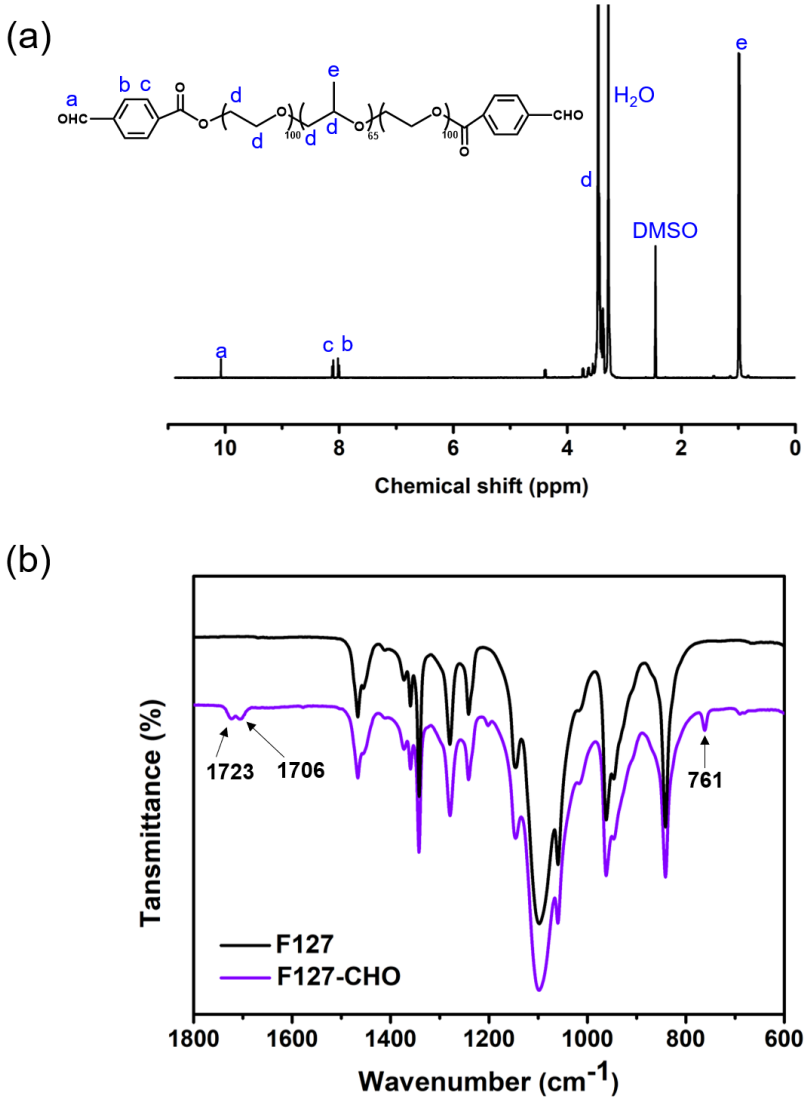

Figure S3.1. (a) ^{1}H NMR and (b) FTIR spectra of F127-CHO.

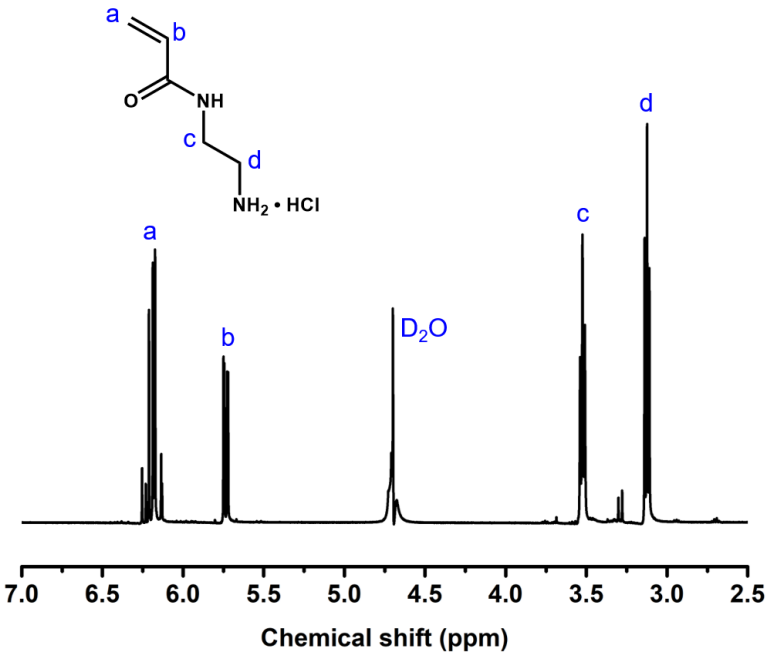

Figure S3.2. ^{1}H NMR spectrum of 2-aminoethyl acrylamide hydrochloride (AEAM).

Table S3.1. Water contents of hydrogels with different compositions.

Sample	Water content (%)
PAM	75.7
PAMF	78.8
PAAF	75.8
PAAFC	75.6
PAAFC-L	73.9

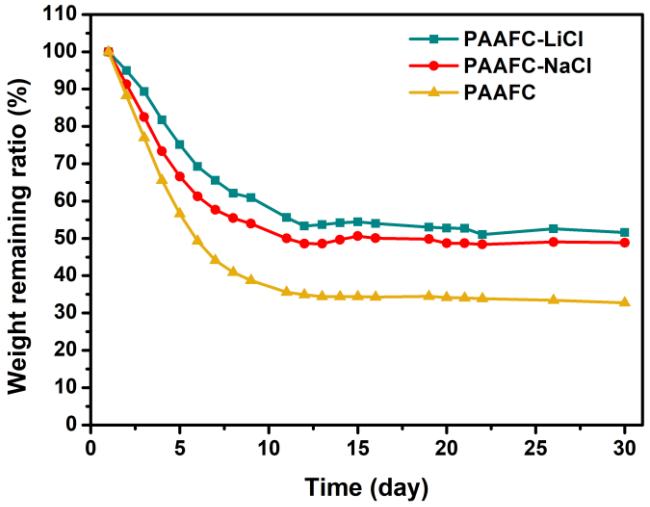

Figure S3.3. Weight change of PAAFC hydrogel with LiCl, NaCl and without addition of ions under ambient condition (70−80 RH%, 20 °C).

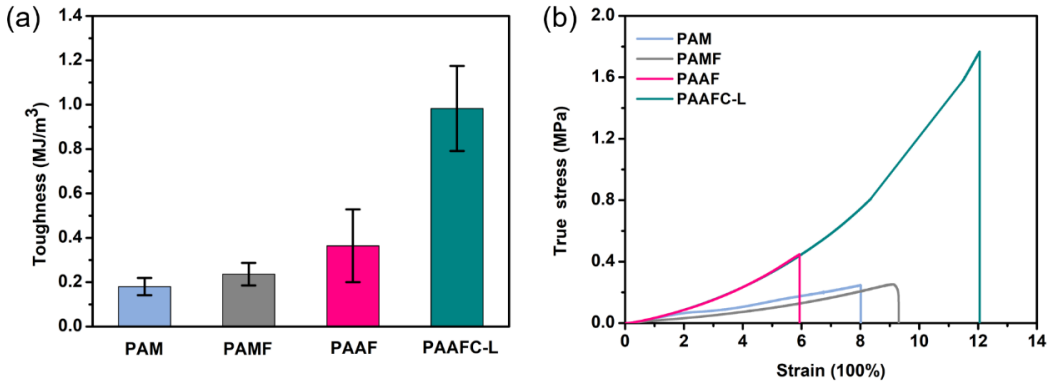

Figure S3.4. (a) Toughness and (b) true stress of hydrogels with different compositions.

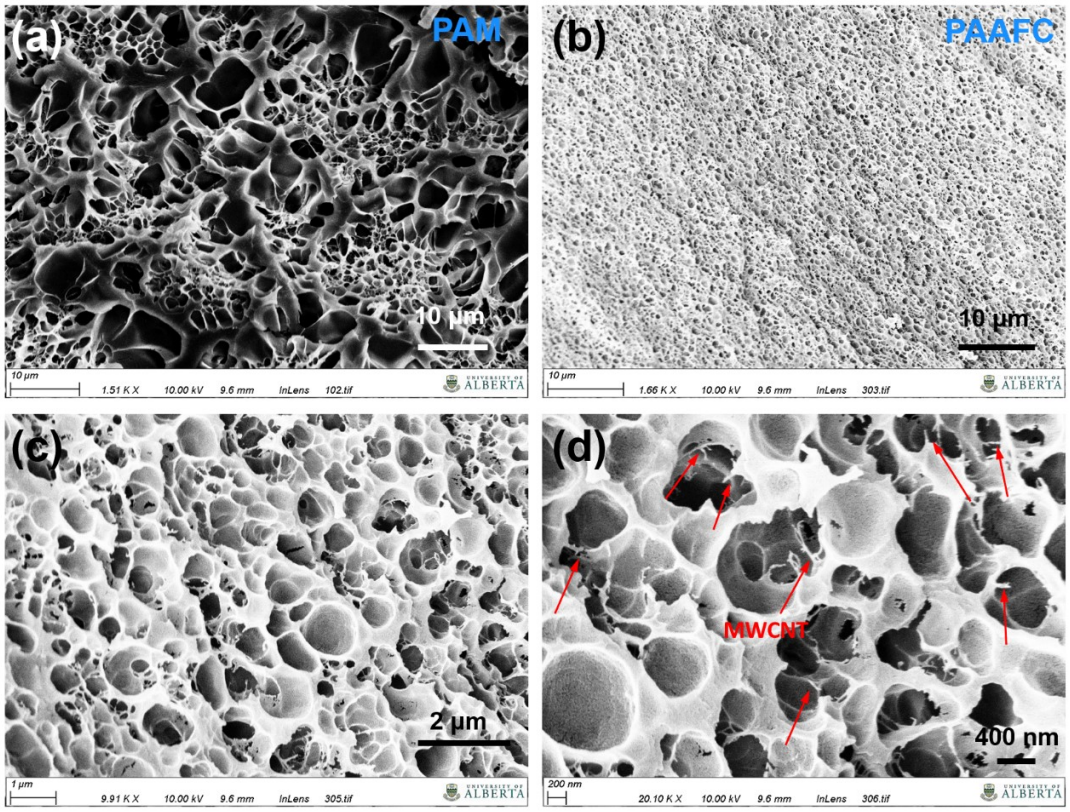

Figure S3.5. SEM images of the cross-sections of freeze-dried (a) PAM hydrogel, (b) PAAFC hydrogel, (c) and (d) PAAFC at higher magnifications. Red arrows indicating the MWCNTs.

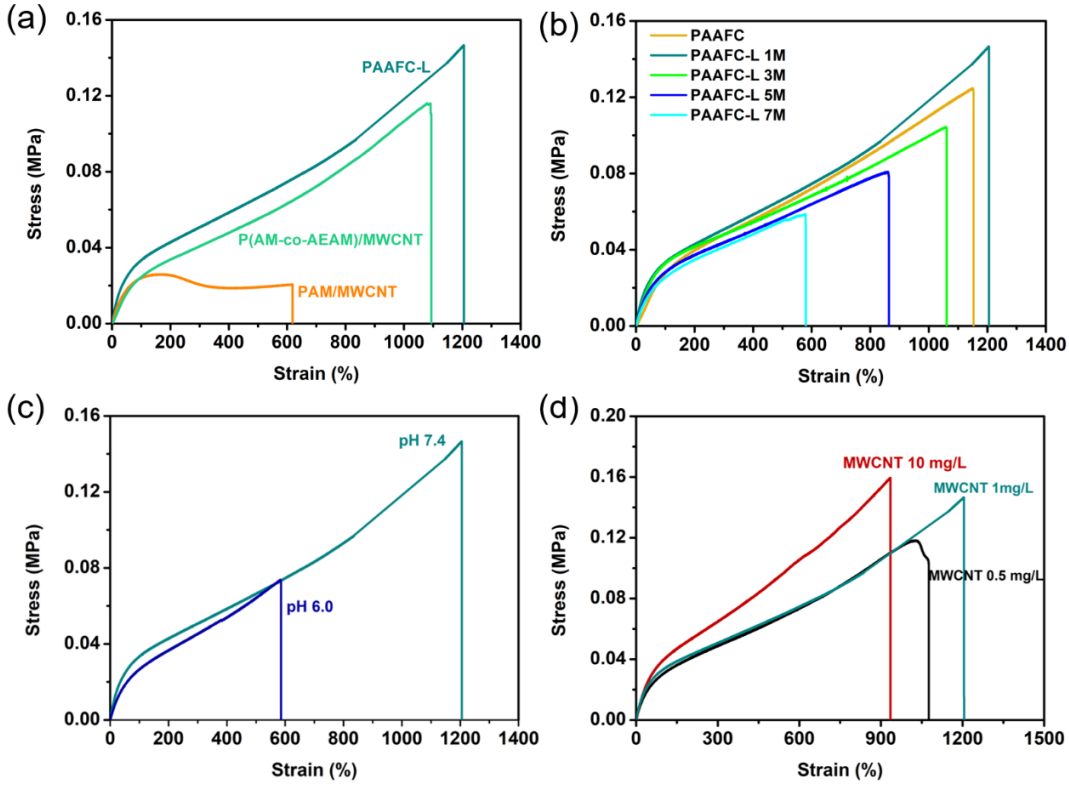

Figure S3.6. Stress-strain curves of (a) PAAFC-L, PAM/MWCNT and P(AM-co-AEMA)/MWCNT hydrogels, (b) hydrogels with different concentrations of LiCl, (c) PAAFC-L hydrogels prepared at different pH, and (d) PAAFC-L hydrogels with various MWCNT concentrations.

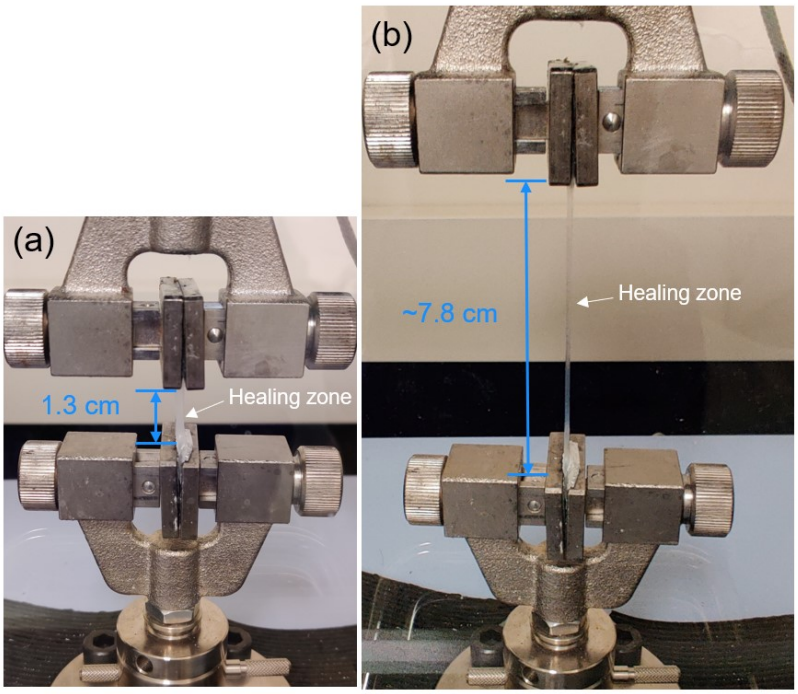

Figure S3.7. Photographs showing the PAAFC-L hydrogel self-healing for 24 h (a) before and (b) during stretching.

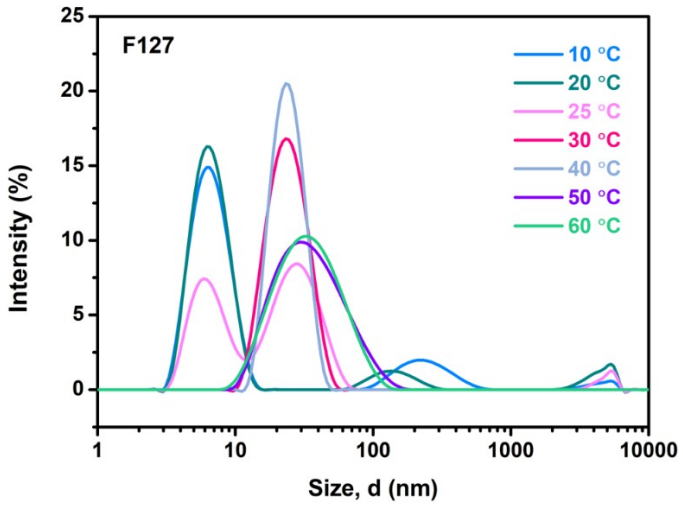

Figure S3.8. DLS size characterization results of unmodified F127 micelles at various temperatures ranging from 10 to 60 °C.

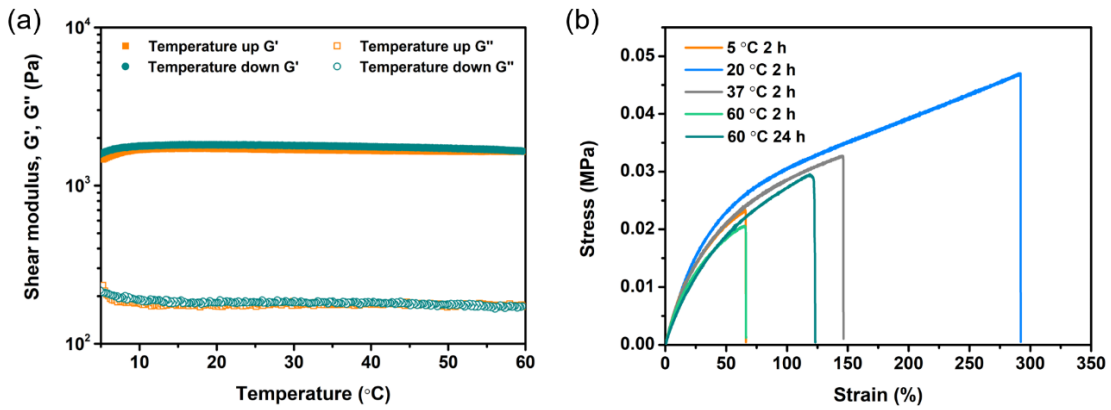

Figure S3.9. (a) Rheological oscillatory temperature sweeps of PAAFC-L hydrogel at an angular frequency of 10 rad/s and a strain of 1%. (b) Stress-strains curves of PAAFC-L hydrogels healed at different temperatures.

As shown in Figure S9b, the hydrogel healed at room temperature displayed the best anti-stretching performance. Both lowering and raising temperature would impair the stretchability of self-healed PAAFC-L hydrogel. It is known the self-healing property of a hydrogel relies on several factors, where the most important ones are the dynamic nature of the cross-linking bonds and the mobility of polymer chains within the hydrogel. At 5 °C, the low chain mobility and increased hydrophobic associations in PAAFC-L hydrogel hinder the self-healing of the hydrogel. Considering the molecular mobility should be enhanced at higher temperatures (37 and 60 °C), the decreased self-repairing efficiency with the increasing of temperature above room temperature is most likely caused by the reduction of dynamicity of the cross-linking bonds. Among the dynamic bonds involved for PAAFC-L hydrogel construction, imine bonds play an important role in self-healing of the hydrogel. The dynamic nature of imine bond originates from the reversible imine formation reaction, i.e., imine hydrolysis and re-formation reach a thermodynamic

equilibration under experimental conditions, and imine exchange reactions.[320, 321] Although raising temperature is favorable for exchange reactions, imine formation is also facilitated at the same time.[322] That is, at elevated temperatures, the equilibrium of Schiff base reaction is pulled toward imine formation and the hydrolysis process would be suppressed, which might lead to reduced reversibility of the bond and the impaired self-healing behavior.

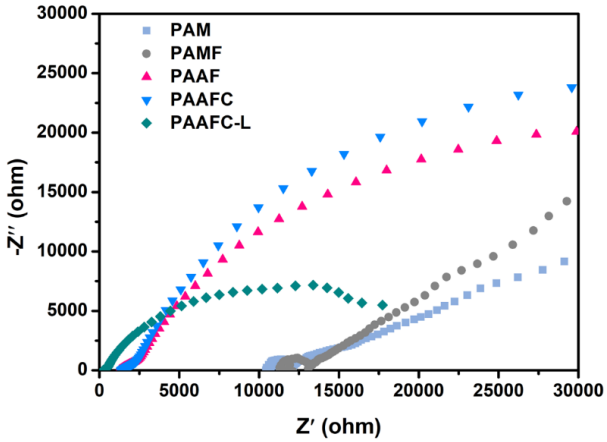

Figure S3.10. Electrochemical impedance spectra of hydrogels of various compositions.

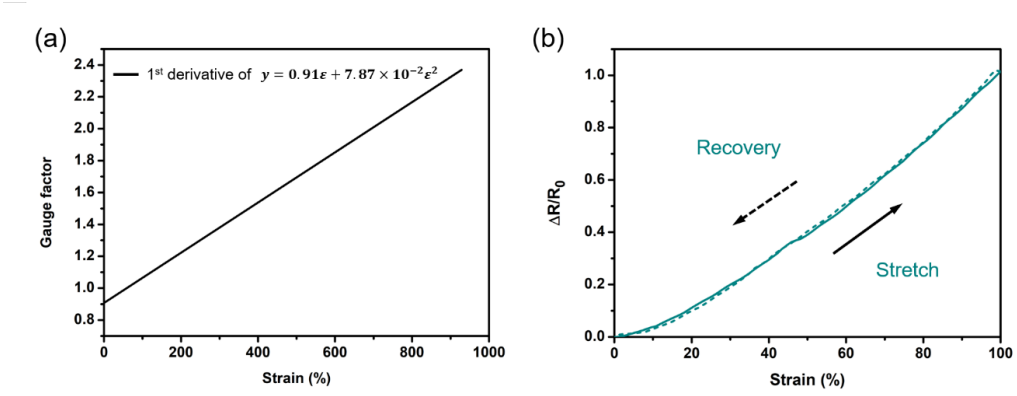

Figure S3.11. (a) Plot of gauge factor versus strain for PAAFC-L hydrogel calculated from the differentiation of the fitting curve of relative resistance change versus strain

experimental data. (b) Relative resistance change-tensile strain loading-unloading curves of PAAFC-L hydrogel. Dash line indicating the recovery process.

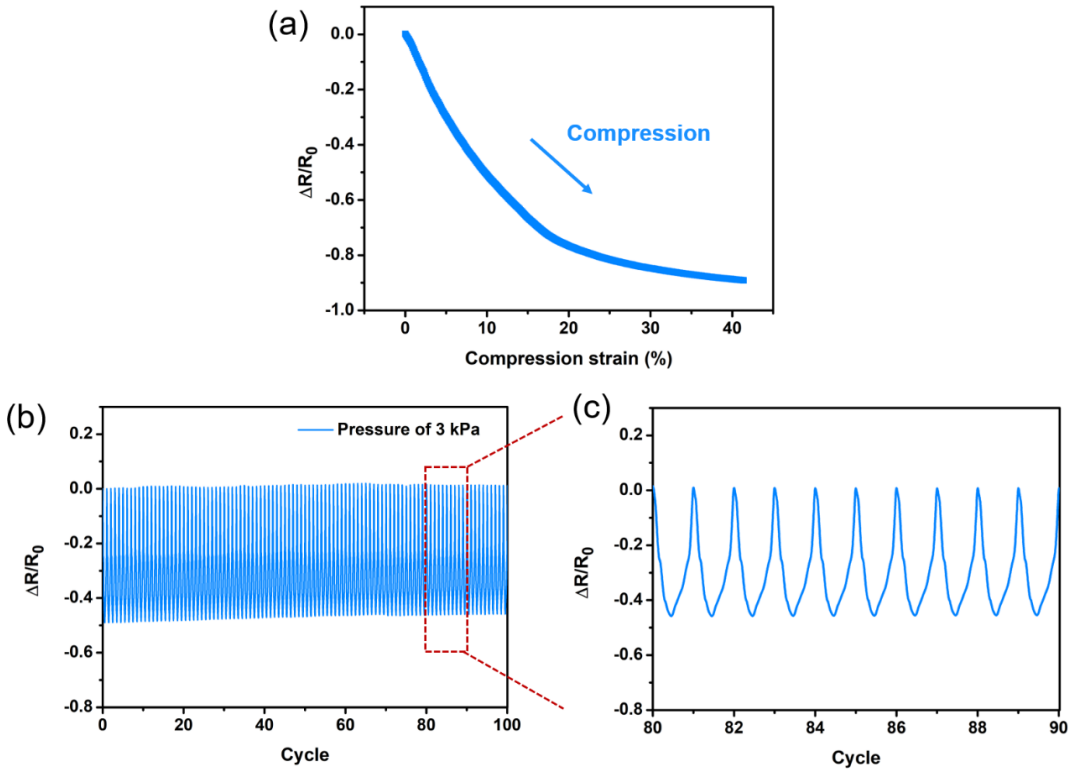

Figure S3.12. (a) Relative resistance variation as a function of compression strain for PAAFC-L hydrogel. (b) Relative resistance response of the PAAFC-L hydrogel under cyclic pressure loading of 3 kPa (compression strain of 10%) for 100 cycles. (c) Magnified signal during 80-90 cycles.

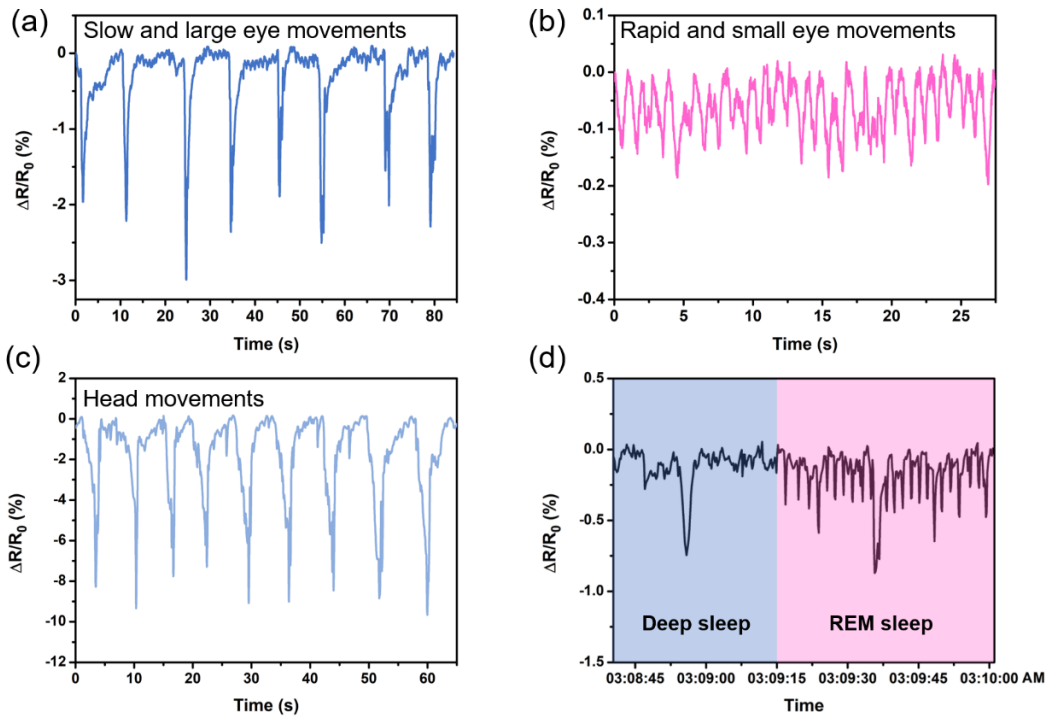

Figure S3.13. Relative resistance changes of (a) slow and large eye movements, (b) rapid and small eye movements, and (c) head movements measured under awake state. (d) Relative resistance change curve showing the transition from deep to REM sleep.

Table S3.2. Comparison of reported elastic hydrogels with this work

Components of hydrogels	Stretchability	Stress at break (MPa)	Elasticity[a]		Self-healing efficiency[b]	Stretchability after self-healing	Stimuli-responsiveness	Conductivity (S/m)	Ref.
			Stretching	Compression					
P(AM-co-AEAM) /MWCNT /F127-CHO/LiCl	1205%	0.147	97% Strength recovery for 1000% strain at 20th cycle	Complete recovery for 90% strain	53%	636%	Thermo-responsive	3.96	**This work**
Sodium alginate /NaCl/PAM	3120%	0.75	98% Energy dissipation recovery for 1000% strain at 20th cycle	Complete recovery for 98% strain	n/a	n/a	n/a	0.023	282
UPyHCBA/SDS /NaCl /PAM	>10000%	0.004	93% Energy dissipation recovery for 500% strain at 2nd cycle	n/a	100%	>10000%	n/a	n/a	56
Hydroxypropyl cellulose/PVA/NaCl	975%	1.3	n/a	Recovery after compression	n/a	n/a	n/a	3.4	246
GO/MeTro	~210%	~0.02	~60% Strength recovery for 100% strain at 1000th cycle	n/a	n/a	n/a	n/a	n/a	323
PVA/PVP/CNC/Fe^{3+}	830%	2.1	60% Energy dissipation recovery for 500% strain at 2nd cycle	n/a	n/a	~150%	n/a	n/a	324
PAM/AETA/sulfonate-modified silica nanoparticles	370%	0.006	97% Energy dissipation recovery for 100% strain at 100th cycle	n/a	n/a	n/a	n/a	2.9	325
Agar/PAM/Stearyl methacrylate (SMA)/SDS	5260%	0.267	40% of Energy dissipation recovery for 900% strain at 2nd cycle (2 min)	n/a	40%	170%	n/a	n/a	180
PAM/Alginate/Ca^{2+}	2200%	0.156	74% of Energy dissipation recovery for 600% strain at 2nd cycle (80 °C, 1 day)	n/a	n/a	n/a	n/a	n/a	60

PAM/F127 diacrylate	2300%	0.27	98% Shape recovery for 1000% strain at 2nd cycle (30 h)	Complete recovery for 90% strain	n/a	n/a	Thermo-responsive	n/a	269
PAAc/SMA/CTAB /NaBr	800−900%	0.7−1.7	97% Strength recovery for 500% strain (5 min)	Complete recovery for 92% strain	60−100% (treated at 35 °C with surfactant)	600−900%	Thermo-responsive	n/a	51
PAM/cucurbit[8]uril/ 1-benzyl-3-vinylimidazolium (host-guest)/MBAA	2400%	0.13	100% Strength recovery for 800% strain at 2nd cycle (2 min)	n/a	n/a	n/a	n/a	n/a	71
DMAA/MAAc	800%	1.3	100% of Energy dissipation recovery for 300% strain at 2nd cycle (60 min)	n/a	n/a	n/a	Thermo-responsive	n/a	57
SBMA/dopamine-modified clay/MBAA	900%	0.077	85% Strength recovery for 400% strain at 2nd cycle (3 min)	n/a	80%	859%	n/a	0.02	326
PMPTC/ PNaSS	750–800%	3.7	100% of Energy dissipation recovery for 300% strain at 2nd cycle (120 min)	n/a	66% (treated with NaCl)	630%	n/a	n/a	47
PAM/GO/Ca^{2+}	1100%	0.143	~90% Strength recovery for 700% strain	~90% recovery for 80% strain	n/a	n/a	n/a	n/a	168
PAM/CNT/SDS/ lauryl methacrylate	3000%	0.267	~90% Strength recovery for 1000% strain	Recovery from 70% strain	n/a	n/a	n/a	0.017	155
PAM/oxCNT/gelatin	1041%	0.71	Recovery from 500% strain	n/a	n/a	n/a	n/a	0.067	156

[a] The recovery percentages of the elasticity were obtained at room temperature with the wait time between cycles set within 1 min unless otherwise noticed.
[b] The self-healing efficiencies were obtained by tensile tests at room temperature without external stimuli unless otherwise noticed.

Appendix C Supporting Information for Chapter 4

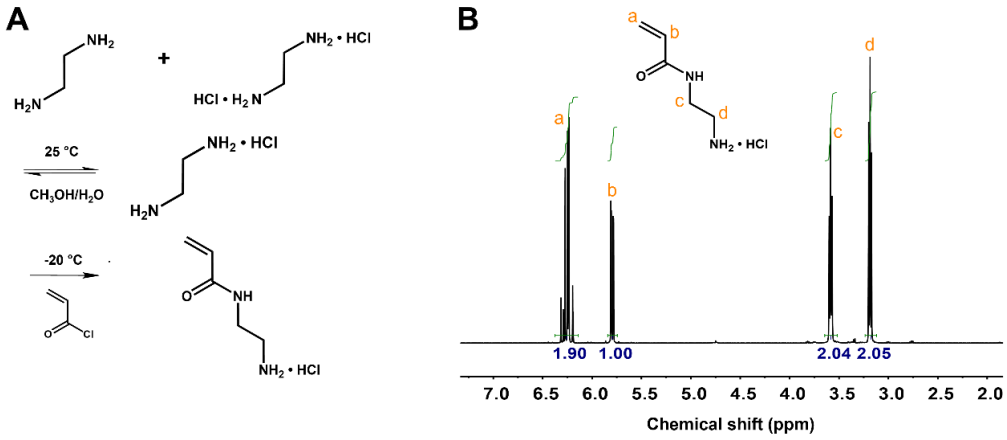

Figure S4.1. (a) Synthetic route and (b) ^{1}H NMR spectrum of 2-aminoethyl acrylamide hydrochloride (AEAM).

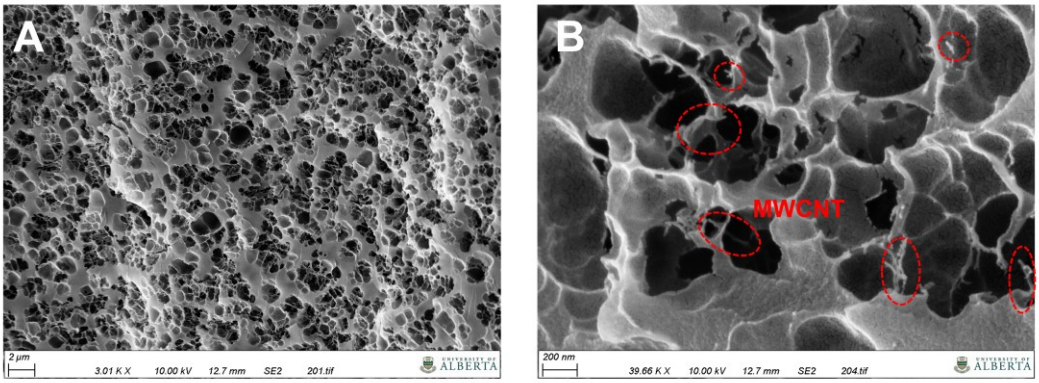

Figure S4.2. SEM images of the cross-sections of freeze-dried PAMAC-L hydrogel at (a) lower magnification and (b) higher magnification. Red arrows indicating the MWCNTs.

Table S4.1. Water contents of hydrogels with different compositions.

Sample	Water content (%)
PAM	69.3
PAM-MT-C	70.8
PAM-AE-C	69.7
PAMAC	69.8
PAMAC-L	69.9

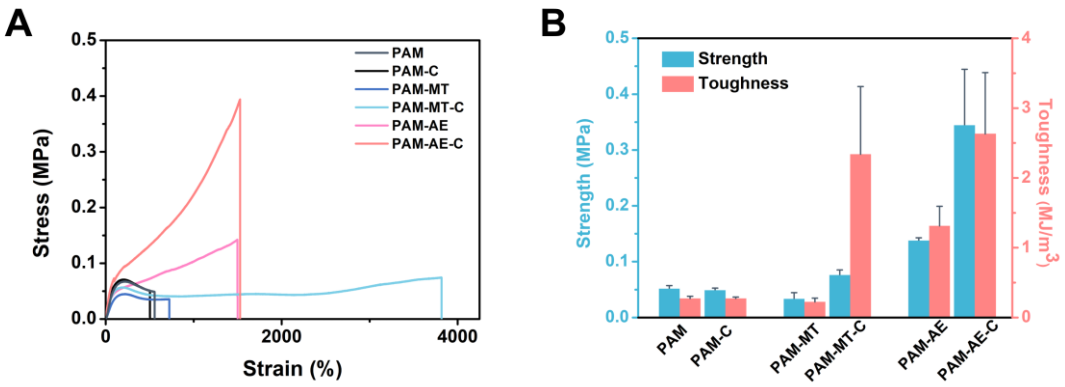

Figure S4.3. (a) Tensile stress−strain curves and (b) Average strength and toughness of PAM, PAM-MT, PAM-AE hydrogels with or without MWCNTs.

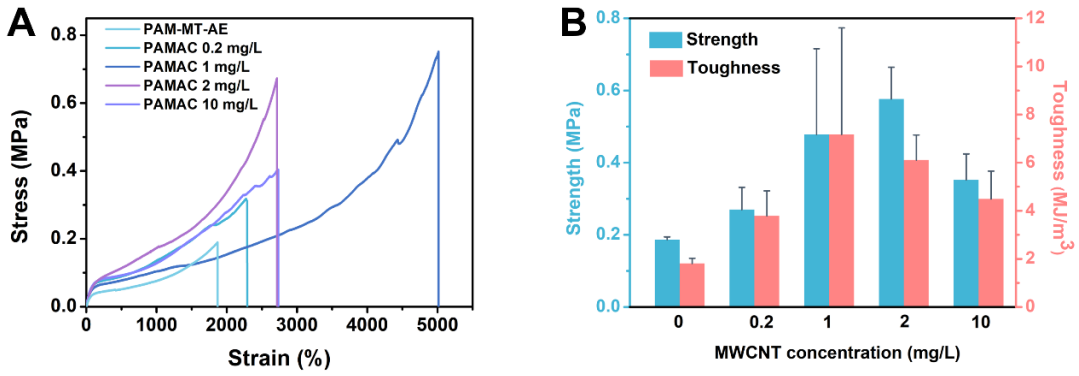

Figure S4.4. (a) Tensile stress−strain curves and (b) Average strength and toughness of PAMAC hydrogels with various concentrations of MWCNTs.

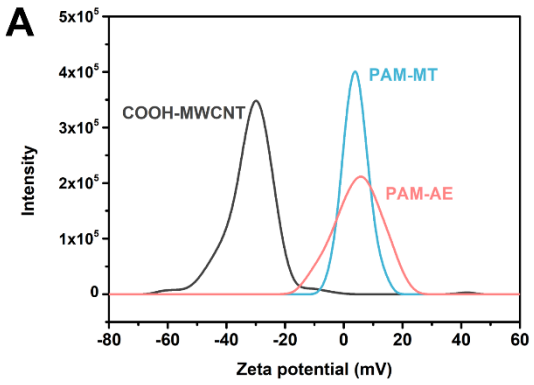

B

Material	Average zeta potential (mV)
COOH-MWCNT	-30.4 ± 0.8
PAM-MT	3.91 ± 0.14
PAM-AE	5.13 ± 0.31

Figure S4.5. (a) Zeta potentials of COOH-MWCNT, PAM-MT and PAM-AE. (b) Average zeta potentials calculated from three runs.

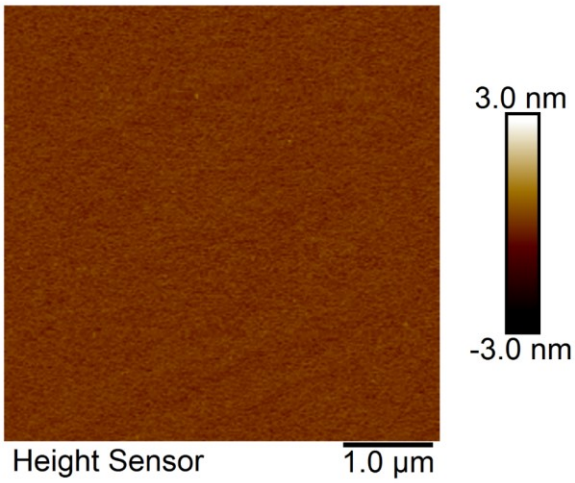

Figure S4.6. Topographic AFM images of bare mica.

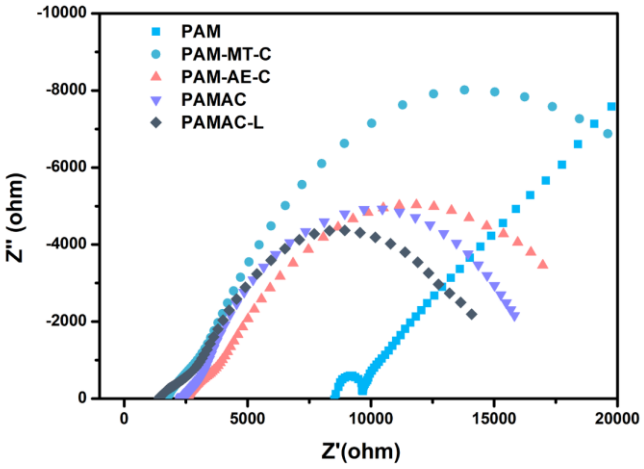

Figure S4.7. Electrochemical impedance spectra of hydrogels of different compositions.

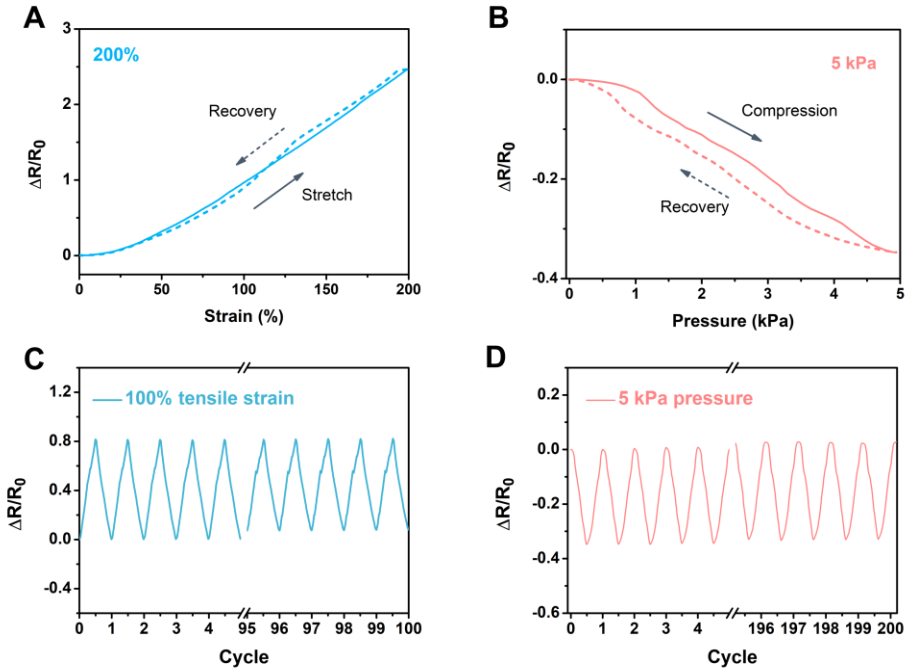

Figure S4.8. Relative resistance changes for PAMAC-L hydrogel during a loading-unloading cycle for (a) 200% tensile strain and (b) 5 kPa pressure, and subjected to (c) 100 loading/unloading tensile cycles of 100% maximum strain, and (d) 200 loading/unloading compressing cycles of 5 kPa maximum pressure.

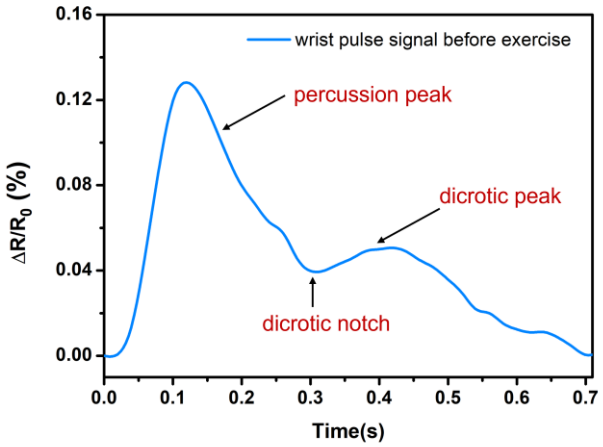

Figure S4.9. Waveform of a single wrist pulse before exercise.

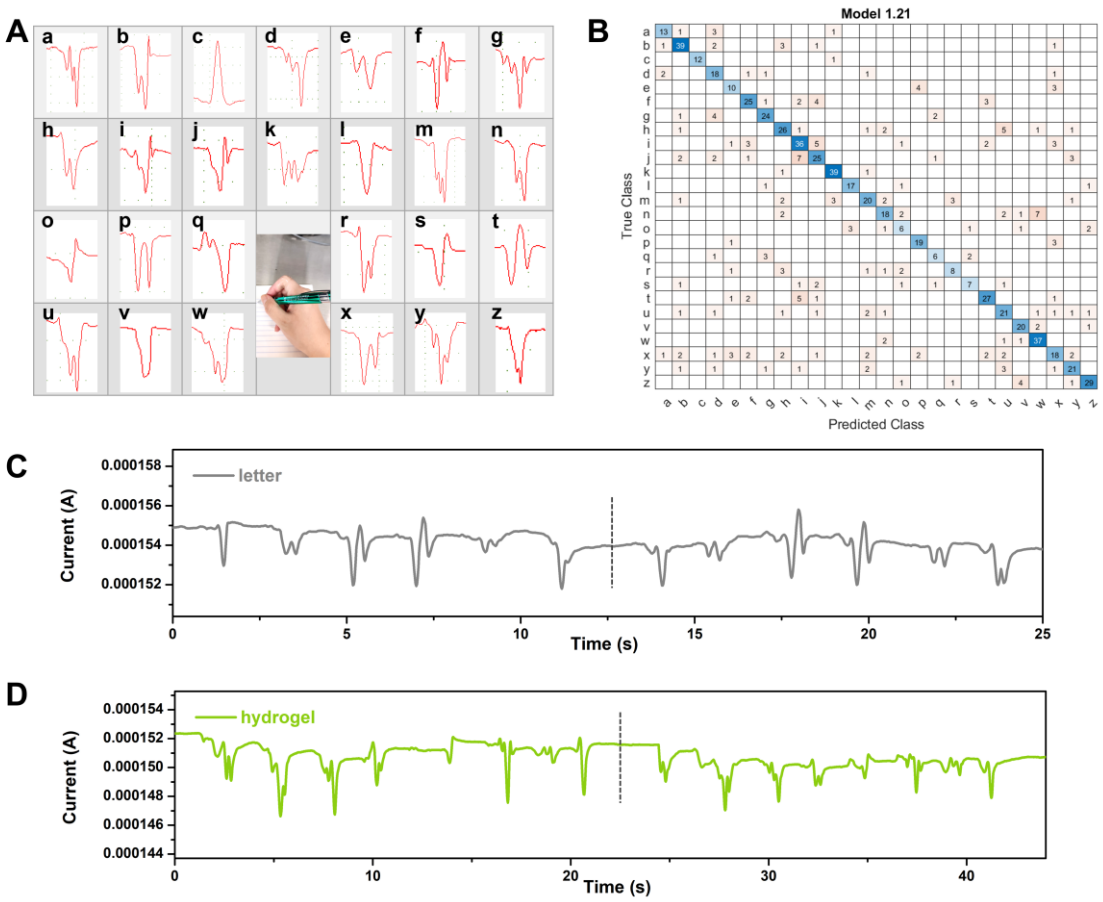

Figure S4.10. (a) Representative current signals for writing English letters from "a" to "z" on paper. (b) Confusion matrix that validates the classifier performance of the trained model. Typical current−time curves of writing words (c) "letter" and (d) "hydrogel".

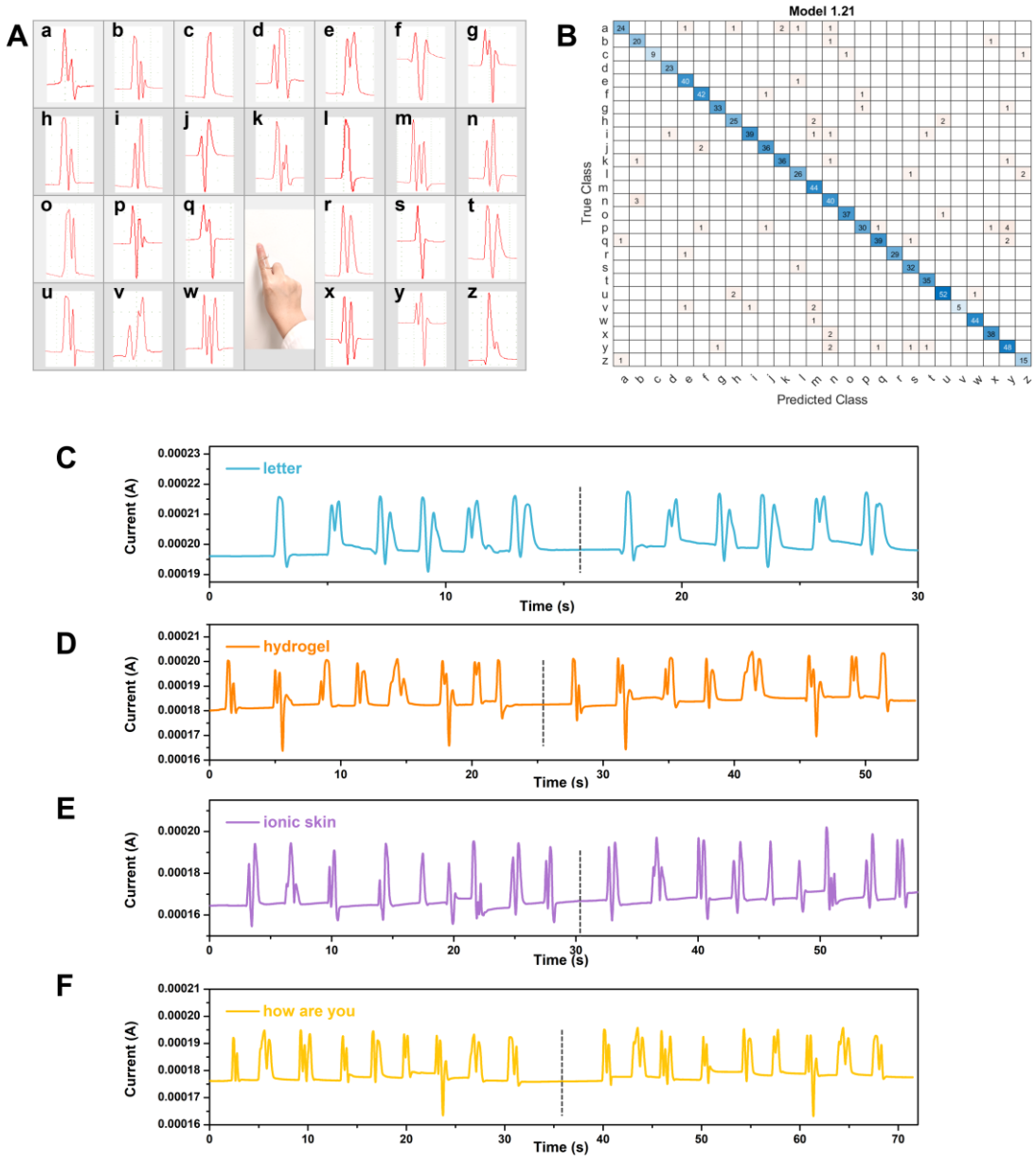

Figure S4.11. (a) Representative current signals for writing English letters from "a" to "z" in air. (b) Confusion matrix that validates the classifier performance of the trained model. Typical current−time curves of writing words (c) "letter", (d) "hydrogel", (e) "ionic skin" and (f) "how are you".

Table S4.2. Comparison of reported tough hydrogels and ionic skins or e-skins with this work

	Components of hydrogels	Strain at break	Stress at break (MPa)	Elastic modulus (kPa)[a]	Toughness (MJ/m^3)	Elasticity[b]	Water content (wt%)	Transparent	Self-healing	GF
This work	P(AM-MT-AE) /MWCNT/LiCl	4075%	1.09	65.4 (tensile) 96.0 (compressive)	12.8 (average 9.11)	90% recovery from 1000% strain	70	yes	yes	0.98−3.35
Tough hydrogel	PAM/Alginate /Ca^{2+} [60]	2200%	0.156	29	n/a	74% recovery from 600% strain (80 °C, 1 day)	86	partially	n/a	n/a
	PAM/GO/Ca^{2+} [168]	1100%	0.143	31.6	n/a	~90% recovery from 700% strain	88	no	n/a	n/a
	PAM/PBMA-PMAA-PBMA[136]	600%	10	2000	~30	recovery from 100% strain (heating-cooling treatment)	42	partially	yes	n/a
	Fe^{3+}/P(AM-AA)/MBAA[327]	748%	5.9	~1700	27	87.6% recovery from 300% strain (4 h)	60−70	no	n/a	n/a
	PMPTC/ PNaSS[47]	750%	5.1	7900	18.8	100% recovery from 300% strain (2 h)	42.5	no	yes	n/a
	PAM/CB[8] host–guest complexes[71]	2400%	0.13	~4.6	n/a	full recovery from 800% strain (2 min)	n/a	yes	yes	n/a
	Agar/PAM/ SMA/SDS [180]	5260%	0.267	106	9.35	40% recovery from 900% strain (2 min)	~70	no	yes	n/a
	HA-PVA[182]	1400−2900 %	11.5−23.5	2500	175−210	recovery from 500% tensile strain	70–95	no	n/a	n/a
	DMAA/MAAc[57]	800%	1.3	14000	n/a	full recovery from 300% strain	67	no	n/a	n/a
	PAAc/SMA/ CTAB/NaBr[51]	800−900%	1.66	605	n/a	97% recovery for 500% strain (5 min)	70	no	yes	n/a

	Components of hydrogels	Strain at break	Stress at break (MPa)	Elastic modulus (kPa)[a]	Toughness (MJ/m^3)	Elasticity[b]	Water content (wt%)	Transparent	Self-healing	GF
Ionic skin and e-skin	Sodium alginate /NaCl/PAM[282]	2000%	0.65	~50	4.77	98% recovery from 1000% strain	72.7	yes	yes	0−2.7
	PCL/PEG/ionic liquid[328]	327%	1.56	420	n/a	recovery from 200% strain	0	partially	yes	1.23−1.54
	TA/CNC/Ag nanoparticle[146]	4106%	0.246	n/a	n/a	n/a	~85	no	yes	~0.87
	PEGDA/SBMA/ dopamine[305]	n/a	n/a	n/a	n/a	~80% recovery from 80% compression strain	60−80	yes	yes	~0.83
	HPC/PVA/NaCl [246]	975%	1.3	900	5.85	recovery from compression	~66	no	n/a	~0.5−1.95
	PAAm/PAA–Fe^{3+}/NaCl[329]	~580%	1.18	330	n/a	full recovery from 200% strain (4 min)	47.9	no	yes	1.23−1.96
	PAA/gelatin/TA/ Al^{3+} [330]	1200%	0.04	n/a	0.148	~90% recovery from 500% strain	39	yes	n/a	2.5
	LA/EGDMA[331]	1000%	0.04	n/a	n/a	Recovery from 35% compression strain	0	yes	yes	n/a
	PAM/CNT/SDS/ lauryl methacrylate[155]	3000%	0.267	n/a	3.42	~90% recovery for 1000% strain	~80	no	n/a	2.0−4.32
	PAM/oxCNT/ gelatin[156]	1041%	0.71	59.6	2.29	recovery from 500% strain	~78	no	n/a	1.5−3.39

[a] The elastic moduli are obtained from tensile tests unless otherwise noticed.

[b] The elasticity recovery was obtained at room temperature in less than 1 min unless otherwise noticed.